ANALYSIS AND IDENTIFICATION OF LINEAR AND NONLINEAR NORMAL MODES IN VIBRATING SYSTEMS

Thesis by

Alexander F. Vakakis

In Partial Fullfillment

of the Requirements for the Degree of

Doctor of Philosophy

California Institute of Technology

Pasadena, California

1991

(Submitted July 30, 1990)

ACKNOWLEDGEMENTS

I wish to thank my Academic Advisor, Professor Thomas Caughey, for his guidance and care during all my years at Caltech. His continuous advice and suggestions were essential for developing the ideas of this work, and I consider myself fortunate for having the opportunity to share some of his knowledge, experience and thoughts on academic and nonacademic matters.

I am also grateful to my former MSc Thesis Advisor, Professor David Ewins, for kindly providing experimental data from his Modal Analysis Laboratory at Imperial College, London. Without his valuable help, the analysis of Part II of this work would be incomplete. Dr. R. Lin of Imperial College, helped with the electronic transmission of the data sets, and for that I thank him.

Many thanks are due to Professor Richard Rand from Cornell University and Visiting Professor at U.C.L.A., for numerous discussions on aspects of averaging. His essential contributions in the derivation of the results of section 2.4.2.2 are greatly appreciated.

I had the pleasure of cooperating with Professor Joel Burdick on the (now "famous") hopping robot. Although the results of our joint research are not presented in this work due to space limitations, I definitely plan a future encounter with the "hopper."

I am grateful to Caltech for generously providing me with Teaching Assistantships and Fellowships throughout my studies. Also, I would like to acknowledge the financial help of the De Karmam Fellowship Trust for awarding me its Fellowship, and of the NASA Jet Propulsion Laboratory for providing me with a Summer

Research Assistantship.

From all my friends at Thomas Lab, I would like to specially thank Albert ("Al") Moser for helping me with some computer operations, and my roommate at Thomas, Robert ("Bob") McCloskey, for interesting and stimulating discussions on all aspects of life and work.

Finally, I would like to express my deep gratitude and respect for my family members in Greece and Los Angeles. Without the unconditional and continuous love, help and coordination of my Father Fotis and Mother Anneta, this Thesis could never have been completed. The joyful and vivid character of my Sister, Elpida ("Bellina"), was always a source of aspiration and relaxation for me. My Wife, Sotiria, was always there during these three exciting and sometimes hard years in Pasadena, with love, compassion and care. It is to them that this Thesis is dedicated, with love.

ABSTRACT

In the first part of this work, the free and forced oscillations of a class of strongly nonlinear, undamped, discrete oscillators, are studied. The free motions are examined by using the notion of "nonlinear normal mode," originally introduced by Rosenberg. Analytical methods for computing similar and nonsimilar normal modes are presented, and the mode stability is analyzed. Normal mode bifurcations are found to exist in these systems, increasing in complexity as the degree of nonlinearity increases.

A specific application is given with a two degree of freedom, hamiltonian oscillator with cubic nonlinearity. The low energy motions are analyzed by means of *Poincare'* maps and an approximate averaging technique. When the energy is increased, chaotic motions are observed in the *Poincare'* maps, resulting from the transverse intersections of the stable and unstable manifolds of an unstable normal mode. Moreover, the generation of subharmonic orbits resulting from the breakdown of invariant KAM Tori is examined by using Subharmonic Melnikov analysis.

The similar and nonsimilar forced steady state motions are examined by considering special (nonharmonic) periodic excitations. For the case of cubic nonlinearity, a theorem on the necessary and sufficient conditions that a force should satisfy in order to lead to an exact steady state is given.

In the second part of the work, techniques for identifying systems with closely spaced modes and weak nonlinearities are developed. Modal interference in the

Complex plane is modeled by expanding the Frequency Response Function of the "perturbing mode" in Taylor series, and retaining only the two first terms. The distorted Nyquist plots of systems with stiffness and/or damping nonlinearities are analytically studied, by using the concept of "equivalent linearization." Based on the analytical results, refined identification algorithms are proposed, and their applicability is tested by analyzing theoretical and experimental data.

TABLE OF CONTENTS

TABLE OF FIGURES

PART I: NORMAL MODES IN STRONGLY NONLINEAR SYSTEMS

1. INTRODUCTION

1.1. OVERVIEW

In linear vibration theory, the concepts of "normal mode" and "steady-state motion" are implemented in the analysis of free and forced oscillations of discrete systems. The classical theory of n-degree-of-freedom (DOF) linear oscillators is concerned with the determination of the n modes (natural frequencies and eigenvectors); the principle of linear superposition can then be used to express any free or forced response as a superposition of individual modal responses. Moreover, it is well known that harmonic excitations of discrete, linear systems, lead to exact steady-state motions, in which all coordinates vary equiperiodically and pass through their extreme values simultaneously.

In the case of discrete oscillators with nonlinear restoring forces, the principle of superposition generally does not hold, and the aforementioned linear methodology cannot be applied. Therefore, there is a need for the development of special techniques for analyzing the dynamic response of such systems. Two basic options exist for studying nonlinear vibrations.

In the first approach, the nonlinearity is assumed to be "weak," i.e., small in magnitude compared to the linear stiffness (or damping) elements of the structure. Consequently, the nonlinear problem is viewed as a perturbation of a linear one. This leads to an asymptotic series approximation of the response, where higher or-

der terms are often omitted (the series is truncated after several terms). Although useful information concerning the free oscillations and the resonant forced motions is contained in the truncated series, the assumption of "weak" nonlinearity limits the applicability of this formulation, when "strongly" nonlinear systems are encountered. Such cases arise, for example, when one considers finite-amplitude vibrations of structural components (beams, plates, shells); the nonlinear restoring forces are then of comparable magnitude with the linear stiffness forces, and as a result the perturbation analysis is not valid anymore.

In the second approach, that of "strong" nonlinearity, the exact solution of the differential equations of motion of the system, is attempted. The precise dependence of the nonlinear restoring forces upon the amplitude is taken into account and, generally, the resulting closed-form solution is mathematically involved. In such cases, there is a need of introducing certain new concepts, with the goal of better understanding the physics of the nonlinear response. Two such concepts originating from the linear theory are these of the "nonlinear normal mode" and of the "nonlinear exact steady-state."

The notion of "nonlinear normal mode" was introduced by Rosenberg in order to study the free oscillations of strongly nonlinear systems. In direct analogy to the linear mode, the "nonlinear mode" is defined as a motion where all coordinates of the system are equiperiodic and reach their extreme values at the same instant of time. Similarly, the concept of "nonlinear exact steady-state" was applied to the

study of forced motions. What Rosenberg found was that, as in the linear case, nonlinear forced steady motions occur in the neighborhood of normal modes. Thus, the existence and the number of normal mode solutions appear to influence to a certain extent the dynamic behavior of discrete nonlinear oscillators.

1.2. OBJECTIVES - OUTLINE OF WORK

The general objective of this work is to apply the concepts of "normal mode" and "exact steady state" to a class of strongly nonlinear discrete oscillators. This will possibly lead to a better understanding of the dynamics of these systems and to a more complete description of the nonlinear global response.

More specifically, it is of interest to know if all nonlinear modes are analytic continuations of linear ones. In this work it is shown that the number of nonlinear normal modes is not necessarily equal to the number of degrees of freedom of the oscillator. This is the result of nonlinear mode bifurcations that increase in complexity as the degree of stiffness nonlinearity increases. Thus, in the nonlinear case, additional (bifurcating) modes may exist, that do not result as continuations of linear ones.

Another question concerns the representation of the nonlinear modes in the configuration space. In linear normal mode oscillations, all coordinates of the system are linearly related for all times. A unique feature of nonlinear free oscillations is the existence (in some cases) of normal modes, in which the functional relations between the coordinates are *not* linear (nonsimilar normal modes). Conditions for

existence of nonsimilar modes are derived and asymptotic techniques for computing these motions are developed. Moreover, it is found that orbitally unstable free nonlinear oscillations are possible, that lead to unstable backbone curves in response versus frequency diagrams.

The normal modes are very special periodic motions of the system and it is of importance to investigate their effect on the global dynamics of the oscillators. In this context, a challenging problem is to find how the bifurcations of normal modes influence the global structure of the flow in the phase space of the system. In this work, the global dynamics of the oscillators are studied by means of *Poincare'* maps. It is demonstrated that normal mode bifurcations lead to large-scale chaotic motions. In addition, "localized" chaotic trajectories and subharmonic orbits are numerically detected in the vicinity of stable modes. A numerical study of the large-scale chaotic motions is carried out by computing the stable and unstable manifolds of an unstable mode, whereas the subharmonic motions are investigated by use of subharmonic Melnikov-type analysis.

The last part of the work is concerned with forced motions of strongly nonlinear systems. Conventional studies of the forced response of nonlinear systems are carried under the assumption of harmonic excitation. In this work general periodic (but not necessarily harmonic) excitations are applied, and methodologies for computing the steady state responses are given. It is shown that forced resonant motions occur in the neighborhoods of normal modes. This result further underlines the impor-

tant role that normal modes play in the nonlinear response. What is also found is that the topological portrait of the resonance curves changes when a bifurcation of normal modes takes place. A last topic that is addressed in this work concerns the form that a periodic excitation must have in order to produce an exact nonlinear steady-state. This question is discussed for the case of systems with cubic stiffness nonlinearity and a general theorem concerning the admissible waveforms of the excitations is presented.

2. FREE OSCILLATIONS

2.1. CONCEPTS

For n degree-of-freedom (DOF) hamiltonian systems, there exist two basic theorems by Liapounov and Weinstein, regarding the existence of periodic solutions passing through the origin of their configuration space:

Theorem 1 (*Liapounov* 1947)

For analytic Hamiltonians with n DOF whose linearized eigenfrequencies are not integrably related, near each stable equilibrium there exist n families of periodic solutions filling up smooth 2-dimensional manifolds going through the equilibrium point. For any fixed energy, near each stable equilibrium one finds n periodic solutions (normal modes).

This result was extended by Weinstein for the "resonance cases": when the linearized eigenfrequencies are dependent over $\mathbf{Z}$ (the set of integers).

Theorem 2 (*Weinstein* 1973)

For an n DOF analytic Hamiltonian near a stable equilibrium point, there are at least n periodic solutions for fixed energy. Some of these solutions may not be analytic continuations of linear normal modes.

In this work, methodologies for computing the normal modes predicted by the two aforementioned theorems will be given. The following formal definitions are used.

Definition 1 (*Rosenberg* 1962, 1966)

A discrete autonomous n DOF system is oscillating in a normal mode, if it is "vibrating in unison":

1) The motions of all coordinates are periodic, of the same period.

2) All coordinates reach their extremum values at the same instant of time.

3) For a fixed $r \in [\,1, 2, ..., n\,]$, at any instant of time the coordinates of the system must be related by functional equations of the form

$$x_i = \hat{x}_i(x_r)\ , \quad i = 1, 2, ..., n. \tag{2.1}$$

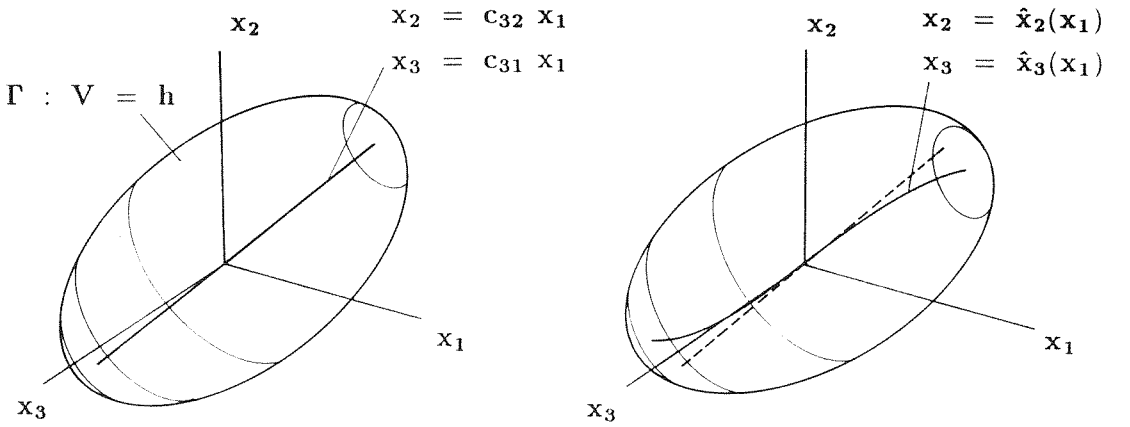

Similar mode *Nonsimilar mode*

Figure 2.1. Modal lines of similar and nonsimilar modes

Hence, in a normal mode, the oscillations of all coordinates can be parametrized

by any one coordinate. The trajectories in the configuration space corresponding to the normal mode are termed "modal lines" and are expressed in a mathematical form by equations (2.1).

Definition 2

If the modal lines corresponding to a nonlinear normal mode are straight, then the mode is termed "similar." In the general case where the modal lines are curved, the normal mode is termed "nonsimilar."

A schematic representation of similar and nonsimilar normal modes is presented at figure 2.1. Note that in the linear case only similar modes exist and the functional relations (2.1) are all linear; thus, nonsimilar modes are unique features of nonlinear oscillators. In what follows, similar and nonsimilar modes will be examined separately.

2.2. SIMILAR NORMAL MODES

2.2.1. PREVIOUS WORK

In a series of papers, Rosenberg introduced the concept of "nonlinear normal mode" (Rosenberg, 1960, 1961, 1962, 1964, 1966). In his work a variety of geometrical and analytical methods were developed for analyzing normal mode trajectories in the configuration space, and certain classes of strongly nonlinear oscillators were investigated: systems with homogeneous nonlinearities, with symmetries, with "linearized" and "nonlinearized" springs, etc. Theorems on the existence of similar nor-

mal modes were derived and stability problems were addressed. In (Atkinson, 1961, 1963), similar normal modes were detected by imposing matching conditions for the coefficients of respective nonlinear terms of the differential equations of motion. In (Cooke, 1966) and (Pak, 1968) the general problem of the existence of normal modes in two DOF conservative systems was addressed. In (Greenberg, 1971), the symmetries of the potential function were used to find subspaces of the configuration space in which the trajectories of the system were confined, and consequently to reduce the dimensions of these "modal subspaces"; a modal subspace of dimension one was then a normal mode. In (Mishra, 1974), group representation theory was used to investigate the existence of nonlinear normal modes of symmetric spring-mass systems of finite DOF, and in (Yang, 1968) the geometrical symmetries of the spatial configuration of certain mechanical systems were shown to reflect in symmetries of the potential function which were then utilized for the derivation of the normal modes. In (Montaldi, 1989), Birkhoff normal forms and techniques from singularity theory were applied for finding normal modes of systems with special symmetries. Some additional methodologies for finding normal modes can be found in (Rand, 1974), (Vito, 1972) and (Van Groesen, 1983).

The general problem of the stability of normal modes was discussed in the aforementioned work by Rosenberg. In (Rosenberg, 1966), the mode stability is approximately analyzed by considering "equivalent" *Mathieu* equations. A similar approach is followed in (Month, 1977). In (Pecelli, 1980), the stability of the normal modes of a planar oscillator with combined geometric and kinematic nonlineari-

ties was examined by means of *Lame'* equations whose stability charts are readily known. In (Rand, 1973), the stability of a normal mode was examined geometrically by establishing a criterion of orbital stability in the configuration space. Analytical methodologies for examining the stability of normal modes were also developed by (Porter, 1962), and in (Auld, 1961), where the mode stability was related to certain topological features of the equipotential curves in the configuration space.

An interesting feature of the free oscillations of strongly nonlinear systems is the fact that the normal modes may exceed the number of degrees-of-freedom (DOF). This is in contrast to the linear case, where the number of normal modes is always equal to the DOF of the system. In (Anand, 1972), an analysis of the free oscillations of a system with two DOF was given. One-term Fourier approximations for the periodic motions were made, and it was found that, depending on the system's parameters, bifurcations of modes were possible. Also, Rosenberg (1961), noted that for the same system with homogeneous springs, more than two modes may exist. In (Yen, 1974), a physical interpretation of the mode bifurcation was given by considering which of the terms in the expression of the potential function dominate for low and large amplitudes of motion. An analytic investigation of the stability of bifurcated modes, based on "stability in the kinemato-statical sense," was carried out in (Pak, 1989). Finally, studies of bifurcations of normal modes were performed by numerical techniques (Johnson, 1979), and by means of *Poincare'* maps (Month, 1980).

2.2.2. FORMULATION OF THE PROBLEM

Consider a n DOF, nonlinear, conservative system. The differential equations of motion are expressed as follows:

$$\ddot{\underline{x}} = -\nabla V = \underline{f}(\underline{x}) \tag{2.2}$$

where $\underline{x} \in R^n$ is the displacement vector, $\underline{f} \in R^n$ is the vector of (nonlinear) stiffness forces, $V : R^n \rightarrow R$ is the potential function of the system, and $\ddot{(\,)} \equiv d^2/dt^2$; it is assumed that the potential function is positive definite and symmetric with respect to the origin in the configuration space. These assumptions guarantee the existence of a stable equilibrium point at $\underline{x} = \underline{0}$. The symmetry of the potential function in the configuration space reflects the fact that the individual stiffnesses of the system respond to an equal amount in compression or extension. The smoothness of the potential function will not be of particular concern in this work: it will be assumed that the potential function is as smooth as required by the mathematical formulations.

The differential equations of motion can be written as follows:

$$\ddot{x}_i = f_i(x_1, ..., x_n) = \sum_{s=1,3,...}^{S} \hat{f}_i^{(s)}(x_1, ..., x_n), \quad i = 1, ..., n \tag{2.3}$$

and must be solved with initial conditions:

$$x_i(0) = X_i \ , \quad \dot{x}_i(0) = V_i \ , \quad i = 1, 2, ..., n. \tag{2.4}$$

In the above equations, each of the terms $\hat{f}_i^{(s)}$ contain monomials $x_1^{d_1} ... x_n^{d_n}$ whose exponents $d_m \geq 0$ satisfy $d_1 + d_2 + ... + d_n = s$. The expressions in

the right-hand-side of equations (2.3) can be regarded as Taylor expansions of the restoring forces f_i with respect to the variables x_i, truncated to order S. Note that the assumed symmetries of the potential function permit only even-order terms in the quantities $\hat{f}_i^{(s)}$.

In order for the system to oscillate in a *similar normal mode* , the coordinates x_i must satisfy the following linear relations for all times:

$$x_i \;=\; c_{ir}\, x_r, \qquad i = 1, ..., n \;,\;\; i \;\neq\; r \;,\;\; c_{rr} = 1 \tag{2.5}$$

where c_{ir} are $(n-1)$ unknown scalar quantities. In the above expressions, the variable x_r was used to parametrize the (straight) modal lines. Substituting the conditions (2.5) into (2.3), n differential equations in x_r result:

$$\begin{aligned} \ddot{x}_r &= \sum_{s=1,3,...}^{S} [\; \hat{f}_i^{(s)}(c_{1r}, ..., c_{nr})/c_{ir} \;]\; x_r^s, \quad i = 1, ..., n, \quad i \neq r \\ \ddot{x}_r &= \sum_{s=1,3,...}^{S} \hat{f}_r^{(s)}(c_{1r}, ..., c_{nr})\; x_r^s, \quad i = r \end{aligned} \tag{2.6}$$

with initial conditions $x_r(0) = X_r$, $\dot{x}_r(0) = V_r$.

It is evident, that the n equations (2.6) will give the same response for $x_r(t)$, if and only if all the coefficients of respective powers of x_r are equal. Thus, a "balancing" of coefficients must be made :

$$\hat{f}_i^{(s)}(c_{1r}, ..., c_{nr})/c_{ir} = \hat{f}_r^{(s)}(c_{1r}, ..., c_{nr}), \quad i = 1, ..., n, \quad i \neq r \tag{2.7}$$

$s = 1, ..., S.$

These "balancing" equations constitute a system of $[(S+1)/2] \times (n-1)$ algebraic equations with $(n-1)$ unknown quantities c_{ir}; hence, the problem of similar normal modes is overdetermined. Because of this, $[(S-1)/2] \times (n-1)$ structural parameters of the oscillators must be treated as unknowns and should be calculated from the "balancing" equations together with the scalars c_{ir}.

After determining the quantities c_{ir} , the response $x_r(t)$ can be formally computed by quadratures, by any one of equations (2.6). The remaining variables $x_i(t)$ can then be evaluated by means of the modal relations (2.5). Integrations by quadratures of differential equations of the form (2.6) can be found in Appendix A. In subsequent sections, applications of the outlined methodology will be given, by considering a strongly nonlinear, two DOF oscillator. It must be stated, however, that the outlined methodology is general and therefore can be formally applied to discrete systems of arbitrary DOF.

2.2.3. SYSTEM WITH "1 TO 1" RESONANCE

As an application of the theory, a two DOF oscillator will be now examined. Assuming that the system consists of two unit masses connected by means of three strongly nonlinear stiffnesses of the form,

$$f_k(u) = \sum_{s=1,3,5,\ldots}^{S} f_{ks} u^s \ , \quad k = 1,2,3$$

the differential equations of motion for the oscillating masses are given by:

$$\begin{aligned} \ddot{x}_1 + \sum_{s=1,3,\ldots}^{S} f_{1s} x_1^s + \sum_{s=1,3,\ldots}^{S} f_{2s}(x_1 - x_2)^s = 0 \\ \ddot{x}_2 - \sum_{s=1,3,\ldots}^{S} f_{2s}(x_1 - x_2)^s + \sum_{s=1,3,\ldots}^{S} f_{3s} x_2^s = 0. \end{aligned} \tag{2.8}$$

Throughout this work it will be assumed that $f_{ij} \geq 0$, unless otherwise stated. This by no means restricts the generality of the analysis since the same methodology can be followed in cases where $f_{ij} < 0$. If the additional symmetry condition is imposed:

$$f_1(u) = f_3(u) \quad \Rightarrow \quad f_{1s} = f_{3s} \ , \ s = 1, 3, ..., S \tag{2.9}$$

then the system is said to be on a "1 to 1" resonance, since its linearized eigenfrequencies are equal; a preliminary remark is that because of resonance this system is expected to have particularly "rich" dynamics.

The similar normal modes of the resonant system will now be calculated. To this end one initially substitutes the modal condition

$$x_2 = c x_1 \tag{2.10}$$

into the equations of motion, to get:

$$\begin{aligned} \ddot{x}_1 + \sum_{s=1,3,\ldots}^{S} [f_{1s} + f_{2s}(1-c)^s] x_1^s = 0 \\ \ddot{x}_1 + \sum_{s=1,3,\ldots}^{S} [f_{1s} c^{s-1} - f_{2s} \frac{(1-c)^s}{c}] x_1^s = 0. \end{aligned} \tag{2.11}$$

Matching the coefficients of respective powers of x_1, leads to the following set of "balancing equations":

$$c(1 - c^{s-1}) f_{1s} = (c-1)^s (c+1) f_{2s} \ , \quad s = 1, 3, ..., S. \tag{2.12}$$

It is clear that there are $[(S+1)]/2$ balancing equations, with only one unknown, c. For a similar normal mode to exist, one must find real values for c that satisfy *all* the balancing equations.

For $s = 1$, one obtains the linear balancing equation:

$$(c^2 - 1)f_{21} = 0. \tag{2.13a}$$

Note that if $f_{21} \neq 0$, i.e., if the linear term of the coupling stiffness f_2 is not zero, the only possible values of c are :

$$\begin{aligned} c = +1 \quad &\Rightarrow \quad Symmetric\ Normal\ Mode \\ c = -1 \quad &\Rightarrow \quad Antisymmetric\ Normal\ Mode \end{aligned} \tag{2.13b}$$

Thus, if one seeks additional nonlinear modes that do not result as continuations of the linear ones, one must require that:

$$f_{21} = 0 \ \ (Condition\ for\ additional\ nonlinear\ modes) \tag{2.14}$$

Assuming that condition (2.14) holds, the balancing equations corresponding to $s = 3, 5, ..., S$, are subsequently examined. It can be verified by direct substitution that $c = \pm 1$ are solutions of all these equations; thus the resonant nonlinear oscillator has the symmetric and antisymmetric modes, irrespective of the particular values of its structural parameters. As far as additional modes are concerned, the following two possibilities exist.

(a) Suppose that all stiffness terms in equations (2.12) are nonzero ($f_{ij} \neq 0$). Then, by dividing each of equations (2.12) by $(1 - c^2)$, one obtains (these equations give

the additional modes):

$$\sum_{p=1}^{(s-1)/2} c^{2p-1} + \frac{f_{2s}}{f_{1s}}(1-c)^{s-1} = 0 \ , \quad s = 3,5,...,S. \tag{2.15}$$

Equations (2.15) are solved for c for various values of the structural parameters $K_s = f_{2s} \ / \ f_{1s}$, and the results are presented in the diagrams of figure 2.2, for $s = 1,3,5$ and 7. In the same diagrams the $c = \pm 1$ modes are also included. Note that, if $f_{21} \neq 0$, the linear balancing diagram restricts the values of c to ± 1 and then the only possible nonlinear modes are the symmetric and antisymmetric ones. If, however, $K_1 = 0$, additional modes are possible, provided that real values of c can be found that satisfy all the remaining nonlinear balancing diagrams.

(b) Suppose now that there exists at least one $s = l > 1$, such that

$$f_{1l} = 0 \quad or \quad f_{2l} = 0 \tag{2.16a,b}$$

Then the $l - th$ equation of the set (2.12) becomes:

$$(c-1)^l(c+1)f_{2l} = 0 \quad or \quad c(1-c^{l-1})f_{1l} = 0 \tag{2.17a,b}$$

Clearly, the only real values of c satisfying any of equations (2.17), are ± 1 ; hence, if at least one f_{ij} $(i,j \neq 1)$ vanishes, no additional modes can exist.

Certain general properties of the real solutions of equations (2.15) (for the additional normal modes) will now be discussed. Since $(s-1)$ is an odd number and $f_{ij} > 0$ (by hypothesis), any real solution c must be negative. Moreover, one can verify by direct substitution that, if c is a real solution, then so is its reciprocal $1/c$. Hence additional nonlinear normal modes occur always in reciprocal pairs and bifurcate from the

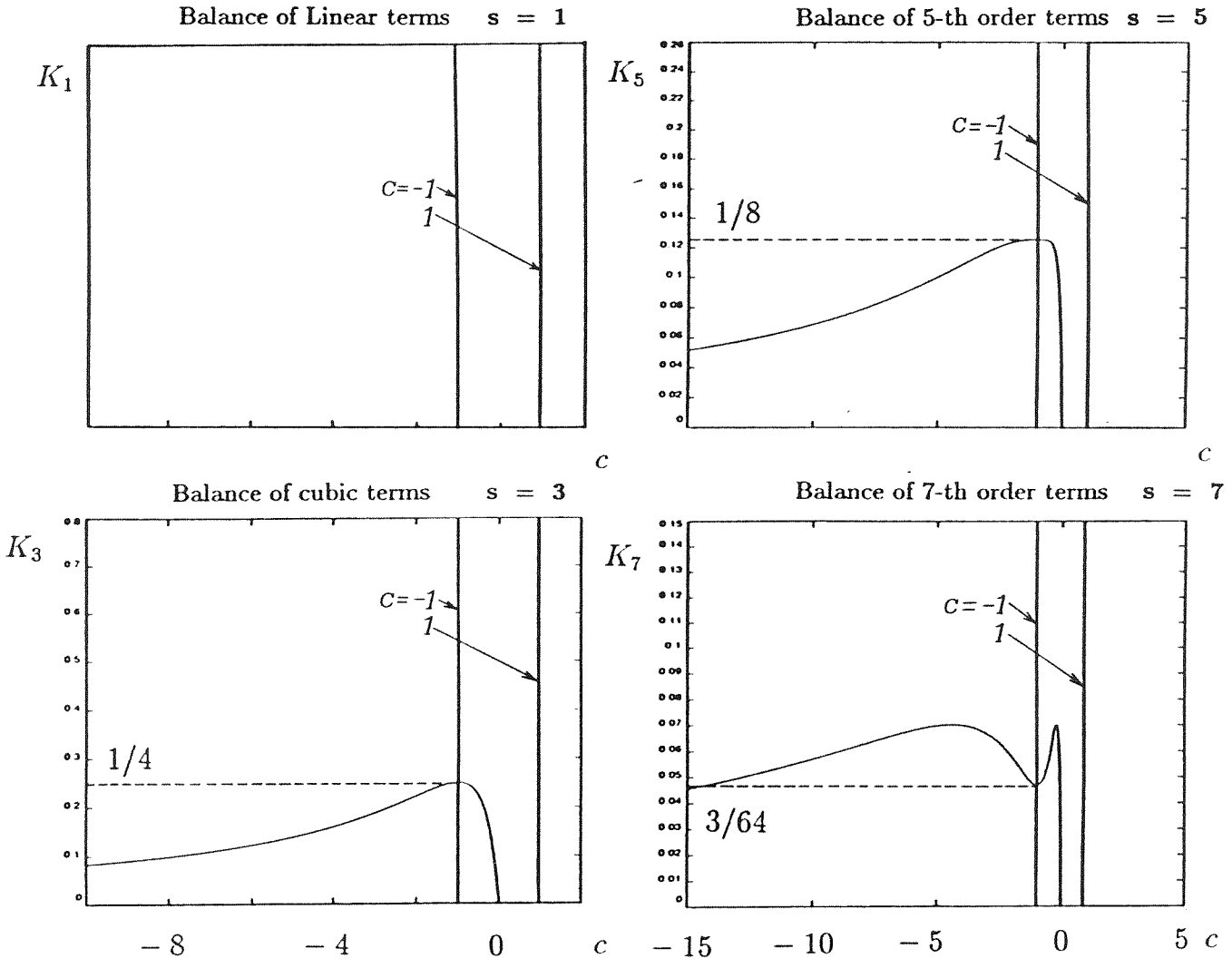

Figure 2.2. Balancing diagrams for similar modes of a system with "1 to 1" resonance.

antisymmetric mode. The bifurcation value for K_s in the balancing diagram of the $s-th$ nonlinearity, can be analytically computed as:

$$(K_s)_{bif} = (\frac{f_{2s}}{f_{1s}})_{bif} = [\sum_{p=1}^{(s-1)/2} (-1)^{2p-1}] \; / \; 2^{s-1} \tag{2.18}$$

$s = 3, 5, ..., S.$

As pointed out by (Anand 1972), this reciprocity of additional modes is the result of the symmetry of the system (the "1 to 1" resonance) and in fact, two reciprocal modes represent the same free oscillation.

As far as the stability of the nonlinear modes is concerned, the fact that the potential energy of the system is not a quadratic form (because of nonlinearities) leads to the conclusion that the normal mode solutions can never be Liapounov stable. Hence, at most, the modes can be orbitally stable and as pointed out by Rosenberg (1966), in general, their stability properties depend not only on the system parameters, but also on the energy level of the oscillation.

Two specific oscillators will now be analyzed, in order to demonstrate the application of the aforementioned theory. Both systems are in "1 to 1" resonance and contain nonlinearities of various orders.

SYSTEM WITH 3rd AND 5th ORDER NONLINEARITIES

Assuming that the coupling stiffness f_2 does not contain any linear term (condition for existence of bifurcating modes), the differential equations of motion of the system

are as follows:

$$\begin{aligned} \ddot{x}_1 + x_1 + x_1^3 + x_1^5 + K_3(x_1 - x_2)^3 + K_5(x_1 - x_2)^5 = 0 \\ \ddot{x}_2 + x_2 + x_2^3 + x_2^5 + K_3(x_2 - x_1)^3 + K_5(x_2 - x_1)^5 = 0 \end{aligned} \tag{2.19}$$

The linear balancing equation is satisfied for any choice of K_3, K_5 and thus only the nonlinear balancing equations are of importance:

$$\begin{aligned} c(1 - c^2) &= -K_3(1 - c)^3(1 + c) \quad (\ 3rd\ order\ ) \\ c(1 - c^4) &= -K_5(1 - c)^5(1 + c) \quad (\ 5th\ order\ ) \end{aligned} \tag{2.20}$$

In addition to the symmetric and antisymmetric modes, however, bifurcating modes may also exist in this system. To find these modes, one requires that the structural parameters K_3 and K_5, be related by $K_5 = 2\,K_3^2\,(1\ /\ 2K_3\ - 1)$. By imposing this condition, the 5-th order balancing equation is transformed to the 3-rd order one and compatibility of the two balancing diagrams of the system is achieved. As a result, the oscillator has effectively only one balancing diagram and the values of c corresponding to the bifurcating modes can then be evaluated as follows:

$$c = 1 - \frac{1}{2K_3} \pm \frac{1}{2}[\frac{1}{K_3}(\frac{1}{K_3} - 4)]\ , \quad K_3 < 1/4 \tag{2.21}$$

Thus, at $(\ K_3,\ K_5\ ) = (\ 1/4,\ 1/8\ )$, two bifurcating modes exist. Their stability will now be analyzed by the "linearized" methodology outlined in (Month, 1977). First, new variables are introduced, along and perpendicular, to the mode under examination:

$$\begin{Bmatrix} x_1 \\ x_2 \end{Bmatrix} = \frac{1}{(1 + c^2)^{1/2}} \begin{bmatrix} -c & -1 \\ 1 & -c \end{bmatrix} \begin{Bmatrix} u \\ v \end{Bmatrix} \tag{2.22}$$

In the new coordinates, the equations of motion become

$$\begin{aligned} \ddot{v} + v + A_4 v^3 + A_5 v^5 + A_3 v u^2 + A_6 v u^4 + A_7 v^2 u^3 \\ + A_8 v^3 u^2 + A_2 u^3 + A_9 u^5 = 0 \\ \ddot{u} + u + A_{10} u^3 + A_{11} u^5 + 3A_2 u^2 v + A_3 u v^2 + 5A_9 u^4 v \\ + \frac{A_3}{2} u v^4 + A_7 u^2 v^3 + 2A_6 u^3 v^2 = 0 \end{aligned} \tag{2.23}$$

where the quantities A_i are listed in Appendix B. Equations (2.23) admit the following set of solutions:

$$\begin{aligned} u(t) &= 0 \\ v(t) &= v^*(t) \end{aligned} \tag{2.24}$$

where $v^*(t)$ is the solution of the differential equation:

$$\ddot{v} + v + A_4 v^3 + A_5 v^5 = 0 \tag{2.25}$$

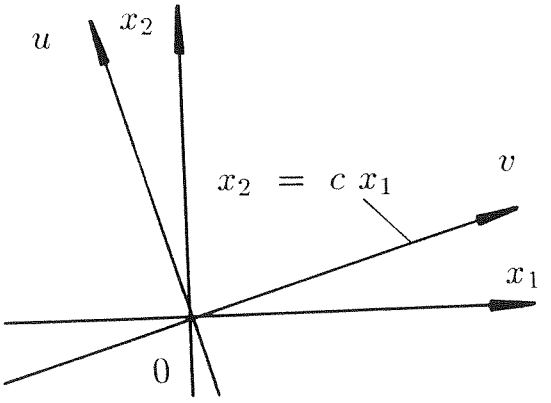

Figure 2.3. Coordinate axes for stability analysis

Under the assumption that the amplitude of $v(t)$ is "small," one can obtain the following approximate solution by Lindsted's method (Nayfeh, 1979):

$$v^*(t) = \beta cos(1 + \frac{3}{8} A_4 \beta^2 + \frac{5}{16} A_5 \beta^4) t + \mathcal{O}(\beta^2) \tag{2.26}$$

where the initial conditions $v^*(0) = \beta,\ \dot{v}^*(0) = 0$ are assumed and $\mathcal{O}(\bullet)$ denotes order of magnitude. The stability of solutions (2.24) determines the stability of the normal mode under consideration, and at this point small variations of the solutions are introduced:

$$\begin{aligned} u(t) &= 0 + \xi(t) \\ v(t) &= v^*(t) + \eta(t) \end{aligned} \tag{2.27}$$

Substituting equations (2.27) into the equations of motion (2.23) and taking into account the approximate solutions (2.24), one obtains two *Hill* - type variational equations in ξ and η. However, under fairly general conditions (Hayashi, 1985), (Van der Pol, 1928), the stability question can be answered by considering only the first two terms of the *Hill* equations. The resulting "equivalent" (Rosenberg, 1966) *Mathieu* variational equations are as follows:

$$\begin{aligned} \eta'' + [\delta_0 + 2\delta_1 cos2\tau]\eta = 0 \\ \xi'' + [\theta_0 + 2\theta_1 cos2\tau]\xi = 0 \end{aligned} \tag{2.28}$$

where, $(\ )'' \equiv d^2 \ / \ d\tau^2$ and

$$\begin{aligned} \theta_0 &= 1 + \frac{A_3\beta^2}{2} - \frac{3A_4\beta^2}{4} + \frac{3A_5\beta^4}{16} - \frac{5A_5\beta^4}{8} \\ \delta_0 &= 1 + \frac{3A_4\beta^2}{4} + \frac{5A_5\beta^4}{4} \\ \theta_1 &= \frac{A_3\beta^2}{4} + \frac{A_8\beta^4}{8} \\ \delta_1 &= \frac{3A_4\beta^2}{4} + \frac{5A_5\beta^4}{4} \end{aligned}$$

Note that since $\delta_0 = 1 + \delta_1$, both characteristic exponents of the $\eta -$ variational equation are zero, irrespective of values of the structural parameters of the system; this is because small perturbations along the v - axis result in neutrally stable

oscillations. Thus, the stability of the mode is determined completely by the ξ - variational equation (or equivalently, by introducing perturbations along the u - axis which is perpendicular to the normal mode). The stability of the ξ - Mathieu equation can be determined by standard methods in the *Stutt* diagram.

In figure 2.4 the stability characteristics of the four modes of the system are presented for $\beta = 0.9$. To produce these diagrams, the values of the coefficients θ_0 and θ_1 were computed for varying K_3, K_5 and were subsequently superimposed in the *Stutt* stability diagram of the *Mathieu* equation. It can be observed that a "Hamiltonian Pitchfork" bifurcation (Guckenheimer, 1984) takes place: the antisymmetric mode loses stability at the bifurcation point ($K_3 = 1/4, K_5 = 1/8$), whereas the bifurcating modes are orbitally stable. Note that the symmetric mode lies on the stability boundary $\theta_0 = 1 + \theta_1$; therefore, its stability cannot be determined by this linearized analysis (nonlinear effects should be taken into account). The reason for this stability indeterminacy is discussed by (Month, 1979), (Hyams, 1984), and as shown later, the use of *Poincare'* maps gives an answer to this problem. A point to note is that both bifurcating modes have the same stability characteristic; this had to be expected since, as mentioned earlier, they correspond to the same free oscillation of the "1 to 1" resonant system. Finally, it must be mentioned that for this example, the stability results do not depend on the amplitude of motion. Thus, even though the stability analysis is only approximate, the stability conclusions hold for relatively large amplitudes of motion. In latter sections such "high energy" motions will be examined by more refined techniques.

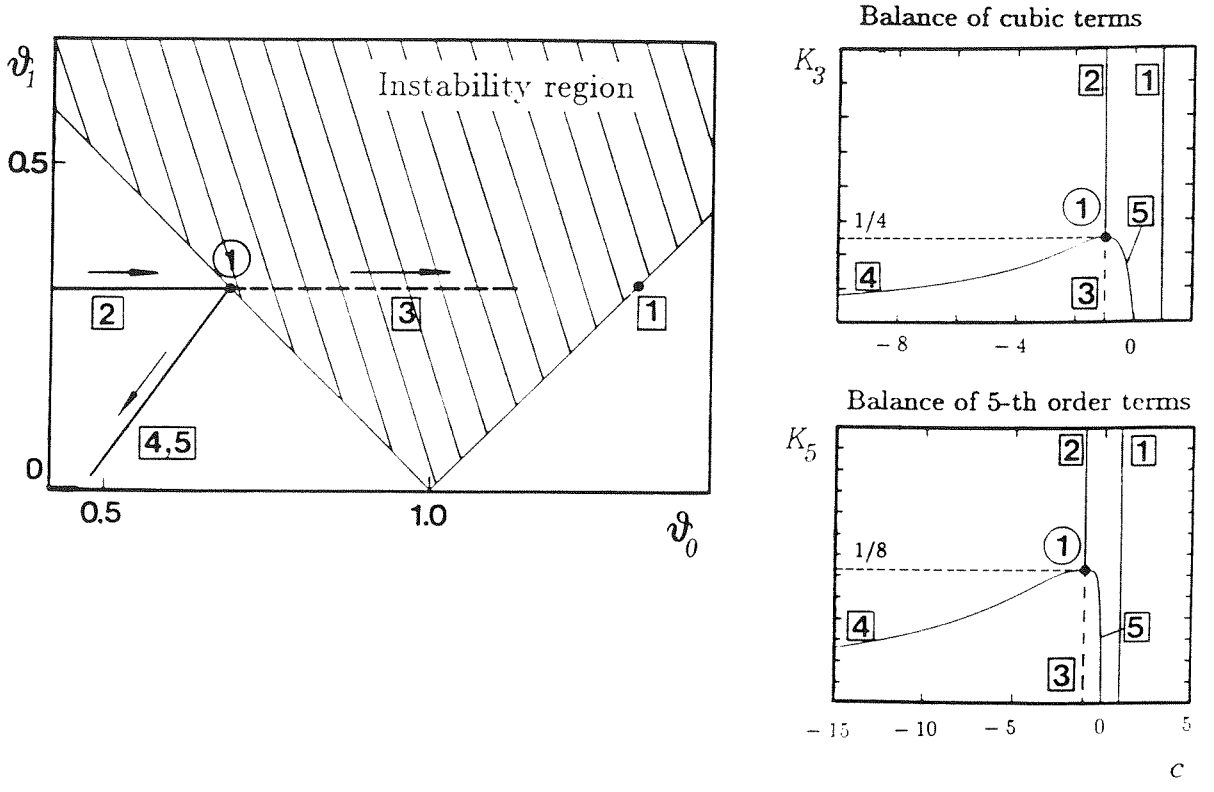

(a) (b)

Figure 2.4. (a) Stability characteristics of normal modes for a system with combined cubic and quintic nonlinearities: arrows in the direction of decreasing K_3, K_5. (b) Bifurcation diagrams.

SYSTEM WITH 7th ORDER NONLINEARITY

In this case, the equations of motion are of the form:

$$\begin{aligned} \ddot{x}_1 + x_1 + x_1^7 + K_7(x_1 - x_2)^7 &= 0 \\ \ddot{x}_2 + x_2 + x_2^7 + K_7(x_2 - x_1)^7 &= 0 \end{aligned} \tag{2.29}$$

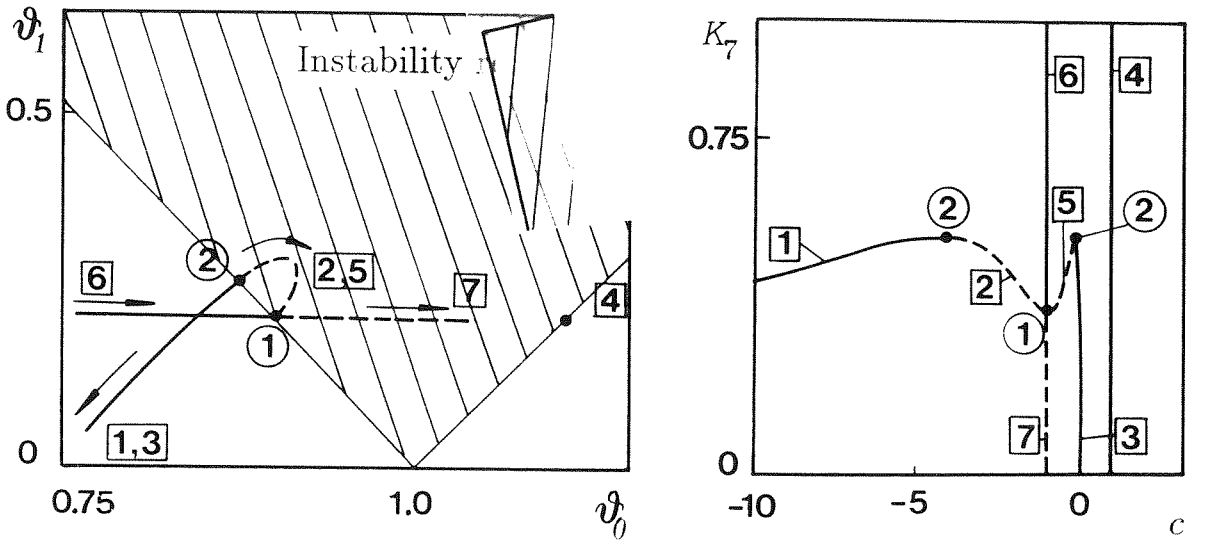

(a) (b)

Figure 2.5. (a) Stability characteristics of normal modes for a system with 7-th order nonlinearity: arrows in the direction of decreasing K_7. (b) Bifurcation diagram.

The linear balancing equation is satisfied for all values of K_7 and therefore the

modal parameter c is computed from the 7-th order balancing equation:

$$c(1-c^6)+K_7(1-c)^7(1+c)=0 \tag{2.30}$$

In addition to the $c = \pm 1$ modes, bifurcating modes may exist, given by the relation:

$$c(1+c^2+c^4)+K_7(1-c)^6=0 \tag{2.31}$$

The stability of the modes is studied with the approximate methodology discussed earlier and the results of the analysis are presented at figure 2.5. For $K_7 > 0.0705$ only the symmetric and antisymmetric modes exist. At $K_7 = 0.0707$ two "Saddle-Node" bifurcations take place and four additional modes are generated in two stable-unstable pairs. At $K_7 = 3/64$ the two additional unstable modes coincide with the stable antisymmetric one in a Pitchfork bifurcation, and for $K_7 < 3/64$, only four modes exist. In this example (as in the previous one) the stability of the symmetric mode cannot be determined by the linearized analysis.

2.2.4. SYSTEM "OFF - RESONANCE"

When the linearized eigenfrequencies of the nonlinear oscillator are not integrably related (independent over $\mathbf{Z}$), then the system is said to be "off-resonance." Consider again the two DOF oscillator and assume that the three nonlinear stiffnesses

are given by:

$$f_1(u) = \sum_{s=1,3,\ldots}^{S} f_{1s}u^s$$
$$f_2(u) = \sum_{s=1,3,\ldots}^{S} f_{2s}u^s \qquad (2.32)$$
$$f_3(u) = \sum_{s=1,3,\ldots}^{S} f_{1s}(1+\epsilon_s)u^s$$

The structural perturbations ϵ_s lead to a break of symmetry of the system and the "1 to 1" resonance (encountered in the previous examples) is eliminated. Throughout this section a system that lacks the "1 to 1" resonance will be referred as "off resonant."

Considering the equations of motion, imposing the modal relation between x_1 and x_2, and balancing coefficients in a way similar to the previous section, one obtains the following modified balancing equations:

$$f_{1s} + f_{2s}(1-c)^s = (1+\epsilon_s)f_{1s}c^{s-1} - f_{2s}\frac{(1-c)^s}{c}\ , \quad s = 1,3,\ldots,S \qquad (2.33)$$

The corresponding modified balancing diagrams appear in figure 2.6, for $s = 1,3,5$ and 7, with $\epsilon_1 = \epsilon_3 = \epsilon_5 = \epsilon_7 = 0.05$. Note that the quantities ϵ_s are not restricted to be small and, therefore, this methodology is also valid for systems with large perturbations off-resonance.

Note that, due to the lack of symmetry, the symmetric and antisymmetric modes cannot be realized in this system and that the bifurcating modes do not appear in reciprocal pairs. Similar modes can only occur if real values of c can be found that satisfy all the modified balancing diagrams. In what follows, two unsymmetric

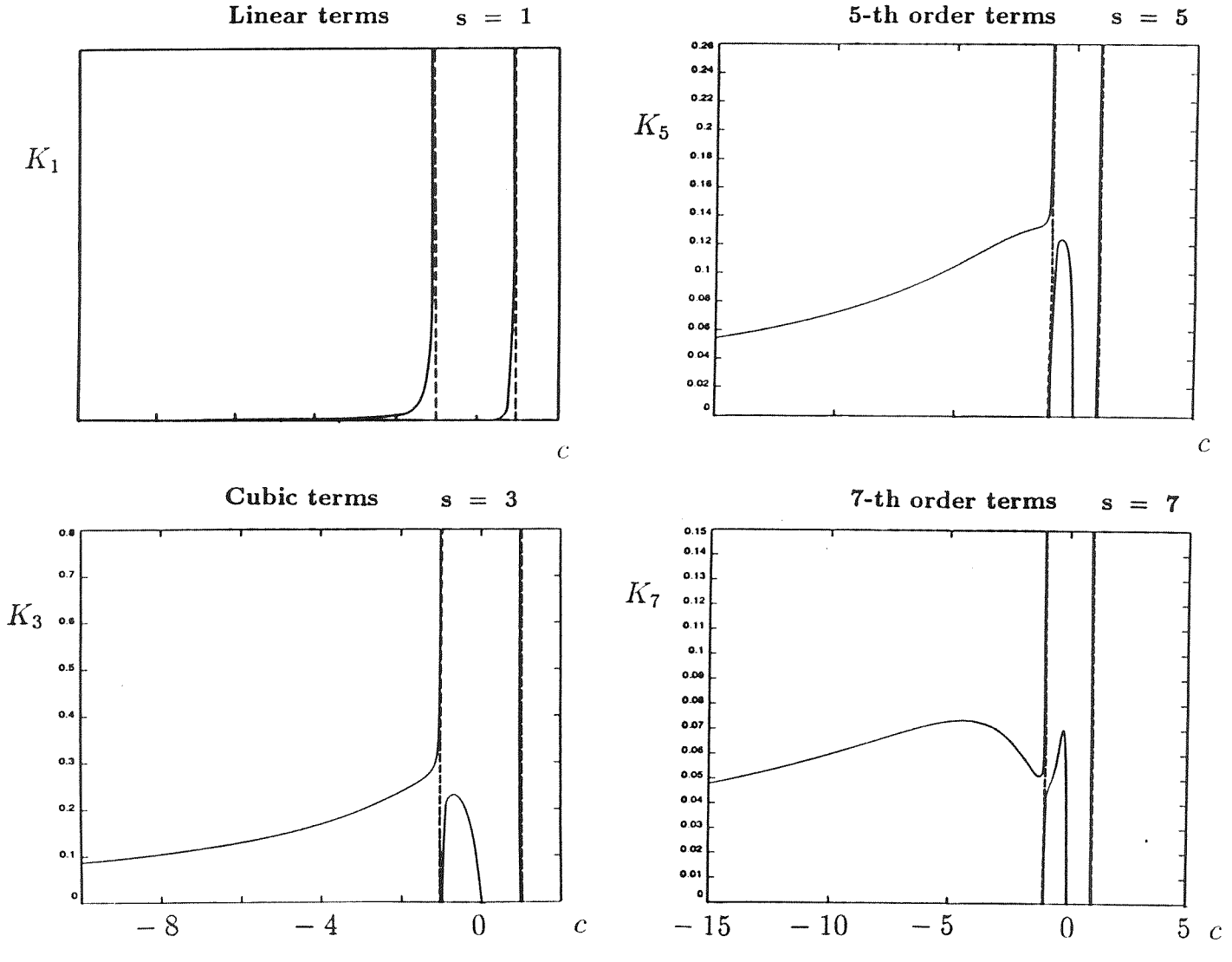

Figure 2.6. Balancing diagrams for similar modes of an unsymmetric system ("off-resonance").

systems will be examined. In the first one, there is a single balancing diagram to be satisfied, whereas in the second system two such diagrams exist. In each case, the similar normal modes are computed and their approximate stability analysis is carried out.

SYSTEM WITH A SINGLE BALANCING DIAGRAM

First, a nonlinear oscillator with 7-th order nonlinearity is examined. The differential equations of motion are as follows:

$$\begin{aligned} \ddot{x}_1 + x_1 + x_1^7 + K_7(x_1 - x_2)^7 &= 0 \\ \ddot{x}_2 + x_2 + \epsilon x_2^7 + K_7(x_2 - x_1)^7 &= 0 \end{aligned} \tag{2.34}$$

In terms of the previous notation, $\epsilon_1 = \epsilon_3 = \epsilon_5 = 0, \epsilon_7 = 1 - \epsilon$. Since $\epsilon_1 = 0$ and since the coupling stiffness does not contain any linear term, there is only one balancing diagram (that of 7th order):

$$1 + K_7(1 - c)^7 = \epsilon c^6 + K_7 \frac{(c-1)^7}{c} \tag{2.35}$$

The mode bifurcation diagram appears in figure 2.7, along with the results of the approximate stability analysis. There can be two, four or six similar normal modes, depending on the value of the parameter K_7. Comparing this bifurcation diagram with that of figure 2.5, it can be stated that the break of symmetry results in the destruction of the Pitchfork bifurcation observed in the resonant system (in its place a Saddle-Node bifurcation exists). This had to be expected, since the Pitchfork bifurcation is the result of the rotational symmetry of the resonant system and is structurally unstable: it can be eliminated by small structural modifications (if the

rotational symmetry is also destroyed). In the contrary, Saddle-Node bifurcations are structurally stable and thus generic for this class of oscillators (Guckenheimer, 1984).

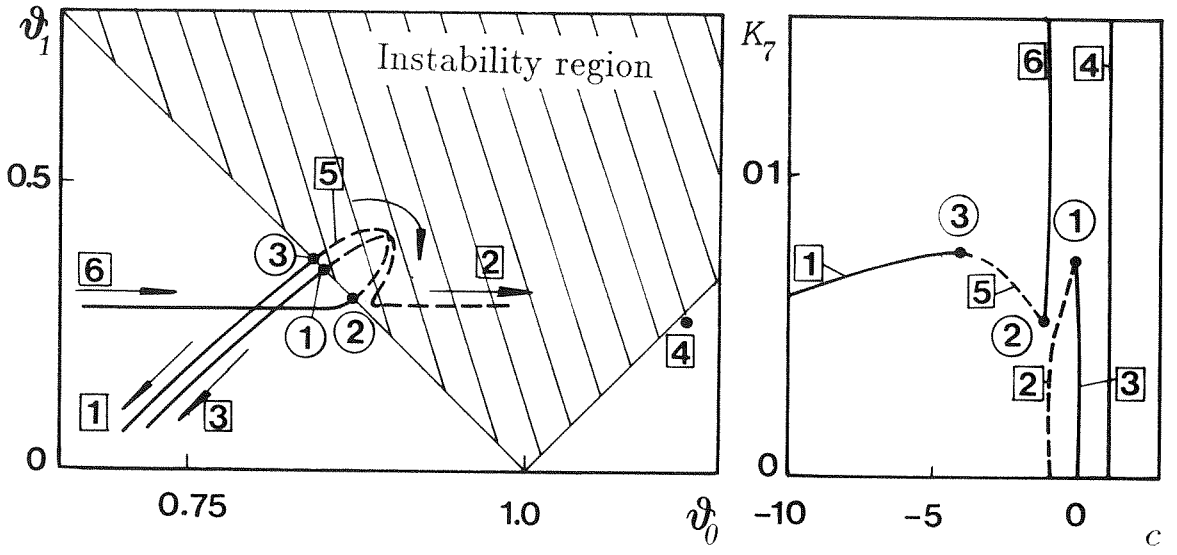

(a) (b)

Figure 2.7. (a) Stability characteristics of normal modes for an unsymmetric system with 7-th order nonlinearity: arrows in the direction of decreasing K_7. (b) Bifurcation diagrams.

Summarizing, the stability analysis indicates that three Saddle-Node bifurcations occur. The bifurcating modes appear in stable-unstable pairs, and at most, three orbitally stable similar normal modes exist. Finally, note that the stability results do

not depend on the amplitude of oscillation. As it will be demonstrated shortly, this does not hold for an unsymmetric system that possesses more than one balancing diagrams.

SYSTEM WITH TWO BALANCING DIAGRAMS

In this example perturbations in the linear stiffnesses of the oscillator of the previous section will be introduced: in addition to the seventh order diagram, a linear balancing diagram exists in this case. The equations of motion are assumed to be of the form:

$$\begin{aligned} \ddot{x}_1 + x_1^7 + K_1(x_1 - x_2) + K_7(x_1 - x_2)^7 = 0 \\ \ddot{x}_2 + \epsilon x_2 + \epsilon x_2^7 + K_1(x_2 - x_1) + K_7(x_2 - x_1)^7 = 0 \end{aligned} \tag{2.36}$$

Introducing the modal relation $x_2 = cx_1$ and matching coefficients, the following balancing equations result:

$$\begin{aligned} c(\epsilon - 1) = K_1(1 - c^2) \quad (Linear) \\ c(\epsilon c^6 - 1) = K_7(1 - c^2)(1 - c)^6 \quad (7th\ order) \end{aligned} \tag{2.37}$$

As mentioned earlier, a necessary condition for similar normal modes is that c satisfies both equations (2.37). The stability of the resulting free oscillations is then examined by the approximate methodology outlined in previous sections. Two numerical examples are given. The first corresponds to $\epsilon = 1.05$ and to an amplitude of oscillation $\beta = 0.9$ (β is the approximate amplitude of motion along the normal mode - equation (2.26)); the results of the analysis are presented in figure 2.8a. In the second example, the parameters are $\epsilon = 1.2$, $\beta = 0.9$ and the results are shown in figure 2.8b. Note that for values of c in the range $c \in (-1, 0)$, it is necessary

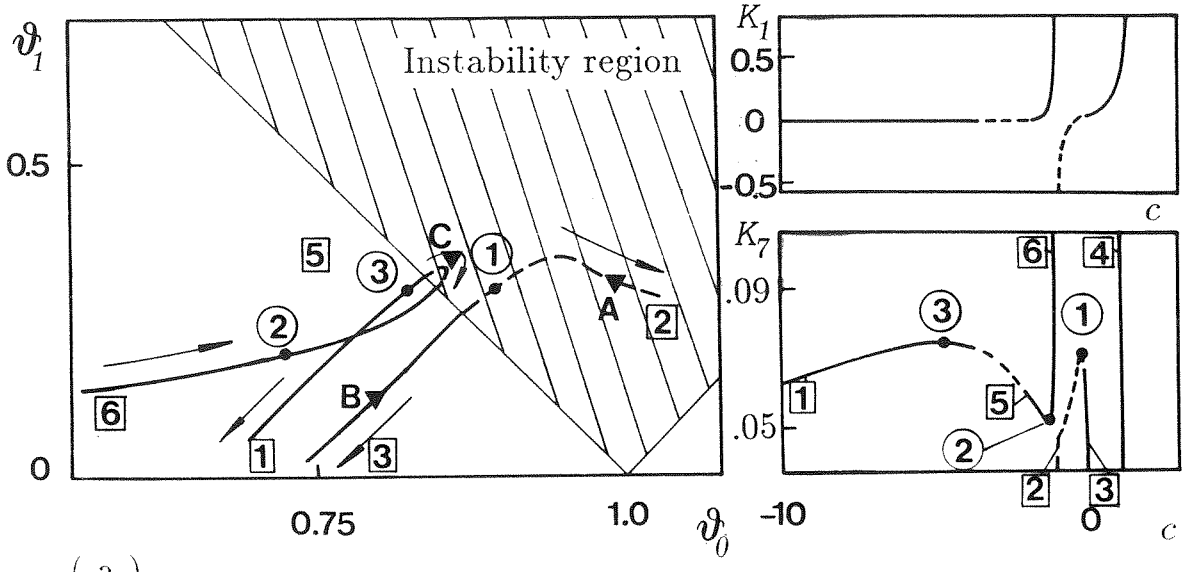

(a)

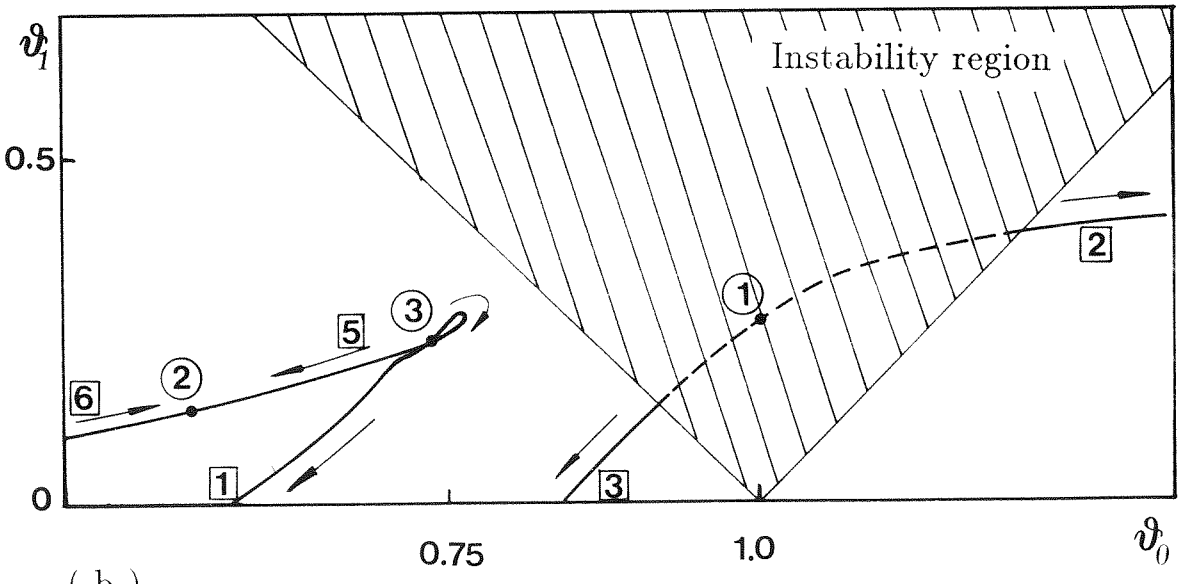

(b)

Figure 2.8. Similar normal modes of an unsymmetric system with two balancing diagrams: arrows in the direction of decreasing K_7:

(a) $\epsilon = 1.05,\ \beta = 0.9$ (b) $\epsilon = 1.20,\ \beta = 0.9$

that $K_1 < 0$. Hence, if K_1, K_7 are restricted to positive values, then c must also be restricted to the range $c \in (-\infty, -1) \cup (0, 1)$. The stability characteristic of mode 4 is not presented in the figures; it is well inside the stable region, indicating orbital stability.

A note of caution should be made here, concerning the way that the results should be interpreted. In previous examples, one can compute the number of modes corresponding to any (fixed) value of the structural parameter K_s. In this example this is not possible, since the two balancing diagrams must be simultaneously satisfied; thus, if the value of K_7, say, is changed, so must be the value of K_1. Hence, values of c in the plots, corresponding to the same value of K_7, correspond to different oscillators and as such, cannot be related. One possible way, however, to interpret the results, is to move *along* the lines of the graphs by varying both K_7 and K_1.

It is evident that no Saddle-Node bifurcations occur in this case. Moreover, it is observed that by varying the parameter ϵ (which indicates the amount of asymmetry of the system), the stability of the free oscillations is also altered. At points where one of the modes becomes orbitally unstable, possible nonsimilar mode bifurcations occur: this conjecture can be tested by implementing global numerical techniques (*Poincare'* maps), but in this work no such attempt will be made.

It can also be shown that the stability results depend on the amplitude of motion β, in contrast to the system examined previously (which had, however, only *one* balancing diagram). So, when more than one balancing diagrams exist, the stability of the resulting modes depends on the amplitude of motion and on the degree of

asymmetry of the system. On the contrary, when only one balancing diagram exists, the stability results are independent of these parameters, and Saddle-Node bifurcations replace the Pitchfork bifurcations observed in the resonant (symmetric) system.

To verify the analytical predictions, the equations of motion (2.36) were numerically integrated by a 4-th order Runge-Kutta algorithm. The existence of the theoretically predicted similar modes was verified, and their stability was examined by considering small perturbations in their initial conditions. The numerical values of the parameters are those of figure 2.8a, and the time-histories corresponding to three different initial conditions are shown in figure 2.9. It can be seen that free oscillations corresponding to points in the *Stutt* diagram well inside the primary instability region, are orbitally unstable: small perturbations in the initial conditions result in large amplitude modulations and no periodic motion is possible. Modes with stability characteristics outside the primary instability region were found to be orbitally stable, since relatively large perturbations in their initial conditions resulted in small amplitude modulations. For mode 5, which is just inside the primary instability region, the instability was manifested by amplitude modulations of large period.

Finally, it must be stated that in (Rosenberg, 1966), it was predicted that the stability of modes of "homogeneous" systems (systems with nonlinearities that are proportional to the same power of the displacement), is independent of the amplitude. In this work, the same result was observed for systems that have a single

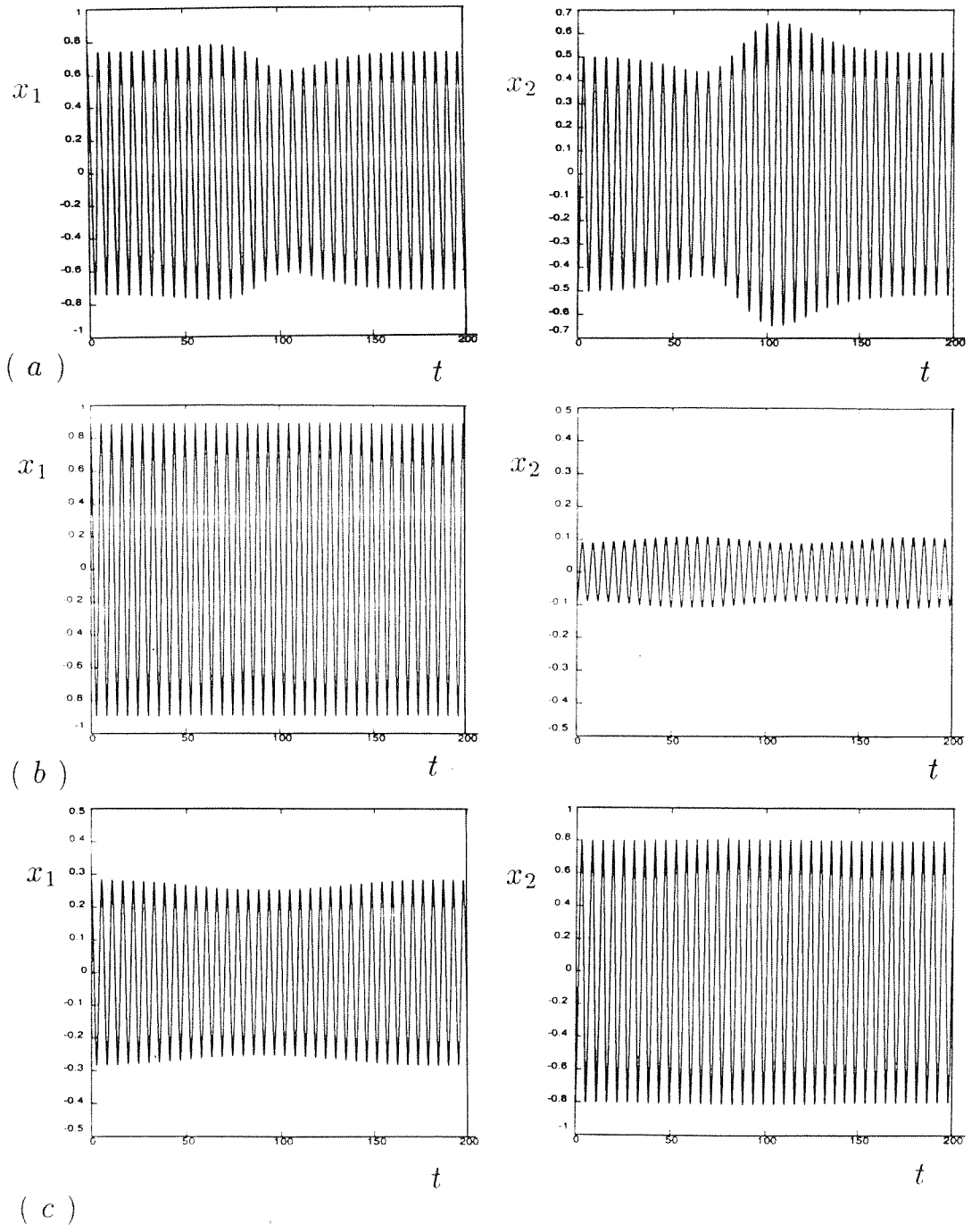

Figure 2.9. Numerical integrations of the equations of motion.

(a) Unstable mode (point A in fig. 2.8a): perturbation 2.6% in $x_2(0)$

(b) Stable mode (point B in fig. 2.8a): perturbation 10.2% in $x_2(0)$

(c) Weakly unstable mode (point C in fig. 2.8a): perturbation 6.2% in $x_2(0)$

balancing diagram (but are not necessarily homogeneous). Thus, if an oscillator has a single balancing diagram, the stability of its similar modes is independent of the amplitude. In cases, however, with more than one diagram, the mode stability depends on the amplitude (or equivalently on the energy of oscillation), and stability analysis should be carried on a case by case basis.

2.3. NONSIMILAR NORMAL MODES

2.3.1. PREVIOUS WORK

In previous sections, similar normal modes of free oscillations were examined. As pointed out, the set of algebraic equations which is used to compute these motions is overdetermined; as a result, similar modes can only be realized for real values of the modal constants c_{ij} that satisfy *all* the balancing diagrams of the system. If no such real values of c_{ij} exist, the periodic oscillations predicted by the Liapounov - Weinstein theorems are nonsimilar normal modes, i.e., they are represented by curved lines in the configuration space of the system.

A general discussion of nonsimilar normal modes can be found in (Rosenberg, 1966); based on geometrical arguments in the configuration space, properties of curved modal lines are given and mathematical formulas for their computation are derived. As pointed out in the same reference, nonsimilar normal modes decouple the nonlinear equations of motion only for a certain level of energy. If a different level of energy is chosen, then the modal line defining the mode should be modified accordingly. This is in contrast to straight modal lines (representing similar modes), which are independent of the particular energy of oscillation.

Since the differential equations describing the curved modal lines in the configuration space are singular at the maximum equipotential surface (Rosenberg, 1966), it is necessary to develop asymptotic solutions that approximate the nonsimilar mode close to the origin. Such asymptotic approximations can be found in (Rosen-

berg, 1964), (Rand, 1971a,b) and (Manevich, 1972). A different methodology was used in (Vito, 1972), where assuming low amplitudes, the nonsimilar modes were approximated by harmonic functions; in the sequence, "backbone" curves (amplitude of free oscillation versus frequency) corresponding to the nonsimilar modes of a two DOF system were plotted. Finally, in (Atkinson, 1962,1965), the nonsimilar modes of a class of strongly nonlinear, discrete oscillators were studied by certain "nonlinear superposition techniques." The nonsimilar free oscillation of the system was expressed as a superposition of the similar normal modes of its "homogeneous" subsystems. Although the numerical results approximated quite satisfactory the free nonlinear response, no mathematical justification for this superposition method was given.

The following sections are arranged as follows. First, a mathematical formulation of the problem of nonsimilar free oscillations is presented. Then, the perturbation methodology of (Manevich, 1972) is implemented for the study of the nonsimilar modes of a strongly nonlinear oscillator. Although the asymptotic solutions presented in this work are new, the perturbation methodology is not. It is only included here for the sake of completeness.

2.3.2. FORMULATION OF THE PROBLEM - ASYMPTOTIC SOLUTIONS

Consider an n - DOF, nonlinear, conservative system. The differential equations of

motion are of the form

$$\ddot{x}_i = f_i(x_1, ..., x_n) \ , \quad i = 1, ..., n \tag{2.38}$$

with initial conditions,

$$x_i(0) = X_i \ , \quad \dot{x}_i(0) = 0 \ , \quad i = 1, 2, ..., n \tag{2.39}$$

The same analysis can be applied, however, for a different set of initial conditions. A necessary condition for nonsimilar free oscillation is that the coordinates x_i be related by:

$$x_i = \hat{x}_i(x_r) \ , \quad i = 1, ..., n, \quad i \neq r. \tag{2.40}$$

The above functional relations must hold at every instant of time. Note that coordinate x_r was used to parametrize the nonsimilar motion and that the functions $\hat{x}_i(\bullet)$ (which are in general nonlinear in x_r), define a curve in the n - dimensional configuration space of the oscillator (instead of a straight line as in the case of similar normal modes).

Expressing the time derivatives in the equations of motion in terms of the functions $\hat{x}_i(\bullet)$ and the coordinate x_r, one finds that a nonsimilar normal mode can occur only if the following $(n-1)$ functional equations are satisfied (Manevich, 1972):

$$2\Big[h - V(\hat{x}_1(x_r), ..., \hat{x}_n(x_r))\Big] \left[1 + \sum_{k=1, k\neq r}^{n} \left(\frac{d\hat{x}_k}{dx_r}\right)^2\right]^{-1} \frac{d^2\hat{x}_i}{dx_r^2} +$$

$$+ f_r\left(\hat{x}_1(x_r), ..., \hat{x}_n(x_r)\right) \frac{d\hat{x}_i}{dx_r} = f_i(\hat{x}_1(x_r), ..., \hat{x}_n(x_r)) \tag{2.40}$$

where, $i = 1, 2, ..., n \quad , i \neq r$, h is the total (fixed) energy, and V is the potential energy of the system.

The above set of $(n-1)$ functional equations must be solved for the $(n-1)$ functions $\hat{x}_i(\bullet)$ that determine the nonsimilar normal mode. Since no exact solutions exist for this problem, it is necessary to develop asymptotic techniques for approximating the modal lines in the configuration space.

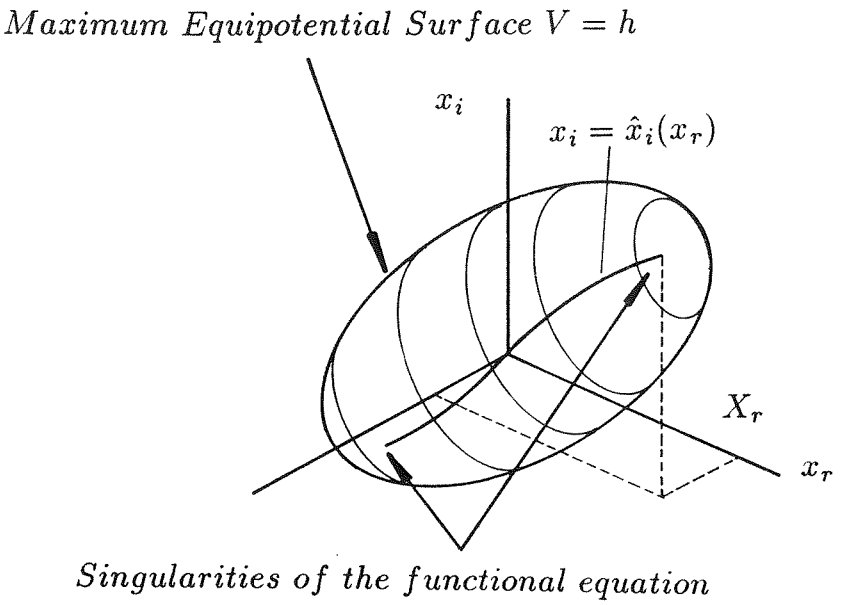

Figure 2.10. Curved Modal line corresponding to a Nonsimilar Normal mode.

Note that the functional equations (2.40) are singular at the maximum equipotential surface (defined by $V = h$). This happens because the coefficients of the second derivatives of the functions $\hat{x}_i$ vanish at these points. These singularities at the points of intersection of the modal lines with the surface $V = h$ (figure 2.10) further complicate the solution of the problem. It can be shown, however, (Erdelyi, 1956), that for differential equations with "regular singular points" (as in the present problem), asymptotic solutions can be constructed which are valid for intervals of the independent parameter that are open and do not contain the singular points. Hence,

it can be proved that an asymptotic solution exists for the nonsimilar mode, valid in open intervals of the coordinate x_r :

$$x_r \in (a, b) \quad , \ |a| \ , \ |b| \ < \ X_r. \tag{2.41}$$

X_r is the maximum value of x_r and corresponds to the point of intersection of the modal curve with the maximum equipotential surface (figure 2.10). To construct the asymptotic solution, one must consider the following general properties of the modal curves (Rosenberg, 1966).

(a) Since the nonsimilar normal mode is a periodic motion passing through the origin of the configuration space, it is necessary that:

$$\hat{x}_i(0) = 0 \quad , \quad i = 1, 2, ..., n \ , \ i \neq r. \tag{2.42}$$

(b) Because of the symmetry of the potential function with respect to the origin of the configuration space, the functions $\hat{x}_i(\bullet)$ describing the nonsimilar mode must be even functions of x_r:

$$\hat{x}_i(-x_r) = -\hat{x}_i(x_r) \ , \quad i = 1, ..., n \quad , \ i \neq r. \tag{2.43}$$

(c) The nonsimilar normal mode must intersect orthogonally the maximum equipotential surface in the configuration space. In mathematical terms, this requirement is expressed by the following $(n-1)$ equations,

$$f_r(\hat{x}_1(X_r), ..., \hat{x}_n(X_r)) \ \left\{ \frac{d\hat{x}_i}{dx_r} \right\}_{x_r = X_r} = f_i \ (\hat{x}_1(X_r), ..., \hat{x}_n(X_r)) \tag{2.44}$$

which hold at the points of intersection of the modal lines with the maximum equipotential surface. There are $(n-1)$ orthogonality relations, and they can be

regarded as "boundary conditions" to the $(n-1)$ functional equations (2.40). It is evident that any asymptotic solution to the problem must necessarily satisfy this set of equations.

The perturbation methodology of Manevich and Mikhlin will now be presented. To apply this analysis one assumes that the nonsimilar normal modes are located in the neighborhood of similar ones. Thus, the nonsimilar modes will be considered to be perturbations of similar free oscillations: an asymptotic series solution will be developed, in which the first order approximation is the similar normal mode. Equivalently, one can consider structural perturbations of oscillators that have similar normal modes: the resulting new system does not have similar modes but its nonsimilar solutions are "close" to the similar ones of the unperturbed system. A final remark is that, this method mainly applies to the analysis of finite-amplitude oscillations of strongly nonlinear systems, in contrast to existing perturbation methodologies which require "weak" nonlinearities and/or small amplitudes of motion. In what follows, the basic steps of the asymptotic method are outlined.

(a) The asymptotic solution is of the form:

$$\hat{x}_i(x_r) = \sum_{k=0}^{\infty} \hat{x}_i^{(k)}(x_r) \ , \quad i = 1, ..., n \ , i \neq r. \tag{2.45}$$

The functions $\hat{x}_i^{(k)}(\bullet)$ represent successive approximations to the solution, and the zero-th order approximation ($k = 0$) is the solution corresponding to a *similar mode*: $\hat{x}_i^{(0)} \ (\ x_r \ ) = c_{ir} \ x_r$.

(b) If the approximations of order $0, ..., (k-1)$ are known, the $k-th$ order

approximation can be found by substituting equation (2.45) into the functional equations (2.40) and the boundary conditions (2.44), and disregarding higher order approximations (of order $k+1$,...). Thus, $(n-1)$ "$k-th$ order functional relations" and $(n-1)$ "$k-th$ order boundary conditions" result that have as unknowns the $(n-1)$ functions $\hat{x}_i^{(k)}(\bullet)$. Each of these functions is expressed in a series representation as follows:

$$\hat{x}_i^{(k)}(x_r) = \sum_{j=1,3,5,\ldots}^{\infty} a_{ij}^{(k)} x_r^j \tag{2.46}$$

$i = 1, 2, ..., n \ , \quad i \neq r.$

Note that only even terms are included in the series, because of the symmetries of the modal line in the configuration space (see previous discussion). The real scalars $a_{ij}^{(k)}$ are determined by substituting expressions (2.46) in the "$k-th$ order functional relations" and the "$k-th$ order boundary conditions," and by matching coefficients of respective powers of x_r. The asymptotic solution converges in any open interval $x_r \in (a, b) \in [-X_r, X_r]$, but not at the limiting values $x_r = \pm X_r$. A rigorous mathematical proof of convergence can be found in (Manevich, 1972).

(c) The approximate asymptotic expressions for $\hat{x}_i(x_r)$ can be used for computing the time response $x_r(t)$ as follows. The coordinates x_i in the equations of motion (2.38) are expressed as functions of x_r (this can be done only when the system oscillates in a nonsimilar mode). In the sequence, the time response for x_r is obtained by integrating by quadratures any one of the resulting equations of motion. The time responses of the remaining coordinates can then be conveniently obtained by direct computation, using the (known) modal relations (2.40).

(d) The stability of the nonsimilar normal modes can be determined rather easily by applying the stability theorem derived in (Rosenberg ,1966). According to this theorem, if a nonsimilar mode results as a perturbation of a similar one, then its stability is identical to that of the similar mode. Thus, the problem of the stability of a nonsimilar mode is converted to an equivalent one involving a similar mode, which can be solved with the techniques outlined in section 2.2.

2.3.3. APPLICATION OF THE METHOD

An application of the outlined asymptotic methodology will now be given with a two DOF system with cubic nonlinearity. The analysis, however, is quite general and can be used for computing nonsimilar modes of oscillators with many DOF and arbitrary degree of stiffness nonlinearities.

At this point, consider a two DOF "resonant" oscillator with differential equations of motion:

$$\begin{aligned} \ddot{x}_1 + x_1 + x_1^3 + K_1(x_1 - x_2) + K_3(x_1 - x_2)^3 &= 0 \\ \ddot{x}_2 + x_2 + (1+\epsilon)x_2^3 + K_1(x_2 - x_1) + K_3(x_2 - x_1)^3 &= 0 \end{aligned} \tag{2.47}$$

and initial conditions $x_1(0) = X_1, \dot{x}_1(0) = 0, x_2(0) = X_2, \dot{x}_2(0) = 0$.

For $\epsilon = 0$, the oscillator has two similar modes of free oscillation (this can be easily shown by considering the balancing diagrams of linear and cubic terms): a symmetric mode corresponding to $c = 1$ and an antisymmetric one for $c = -1$. However, for $\epsilon \neq 0$, no similar normal modes exist for this oscillator since no real values of the modal constant c can be found that satisfy *simultaneously* the linear and cubic

balancing diagrams (figure 2.11). Thus, the structural perturbation of the system (represented by the ϵ term) eliminates the possibility of similar modes and the only possible periodic free motions of the "perturbed system" can be nonsimilar modes. However, for "small" values of the parameter ϵ, it is reasonable to expect that these nonsimilar modes will be "close" to the similar ones (of the unperturbed system), and that the asymptotic analysis outlined in the previous sections can be applied.

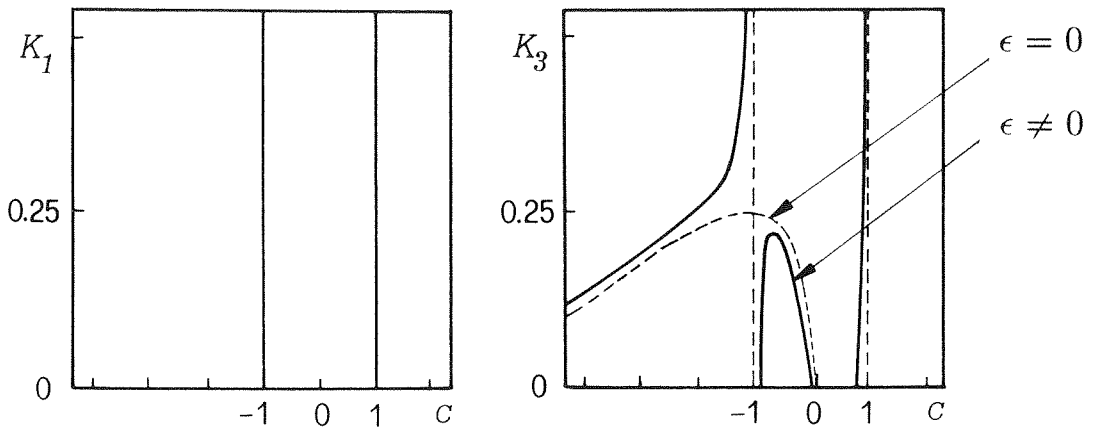

Figure 2.11. Linear and cubic balancing diagrams of a system with nonsimilar modes.

In seeking nonsimilar modes of free oscillation, one requires that the coordinates of the system be related by an expression of the form:

$$x_2 = \hat{x}_2(x_1) \tag{2.48}$$

Since this relation must hold for every value of time, the derivatives of the coordi-

nates during a nonsimilar normal mode can be computed as follows:

$$\dot{x}_2 = \hat{x}_2' \dot{x}_1 \ , \quad \ddot{x}_2 = \hat{x}_2''(\dot{x}_1)^2 + \hat{x}_2' \ddot{x}_1 \tag{2.49}$$

where $(\bullet)' \equiv d/dx_1$ and $\dot{(\bullet)} \equiv d/dt$. Substituting for $x_2, \dot{x}_2$ and $\ddot{x}_2$ into the equations of motion, one obtains the following set of differential equations that describe the oscillation on the nonsimilar mode:

$$\begin{aligned} \ddot{x}_1 + x_1 + x_1^3 + K_1(x_1 - \hat{x}_2)^3 + K_3(x_1 - \hat{x}_2)^3 = 0 \\ \hat{x}_2''(\dot{x}_1)^2 + \hat{x}_2' \ddot{x}_1 + \hat{x}_2 + (1+\epsilon)\hat{x}_2^3 + K_1(\hat{x}_2 - x_1) + K_3(\hat{x}_2 - x_1)^3 = 0 \end{aligned} \tag{2.50}$$

An expression for the velocity $\dot{x}_1$ can be obtained by integrating the first of the above equations by quadratures (in the following expressions, X_1 denotes the amplitude of coordinate x_1).

$$(\dot{x}_1)^2 = -2 \int_{X_1}^{x_1} \{\xi(1+K_1) + \xi^3 - K_1 \hat{x}_2(\xi) + K_3[\xi - \hat{x}_2(\xi)]^3\} d\xi \tag{2.51}$$

Then, substituting (2.51) into the second of equations (2.50), and eliminating the variable $\ddot{x}_1$, one obtains the following functional equation for the (unknown) "modal function" $\hat{x}_2(\bullet)$:

$$\begin{aligned} -2\hat{x}_2''\{ \frac{(x_1^2 - X_1^2)}{2}(1+K_1) + \frac{(x_1^4 - X_1^4)}{4} + \int_{X_1}^{x_1} [K_3(\xi - \hat{x}_2(\xi))^3 - K_1 \hat{x}_2(\xi)] d\xi \ \} - \\ -\hat{x}_2'\{ \ x_1 + x_1^3 + K_1 x_1 - \hat{x}_2 K_1 + K_3(x_1 - \hat{x}_2)^3 \ \} + \\ +\hat{x}_2 + (1+\epsilon)\hat{x}_2^3 + K_1 \hat{x}_2 - K_1 x_1 + K_3(\hat{x}_2 - x_1)^3 = 0 \end{aligned} \tag{2.52}$$

This functional equation is analogous to the general expression (2.40) that was derived earlier for the general n DOF oscillator. Note that the coefficient of the second

derivative of $\hat{x}_2$ becomes zero at $x_1 = \pm X_1$. As a result, the asymptotic approximation to the solution will be valid only in open intervals contained in $[-X_1, X_1]$. To guarantee that the series solution intersects the maximum equipotential surface at the points $(x_1,\ x_2) = (\pm X_1, \pm X_2)$, one imposes the additional boundary condition:

$$-\hat{x}_2'(X_1)\{\ X_1 + X_1^3 + K_1 X_1 - \hat{x}_2(X_1)K_1 + K_3(X_1 - \hat{x}_2(X_1))^3\ \}+$$

$$+\hat{x}_2(X_1) + (1+\epsilon)\hat{x}_2(X_1)^3 + K_1\hat{x}_2(X_1) - K_1 X_1 + K_3(\hat{x}_2(X_1) - X_1)^3 = 0 \quad (2.53)$$

This is equivalent to the boundary orthogonality condition (2.44) that was given in the general formulation of the problem.

The asymptotic solution is written in the form:

$$\hat{x}_2(x_1) = \hat{x}_2^{(0)}(x_1) + \hat{x}_2^{(1)}(x_1) + ... \quad (2.54)$$

It will be assumed at this point that the first term of this series is much "larger" in magnitude than the other terms. Specifically, the orders of magnitude of the terms are assumed to be as follows:

$$\mathcal{O}(\hat{x}_2^{(0)}) = 1\ ,\quad \mathcal{O}(\hat{x}_2^{(1)}) = \mathcal{O}(\hat{x}_2^{(1)\prime}) = \mathcal{O}(\hat{x}_2^{(1)\prime\prime}) = \mathcal{O}(\epsilon) << 1. \quad (2.55)$$

The displacement x_1 is assumed to be finite (of $\mathcal{O}(1)$), and higher approximations $\hat{x}_2^{(k)}$, $k \geq 2$ are assumed to be of $\mathcal{O}(\epsilon^2)$ or higher. It is clear that these assumptions must be verified when the actual solution is computed.

The zero-th order solution corresponds to the similar modes of the "unperturbed system" (resulting when $\epsilon = 0$). Thus, the first term of the series (2.54) has the

form,

$$\hat{x}_2^{(0)}(x_1) = cx_1 \tag{2.56}$$

where the modal constant c is of $\mathcal{O}(1)$.

Substituting relation (2.54) into the functional equation (2.52), taking into account the zero-th order solution, (2.56), and retaining terms only up to $\mathcal{O}(\epsilon)$, one obtains:

$$-2\hat{x}_2^{(1)\prime\prime}\{\ [1+K_1(1-c)]\frac{(x_1^2-X_1^2)}{2}+[1+K_3(1-c)^3]\frac{(x_1^4-X_1^4)}{4}\ \}-$$

$$-\hat{x}_2^{(1)\prime}\{\ [1+K_1(1-c)]x_1+[1+K_3(1-c)^3]x_1^3\ \}+$$

$$+\hat{x}_2^{(1)}\{\ [1+K_1(1+c)]+[3K_3(1-c)^2c+3(1+\epsilon)c^2+3K_3(c-1)^2]x_1^2\ \}+$$

$$+\{\ (c^2-1)x_1+[-c-cK_3(1-c)^3+(1+\epsilon)c^3+K_3(c-1)^3]x_1^3\ \}=0 \tag{2.57}$$

$\mathcal{O}(1)$ terms

Considering only terms of O(1), the following equality results:

$$(c^2-1)x_1+[-c-cK_3(1-c)^3+c^3+K_3(c-1)^3]x_1^3=0 \tag{2.58}$$

Since the above relation must hold for arbitrary values of $x_1 \in [-X_1, X_1]$, it is necessary that the coefficients of all powers of x_1 be equal to zero :

$$c^2=1 \quad \textit{and} \quad -c-cK_3(1-c)^3+c^3+K_3(c-1)^3=0 \tag{2.59}$$

The above relations can be easily identified as being the balancing equations for similar normal modes of the "unperturbed" system ($\epsilon = 0$); they are satisfied if

and only if $c = \pm 1$. Thus, there are only two similar modes in the "unperturbed" oscillator (a symmetric and an antisymmetric one); for $\epsilon \neq 0$ they are perturbed, giving rise to nonsimilar normal modes.

$\mathcal{O}(\epsilon)$ terms

To compute the second term of the series, $\hat{x}_2^{(1)}$, one has to consider the balance of $\mathcal{O}(\epsilon)$ terms in equation (2.57):

$$-2\hat{x}_2^{(1)\prime\prime}\{\ [1+K_1(1-c)]\frac{(x_1^2-X_1^2)}{2}+[1+K_3(1-c)^3]\frac{(x_1^4-X_1^4)}{4}\ \}-$$

$$-\hat{x}_2^{(1)\prime}\{\ [1+K_1(1-c)]x_1+[1+K_3(1-c)^3]x_1^3\ \}-$$

$$-\hat{x}_2^{(1)}\{\ [1+K_1(1+c)]+[3K_3(1-c)^2c+3(1+\epsilon)c^2+3K_3(c-1)^2]x_1^2\ \}+$$

$$+\epsilon c^3 x_1^3 = 0 \tag{2.60}$$

This is the "functional equation of first order" that must be satisfied by $\hat{x}_2^{(1)}$. In addition to this equation, the following "boundary condition of first order" must be considered (this is derived from (2.53) by considering only terms of $\mathcal{O}(\epsilon)$):

$$-\hat{x}_2^{(1)\prime}(X_1)\{\ [1+K_1(1-c)]X_1+[1+K_3(1-c)^3]X_1^3\ \}+$$

$$+\hat{x}_2^{(1)}\{\ [1+K_1(1+c)]+[3K_3(1-c)^2c+3(1+\epsilon)c^2+3K_3(c-1)^2]X_1^2\ \}+$$

$$+\epsilon c^3 X_1^3 = 0 \tag{2.61}$$

The solution for $\hat{x}_2^{(1)}$ is now expressed in the form:

$$\hat{x}_2^{(1)} = a_{21}^{(1)}x_1 + a_{23}^{(1)}x_1^3 + a_{25}^{(1)}x_1^5 + \ldots \tag{2.62}$$

When this series solution is substituted in the functional equation of first order (2.60) and coefficients of respective powers of x_1 are set equal to zero, the following equations for the unknowns $a_{2j}^{(1)}$ result:

$$a_{23}^{(1)} = \frac{(T_1^{(1)} - T_3^{(1)})a_{21}^{(1)}}{6T_1^{(1)}X_1^2 + 3T_2^{(1)}X_1^4} \equiv L_1^{(1)}a_{21}^{(1)}$$

$$a_{25}^{(1)} = \frac{-T_5^{(1)}}{20T_1^{(1)}X_1^2 + 10T_2^{(1)}X_1^4} + \frac{[L_1^{(1)}(-T_3^{(1)} + 9T_1^{(1)}) + T_2^{(1)} - T_4^{(1)}]a_{21}^{(1)}}{20T_1^{(1)}X_1^2 + 10T_2^{(1)}X_1^4} \equiv$$

$$\equiv L_2^{(1)} + L_3^{(1)}a_{21}^{(1)} \tag{2.63}$$

Similar analytic expressions (albeit of increasing complexity) can be computed for the coefficients $a_{2j}^{(1)}$, $j \geq 7$, but these will not be presented in this work. The quantities $T_p^{(1)}$ depend on the value of c (of the zero-th order approximation) and the structural parameters of the oscillator:

$$\begin{aligned} T_1^{(1)} &= 1 + K_1(1-c) \\ T_2^{(1)} &= 1 + K_3(1-c)^3 \\ T_3^{(1)} &= 1 + K_1(1+c) \\ T_4^{(1)} &= 3K_3(1-c)^2c + 3(1+\epsilon)c^2 + 3K_3(1-c)^2 \\ T_5^{(1)} &= \epsilon c^3 \end{aligned} \tag{2.64}$$

To compute the quantity $a_{21}^{(1)}$, one substitutes the series (2.62) into the boundary condition of first order, taking simultaneously into account expressions (2.63). The resulting formula for $a_{21}^{(1)}$ is :

$$a_{21}^{(1)} =$$

$$\frac{-T_5^{(1)}X_1^2 - L_2^{(1)}X_1^4(T_3^{(1)} + T_4^{(1)}X_1^4) + 5L_2^{(1)}X_1^4(T_1^{(1)} + T_2^{(1)}X_1^2)}{-(1 + 3L_1^{(1)}X_1^2 + 5L_3^{(1)}X_1^4)(T_1^{(1)} + T_2^{(1)}X_1^2) + (1 + L_1^{(1)}X_1^2 + L_3^{(1)}X_1^4)(T_3^{(1)} + T_4^{(1)}X_1^2)} \tag{2.65}$$

Thus, by making use of relations (2.63) and (2.65), one approximates the nonsimilar normal mode as follows:

$$\hat{x}_2(x_1) = (c + a_{21}^{(1)})x_1 + a_{23}^{(1)}x_1^3 + +a_{25}^{(1)}x_1^5 + \mathcal{O}(\ \epsilon x_1^7,\ \epsilon^2) \tag{2.66}$$

Considering the analytical expressions (2.63-65), one can show that, indeed, all the coefficients $a_{2j}^{(1)},\ j = 1, 3, 5$ appearing in (2.66) are of $\mathcal{O}(\epsilon)$. Thus, the assumptions of the outlined perturbation analysis are met.

Since (2.66) is a truncated form of the general expression (2.54), it only approximates the actual solution for small values of the structural parameter ϵ and for small values of the amplitude x_1. However, one can extend the validity of the solution for relatively large amplitudes by computing additional terms in (2.66), of higher order in x_1 (this can be achieved by computing additional constants $a_{2j}^{(1)}$). Note also that since the coefficients $a_{2j}^{(1)}$ depend on the amplitude X_1, the resulting expression for the modal curve depends on the magnitude of oscillation (or equivalently on the total energy). This is in agreement with the prediction made by (Rosenberg, 1966) concerning nonsimilar normal modes.

After determining the approximation to the modal curve, the time responses can be computed by substituting (2.66) into the differential equations of motion (2.47).

In particular, the first of these equations takes the form:

$$\ddot{x}_1 + I_1^{(1)} x_1 + I_3^{(1)} x_1^3 + I_5^{(1)} x_1^5 + \mathcal{O}(\epsilon x_1^7,\ \epsilon^2) = 0 \tag{2.67}$$

where

$$\begin{aligned} I_1^{(1)} &= 1 - a_{21}^{(1)} + K_1(1-c) \\ I_3^{(1)} &= 1 - K_1 a_{23}^{(1)} + K_3(1 - c - a_{21}^{(1)})^3 \\ I_5^{(1)} &= -K_1 a_{51}^{(1)} - 3K_3(1 - c - a_{21}^{(1)})^2 a_{23}^{(1)} \end{aligned} \tag{2.68}$$

The time response of the coordinate x_1 can be computed from (2.67) by quadratures:

$$t = t(x_1) = \pm \int_{X_1}^{x_1} G(X_1, \xi) d\xi \tag{2.69a}$$

where,

$$G(X_1, \xi) \equiv \frac{1}{\{\ I_1^{(1)}(X_1^2 - \xi^2) + \frac{I_3^{(1)}}{2}(X_1^4 - \xi^4) + \frac{I_5^{(1)}}{3}(X_1^6 - \xi^6) + \mathcal{O}(\epsilon x_1^7, \epsilon^2)\ \}^{1/2}} \tag{2.69b}$$

The $(+)$ or $(-)$ signs are used alternatively so that a monotonic increase of the time variable results. Note that in writing expressions (2.69), it was assumed that the initial conditions of the system are $x_1\ (0) = X_1, \dot{x}_1(0) = 0, x_2(0) = X_2, \dot{x}_2(0) = 0$. For a different set of initial conditions, the limits of integration must be modified accordingly. Once the relation $x_1 = x_1(t)$ has been determined, the time response of the coordinate x_2 can be easily computed by use of the (nonlinear) modal relation (2.66).

One can "invert" (2.69a) to obtain a functional relation of the form $x_1 = x_1(t)$. However, this inversion may introduce difficulties of interpretation of the results,

since the associated expressions might not be (known) tabulated functions. A special case where the results are in terms of tabulated functions is when one retains only terms up to $\mathcal{O}(\xi^4)$ in the denominator of expression (2.69). The response can then be expressed in terms of elliptic functions, whose properties have been studied in the literature (Byrd, 1954), (Abramowitch, 1970).

The frequency of free oscillation can be evaluated directly from (2.69a), by a suitable choice of the limits of integration :

$$\omega = \frac{\pi}{-\int_{X_1}^{0} G(X_1, \xi) d\xi} \tag{2.70}$$

From the above relation the so called "backbone curves" of the nonsimilar modes can be evaluated. These are plots of the frequencies of oscillation ω versus the maximum amplitudes X_1, and are commonly used for describing the free oscillation in the frequency domain.

For a numerical application of the aforementioned analysis, let $K_1 = 1.3$ and $K_3 = 0.7$. For $\epsilon = 0.5$ and $X_1 = 0.6$, the asymptotic approximations of the two nonsimilar modes of the system were found to be as follows:

$$\begin{aligned} \hat{x}_2(x_1) &= -1.0325432x_1 - 0.0163626x_1^3 + 0.0054876x_1^5 + ... \\ \hat{x}_2(x_1) &= 0.9404508x_1 + 0.1214908x_1^3 + ... \end{aligned} \tag{2.71}$$

The two nonsimilar modes result as perturbations of the symmetric and antisymmetric similar modes of the oscillator with $\epsilon = 0$. Note that the high order terms are small compared to the dominant linear ones, even for a relatively large value of ϵ (in this example, $\epsilon = 0.5$).

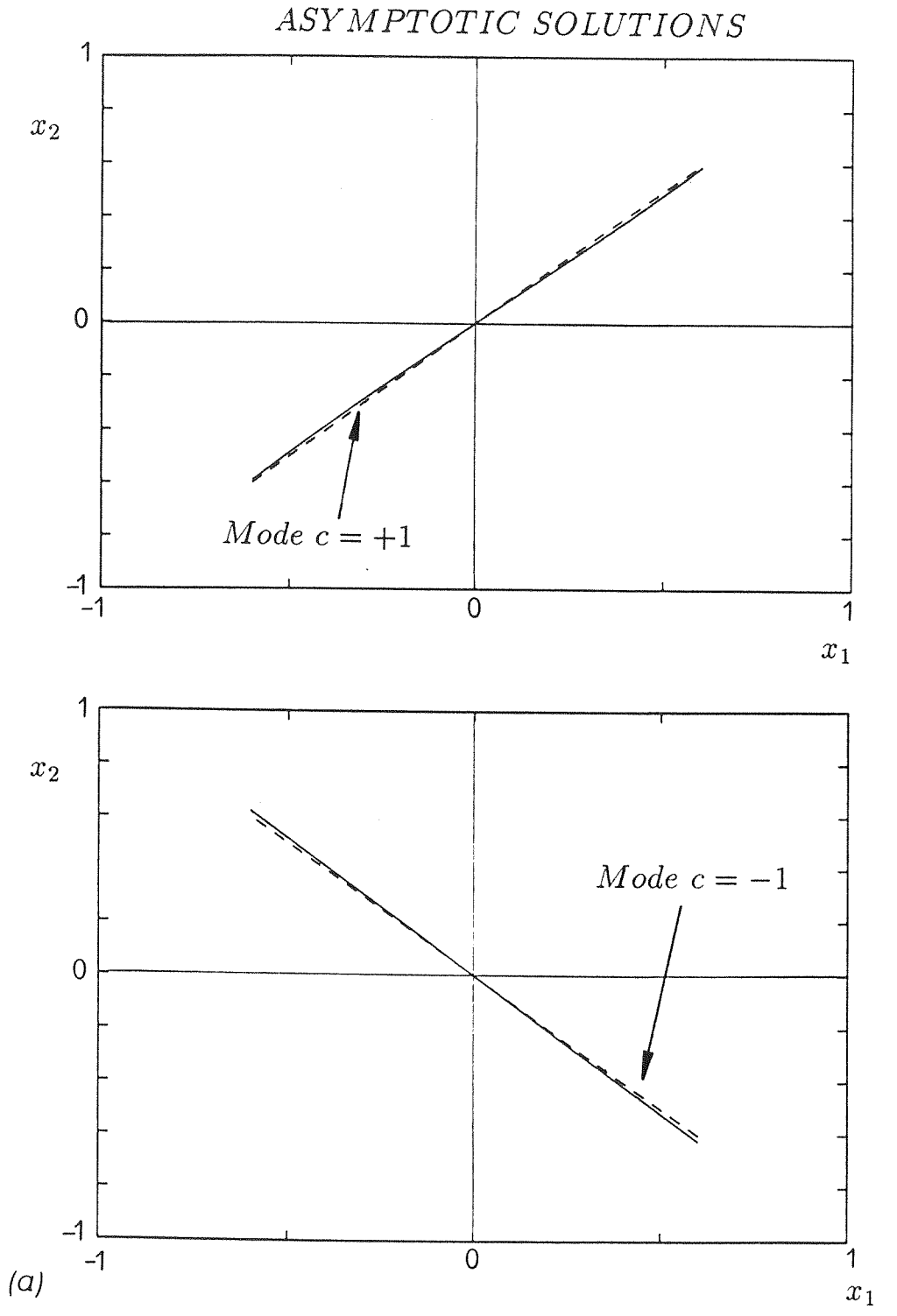

Figure 2.12. Modal curves of the two nonsimilar normal modes. (a) Asymptotic approximations.(b) Numerical (exact) solutions.

NUMERICAL SOLUTIONS

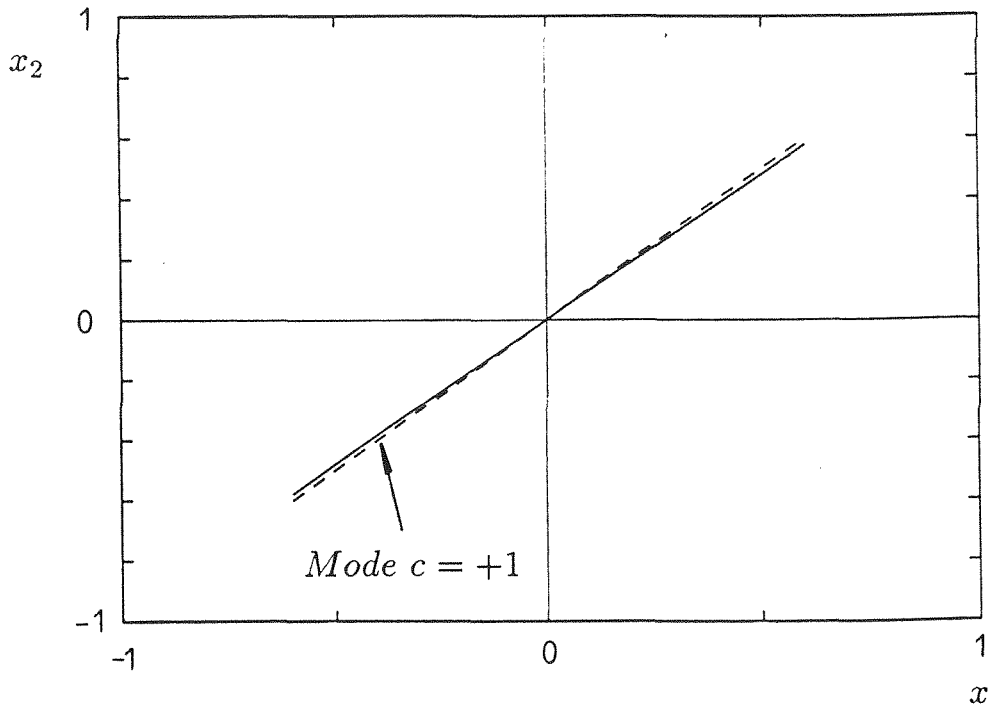

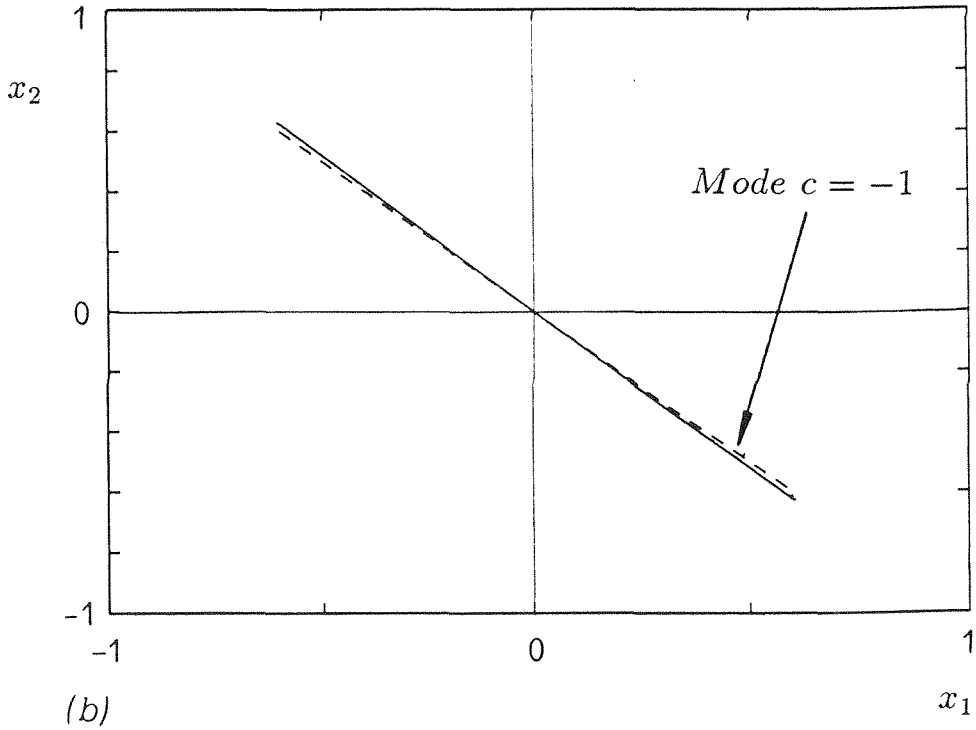

(b)

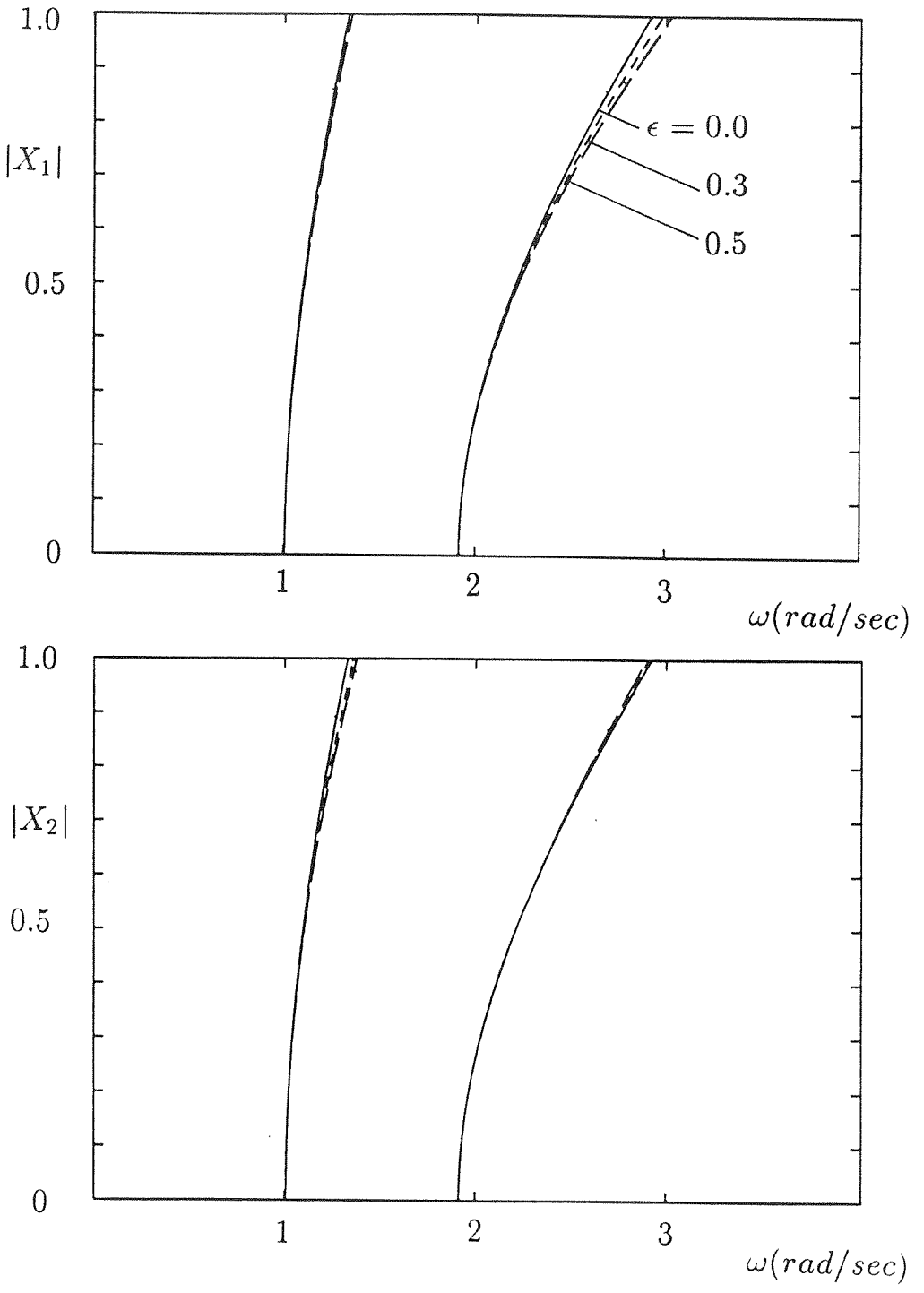

Figure 2.13. Backbone curves corresponding to nonsimilar normal modes.

To test the accuracy of the asymptotic solution, a numerical integration of the equations of motion was carried out, using a 4-th order Runge-Kutta algorithm. For $X_1 = 0.6$, the values of X_2 corresponding to the two nonsimilar modes were numerically detected. This was achieved by observing the simulated oscillation in the configuration plane of the system for different choices of X_2: for a nonsimilar mode, the oscillation was represented by a curve. For the nonsimilar mode close to the symmetric, similar one, the numerical (exact) value for X_2 was found to be 0.579, compared to the approximate asymptotic estimate of $X_2 = 0.5905$. For the nonsimilar mode close to the antisymmetric, similar one, the corresponding estimates are -0.6253 and -0.62263 respectively. The associated modal curves are shown at figures 2.12. From these plots, a good agreement between the asymptotic and the numerical results is observed, particularly when the amplitude of oscillation is small. The asymptotic approximations can be improved if more terms are added to the solutions (2.71).

As far as stability is concerned, the computed nonsimilar modes are orbitally stable since they result as perturbations of orbitally stable similar modes (the fact that the "unperturbed" system has stable similar modes can be easily verified by implementing the linearized stability analysis of section 2.2).

In figure 2.13, the "backbone" curves of the nonsimilar modes are presented for various values of the parameter ϵ. Note that the nonsimilar mode backbone curves are very close to the ones corresponding to the similar modes $c = \pm 1$, even for relatively large values of the perturbation ϵ.

2.4. STUDY OF THE GLOBAL DYNAMICS

2.4.1. *POINCARE'* MAPS

In previous sections, analytic methods for detecting nonlinear normal modes were presented. As pointed out, for nonlinear systems the analytically detected periodic motions are not always physically realizable, since they must also be stable in a certain sense (orbitally or Liapounov).

Until now the linearized stability of the normal modes was considered. Although this approximate analysis leads to important conclusions about the bifurcations of normal modes, it cannot predict the stability of the symmetric mode in the "1-1 resonant" system. The reason for this limitation is examined in (Hyams, 1984), where it is shown that, for low energies, this stability indeterminacy is caused by a bifurcation of periodic motions (which are not nonlinear normal modes) from the symmetric mode.

In this section, a more complete stability analysis will be presented. This is based on *Poincare'* maps, and enables the study of the global dynamics of the flow of the dynamical system. Certain deficiencies of the approximate, linearized stability analysis are resolved with this refined methodology, such as the determination of the mode stability for large amplitudes and the stability indeterminacy of the symmetric mode of the "1-1 resonant" oscillator. Application of *Poincare'* maps to the study of the dynamics of undamped, discrete oscillators can be found in (Month, 1979,1980). In these references, analytic techniques for approximating the *Poincare'* maps in

low energies (such as Birkhoff-Gustavson canonical transformations, Whittaker's adelphic integrals and Lie transforms), are given. By applying these techniques, one can determine analytically the global flow of the dynamical system sufficiently close to a normal mode, and thus obtain a more complete description of the mode stability. This section starts by a brief description of the construction of the *Poincare'* map.

The free oscillations of a two DOF oscillator are examined. The equations of motion for this system are given by:

$$\begin{aligned} \ddot{x}_1 + \sum_{s=1,3,\ldots}^{S} f_{1s} x_1^s + \sum_{s=1,3,\ldots}^{S} f_{2s}(x_1 - x_2)^s = 0 \\ \ddot{x}_2 - \sum_{s=1,3,\ldots}^{S} f_{2s}(x_1 - x_2)^s + \sum_{s=1,3,\ldots}^{S} f_{3s} x_2^s = 0. \end{aligned} \tag{2.72}$$

This is a hamiltonian system with a 4-dimensional phase space (x_1, $\dot{x}_1$, x_2, $\dot{x}_2$). By fixing the total energy of the system to a constant level, one restricts the flow of this dynamical system to an isoenergetic 3-dimensional manifold. This is achieved by setting:

$$H(x_1, \dot{x}_1, x_2, \dot{x}_2) = h \tag{2.73}$$

where $H(\bullet)$ is the expression of the hamiltonian of the system (to be given later), and h is the constant energy level. The hamiltonian H is a first integral of motion for the system, and for autonomous oscillators it represents conservation of energy during free oscillations. If an additional independent first integral of motion exists, the two DOF system is said to be "integrable" and the isoenergetic manifold $H = h$ is fibered by invariant 2-dimensional tori (Guckenheimer, 1984). This "integrability" property is not generic in hamiltonian systems and in general, one does not expect

the existence of a second integral of motion (in fact, the "integrable" cases are of measure zero in the "space" of this class of nonlinear systems). It must be noted, however, that for low energies even nonintegrable oscillators appear to have an "approximate" second integral of motion. This is because for low amplitudes their isoenergetic manifolds appear to be fibered by approximate invariant tori which, as the energy increases, "break" giving rise to random-like chaotic motions (Lichtenberg, 1983).

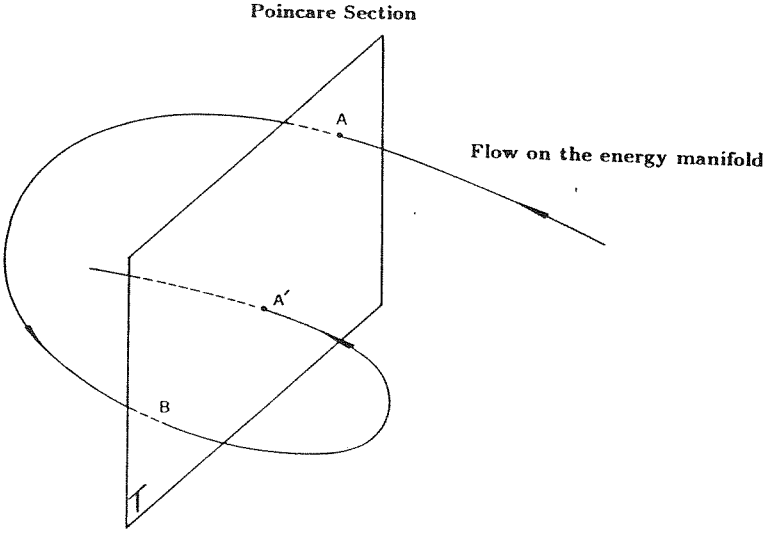

Figure 2.14. Construction of the *Poincare'* map.

Now suppose that one intersects the 3-dimensional isoenergetic manifold defined by (2.73), by a 2-dimensional cut-plane. If the intersection of the two manifolds is transverse (Guckenheimer, 1986), the resulting cross-section Σ is 2-dimensional, and the flow of the dynamical system intersecting the cut-plane defines a "*Poincare'* map." A schematic representation of a *Poincare'* map is shown at figure 2.14, where the

cut plane is chosen as:

$$T : \{x_1 = 0\} \tag{2.74}$$

and the *Poincare'* section Σ is defined by:

$$\Sigma = \{x_1 = 0,\ \dot{x}_1 > 0\} \cap \{H = h\} \tag{2.75}$$

Note that an additional restriction on the sign of the velocities of the intersecting points was posed. This is because one requires the *Poincare'* map to be orientation preserving (Guckenheimer, 1984),(Wiggins, 1989) (in figure 2.14 this is done by recording only points A and A', but not point B which corresponds to a negative velocity at the point of intersection). Also note that transverse intersections of the flow with the cut-plane will only occur if the following condition is satisfied:

$$(\dot{x}_1, \ddot{x}_1, \dot{x}_2, \ddot{x}_2) \bullet (1, 0, 0, 0) \neq 0 \Rightarrow \dot{x}_1 \neq 0 \ \ (\textit{Transversality Condition}\ ) \tag{2.76}$$

A free oscillation of the system corresponding to a normal mode is a periodic motion and therefore pierces the cut-section only once. As a result, the *Poincare'* section, Σ, of a normal mode is a single point and the mode stability can be determined by examining the *Poincare'* sections of "near-by" trajectories (corresponding to initial conditions that are very close to those of the normal mode). If the point corresponding to the normal mode appears as a center, then orbital stability can be concluded. In that case, the modes appear to be surrounded by closed curves that result as intersections of invariant tori with the cut-section. On the contrary, if the mode appears as a saddle point, then orbital instability is inferred.

Before proceeding with numerical results, a note of caution is appropriate. The outlined stability methodology is only valid for small values of energies h. This is because, in general, the two DOF nonlinear oscillator will not possess a second independent integral of motion and hence it will not be integrable. For such nonintegrable two DOF systems, KAM (Kolmogorov - Arnold - Moser) theory predicts that "rational" tori break, resulting in layers of ergodic motion, filling the phase space between sufficiently "irrational" preserved tori (Lichtenberg, 1983). As the energy increases, one typically expects all the tori to break, resulting in the filling of the whole phase space of the system with ergodic motion. This topic will be further investigated in subsequent sections.

At this point, a specific oscillator will be examined. Assuming cubic nonlinearity and "1-1 resonance," the equations of motion are as follows:

$$\begin{aligned} \ddot{x}_1 + x_1 + x_1^3 + K_3(x_1 - x_2)^3 &= 0 \\ \ddot{x}_2 - K_3(x_1 - x_2)^3 + x_2 + x_2^3 &= 0 \end{aligned} \tag{2.77}$$

Note that the oscillator is strongly nonlinear and that K_3 characterizes the modulus of the coupling stiffness. The hamiltonian of this system is given by:

$$H(x_1, \dot{x}_1, x_2, \dot{x}_2) = \frac{1}{2}(x_1^2 + x_2^2) + \frac{1}{4}(x_1^4 + x_2^4 + K_3(x_1 - x_2)^4) + \frac{1}{2}(\dot{x}_1^2 + \dot{x}_2^2) \tag{2.78}$$

where $\dot{x}_1$ and $\dot{x}_2$ are equal in this case to the generalized momenta of the oscillator. Restricting the flow to the isoenergetic manifold $H = h$, the *Poincare'* map is computed by requiring that $x_1 = 0$. This results in the following expression for $\dot{x}_1$:

$$\dot{x}_1 = \pm[2h - \frac{1}{2}(1 + K_3)x_2^4 - x_2^2 - \dot{x}_2^2]^{1/2} \tag{2.79}$$

By construction the *Poincare'* map will contain intersections $(x_2, \dot{x}_2)$ corresponding to $x_1 = 0$ and $\dot{x}_1 > 0$. These points will fill the interior of a region with boundary

$$2h = \frac{1}{2}(1 + K_3)x_2^4 + x_2^2 + \dot{x}_2^2 \tag{2.80}$$

corresponding to $\dot{x}_1 = 0$. The plan is to integrate numerically the differential equations of motion of the system and to sample the values of $(x_2, \dot{x}_2)$ corresponding to $x_1 = 0, \dot{x}_1 > 0$. The *Poincare'* maps of the free oscillation of the system will be constructed and the global picture of the dynamics of the oscillator will be obtained.

2.4.2. DYNAMICS FOR LOW ENERGIES

2.4.2.1. NUMERICAL SIMULATIONS

The oscillator described by the equations of motion (2.77) was examined in previous sections and it was found that a bifurcation of similar normal modes exists. Considering the balancing diagram of cubic terms of figure 2.15, note that depending on the value of K_3, two or four similar normal modes can be realized. Recall that although the linearized stability analysis indicates that a pitchfork bifurcation occurs, it cannot predict the stability of the in-phase (symmetric) mode that corresponds to $c = +1$.

The *Poincare'* maps of free oscillation of the system are shown at figure 2.16. The total energy of the system, h, was fixed to a small value $h = 0.5$, and two values of the parameter K_3 were considered: one above and one below the bifurcation value of $K_3 = 1/4$. The following remarks can be made as far as these plots are concerned.

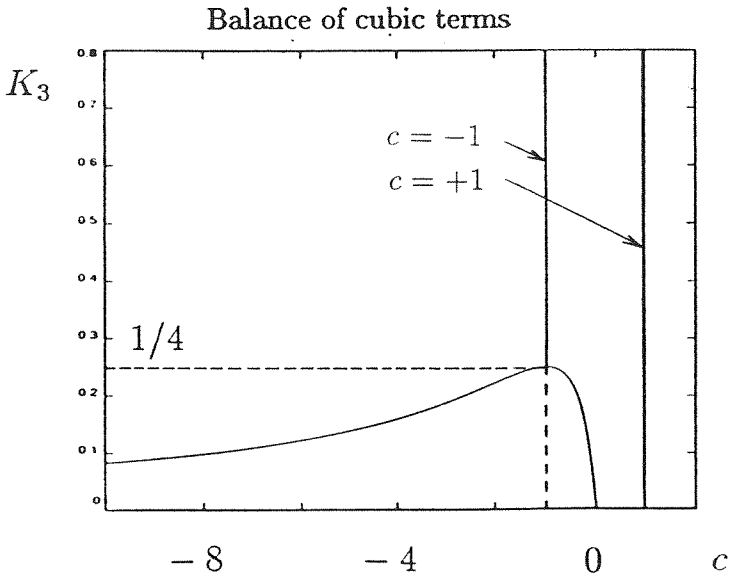

Figure 2.15. Balancing diagram of cubic terms.

Stable mode ———— Unstable mode – – – – – –

- The symmetric normal mode (the upper fixed point in both maps) is orbitally stable. This is concluded from the fact that it appears as a center in the plots, surrounded by closed curves which are intersections of invariant tori with the *Poincare'* section. Thus, the problem of the stability of the symmetric mode which could not be resolved by the linearized stability analysis, is answered by using these maps.

- A qualitative change of the global flow of the system occurs as the parameter K_3 is decreased below the value $K_3 = 1/4$. For $K_3 > 1/4$ the antisymmetric mode (the lower fixed point in the Poincare plot) is orbitally stable. For $K_3 < 1/4$ the mode becomes orbitally unstable (since it appears as a saddle point in the plots), whereas the bifurcating modes are orbitally stable. Note the closed "loop" starting and ending at the unstable mode (in fact, there are two such "loops," but

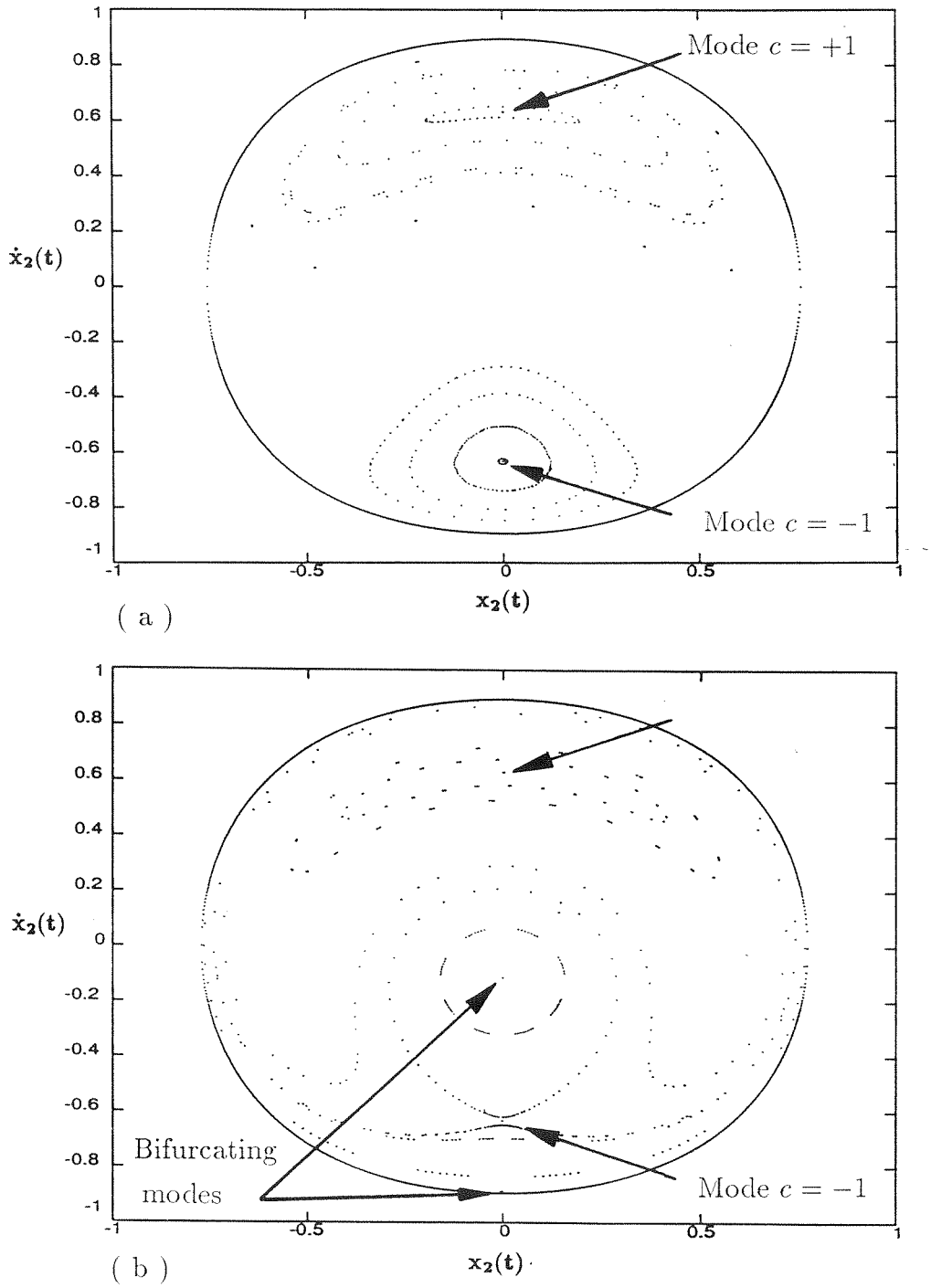

Figure 2.16. Poincare Maps of the system for a low level of energy ($h = 0.5$).

(a) $K_3 = 0.4 > 1/4$ (b) $K_3 = 0.1 < 1/4$.

the second is difficult to observe since it is very close to the boundary curve of the plot). This path is a "homoclinic orbit" and is formed by trajectories that approach the saddle point after infinite positive and negative times (points on the homoclinic orbit have the same past and future). The homoclinic orbit is formed when the stable and unstable invariant manifolds of the unstable point, coalesce (Guckenheimer, 1984),(Wiggins, 1989), and it represents the boundary between trajectories that enclose only one of the bifurcating centers and those that enclose both. The homoclinic orbits are recognized as a mechanism for generation of chaos in hamiltonian systems, and it will be shown in latter sections that for this oscillator, the observed homoclinic trajectories give rise to large-scale chaotic motions.

- As a last remark, note that the observed *Poincare'* plots correspond to a low value of the energy h. In fact, these results can be deceiving, since they may lead to the impression that the dynamics of the oscillator are "smooth" and totally predictable. In fact, since the oscillator under investigation is *not integrable*, certain invariant tori of the flow "break" according to the KAM theorem, giving rise to random-like chaotic motions. These complicated trajectories occur in "stochastic layers" which have a very small measure for low energies and thus are not easily observable in numerical simulations. In addition, transverse homoclinic intersections between the stable and unstable manifolds occur in the smooth-looking homoclinic trajectories that lead to large-scale chaotic motions. So, the dynamics of free oscillations of the system are more complicated than what they appear in the low-energy *Poincare'* plots. This will become evident in subsequent sections, where the energy of the

oscillation will be increased.

In what follows, a two-timing perturbation analysis will be used to study the dynamics of the system for low energies, and to compute analytically the various trajectories of free oscillation that are observed in the numerical simulations.

2.4.2.2. PERTURBATION ANALYSIS: AVERAGING

In this section an approximate perturbation analysis will be performed for the two-DOF nonlinear oscillator. In order for the perturbation expansions to be justified, it is assumed that the nonlinear system "neighbors" a linear one so that the nonlinear solution is regarded as a perturbation of a linear one. This is the case of an oscillator with cubic, "weak" nonlinearities (of perturbation order), and equations of motion of the form:

$$\begin{aligned} \ddot{x}_1 + x_1 + \epsilon x_1^3 + \epsilon K_3 (x_1 - x_2)^3 = 0 \\ \ddot{x}_2 - \epsilon K_3 (x_1 - x_2)^3 + \epsilon x_2^3 + x_2 = 0 \end{aligned} \tag{2.81}$$

where $|\epsilon| \ll 1$, is a small parameter. At this point, the additional parameter μ is introduced, defined by the relation,

$$K_3 = \frac{1}{4} - \mu \tag{2.82}$$

Note that μ is a measure of the distance of the value of K_3 from the bifurcation value of $1/4$ (μ is assumed to be a nonnegative quantity). At $\mu = 0$ the pitchfork bifurcation occurs, whereas for positive values of μ, two bifurcating normal modes exist.

The two-timing perturbation method will be implemented (for more information about this method see (Nayfeh, 1979)). The following set of dependent coordinates

are introduced

$$u = (x_1 + x_2)/2 \quad , \quad v = (x_1 - x_2)/2 \tag{2.83a}$$

and "slow" and "fast" time variables are defined:

$$\eta = \epsilon t \quad , \quad \xi = t \tag{2.83b}$$

Then, expressing the time derivatives of u and v by the chain-rule, one obtains:

$$u_t = u_\xi + \epsilon u_\eta + \mathcal{O}(\epsilon^2) \qquad u_{tt} = u_{\xi\xi} + 2\epsilon u_{\xi\eta} + \mathcal{O}(\epsilon^2) \tag{2.84}$$

Writing the equations of motion (2.81) in terms of the new variables u and v and using expressions (2.84), the following approximate transformed equations of motion result (correct to $\mathcal{O}(\epsilon^2)$):

$$\begin{aligned} u_{\xi\xi} + 2\epsilon u_{\xi\eta} &= -3\epsilon u v^2 - \epsilon u^3 - u + \mathcal{O}(\epsilon^2) \\ v_{\xi\xi} + 2\epsilon v_{\xi\eta} &= 8\epsilon\mu v^3 - 3\epsilon v^3 - 3\epsilon u^2 v - v + \mathcal{O}(\epsilon^2) \end{aligned} \tag{2.85}$$

In these equations the "shortened" notation for the derivatives was used, for example, $(\bullet)_{\xi\eta} \equiv \frac{\partial^2(\bullet)}{\partial\xi\partial\eta}$. Note that all variables other than ϵ are assumed to be of $\mathcal{O}(1)$.

The solutions of equations (2.85) are expressed in the series form:

$$\begin{aligned} u(\xi,\eta) &= \sum_{n=0}^{\infty} \epsilon^n u_n(\xi,\eta) \\ v(\xi,\eta) &= \sum_{n=0}^{\infty} \epsilon^n v_n(\xi,\eta) \end{aligned} \tag{2.86}$$

where u_n, v_n are the $n-th$ order approximations to the solution. These are computed by substituting the series expressions for u and v into equations (2.85), and matching coefficients of respective powers of ϵ.

$\mathcal{O}(\epsilon^0)$ terms

The zero-th order approximate solutions are given by the following set of differential equations:

$$u_{0\xi\xi} + u_0 = 0$$
$$v_{0\xi\xi} + v_0 = 0 \tag{2.87}$$

The general solutions of these equations are of the form:

$$u_0(\xi,\eta) = A(\eta)cos\xi + B(\eta)sin\xi$$
$$v_0(\xi,\eta) = C(\eta)cos\xi + D(\eta)sin\xi \tag{2.88}$$

where the (unknown) quantities A, B, C and D are computed by eliminating the "secular" terms of the equations of the next approximation (Nayfeh, 1979).

$\mathcal{O}(\epsilon^1)$ terms

The equations of the first approximation are obtained by matching terms of order ϵ:

$$u_{1\xi\xi} + u_1 = -2u_{0\xi\eta} - 3u_0v_0^2 - u_0^3$$
$$v_{1\xi\xi} + v_1 = -2v_{0\xi\eta} + 8\mu v_0^3 - 3v_0^3 - 3u_0^2v_0 \tag{2.89}$$

Substituting the expressions for u_0 and v_0 into the left-hand sides of equations (2.89) and setting to zero the coefficients of $cos\xi$ and $sin\xi$ (since they represent resonant excitations for the system (2.89) leading to unbounded solutions), one obtains four differential equations for the unknown quantities A, B, C and D. This operation was performed with the symbolic manipulation software package "MACSYMA" and the expressions are too lengthy to be reported here. However, the results can be significantly simplified if one uses a new set of polar coordinates, $R_1(\eta), R_2(\eta)$, and

$\phi(\eta)$, defined by:

$$A = R_1 cos\theta_1 \qquad B = R_1 sin\theta_1$$

$$C = R_2 cos\theta_2 \qquad D = R_2 sin\theta_2 \tag{2.90}$$

$$\phi = \theta_2 - \theta_1$$

In terms of these new variables, the equations that result from the elimination of the secular terms of equations (2.85), are as follows:

$$\begin{aligned} \frac{dR_1}{d\eta} &= \frac{3}{8} R_1 R_2^2 sin2\phi \\ \frac{dR_2}{d\eta} &= -\frac{3}{8} R_1^2 R_2 sin2\phi \\ \frac{d\phi}{d\eta} &= -\frac{3}{8}(R_1^2 + R_2^2) + 3\mu R_2^2 + \frac{3}{8}(R_2^2 - R_1^2)cos2\phi \end{aligned} \tag{2.91}$$

where the variable ϕ is modulo π. Combining the first two equations of the above set, one obtains:

$$\frac{dR_1}{dR_2} = -\frac{R_2}{R_1} \Rightarrow R_1^2 + R_2^2 = \rho^2 \tag{2.92}$$

where ρ is a constant scalar quantity. Note that the quantity $(R_1^2 + R_2^2)$ is related to the total energy of the motion; thus, expression (2.92) indicates that the total energy of the system is conserved during free oscillation (as expected). Note, however, that this form of the conservation law holds only for this level of approximation, since all terms of order ϵ^2 or higher are neglected.

Equations (2.91) represent a dynamical system with a 3-dimensional phase space. However, since the energy is fixed during free oscillation, the motion of the dynamical system is confined to a 2-dimensional isoenergetic manifold, represented by the cylindrical surface of figure 2.17. In that figure, a schematic description of the flow of the dynamical system is given. It has been assumed that $\mu > 0$, so

that the pitchfork bifurcation of modes has already occurred. The variable ϕ is confined in the range $[0, \pi)$, and the plot is symmetric with respect to the plane $\phi = \pi/2$. Points that are symmetric with respect to that plane must be identified since they represent the same motion of the dynamical system (this is due to the applied mathematical transformations).

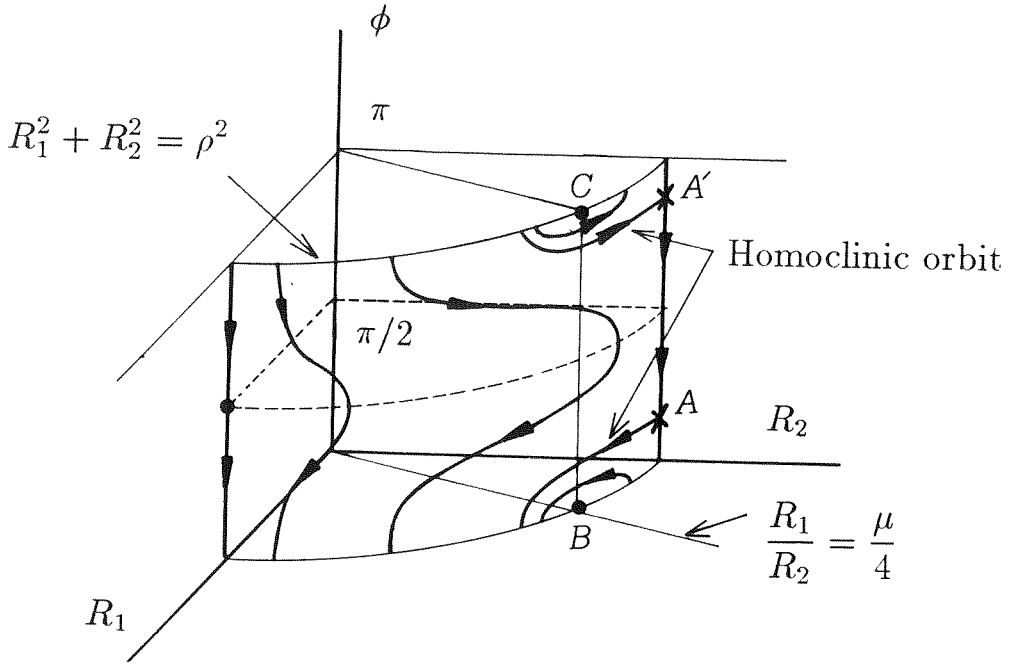

Figure 2.17. Schematic representation of the flow on the isoenergetic manifold for positive values of μ.

For example, points A and A' represent the same (unstable) antisymmetric mode; as a result the homoclinic orbit appears as an open loop in this plot (compare with the *Poincare'* maps of figure 2.16). Similarly, the two additional bifurcating modes are represented by the fixed points B and C, and are centers, indicating orbital stability.

The motion on the isoenergetic manifold can be better described if one introduces

a second polar transformation according to the formulas:

$$R_1 = \rho\, cos\psi$$
$$R_2 = \rho\, sin\psi \tag{2.93}$$

where ρ is the scalar constant of equation (2.92), and ψ is a new polar variable. Substituting expressions (2.93) into equations (2.91) and eliminating the constant ρ, one obtains the following set of differential equations that describe the free oscillation of the system on the isoenergetic manifold:

$$\begin{aligned} \frac{d\phi}{d\eta} &= -\frac{3\rho^2}{16}[8\mu(cos2\psi - 1) + 2 + 2cos2\psi cos2\phi] \\ \frac{d\psi}{d\eta} &= -\frac{3\rho^2}{16} sin2\phi sin2\psi \\ \rho &= constant \end{aligned} \tag{2.94}$$

Note that the above equations represent a dynamical system on a two-Torus, since the variables ϕ and ψ are modulo π. Thus, by applying subsequent transformations, one finally relates the free oscillation of the two-DOF system with a flow of a vector field on a two-Torus.

An interesting feature of equations (2.94) is that they can be integrated exactly. Indeed, the integrating factor for this system of ordinary differential equations is (Rand, 1990):

$$F(\phi, \psi) = sin2\psi \tag{2.95}$$

and the first integral of motion is computed as:

$$K(\phi, \psi) = -\frac{1}{2} sin^2 2\psi cos2\phi + cos2\psi \tag{2.96}$$

The level curves of the integral (2.96) are plotted in figure 2.18 for $\mu = 0.05$. Each curve corresponds to a different value for the integral K, but all are on the same

"energy level" ρ. Observe that the flow is symmetric with respect to the lines $\phi = \pi/2$ and $\psi = \pi/2$. The symmetric mode corresponds to $(\phi,\ \psi) = (\pi/2,\ 0)$ and appears to be surrounded by closed curves. This is an analytic proof of the orbital stability of the symmetric mode (recall that a numerical proof was obtained with *Poincare'* maps, where it was found that the symmetric mode was surrounded by closed curves that result as intersections of invariant tori with the cut plane). The two bifurcating modes are orbitally stable (since they appear as centers) and correspond to the fixed points $(\phi,\ \psi) = (0,\ \frac{1}{2}cos^{-1}(\frac{4\mu-1}{4\mu+1}))$ and $(\pi,\ \frac{1}{2}cos^{-1}(\frac{4\mu-1}{4\mu+1}))$ respectively. Finally, the unstable antisymmetric normal mode is represented by the fixed points $(\phi,\ \psi) = (\frac{1}{2}cos^{-1}(1-8\mu),\ \frac{\pi}{2})$ and $(\pi\ -\ \frac{1}{2}cos^{-1}(1-8\mu),\ \frac{\pi}{2})$. Note that the homoclinic orbit Γ appears as an open curve; this paradox is due to the applied polar transformations, and it is resolved if one identifies points that are symmetric with respect to the line $\phi = \pi/2$. Note that in section 2.1 similar normal modes were investigated and it was found that for the "1-1 resonant" system, the two bifurcating modes actually represent the same free oscillation. Exactly the same conclusion can be made from the phase plane of figure 2.18, if one identifies points symmetric with respect to line $\phi = \pi/2$: the two bifurcating modes are actually the same motion and in addition, the homoclinic orbit originates from and ends at the unstable mode.

In figure 2.19, the phase plane of the oscillator for different values of μ is shown (only values of ϕ and ψ between 0 and $\pi/2$ are presented). Observe that at $\mu = 0$ only the symmetric and antisymmetric modes exist. As μ is increased from zero,

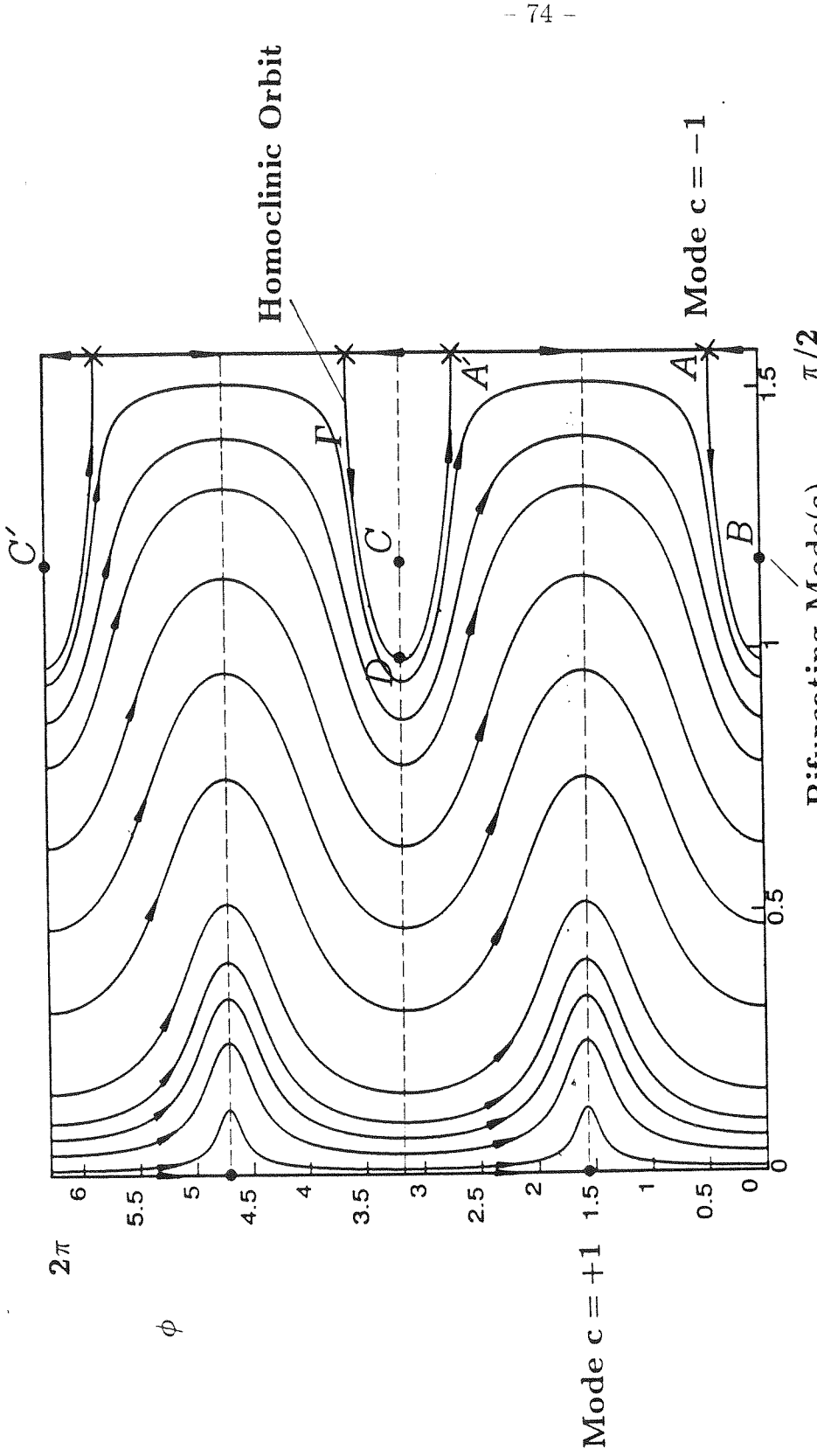

Figure 2.18. Flow of the vector field on the two-Torus, for $\mu = 0.05$.

the homoclinic orbit increases in length. At the limit $\mu = 1/4$, the coupling stiffness of the oscillator vanishes and the two-DOF system degenerates into two single DOF disjoint oscillators. Note that as $\mu \rightarrow 1/4$, the homoclinic orbit becomes more and more "curved," until it reaches a nonsmooth limit.

By using the analytic expression of the first integral of motion (eq. 2.96), it is possible to find exact expressions for the time responses of the coordinates of the oscillator. In the sequence, the time responses corresponding to a homoclinic motion of the system will be computed. To obtain the value of $K(\phi, \psi)$ for the homoclinic level curve, substitute in (2.96) the values of ϕ and ψ corresponding to the anti-symmetric mode (since the level curve corresponding to the homoclinic orbit passes through that mode):

$$(\ \phi, \ \psi \ ) = (\ \frac{1}{2} cos^{-1}(1 - 8\mu), \ \frac{\pi}{2} \ ) \quad (Antisymmetric \ mode) \tag{2.97}$$

Then the first integral of motion takes the value:

$$K(\phi, \psi) = (1 - 4\mu)(-1) + \mu = 5\mu - 1 \quad (Homoclinic \ orbit) \tag{2.98}$$

Using the computed value of K, find the relation between ϕ and ψ for a motion on the homoclinic orbit (this is achieved by solving for $cos2\phi$ in expression (2.96)):

$$cos2\phi = \frac{2 - 10\mu + 2(1 - 4\mu)cos2\psi + 2\mu cos4\psi}{sin^2 2\psi} \quad (Homoclinic \ Orbit) \tag{2.99}$$

Using expression (2.99), one can eliminate the variable ϕ from the second of equations (2.94), to obtain the following differential equation for ψ:

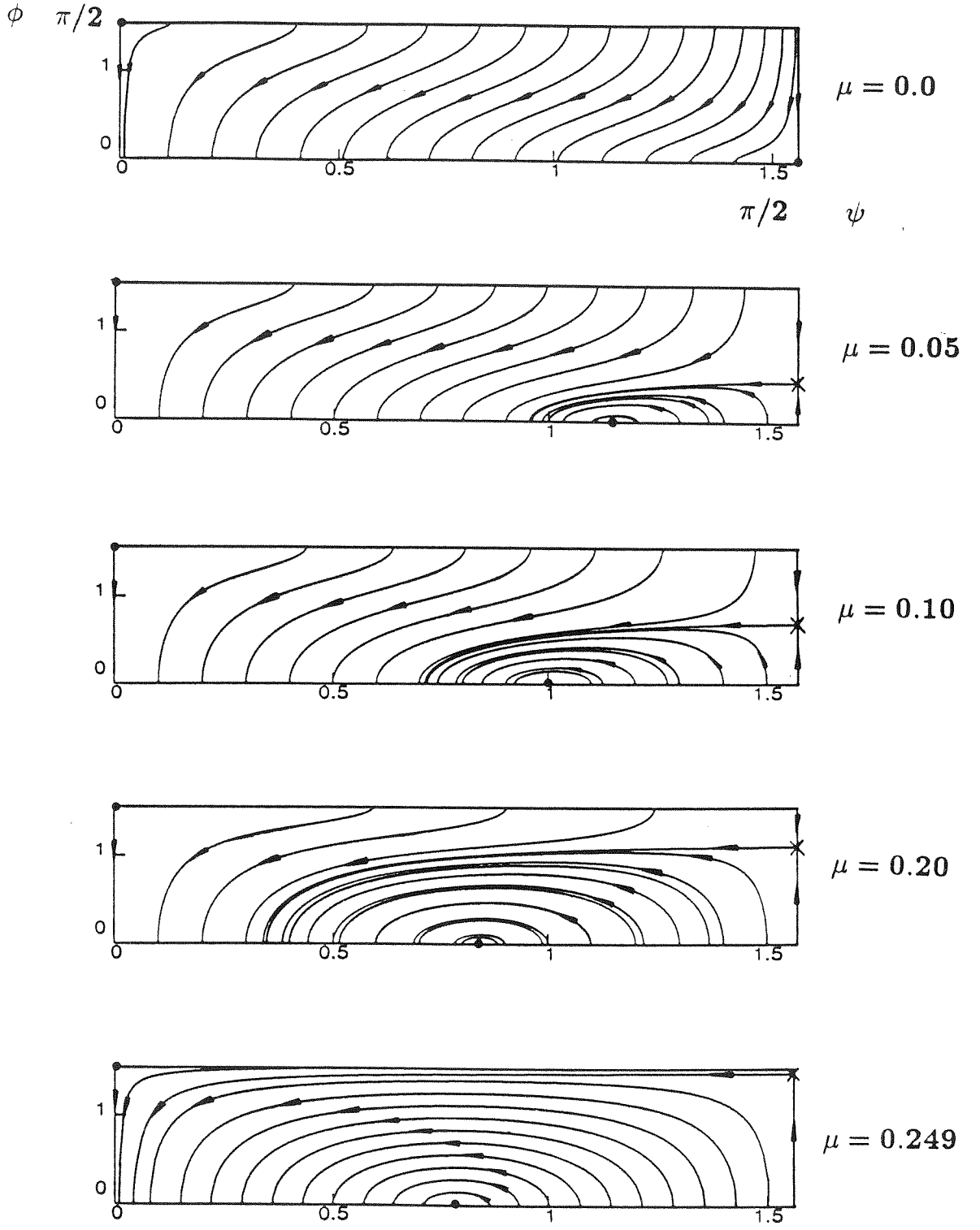

Figure 2.19. Bifurcation to a homoclinic orbit as μ increases.

$$\frac{d\psi}{d\eta} = \mp\frac{3\rho^2}{16}\{\frac{[(12\mu-1)+(8\mu-2)cos2\psi-(4\mu+1)cos^2 2\psi]}{sin^2 2\psi}\bullet$$

$$\bullet[(3-12\mu)+(2-8\mu)cos2\psi+(4\mu-1)cos^2 2\psi]\}^{1/2} \qquad (2.100)$$

where the upper $(-)$ and lower $(+)$ signs are used for $\phi \in [0,\ \pi/2)$ and $[\pi/2,\ \pi)$ respectively. Introducing a new dependent variable, x given by,

$$x = cos2\psi \qquad (2.101)$$

the differential equation (2.100) can be written in the following simplified form :

$$\frac{Q_1 dx}{\{(A_1+B_1x-x^2)(3+2x-x^2)\}^{1/2}} = \pm d\eta \qquad (2.102)$$

where

$$Q_1 = \frac{8}{3\rho^2(1-16\mu^2)^{1/2}}$$

$$A_1 = \frac{12\mu-1}{4\mu+1}$$

$$B_1 = \frac{8\mu-2}{4\mu+1}$$

Equation (2.102) can be integrated formally by quadratures (although the process is tedious!) as follows. Assume that at $\eta = 0$ (or equivalently at time $t = 0$), the system is at position $(\phi, \psi) = (\pi, \frac{1}{2}cos^{-1}(\frac{12\mu-1}{4\mu+1}))$, i.e., at point D of the phase plane of figure 2.18. Then, arbitrary (positive or negative) values of η are obtained by performing an integration of expression (2.102) with the following limits:

$$\int_{\frac{12\mu-1}{4\mu+1}}^{x} \frac{Q_1 d\xi}{\{(A_1+B_1\xi-\xi^2)(3+2\xi-\xi^2)\}^{1/2}} = \pm\int_0^{\eta} d\tau = \pm\eta \qquad (2.103)$$

Fortunately, the associated integrals can be found in standard tables (Byrd, 1954), so that the final result of the above integration can be analytically expressed in

terms of elementary functions as:

$$\frac{16\mu^{1/2}}{(1+4\mu)^{1/2}}\{1-\frac{4(8\mu+1)}{(4\mu+1)(x+1)}+\frac{64\mu}{(4\mu+1)(x+1)^2}\}^{1/2}+\frac{128\mu}{(4\mu+1)(x+1)}=$$

$$=\frac{32\mu+4}{4\mu+1}+\frac{4}{4\mu+1}e^{\mp 3\eta[\mu(1-4\mu)]^{1/2}\rho^2} \qquad (2.104)$$

Equation (2.104) gives the exact relation between the variables η and x (or equivalently t and ψ) for the motion on the homoclinic orbit. Certain remarks can be made as far as the above expression is concerned.

- This algebraically complex expression represents a solution for the homoclinic motion that is correct to $\mathcal{O}(\epsilon^2)$. Moreover, one can easily express the slow-time variable η as a function of x (and thus ψ), by rearranging terms and taking the logarithms of both sides of the equation. Note that η (the time variable) appears as an exponent of an exponential function. This is typical in time responses of homoclinic orbits, since as discussed earlier the homoclinic trajectory reaches the same limit for positive or negative infinite times.

- The upper $(-)$ sign corresponds to $\phi \in [0, \pi/2)$, and gives negative values for η that decrease as x increases. Moreover, as x approaches the limiting value $x = cos2\psi = -1$ (corresponding to the antisymmetric mode), one obtains:

$$lim_{x\to -1}\ \eta = -\infty \quad (\ \phi \in [\ 0,\ \pi/2\ )\ )$$

This result confirms that the motion on the homoclinic orbit originates from the antisymmetric normal mode (since it approaches this state of motion for negative infinite times).

- Similarly, the lower $(+)$ sign is used when $\phi \in [\pi/2, \pi)$, and results in positive values of η. One finds that η increases as x increases, reaching the limit,

$$lim_{x \to -1}\ \eta = +\infty \quad (\ \phi \in [\ \pi/2,\ \pi\ )\ )$$

which implies that the motion reaches the antisymmetric mode for infinite positive times.

- Solution (2.104) is an approximation to the homoclinic motion for low energies of the system. When the level of energy is increased, the stable and unstable invariant manifolds comprising the homoclinic orbit intersect transversally and Smale horseshoes are formed, leading to chaotic motions. Unfortunately, one cannot use the exact solution of this section as a basis for a homoclinic Melnikov analysis (Guckenheimer, 1984), (Wiggins, 1989), since the resulting Melnikov functions become exponentially small as $\epsilon \to 0$. Although one cannot prove analytically the existence of transverse homoclinic intersections, this can be proven numerically, by computing the stable and unstable invariant manifolds of the unstable antisymmetric normal mode.

2.4.3. DYNAMICS FOR HIGH ENERGIES

The results of previous sections corresponded to low levels of energies of oscillation, and it was found (both numerically and analytically) that in such cases, the dynamics could be completely analyzed and predicted. In this section, however, it will be shown that, when the energy of oscillation is increased, complicated, random-like

chaotic motions result that cannot be predicted by any standard method of analysis. In order to study such complicated motions, numerical techniques must be implemented, and in fact, the *Poincare'* map will be the basic tool in the following investigations of the large amplitude motions of the system.

The differential equations of motion (2.77) were numerically integrated with a fourth-order Runge-Kutta algorithm, and the dynamics were sampled with the *Poincare'* section described in section 2.4.1. The coupling stiffness parameter K_3 was assigned the value $K_3 = 0.1 < 1/4$ (corresponding to four normal modes of free oscillation). The *Poincare'* maps corresponding to levels of energy $h = 50, 150$ and 5×10^5 are presented at figure 2.20. In the same figure, the plot of figure 2.16(b) is reproduced for comparison purposes (that plot corresponds to a system with $K_3 = 0.1$ and a lower level of energy $h = 0.1$). Observe the global changes that occur in the *Poincare'* plots as the energy is increased:

- There are certain regions in the maps where the orbits of the oscillator seem to wander erratically. These regions, the so-called "seas of stochasticity" (Lichtenberg, 1983), contain chaotic motions of the hamiltonian system, i.e., motions that have extreme sensitivity on initial conditions. It must be stated that the chaotic regions of the maps of figures 2.20 were generated by a *single initial condition.* In each of the maps, one can detect a large "sea of stochasticity" surrounding the (unstable) antisymmetric and the two (stable) bifurcated normal modes. In that region, large-scale chaotic motions occur.

- A careful examination of the plots indicates that there also exist some "islands

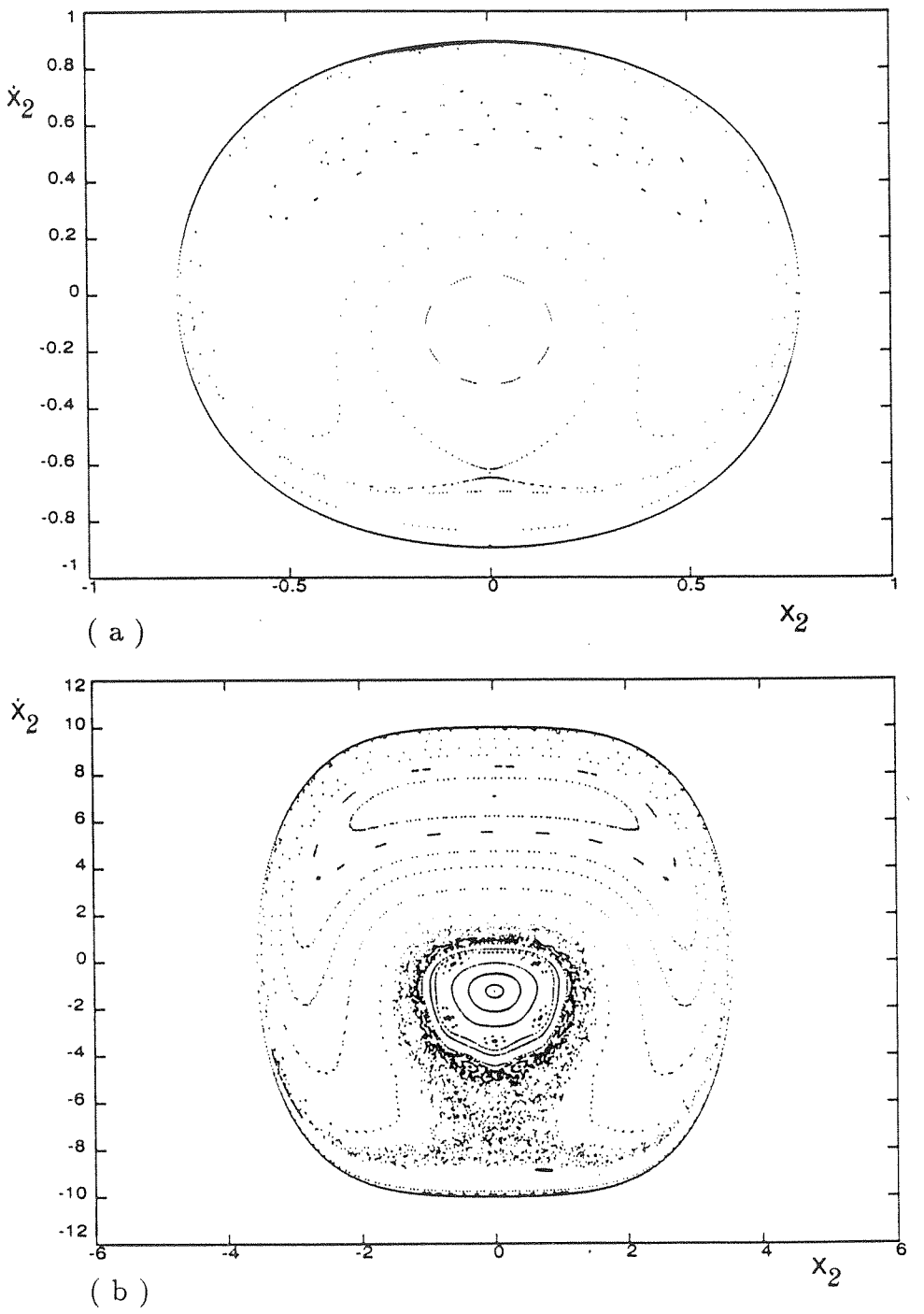

Figure 2.20. Poincare Maps for the oscillator with $K_3 = 0.1 < 1/4$.

(a)$h = 0.1$ (b)$h = 50.0$ (c)$h = 150.0$ (d) $h = 5 \times 10^5$.

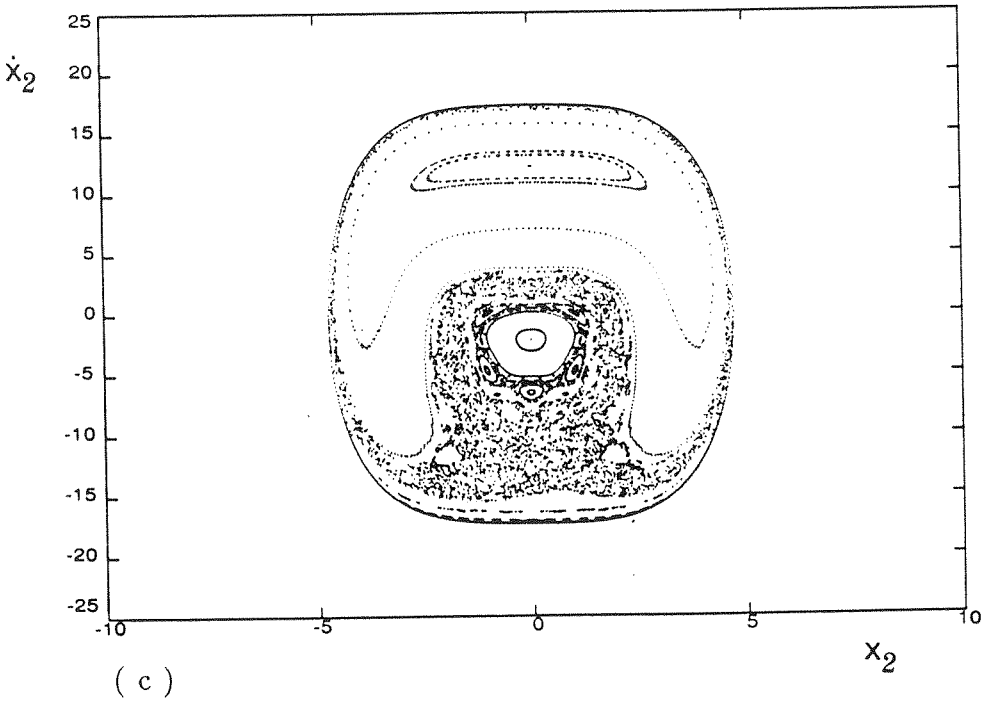
$\dot{x}_2$
25
20
15
10
5
0
-5
-10
-15
-20
-25
-10
-5
0
5
10
x_2

(c)

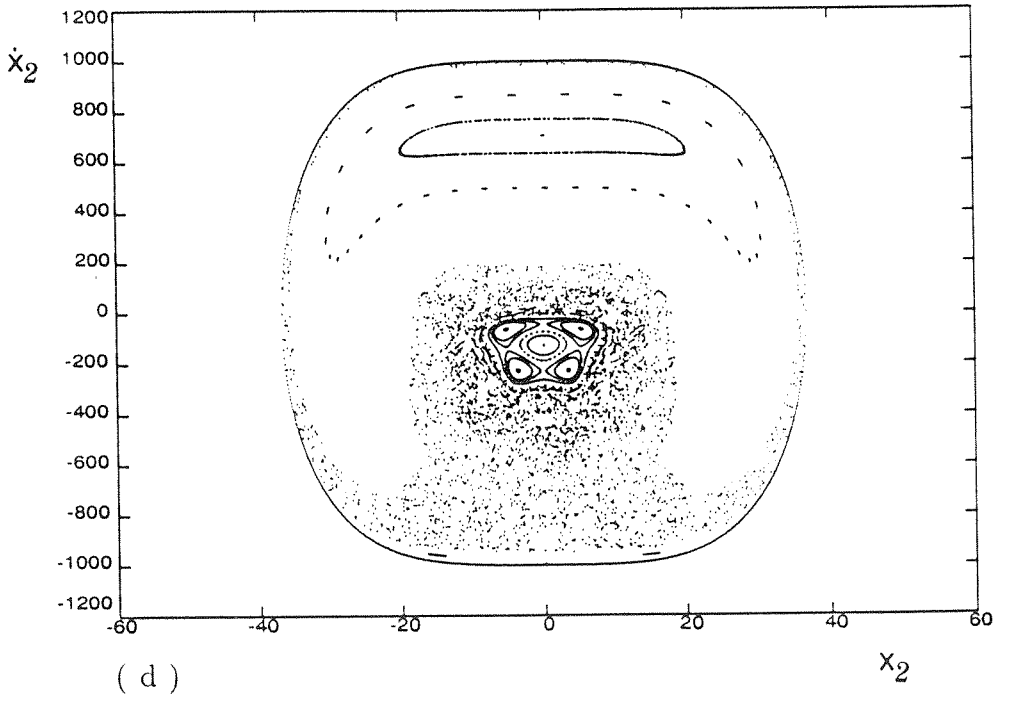
$\dot{x}_2$
1200
1000
800
600
400
200
0
-200
-400
-600
-800
-1000
-1200
-60
-40
-20
0
20
40
60
x_2

(d)

in the stochastic sea"; these consist of stable and unstable subharmonic orbits that are surrounded by small-scale chaotic motions. For example, in the *Poincare'* map of figure 2.20(d) a period-4 stable subharmonic orbit can be clearly seen, lying in the vicinity of one of the bifurcated modes. There exist small-scale chaotic motions in the neighborhood of this subharmonic orbit but these cannot be detected due to the restricted, finite resolution of the plot. In later sections it will be shown that both large and small-scale chaotic motions are generated by the same mechanism (transverse homoclinic intersections of invariant manifolds).

- In figure 2.20(b), two closed curves appear to separate two subharmonic orbits of periods 6 (the outer) and 5 (the inner). Thus, small-scale chaotic motions surrounding the two subharmonics are necessarily disconnected from each other, since they cannot cross the aforementioned closed curves. It will be shown that this confinement of chaotic motions is a unique feature of the 2-DOF hamiltonian oscillator and is not encountered in oscillators with more DOF (in systems with n-DOF, $n \geq 3$, "Arnold diffusion" occurs). The closed curves are the intersections with the cut-plane of "sufficiently irrational" KAM tori, whereas the subharmonic orbits result from the breakdown of the "rational" ones. A definition of these terms and an analytic proof of the existence of subharmonic orbits, are given in the next section.

- Note that the region of the phase space occupied by the "stochastic sea" increases with increasing energy. However, even for large energies there exist regions in the phase plane where the free oscillation of the system is regular. For example, the symmetric mode is orbitally stable even for large energies and is surrounded

by smooth closed curves that are intersections of tori with the cut section. So an interesting observation for the oscillator under investigation is that although the chaotic region expands with increasing energy, it remains confined to a certain region close to the antisymmetric and bifurcating modes, but away from the symmetric one.

In what follows, the large-scale chaotic motions (in the "stochastic sea"), and the small-scale ones (close to the subharmonic orbits), are examined separately.

2.4.3.1. TRANSVERSE HOMOCLINIC INTERSECTIONS OF INVARIANT MANIFOLDS

To study the chaotic motions that surround the antisymmetric and bifurcated modes, it is necessary to compute the stable and unstable invariant manifolds of the unstable mode. A rigorous definition of the notion of "invariant manifold" can be found in (Wiggins, 1989). Basically, the aforementioned manifolds are the extensions for the nonlinear case of the linear eigenspaces that are encountered in linear theory. For 2-dimensional maps (as the *Poincare'* maps under investigation), it can be shown that "unstable hyperbolic fixed points" (such as the unstable antisymmetric mode in this case) have one-dimensional stable and unstable invariant manifolds. Points on the stable (unstable) manifold approach the fixed point under infinite forward (backward) iterations.

For low energies it was found that the two manifolds of the antisymmetric mode approximately coincide to a homoclinic orbit. When the energy is increased, it will

be shown that the stable and unstable manifolds intersect transversely infinitely many times; this is the mechanism that generates the observed large-scale chaos in the system. The manifolds are numerically computed by integrating the equations of motion on the energy manifold, with initial conditions that are sufficiently close to those of the antisymmetric mode. Forward iterations of points close to the unstable mode give the unstable manifold, whereas backward iterations lead to the stable one.

In figure 2.21(a), the unstable manifold of the antisymmetric mode is shown. Note that it consists of discrete points since the dynamical system under investigation is a map (and not a vector field). Observe that, under forward iterations of the map, there are "violent windings" of the manifold as it approaches the unstable mode. It can be proven that there exist an infinite number of these "windings"; as a result the manifold accumulates on itself ("lambda-lemma" (Guckenheimer, 1984)) and approaches the unstable mode after infinite forward iterations. A similar numerical simulation can be carried out for the stable manifold (one considers backward iterations of an initial point close to the unstable mode), and the two manifolds are superimposed on each other at figure 2.21(b). Clearly, transverse intersections of the two manifolds can be detected (the so called "homoclinic tangles"). There is an infinite number of these intersections (Guckenheimer, 1984) and these result in an infinite number of "Smale horseshoes."

The creation of one such "horseshoe" will be discussed by examining an enlarged neighborhood of the unstable mode (figure 2.22). Consider the strip U_0 of the phase

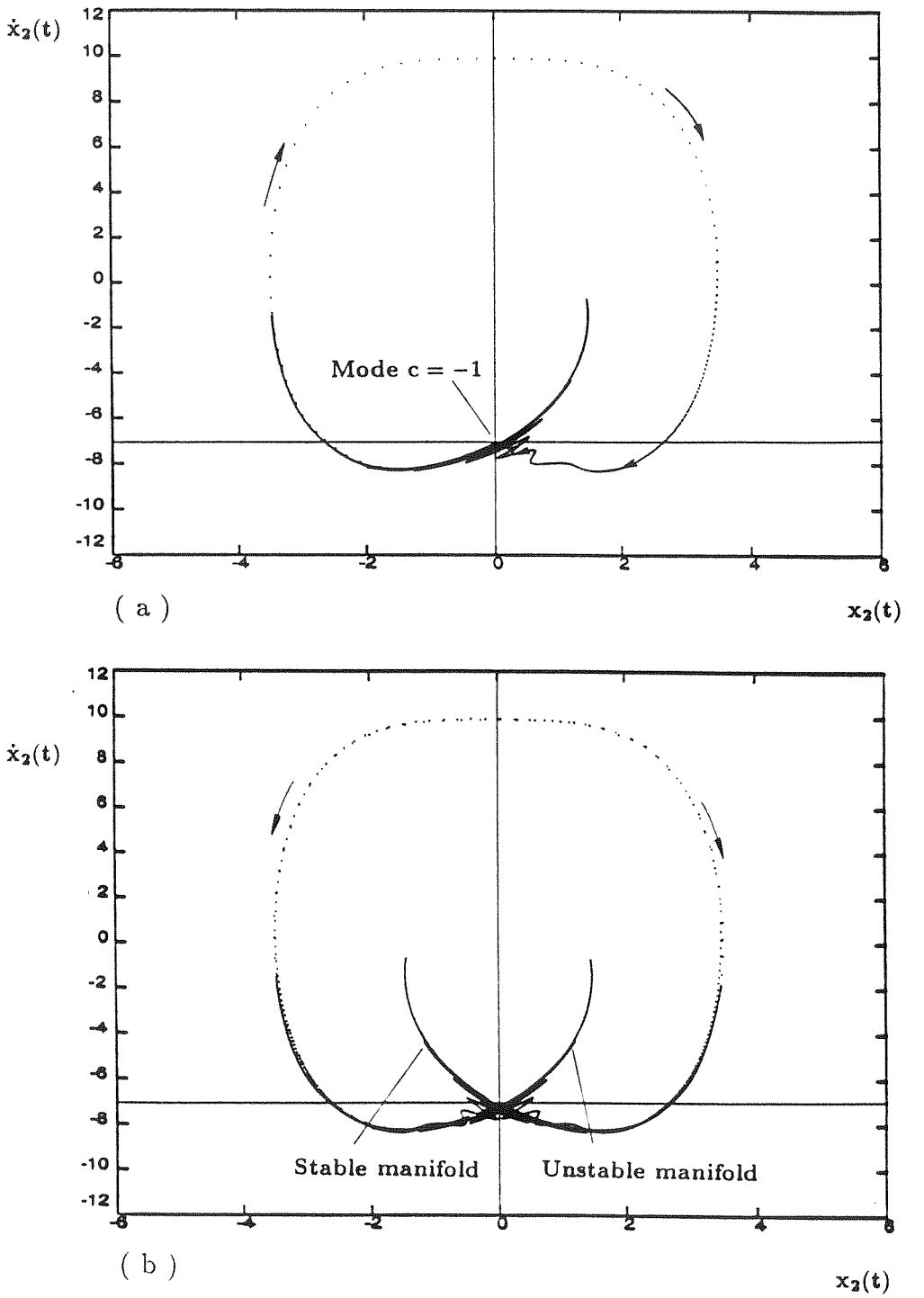

Figure 2.21. (a) Unstable manifold of the unstable mode. (b) Transverse intersections of the stable and unstable manifolds.

plane, with boundaries on the stable and unstable manifolds, and observe how it is mapped under forward iterations of the map. Under a single forward iteration, the strip is mapped to U_1. The second iteration transforms the strip to U_2, etc. The $n-th$ iterate of the strip (for some n), will be in the position U_n, so that the $n-th$ iterate intersects the original strip transversely. This is a "Smale horseshoe" mapping and it has interesting implications in the dynamics of the $Poincare'$ map. In fact, using the Smale-Birkhoff homoclinic theorem (Wiggins, 1989), it can be shown that for some iterate, the Poincare map contains:

- A countable infinity of periodic orbits

- An uncountable infinity of nonperiodic orbits

- A dense orbit

Thus, the dynamics of the map in the vicinity of the unstable mode have sensitive dependence on initial conditions and are virtually unpredictable. Note that this numerical demonstration of the existence of "homoclinic tangles" shows that transient chaos occurs in the map, but it does not imply the existence of a "strange attractor." Such attractors are only realizable in dissipative dynamical systems, and thus cannot be found in the dynamics of this hamiltonian oscillator. No more details will be provided about these chaotic motions at this point, since a complete analysis of "horseshoe"maps can be found elsewhere (Wiggins, 1989).

An interesting observation is that this type of large-scale, global chaos, occurs only if the antisymmetric mode is orbitally unstable, since only then do one-dimensional

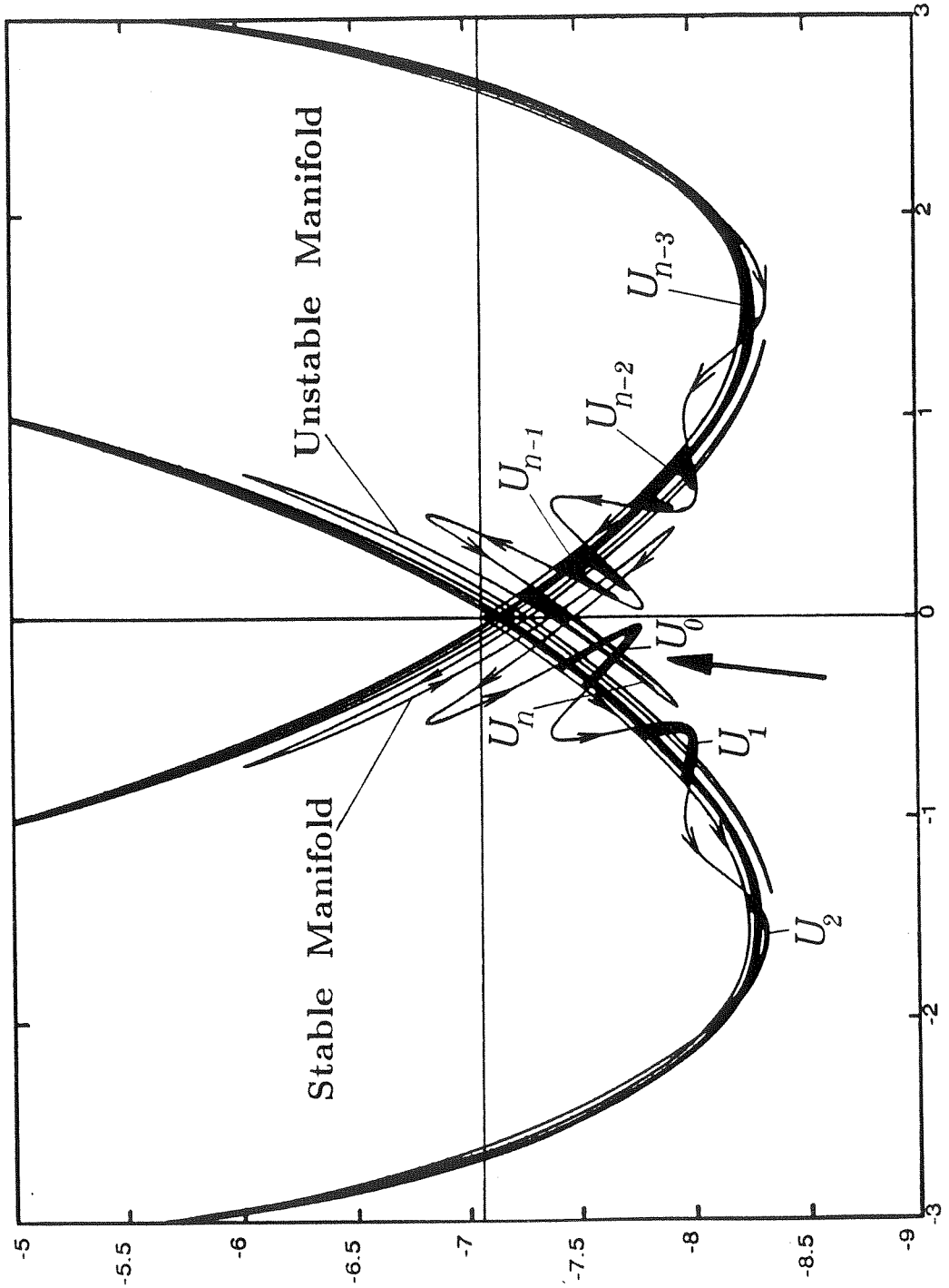

Figure 2.22. Creation of a Smale Horseshoes in the neighborhood of the unstable antisymmetric mode.

invariant manifolds exist. For values of the coupling stiffness parameter K_3 greater than 1/4, no such motions can occur, since then the antisymmetric mode is orbitally stable and no bifurcating modes exist (however, as shown in the next section, small-scale, local chaotic motions are encountered in that case).

In certain cases, homoclinic Melnikov functions can be used to analytically prove the existence of the aforementioned transverse intersections. Unfortunately, one cannot implement this kind of analysis in the present case, since the resulting Melnikov functions become exponentially small as the nonlinearity decreases (this is because, for low energies, the homoclinic orbit appears in the *averaged* hamiltonian equations–for a discussion see (Guckenheimer, 1984)). However, subharmonic Melnikov analysis will be successfully used to prove the existence of subharmonic orbits in the *Poincare'* map.

2.4.3.2. SUBHARMONIC ORBITS

An additional feature of the maps of figure 2.20 is the existence of subharmonic periodic orbits. These orbits result from the breakdown of the invariant tori that appear for low energies. In figure 2.23 two such orbits appear of periods 5 and 6. In each of these plots, a pair of subharmonic orbits exist, the one being orbitally stable (the points of the orbit appearing as centers), and the other orbitally unstable (the orbit containing hyperbolic saddle points). The stable and unstable manifolds of the unstable subharmonic points intersect with each other transversely in a manner completely analogous to that described in the previous section, giving rise to small-

scale chaotic trajectories (figure 2.23). These chaotic trajectories are of a local nature since they occupy only a small neighborhood of the subharmonic orbit. In that sense, they differ from the global, large-scale chaotic motions encountered in previous sections (which result from the "homoclinic tangles" of the antisymmetric mode).

The subharmonic orbits are generated from the "breakdown" of "irrational" tori (Arnold, 1978a,b). However, according to the KAM (Kolmogorov-Arnold-Moser) theorem (Arnold, 1964), for sufficiently small levels of energy there exist "sufficiently irrational" tori that are preserved. As the energy of motion is increased, the measure of these preserved tori diminishes to zero. The terms "rational" and "sufficiently irrational," refer to rational or irrational ratios of the frequencies of the two angle-variables of the tori under investigation (the angle-variables, together with the action ones, result from a canonical symplectic transformation of the generalized coordinates and the generalized momenta of the hamiltonian system (Persival, 1982)(Arnold, 1978a)). The preserved "irrational" tori confine the small-scale chaotic motions into certain regions of the phase plane. This is because the one-dimensional intersections of the tori with the *Poincare'* section, partition the 2-dimensional *Poincare'* map into disconnected regions. Thus, chaotic motions inside a preserved invariant torus cannot "escape" outside it. This is not the case for hamiltonian systems of higher dimensions, where the small-scale chaotic trajectories are in a continuous "web" and "Arnold diffusion" occurs (Arnold, 1964).

Summarizing, small-scale chaotic motions result from the destruction of the invari-

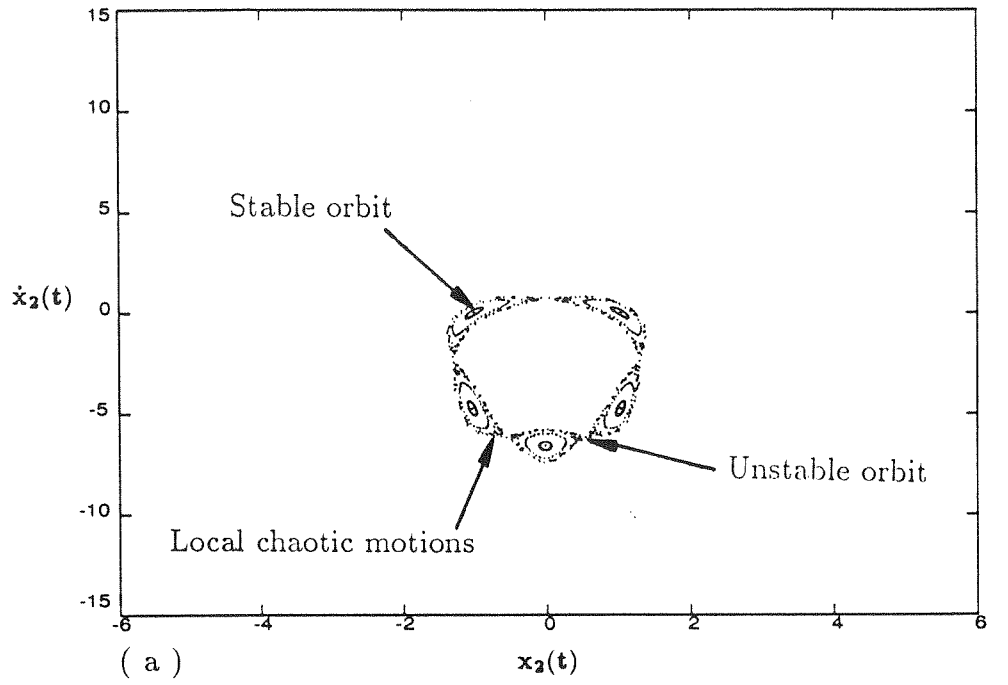

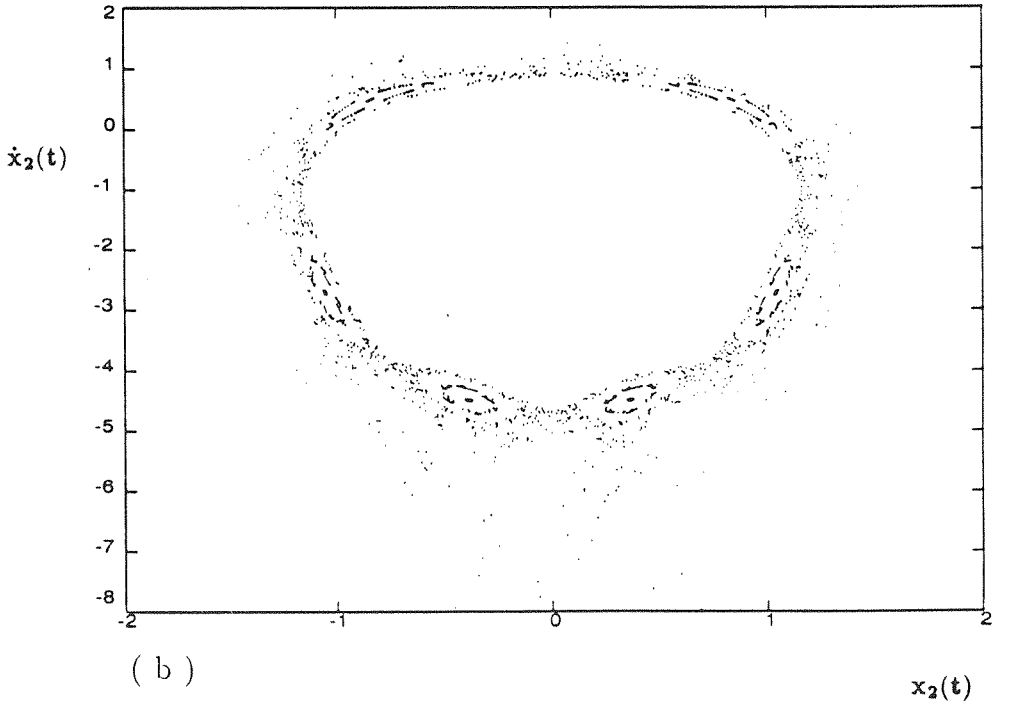

Figure 2.23. Subharmonic and local chaotic motions: subharmonic orbit of (a) period 5, (b) of period 6.

ant tori of the hamiltonian system, and are local in nature. Moreover, they occur irrespective of the pitchfork bifurcation of normal modes (at $K_3 = 1/4$) since they result from the breakdown of "rational" tori, which take place before and after the bifurcation. On the contrary, the large-scale chaotic motions (encountered in the previous section) resulted because of homoclinic intersections of the manifolds of the unstable mode, and occurred only because the bifurcation of normal modes had already taken place (i.e., only for $K_3 < 1/4$). This is because for $K_3 > 1/4$, the antisymmetric mode was a (stable) center and it did not possess one-dimensional invariant manifolds. Thus, a first physical implication of the pitchfork bifurcation of normal modes is that they make the system "more chaotic," since they give rise to global, chaotic trajectories. A final remark is that as the energy of the system is increased, all the invariant tori of the system "break" and the whole phase plane is filled with chaotic motions.

In the next section, a Melnikov-type analysis is implemented to study the generation of subharmonic orbits that result from the destruction of the "rational" tori.

2.4.4. STUDY OF THE SUBHARMONIC ORBITS OF THE "1-1 RESONANT" OSCILLATOR

In this section, the perturbation methods developed by Holmes and Marsden (Holmes, 1982a,b) will be implemented, to prove the existence of arbitrarily many subharmonic orbits in the neighborhood of an orbit of the two-DOF, "1-1 resonant," hamiltonian oscillator with cubic nonlinearity. In (Holmes, 1982a,b), a similar methodology was applied to prove the nonexistence of analytic second integrals of motion of a certain type, and to study the way in which "resonant" tori break-up between KAM "irrational" preserved tori, for a pair of weakly coupled pendula. The methodology of these references will be followed, and an analytic proof of the existence of the subharmonic orbits that were observed in the (numerical) *Poincare'* plots will be given.

2.4.4.1. VEERMAN - HOLMES THEOREM

Throughout this analysis, the two-DOF oscillator that was examined in previous sections will be considered. The system consists of two nonlinear, single DOF (SDOF) oscillators, connected by means of a cubic nonlinear stiffness. In order to apply the perturbation methodology of this section, it is necessary to assume that the coupling stiffness is weakly nonlinear; however, no such assumption is needed for the uncoupled, nonlinear, single DOF (SDOF) systems. Thus, the system under investigation is slightly different than that examined in section 2.4.2.2., since in the present case only one nonlinear stiffness depends on the small parameter ϵ, and the

differential equations of motion are of the form:

$$\begin{aligned} \ddot{x}_1 + x_1 + x_1^3 + \epsilon K_3 (x_1 - x_2)^3 = 0 \\ \ddot{x}_2 - \epsilon K_3 (x_1 - x_2)^3 + x_2^3 + x_2 = 0 \end{aligned} \tag{2.105}$$

The parameter ϵ is of perturbation order, i.e., it is assumed that $\mid \epsilon \mid \ll 1$. Note that when $\epsilon = 0$, the system degenerates into two (strongly) nonlinear oscillators.

The system (2.105) is hamiltonian, and from classical theory, its generalized coordinates q_1, q_2, and momenta p_1, p_2, are expressed as follows:

$$\begin{aligned} q_1 = x_1 \quad , \quad p_1 = \dot{x}_1 \\ q_2 = x_2 \quad , \quad p_2 = \dot{x}_2 \end{aligned} \tag{2.106}$$

The hamiltonian function of the oscillator can then be expressed as:

$$H^\epsilon(\underline{p}, \underline{q}) = \frac{p_1^2 + p_2^2}{2} + \frac{q_1^2 + q_2^2}{2} + \frac{q_1^4 + q_2^4}{4} + \epsilon \frac{(q_1 - q_2)^4}{4} \Rightarrow$$

$$\Rightarrow H^\epsilon(\underline{p}, \underline{q}) = H^0(\underline{p}, \underline{q}) + \epsilon H^1(\underline{p}, \underline{q}) \tag{2.107}$$

where the notation of (Veerman, 1985,1986) was followed, in denoting by $H^0(\underline{p}, \underline{q})$ and $H^\epsilon(\underline{p}, \underline{q})$ the unperturbed and perturbed hamiltonians respectively, and by $H^1(\underline{p}, \underline{q})$ the perturbation term that contains the weak coupling stiffness. In the previous expressions, $\underline{p} \equiv (p_1, p_2)$ and $\underline{q} \equiv (q_1, q_2)$.

Note that for $\epsilon = 0$, the oscillator is integrable (since as mentioned earlier, it degenerates into two SDOF oscillators), and the addition of the term $H^1(\underline{p}, \underline{q})$ results in a perturbation of the integrability. In what follows, it will be shown that this perturbation results in the creation of arbitrarily many "perturbed" subharmonic orbits that exist in the neighborhood of "unperturbed" periodic ones.

The first step of the analysis is to consider the unperturbed integrable hamiltonian system (corresponding to $\epsilon = 0$ in equations (2.105)). The unperturbed hamiltonian is expressed as follows:

$$H^0(\underline{p}, \underline{q}) = F_1(p_1, q_1) + F_2(p_2, q_2) \tag{2.108}$$

where the terms F_1, F_2 are given by:

$$F_i(p_i, q_i) = \frac{p_i^2}{2} + \frac{q_i^2}{2} + \frac{q_i^4}{4} \quad , \; i = 1, 2 \tag{2.109}$$

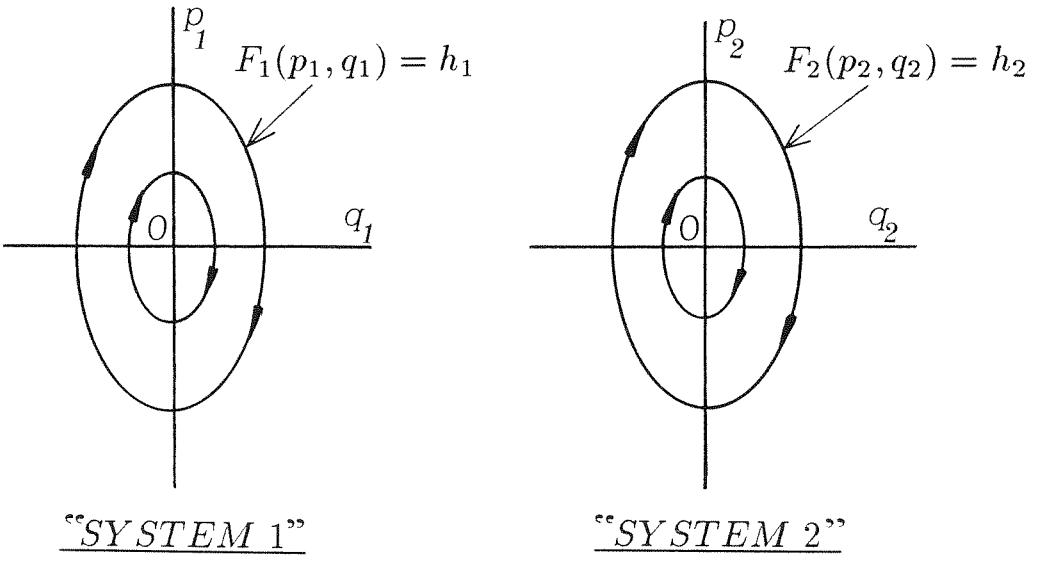

Figure 2.24. Phase planes of the two unperturbed, SDOF systems.

Each of the unperturbed, SDOF oscillators (referred from here on as "systems 1 and 2"), has a phase plane consisting of elliptic periodic orbits, which are level curves of the individual SDOF hamiltonian functions F_1 and F_2 (i.e., they correspond to $F_i = c$, where c is an arbitrary constant). Consider the flow in the neighborhood of the

elliptic periodic orbit $\underline{p} = (0, p_2(t))$, $\underline{q} = (0, q_2(t))$, on the fixed energy surface $H^\epsilon = h$. Since the conditions (H1-H3) of reference (Veerman, 1985), are satisfied for the system under consideration, it is possible to reduce the 2-dimensional hamiltonian oscillator to the form (Holmes, 1982a,b),(Veerman, 1985):

$$\begin{aligned} \frac{dq_1}{d\theta_2} &= -\frac{\partial \mathcal{L}^0}{\partial p_1} - \epsilon \frac{\partial \mathcal{L}^1}{\partial p_1} + \mathcal{O}(\epsilon^2) \\ \frac{dp_1}{d\theta_2} &= \frac{\partial \mathcal{L}^0}{\partial q_1} + \epsilon \frac{\partial \mathcal{L}^1}{\partial q_1} + \mathcal{O}(\epsilon^2) \end{aligned} \tag{2.110}$$

where

$$\begin{aligned} \mathcal{L}^0(q_1, p_1; h) &= F_2^{-1}(h - F_1(q_1, p_1)) \\ \mathcal{L}^1(q_1, p_1, \theta_2; h) &= -\frac{H^1(q_1, p_1, \theta_2; \mathcal{L}^0(q_1, p_1; h))}{\Omega(\mathcal{L}^0(q_1, p_1; h))} \\ \Omega(I_2) &= \frac{dF_2(I_2)}{dI_2} \end{aligned} \tag{2.111}$$

The quantities (I_2, θ_2) are the action-angle variables of the unperturbed system 2, and result from the original generalized variables (q_2, p_2) by means of a canonical symplectic transformation of coordinates. Note that the expression for $\mathcal{L}^0$ results from the "symbolic inversion" of the quantity F_2. For a rigorous derivation of expressions (2.110-2.111), the reader is referred to (Holmes, 1982a,b).

The "reduced" system (2.110) is in the form of a periodically perturbed planar oscillator. When $\epsilon = 0$ the system is hamiltonian with hamiltonian function $\mathcal{L}^0$, and "time-like" variable θ_2. For $\epsilon \neq 0$, the hamiltonian system is perturbed by "time-dependent" terms (this happens because the term $\mathcal{L}^1$ has explicit periodic dependence on the "time-like," angle variable θ_2 which is modulo 2π). Thus, one can apply the Melnikov theory for subharmonic orbits (Guckenheimer, 1984) to the study of the reduced system. In fact, considering the "reduced" phase space

(q_1, p_1, θ_2), one can find a countable infinity of "resonant" tori for the unperturbed system (corresponding to $\epsilon = 0$ in equations (2.110)). These tori are direct products of the periodic orbits of the two SDOF uncoupled oscillators (shown in figure 2.24). In order for a torus to be "resonant," it is necessary that the periods T_1 and T_2 of the SDOF "unperturbed" systems satisfy a relation of the following form:

$$T_1 = \frac{mT_2}{n} \qquad (Resonance\ condition) \tag{2.112a}$$

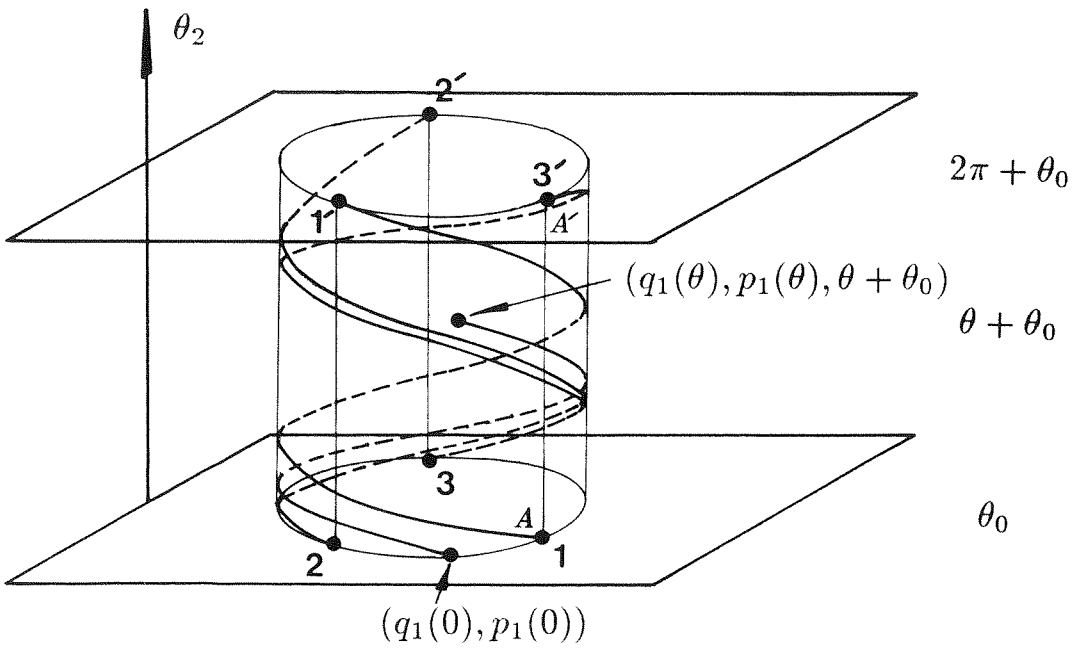

Figure 2.25. Unperturbed motion on a resonant torus, in the reduced phase space ($m/n = 3/1$).

Equivalently, the resonance condition for the period of "system 1" can be expressed in terms of the time-like angle variable θ_2 of "system 2," as follows:

$$\overline{T_1} = \frac{2\pi m}{n} \qquad (Resonance\ condition) \tag{2.112b}$$

In the above expressions, m and n are relatively prime positive integers. Relations (2.112), combined with the fact that the total energy of the perturbed hamiltonian system is preserved, define a unique unperturbed resonant two-torus for each pair of integers (m, n).

Considering the unperturbed, reduced equations (2.110) (with $\epsilon = 0$), and assuming that the resonance conditions (2.112) are satisfied, the motion on a "resonant" torus corresponding to initial conditions ($q_1(0), p_1(0), \theta_0$) and unperturbed energy level $F_1(q_1, p_1) = h_1$ is denoted by:

$$(q_1(\theta), p_1(\theta), \theta + \theta_0) \quad (\textit{ Unperturbed solution }) \tag{2.113}$$

where θ is a variable parametrizing the motion on the resonant torus. Referring to figure 2.25, since the resonance condition (2.112b) is satisfied, point A corresponding to $\theta = \theta_0$ coincides with its image under the unperturbed flow at $\theta = \theta_0 + 2\pi\, m$, point A'.

When the "perturbed," reduced flow is considered ($\epsilon \neq 0$ in (2.110)), the distance between the initial point at θ_0 and its image at $\theta_0 + 2\pi\, m$ will not be zero, but to the first order of accuracy it can be expressed as (Guckenheimer, 1984):

$$d(\theta_0) = \epsilon \frac{\mathcal{M}(\theta_0; m, n, h)}{||X_F(0)||} + \mathcal{O}(\epsilon^2) \tag{2.114}$$

where

$$||X_F(0)|| = \left(\frac{\partial F_1}{\partial p_1} - \frac{\partial F_1}{\partial q_1}\right)_{(q_1(0), p_1(0))} \tag{2.115}$$

is a normalization factor, and $\mathcal{M}(\ \theta_0, m, n, h\ )$ is the subharmonic-Melnikov function

given by:

$$\mathcal{M}(\theta_0, m, n, h) = \int_0^{2\pi m} \{\mathcal{L}^0, \mathcal{L}^1\}_{(q_1(\theta_2-\theta_0), p_1(\theta_2-\theta_0), \theta_2, h)} d\theta_2 \qquad (2.116)$$

or in terms of the time t,

$$\mathcal{M}(t_0, m, n, h) = \frac{T_2}{2\pi} \int_{-mT_2/2}^{mT_2/2} \{F_1, H^1\}_{(q_1(t), p_1(t), q_2(t+t_0), p_2(t+t_0))} dt \qquad (2.117)$$

In the above expressions, $\{\bullet, \bullet\}$ is the Poisson bracket (Guckenheimer, 1984).

As the following theorem states, when the distance (2.114), between the image points in the perturbed flow, vanishes, a subharmonic orbit results.

Theorem (Veerman, Holmes , 1985)

Fix the total energy level of the system to $h > 0$. Assume that m, n are integers relatively prime and choose ϵ sufficiently small. Then, if $\mathcal{M}(\theta_0, m, n, h)$ has j simple zeros as a function of θ_0 in $[0, 2\pi m/n)$ (or equivalently $\mathcal{M}(t_0, m, n, h)$ as a function of t_0 in $[0, T_1)$), the resonant torus given by $(q_1, p_1, \theta_2) = (q_1(\theta_2 - \theta_0), p_1(\theta_2 - \theta_0), \theta_2)$ breaks into $2k = j/m$ distinct $2\pi m$-periodic orbits and there are no other $2\pi m$-periodic orbits in its neighborhood.

As pointed out in (Veerman, 1985), this Melnikov-function technique proves the existence of only a finite number of periodic orbits in the vicinity of an unperturbed resonant torus. This is because as the integers $m, n \to \infty$, one must let $\epsilon \to 0$, in order to guarantee that the term $\epsilon\, \mathcal{M} \,/\, ||X_F||$ dominates over the $\mathcal{O}(\epsilon^2)$ terms. Thus, one cannot prove the existence of infinitely many periodic orbits, and as a result, one cannot rigorously prove the nonintegrability of the hamiltonian system.

Note that if a homoclinic orbit existed in the unperturbed reduced system (2.110), then by means of the Smale-Birkhoff homoclinic theorem, one would be able to prove the existence of an infinity of transverse homoclinic intersections for the perturbed system (homoclinic Melnikov-functions should be used in that case). As a result, one would be able to prove that the perturbed hamiltonian system does not contain any integrals of motion that are independent from the hamiltonian function.

2.4.4.2. SUBHARMONIC MELNIKOV ANALYSIS

The outlined theory will now be applied for the analysis of the oscillator under consideration. The unperturbed response of the system will first be computed. When $\epsilon = 0$, the equations of motion (2.105) uncouple:

$$\begin{aligned} \ddot{x}_1 + x_1 + x_1^3 &= 0 \\ \ddot{x}_2 + x_2 + x_2^3 &= 0 \end{aligned} \tag{2.118}$$

These equations describe the free motions of "systems 1 and 2," and correspond to two uncoupled, SDOF oscillators. Integrating the equations by quadratures, and taking into account expressions (2.106) for the generalized coordinates and momenta, one obtains the following analytic solution for the time response of the unperturbed system:

$$q_i = X_i cn([1 + X_i^2]^{1/2} t \ , k_i) \ \ , \ k_i = \frac{X_i^2}{2(1 + X_i^2)} \ \ , \ i = 1, 2 \tag{2.119}$$

where the following set of initial conditions was assumed:

$$q_i(0) = X_i \quad \dot{q}_i(0) = 0 \ \ , \ i = 1, 2 \tag{2.120}$$

In the above expressions, $cn(\bullet,\bullet)$ is the elliptic cosine, and k_i is the elliptic modulus. Note that if one assumes a different set of initial conditions, a different elliptic function results, but this does not affect the generality of the analysis.

Assuming that the energy of oscillation of "system i," is h_i ($i = 1, 2$), its amplitude of oscillation X_i can be related to h_i by:

$$X_i^2 = -1 + (1 + 4h_i)^{1/2} \quad , \quad h_i > 0 \quad , \; i = 1, 2 \tag{2.121}$$

Combining expressions (2.119) and (2.121), one can express the oscillations of the two unperturbed systems, in terms of their energies, as follows:

$$\begin{aligned} q_i(t) &= \left(\mathcal{H}_i{}^{1/2} - 1\right)^{1/2} \, cn(\mathcal{H}_i{}^{1/4} t \; , k_i) \\ k_i^2 &= \frac{\mathcal{H}_i{}^{1/2} - 1}{2\mathcal{H}_i{}^{1/2}} \quad , \; i = 1, 2 \end{aligned} \tag{2.122}$$

where the notation, $\mathcal{H}_i \equiv (1 + 4h_i)$, was used. The generalized momenta of the uncoupled system result by direct differentiation of expressions (2.122) with respect to time:

$$p_i(t) = \dot{q}_i(t) = -\mathcal{H}_i{}^{1/4}(\mathcal{H}_i{}^{1/2} - 1)^{1/2} \, sn(\mathcal{H}_i{}^{1/4} t \; , k_i) \; dn(\mathcal{H}_i{}^{1/4} t \; , k_i)$$

$$i = 1, 2 \tag{2.123}$$

where $sn(\bullet,\bullet), dn(\bullet,\bullet)$ are elliptic functions (Byrd, 1954).

The orbits represented by equations (2.122-123) are based on the initial points $(q_i(0), p_i(0)) = (X_i, 0)$, $i = 1, 2$, and describe the motion on a two-torus of the unperturbed system. In order for this torus to be in "resonance of order m/n," it is necessary that the periods of oscillation of "systems 1 and 2" be integrably related:

$$nT_1 = mT_2 \Rightarrow \frac{nK(k_1)}{\mathcal{H}_1{}^{1/4}} = \frac{mK(k_2)}{\mathcal{H}_2{}^{1/4}} \tag{2.124}$$

In writing (2.124), the actual expressions for the periods of oscillation of the motions (2.119) were used. In this equation $K(\bullet)$ is the complete elliptic integral of the first kind.

Equation (2.124) is the resonance condition for the oscillator. Taking into account the fact that the total energy of the unperturbed motion is the sum of the energies of "systems 1 and 2," i.e., that $h = h_1 + h_2$, the resonance condition (2.124) becomes:

$$\frac{nK\left(\frac{(\mathcal{H}_1{}^{1/2}-1)^{1/2}}{2^{1/2}\mathcal{H}_1{}^{1/4}}\right)}{\mathcal{H}_1{}^{1/4}} = \frac{mK\left(\frac{(\overline{\mathcal{H}_1}^{1/2}-1)^{1/2}}{2^{1/2}\overline{\mathcal{H}_1}^{1/4}}\right)}{\overline{\mathcal{H}_1}^{1/4}} \tag{2.125}$$

where

$$\mathcal{H}_1 = 1 + 4h_1 \quad , \; \overline{\mathcal{H}_1} = 1 + 4(h - h_1) \tag{2.126}$$

It will be shown that for fixed h, m and n, equation (2.125) gives a unique solution for h_1. This implies that the unperturbed oscillator has a dense set of resonant tori in any neighborhood of the orbit $\underline{q} = (0, q_2(t)), \underline{p} = (0, p_2(t))$ at every energy level h (Veerman, 1985). Equation (2.125) can be regarded as a transcedental equation in h_1. To show uniqueness of solutions for h_1, the monotonicity of the following quantity is examined:

$$D(u) \equiv K\left(\frac{\left((1+4u)^{1/2}-1\right)^{1/2}}{2^{1/2}(1+4u)^{1/4}}\right)/(1+4u)^{1/4} \quad , \quad u \in [0, h) \tag{2.127}$$

By numerical computation (figure 2.26a) it can be shown that $D(u)$ is a monotonically decreasing function of u in the domain $u \in [0, h)$. Thus, the left-hand side of equation (2.125) is monotonically decreasing, whereas the right-hand side is monotonically increasing for $h_1 \in [0, h)$. Therefore, equation (2.125) is guaranteed

to have a unique solution for h_1, when the following inequalities are satisfied (see figure 2.26b):

$$\begin{aligned} mK\left(\frac{\left((1+4h)^{1/2}-1\right)^{1/2}}{2^{1/2}(1+4h)^{1/4}}\right)/(1+4h)^{1/4} &\leq nK(0) \\ nK\left(\frac{\left((1+4h)^{1/2}-1\right)^{1/2}}{2^{1/2}(1+4h)^{1/4}}\right)/(1+4h)^{1/4} &\leq mK(0) \end{aligned} \tag{2.128}$$

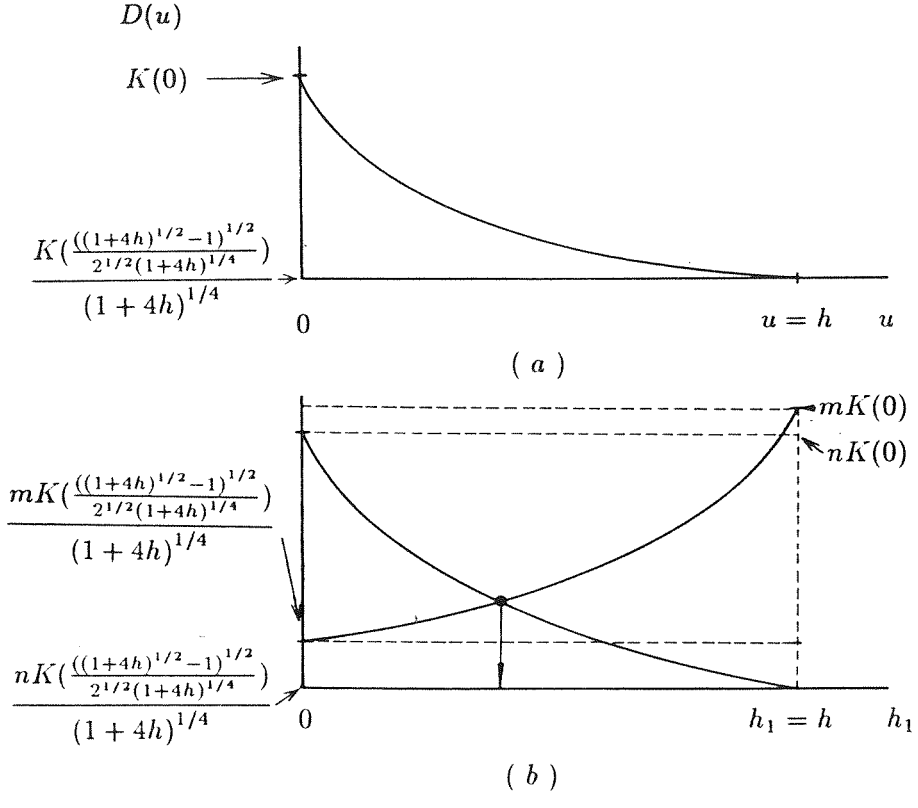

Figure 2.26. (a) Numerical plot of the quantity $D(u)$. (b) Existence of a unique solution for h_1 in equation (2.125).

The inequalities (2.128) pose certain restrictions on the values of m and n. For example, for $h = 1$, the ratio m/n must be in the range,

$$0.72411 \leq m/n \leq 1.38100 \qquad (\ h = 1\ )$$

If the value of m/n is out of the aforementioned range, equation (2.125) does not have a unique solution for h_1 in $[0, h)$, and the perturbation analysis fails.

Hence, only resonant orbits satisfying inequalities (2.128) are guaranteed to have a resonant torus for the fixed energy level h. It is the perturbations of these orbits that will be examined in the sequence. As mentioned earlier, the existence of subharmonic orbits in the neighborhood of a resonant torus can be proven by examining the subharmonic Melnikov-function (2.116-117):

$$\mathcal{M}(t_0, m, n, h) = \frac{T_2}{2\pi} \int_{-mT_2/2}^{mT_2/2} \left(\frac{\partial F_1}{\partial q_1} \frac{\partial H^1}{\partial p_1} - \frac{\partial F_1}{\partial p_1} \frac{\partial H^1}{\partial q_1} \right)_{(q_1(t), p_1(t), q_2(t+t_0), p_2(t+t_0))} dt =$$

$$= \frac{T_2}{2\pi} \int_{-mT_2/2}^{mT_2/2} -p_1(t)(q_1(t) - q_2(t+t_0))^3 \, dt \qquad (2.129)$$

where $T_2 = K(k_1)/{\mathcal{H}_1}^{1/4}$ is the period of oscillation of the unperturbed motion of "system 2" on the fixed energy level h, $q_i(t), p_i(t)$ are the unperturbed oscillations given by expressions (2.122-123), and F_1, H^1 are the hamiltonian functions defined by equations (2.107-109).

In order to prove the existence of subharmonic motions for the perturbed system, it is necessary that the equation,

$$\mathcal{M}(t_0, m, n, h) = 0, \qquad (2.130)$$

has a finite number of zeros. In order to show this, rewrite equation (2.129) in the form:

$$\mathcal{M}(t_0, m, n, h) = \frac{T_2}{2\pi} \int_{-mT_2/2}^{mT_2/2} [-p_1(t)q_1^3(t) + p_1(t)q_2^3(t+t_0) + 3p_1(t)q_1^2(t)q_2(t+t_0) -$$

$$-3p_1(t)q_1(t)q_2^2(t+t_0)]\ dt \tag{2.131}$$

Since $q_1(t)$ is given in terms of an elliptic cosine, $cn(\bullet,\bullet)$, it is an even function of t (Byrd, 1954). On the other hand, $p_1(t)$ is an odd function of time, since it depends on the product of the elliptic functions $sn(\bullet,\bullet)$ and $dn(\bullet,\bullet)$. Thus, the first term of the integral (2.131) gives a zero contribution and one needs only to consider the remaining three terms.

Note that the period of $q_2(t+t_0)$ is T_2. Thus, by setting,

$$t_0 = \frac{kT_2}{2} = \frac{nkT_1}{2m} \quad , \quad k\ positive\ integer \tag{2.132}$$

the following relation results:

$$q_2(t+t_0) = q_2(t+\frac{kT_2}{2}) = (-1)^k q_2(t) \tag{2.133}$$

Thus, by selecting t_0 according to equation (2.132), the quantity $q_2(t+t_0)$ becomes an even function of t, and since $p_1(t)$ is an odd function of t, it can be concluded that all the terms of the integral (2.131) give zero contributions:

$$\mathcal{M}(t_0 = \frac{kT_2}{2}, m, n, h) = 0 \quad , \quad k\ positive\ integer \tag{2.134}$$

Hence, it was proven that, at $t_0 = kT_2/2$ the Melnikov-function has a zero. As far as the number of these zeros is concerned, as pointed out by (Veerman, 1985), if one computes $kn/2m\ mod.\ 1$, for m and n relatively prime, one finds precisely $2m$ such zeros for t_0 (at $kn\ mod.\ 2m = 0, 1, ..., 2m-1$), in the interval $0 \leq kn/2m < 1$.

Summarizing, it was proved that $\mathcal{M}(t_0, m, n, h)$ has $2m$ zeros for $0 \leq kn/2m < 1$. In order to satisfy completely the conditions of the Veerman-Holmes theorem, one

has to prove that these zeros are simple. This is the case, when the following inequality holds:

$$\left(\frac{d\mathcal{M}(t_0,m,n,h)}{dt_0}\right)_{t_0=kT_2/2} \neq 0 \tag{2.135}$$

Differentiating $\mathcal{M}(t_0,m,n,h)$ with respect to t_0, and taking into account the relations,

$$\left(\frac{dq_2(t+t_0)}{dt_0}\right)_{t_0=kT_2/2} = (-1)^k \frac{dq_2(t)}{dt} \quad , \quad p_1(t) = \frac{dq_1(t)}{dt}, \tag{2.136}$$

one obtains the following expression for the derivative of the Melnikov-function:

$$\mathcal{M}'_{(t_0=kT_2/2)} = \frac{T_2}{2\pi}\int_{-mT_2/2}^{mT_2/2} [\,(-1)^k \frac{dq_2(t)}{dt}\frac{dq_1^3(t)}{dt} +$$

$$+(-1)^k \frac{dq_1(t)}{dt}\frac{dq_2^3(t)}{dt} - \frac{3}{2}\frac{dq_1^2(t)}{dt}\frac{dq_2^2(t)}{dt}\,]\,dt \tag{2.137}$$

where $(\bullet)' \equiv d/dt_0$. In order to compute the above relation, one expands the expressions for $q_1(t)$ and $q_2(t)$ in Fourier series, and evaluates the differentiations appearing in (2.137), as follows (the Fourier expansions of the elliptic functions are listed in Appendix C):

$$\begin{aligned}
\frac{d}{dt}(q_1(t)) &= \sum_{r=0}^{\infty} \Lambda_i^{(r)} sin\gamma_i^{(r)} t \\
\frac{d}{dt}(q_1^3(t)) &= \sum_{r=0}^{\infty} \Gamma_i^{(r)} sin\gamma_i^{(r)} t \\
\frac{d}{dt}(q_1^2(t)) &= \sum_{r=0}^{\infty} \Delta_i^{(r)} cos\gamma_i^{(r)} t
\end{aligned} \tag{2.138}$$

where

$$\Lambda_i^{(r)} = -\frac{\pi^2 2^{1/2}\mathcal{H}_i^{1/2}}{K^2(k_i)}\frac{(2r+1)Q_i^{r+1/2}}{1+Q_i^{2r+1}}$$

$$\Gamma_i^{(r)} = -\frac{\pi^2 2^{1/2}\mathcal{H}_i}{K^2(k_i)}(2r+1)[2k_i^2 - 1 + \frac{(2r+1)^2\pi}{2K(k_i)}]\frac{Q_i^{r+1/2}}{1+Q_i^{2r+1}}$$

$$\Delta_i^{(r)} = -\frac{\pi^2 2^{1/2}\mathcal{H}_i}{K^2(k_i)(\mathcal{H}_i^{1/2}-1)^{1/2}}[1+k_i^2-\frac{(2r+1)^2\pi^2}{4K^2(k_i)}]\frac{(2r+1)Q_i^{r+1/2}}{1-Q_i^{2r+1}}$$

$$\gamma_i^{(r)} = \frac{(2r+1)\pi\mathcal{H}_i^{1/4}}{2K(k_i)} \qquad (2.139)$$

and $Q_i = exp(-\pi K(1-k_i)/K(k_i))$, is the elliptic nome (Byrd, 1954). Substituting these series expressions into equation (2.137), and taking into account orthogonality conditions of the form,

$$\int_{-mT_2/2}^{mT_2/2} cos[\frac{2(2j+1)\pi t}{T_1}]cos[\frac{2(2l+1)\pi t}{T_2}]\ dt =$$

$$= \frac{nT_1}{2}\delta_{n(2j+1),m(2l+1)} = \frac{mT_2}{2}\delta_{n(2j+1),m(2l+1)} \qquad (\delta_{u,v}\ is\ Kronecker's\ function) \qquad (2.140)$$

one obtains the following expression for the derivative of the Melnikov-function (evaluated at its zeros):

$$\mathcal{M}'_{(t_0=kT_2/2)} = \frac{(-1)^k mT_2}{4\pi}\sum_{\mu=0}^{\infty}[\ \Lambda_2^{(l)}\Gamma_1^{(j)} + \Lambda_1^{(j)}\Gamma_2^{(l)} - \frac{3(-1)^k}{2}\Delta_1^{(j)}\Delta_2^{(l)}\ ] \qquad (2.141)$$

where the integers j, l satisfy the relations:

$$n(2j+1) = m(2l+1) \Rightarrow (2j+1) = (2\mu+1)m\ \ ,\ \ (2l+1) = (2\mu+1)n\ \ ,\ \mu = 0,1,2,... \qquad (2.142)$$

Finally, substituting into (2.141) the expressions for $\Lambda_i^{(r)}, \Gamma_i^{(r)}$ and $\Delta_i^{(r)}$ (equations (2.139)), and after some tedious but straightforward algebraic manipulations, one obtains the following relation for $\mathcal{M}'(t_0, m, n, h)$:

$$\mathcal{M}'(t_0,m,n,h) = \frac{(-1)^k m}{T_1^2}[\ -256\pi^3 mn\mathcal{K}_2 + 1024\pi^5 mn(\frac{m^2}{T_1^2}+\frac{n^2}{T_2^2})\mathcal{K}_4 -$$

$$-\frac{12(-1)^k\pi^3(1+4h_1)^{1/4}(1+4h_2)^{1/4}}{2k_1k_2}\{\,(1+k_1^2)(1+k_2^2)mn\mathcal{J}_2-\frac{(1+k_1^2)n^2\pi^2mn}{4K^2(k_2)}\mathcal{J}_4-$$

$$-\frac{(1+k_2^2)m^2\pi^2mn}{4K^2(k_1)}\mathcal{J}_4+\frac{m^3n^3\pi^4}{16K^2(k_1)K^2(k_2)}\mathcal{J}_6\,\}\,] \qquad (2.143)$$

where

$$\mathcal{K}_i=\frac{1}{4}\sum_{\mu=0}^{\infty}(2\mu+1)^i sech[\pi m\tau_1(\mu+\frac{1}{2})]sech[\pi n\tau_2(\mu+\frac{1}{2})]\ ,\ i=2,4$$

$$\mathcal{J}_i=\frac{1}{4}\sum_{\mu=0}^{\infty}(2\mu+1)^i csch[\pi m\tau_1(\mu+\frac{1}{2})]csch[\pi n\tau_2(\mu+\frac{1}{2})]\ ,\ i=2,4,6 \qquad (2.144)$$

and $\tau_i = K(1-k_i)/K(k_i)\ ,\ i=1,2$. Note that the above expression for the derivative of the Melnikov function, evaluated at its zeros, is not identically zero. Thus, the simplicity of its zeros is established and the conditions of the Veerman-Holmes theorem are met. In fact, the series expressions for $\mathcal{K}_i$ and $\mathcal{J}_i$ converge rapidly. Thus, one can obtain a fairly good approximation for these quantities by retaining only their first term, corresponding to $\mu = 0$ (for an estimation of the errors of such an approximation, see (Veerman, 1986)).

It can be verified that the outlined analysis fails as $n, m \to \infty$. In that case,

$$lim_{m,n-\infty}\ \mathcal{M}'(t_0 = kT_2/2, m, n, h) = 0 \qquad (2.145)$$

and the conclusion is that one cannot prove the existence of subharmonic orbits of all resonant tori in any neighborhood of an elliptic orbit (this can only be proved for finite values of m and n).

As a numerical example, consider the energy level $h = 1$, and a resonant torus corresponding to $m/n = 11/13$. The value of the ratio m/n is within the range

specified by inequalities (2.128); hence, equation (2.125) has a unique root for h_1, which was numerically computed as $h_1 = 0.776$. This gives a value for h_2 equal to $h_2 = h - h_1 = 0.224$. At these energy levels of "systems 1,2," a resonant torus exists. There are $2m = 22$ zeros of the Melnikov function, and their simplicity can be examined by evaluating expression (2.143). Retaining only the first terms of the series expressions in (2.144), the derivative of the Melnikov-function at its zeros was numerically evaluated as $\mathcal{M}' = -5.3 \times 10^{-8}$ for k even, and -5.4×10^{-8} for k odd. Thus, the zeros of the Melnikov-function are simple, and from the Veerman-Holmes theorem one concludes that at the energy level $h = 1$, a resonant torus breaks into two distinct, 22π-periodic orbits. The stability of such subharmonic orbits will be examined in the next section.

2.4.4.3. PHASE PLANE REPRESENTATION OF SUBHARMONIC ORBITS

The stability of the subharmonic orbits that result from the destruction of the "rational" tori will be examined by studying their phase plane representation. To achieve this, one introduces a canonical transformation of coordinates. Consider the perturbed hamiltonian function:

$$H^{\epsilon}(\underline{p}, \underline{q}) = H^0(\underline{p}, \underline{q}) + \epsilon H^1(\underline{p}, \underline{q}) = F_1(p_1, q_1) + F_2(p_2, q_2) + \epsilon \frac{(q_1 - q_2)^4}{4} \qquad (2.146)$$

where the terms F_1, F_2 are given by expressions (2.109). The following canonical transformation of coordinates is considered:

$$(p_1, q_1) \rightarrow (I_1, \theta_1) \qquad (2.147)$$

where (I_1, θ_1) are the action-angle variables of the hamiltonian "system 1"(for a definition of "systems 1,2" refer to previous sections and figure 2.24). The action variable is defined as (Percival, 1982):

$$I_1(h_1) = \frac{1}{\pi}\int_{q_1^+}^{q_1^-} p_1 dq_1 = \frac{1}{\pi}\int_{q_1^+}^{q_1^-} 2^{1/2}(h_1 - \frac{q_1^2}{2} - \frac{q_1^4}{4})^{1/2} dq_1 \qquad (2.148)$$

where h_1 is the energy of motion of "system 1," and $q_1^{\pm}$ are its extreme values of oscillation (figure 2.27). The numerical value of I_1 is equal to the area enclosed by the free oscillation of the system in the phase plane.

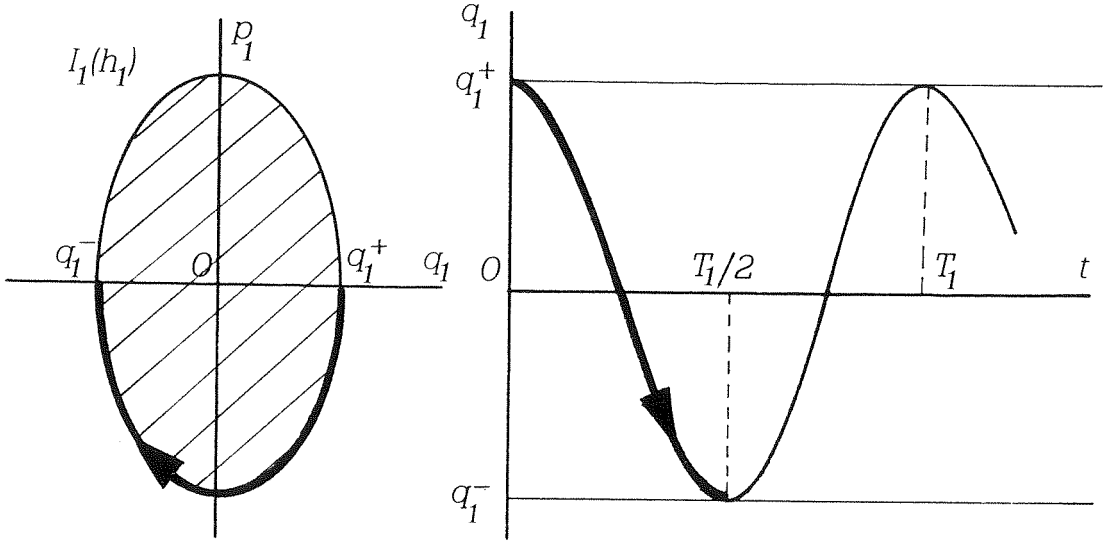

Figure 2.27. Free oscillation of "system 1" : path of integration for evaluating I_1.

Substituting the derived expressions for $q_1(t)$ and $p_1(t)$ (equations (2.122-123)) in (2.148), one obtains the action variable, I_1, as a function of the elliptic modulus of the free oscillation k_1:

$$I_1(k_1) = \frac{4}{3\pi(1-2k_1^2)^{3/2}}[\ E(k_1)(2k_1^2 - 1) + k_1'^2 K(k_1)\ ] \qquad (2.149)$$

where $K(\bullet)$ and $E(\bullet)$ are the complete elliptic integrals of first and second kind respectively, and $k_1'^2 = 1 - k_1^2$ is the complementary elliptic modulus. The elimination of the energy h_1 from (2.148) was achieved by the relation:

$$h_1 = \frac{p_1^2}{2} + \frac{q_1^2}{2} + \frac{q_1^4}{4} = \frac{1}{4}[\ \frac{1}{(1-2k_1^2)^2} - 1\ ] \tag{2.150}$$

The angle variable θ_1 can be computed by expressions given in (Percival, 1982). These computations, however, will not be carried out in this work, since they will not be needed in what follows.

Consider now the reduced system of equations (2.110):

$$\begin{aligned} \frac{dq_1}{d\theta_2} &= -\frac{\partial \mathcal{L}^0}{\partial p_1} - \epsilon \frac{\partial \mathcal{L}^1}{\partial p_1} + \mathcal{O}(\epsilon^2) \\ \frac{dp_1}{d\theta_2} &= \frac{\partial \mathcal{L}^0}{\partial q_1} + \epsilon \frac{\partial \mathcal{L}^1}{\partial q_1} + \mathcal{O}(\epsilon^2) \end{aligned} \tag{2.110}$$

Note that θ_2 is a "time-like" variable, and that for $\epsilon = 0$, the unperturbed system is hamiltonian with hamiltonian function $\mathcal{L}^0$. Introducing the action-angle transformation (2.147),

$$\begin{aligned} I_1 &= I_1(p_1, q_1) \quad , \quad p_1 = p_1(I_1, \theta_1) \\ \theta_1 &= \theta_1(p_1, q_1) \quad , \quad q_1 = q_1(I_1, \theta_1) \end{aligned} \tag{2.151}$$

and substituting for q_1, p_1 in the expressions for $\mathcal{L}^0$ and $\mathcal{L}^1$, one obtains the following symbolic expressions:

$$\begin{aligned} \mathcal{L}^0(q_1, p_1, h) &= \mathcal{L}^0(q_1(I_1, \theta_1), p_1(I_1, \theta_1), h) \equiv \hat{\mathcal{L}}^0(I_1, h) \\ \mathcal{L}^1(q_1, p_1, \theta_2) &= \mathcal{L}^1(q_1(I_1, \theta_1), p_1(I_1, \theta_1), \theta_2) \equiv \hat{\mathcal{L}}^1(I_1, \theta_1, \theta_2) \end{aligned} \tag{2.152}$$

Note that there is no explicit dependence of $\hat{\mathcal{L}}^0$ on θ_1, since (I_1, θ_1) are the action-angle variables of "system 1" (Percival, 1982). The reduced set of equations (2.110)

is now symbolically transformed into the new variables (Veerman, 1985):

$$\begin{aligned} \frac{dI_1}{d\theta_2} &= \epsilon \frac{\partial \hat{\mathcal{L}}^1(I_1, \theta_1, \theta_2)}{\partial \theta_1} + \mathcal{O}(\epsilon^2) \\ \frac{d\theta_1}{d\theta_2} &= -\omega(I_1) - \epsilon \frac{\partial \hat{\mathcal{L}}^1(I_1, \theta_1, \theta_2)}{\partial I_1} + \mathcal{O}(\epsilon^2) \end{aligned} \tag{2.153}$$

where $\omega(I_1) = d\hat{\mathcal{L}}^0(I_1)/dI_1$, and the dependence of $\hat{\mathcal{L}}^0$ on the total energy h has been omitted. Consider now an unperturbed orbit on the resonant torus with $nT_1 = mT_2$, by setting $\epsilon = 0$ in (2.153), and integrating:

$$\begin{aligned} I_1 &= \overline{I}_1 \\ \theta_1 &= -\omega(I_1)\theta_2 = -\frac{n}{m}\theta_2 \end{aligned} \tag{2.154}$$

In the above expressions, $\overline{I}_1$ denotes the fixed value of the action variable on the unperturbed orbit. At this point, small perturbations of the following form are introduced:

$$\begin{aligned} I_1 &= \overline{I}_1 + \epsilon^{1/2} K \\ \theta_1 &= -\frac{n}{m}\theta_2 + \epsilon^{1/2}\psi \end{aligned} \tag{2.155}$$

The quantities K and ψ represent the perturbing terms. Note that the perturbations are assumed to be of $O(\epsilon^{1/2})$ (Veerman, 1985,1986); this is necessary for a correct balancing of the terms in the perturbation analysis that follows.

Substituting the perturbations (2.155) into the reduced system (2.153), and after some manipulations, one obtains the following set of differential equations that must be satisfied by the quantities K and ψ:

$$\begin{aligned} \frac{dK}{d\theta_2} &= \epsilon^{1/2} \frac{\partial \hat{\mathcal{L}}^1(\overline{I}_1, -\frac{n\theta_2}{m} + \psi, \theta_2)}{\partial \theta_1} + \epsilon \frac{\partial \hat{\mathcal{L}}^1(\overline{I}_1, -\frac{n\theta_2}{m} + \psi, \theta_2)}{\partial I_1} K + \mathcal{O}(\epsilon^{3/2}) \\ \frac{d\psi}{d\theta_2} &= -\epsilon^{1/2} \frac{d\omega(\overline{I}_1)}{dI_1} K - \epsilon \Big[\frac{\partial^2 \hat{\mathcal{L}}^1(\overline{I}_1, -\frac{n\theta_2}{m} + \psi, \theta_2)}{\partial I_1^2} + \frac{d^2\omega(\overline{I}_1)}{dI_1^2} \frac{K^2}{2} \Big] + \mathcal{O}(\epsilon^{3/2}) \end{aligned} \tag{2.156}$$

Following the methodology outlined in (Veerman, 1985, 1986) and (Greenspan, 1983), one applies the averaging theorem for $\epsilon^{1/2}$ sufficiently small, in order to remove the explicit dependence of (2.156) from the "fast-variable" θ_2. The resulting averaged equations are:

$$\begin{aligned} \frac{d\overline{K}}{d\theta_2} &= \frac{\epsilon^{1/2}}{2\pi n}\ \mathcal{M}(\frac{\overline{\psi}}{\omega(\overline{I}_1)}, m, n, h) \\ \frac{d\overline{\psi}}{d\theta_2} &= -\epsilon^{1/2}\ \frac{d\omega(\overline{I}_1)}{dI_1}\ \overline{K} \end{aligned} \tag{2.157}$$

In the above averaged equations, the quantity $\mathcal{M}$ is the subharmonic Melnikov-function encountered in the previous section (defined by equation (2.131)), with the argument t_0 replaced by the new variable $\overline{\psi}/\omega(\overline{I}_1)$. Also note that the new variables $\overline{K}$ and $\overline{\psi}$ were used in the averaged equations, in order to distinguish them from expressions (2.156).

Under the Averaging theorem, the hyperbolic and elliptic fixed points of (2.157) correspond to small periodic motions of the variations K and ψ, and therefore to subharmonics of order (m/n) for the reduced system (2.153). However, a necessary and sufficient condition for the existence of such fixed points for equations (2.157) is that the subharmonic Melnikov-function has simple zeros, and that $\omega(\overline{I}_1) \neq 0$ (note that these requirements are in total agreement with those posed by the subharmonic Melnikov analysis of the previous section).

The averaged system (2.157) is hamiltonian, with hamiltonian function given by (Greenspan, 1983),

$$\overline{H}(\overline{K}, \overline{\psi}) = \epsilon^{1/2}[\ \frac{d\omega(\overline{I}_1)}{dI_1}\frac{\overline{K}^2}{2} + \int_0^{\overline{\psi}} \frac{\mathcal{M}(\frac{\eta}{\omega(\overline{I}_1)}, m, n, h)}{2\pi n} d\eta\ ] \tag{2.158}$$

For the specific two-DOF oscillator under consideration, the Melnikov function was computed earlier, and the only unknown quantity in the averaged equations is the derivative $d\omega(\overline{I}_1)/dI_1$. To compute this quantity, one writes:

$$\frac{d\omega(\overline{I}_1)}{dI_1} = \frac{d}{dI_1}\left(\frac{2\pi}{T_1(I_1)}\right)_{(I_1=\overline{I}_1)} \tag{2.159}$$

The variable T_1 is the period of oscillation of the unperturbed "system 1", and is given by

$$T_1(k_1) = \frac{4K(k_1)}{(1+4h_1)^{1/4}} \tag{2.160}$$

where $K(\bullet)$ is the complete elliptic integral of the first kind, and k_1 is the elliptic modulus. The variable h_1 is the energy of "system 1," and is related to k_1 by the formula:

$$h_1 = \frac{1}{4}\left[\frac{1}{(1-2k_1^2)^2} - 1\right] \tag{2.161}$$

Combining expressions (2.160-161), one obtains T_1 as a function of the elliptic modulus k_1:

$$T_1^2(k_1) = 16K^2(k_1)(1-2k_1^2) \tag{2.162}$$

Equation (2.159) can now be rewritten as:

$$\frac{d\omega(\overline{I}_1)}{dI_1} = -\frac{2\pi}{T_1^2(k_1)}\frac{dT_1(k_1)/dk_1}{dI_1(k_1)/dK_1} \tag{2.163}$$

Note that explicit expressions for I_1 and T_1 as functions of k_1 are given by expressions (2.149) and (2.162) respectively. Hence, one can explicitly evaluate the right-hand side of equation (2.163):

$$\frac{d\omega(\overline{I}_1)}{dI_1} = -\frac{\pi[E(k_1)(1-2k_1^2) - K(k_1)(1-k_1^2)](1-2k_1^2)}{8K^3(k_1)k_1^2(1-k_1^2)} \tag{2.164}$$

where $E(\bullet)$ is the complete elliptic integral of the second kind. Thus, the right-hand sides of the averaged, hamiltonian equations (2.157) are explicitly known. In the previous section it was proven that for an (m/n) resonant torus, the associated Melnikov function has $2m$ simple zeros. Considering expression (2.161), note that:

$$1 - 2k_1^2 > 0 \quad for \quad h_1 > 0 \quad , \; and \quad lim_{h_1 \to -\infty} \; k_1^2 = \frac{1}{2} \tag{2.165}$$

For negative values of h_1 , one obtains values of k_1^2 less than $1/2$. Moreover, from simple properties of complete elliptic integrals (Byrd, 1954), it can be proven that the following inequalities hold:

$$E(k_1)(1 - 2k_1^2) - K(k_1)(1 - k_1^2) < E(k_1)(1 - k_1^2) - K(k_1)(1 - k_1^2) <$$

$$< [E(k_1) - K(k_1)](1 - k_1^2) < 0 \tag{2.166}$$

In deriving the aforementioned relations, use was made of the known inequality $E(k) - K(k) \; < \; 0$. Combining relations (2.165-166), one obtains the final basic result:

$$\frac{d\omega(\overline{I}_1)}{dI_1} > 0 \tag{2.167}$$

Considering now the averaged equations (2.157), and taking into account the inequality (2.167), one can prove that for positive (negative) values of $\overline{K}$, the variable $\overline{\psi}$ is a decreasing (increasing) function of the "time-like" variable θ_2:

$$sgn \; (\; \frac{d\overline{\psi}}{d\theta_2} \;) \; = \; - \; sgn \; (\; \overline{K} \;) \tag{2.168}$$

From the aforementioned discussion, one can draw a schematic representation of the phase plane of the averaged equations (2.157). From (2.168), the phase plane

is rotating counterclockwise with increasing θ_2, and its fixed points correspond to the zeroes of the Melnikov-function $\mathcal{M}$.

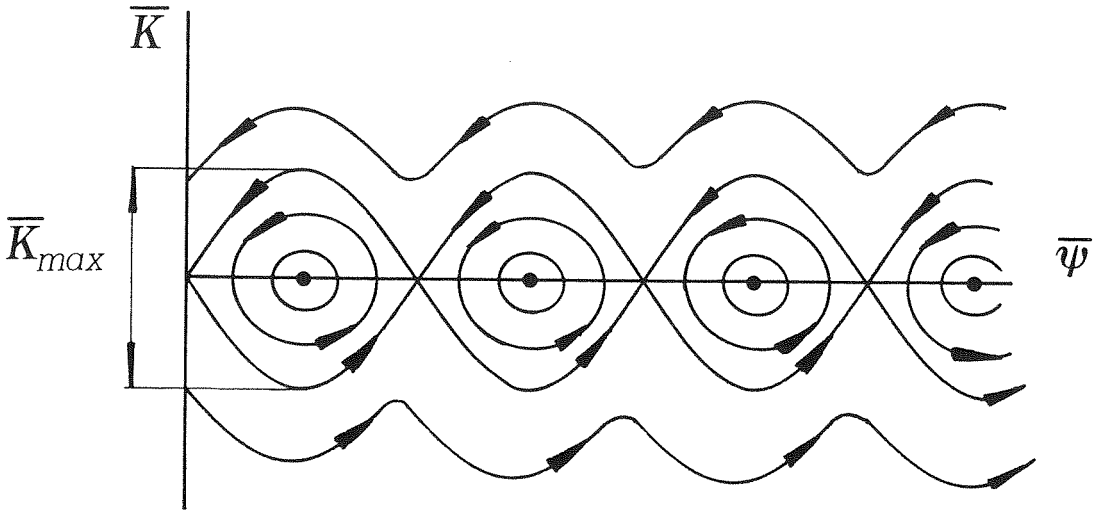

Figure 2.28. Phase plane of the averaged equations (2.157).

Half of the fixed points are elliptic (and thus orbitally stable), whereas the remaining ones are hyperbolic (orbitally unstable). The elliptic and hyperbolic points alternate and the averaging theorem does not guarantee that the families of heteroclinic orbits connecting the hyperbolic points are preserved as smooth manifolds. In fact, the stable and unstable manifolds of the hyperbolic points intersect transversely, leading to chaotic motions (that are confined between preserved "sufficiently irrational" KAM-tori). Unfortunately, one cannot analytically prove the existence of these transverse intersections by a Melnikov-type analysis, since the resulting Melnikov-functions become exponentially small as the perturbation parameter ϵ tends to zero.

Note that the elliptic points are surrounded by closed curves; these correspond to the "islands" observed in the numerical *Poincare'* plots. The maximum "island" width can be estimated from expression (2.158) (that gives the first integral of the averaged equations), by considering the level curves of $\overline{H}$ passing through the hyperbolic fixed points (Veerman, 1985):

$$\overline{K}_{max} = \{ \frac{2}{d\omega(\overline{I}_1)/dI_1} [max_{\overline{\psi} \in [0,2\pi)} (\int_0^{\overline{\psi}} \frac{\mathcal{M}(\frac{\eta}{\omega(\overline{I}_1)}, m, n, h)}{2\pi n} d\eta)] \} \quad (2.169)$$

To this order of approximation, only "primary islands" (Lichtenberg, 1983) are observed. However, by introducing new canonical transformations and rescaling, one could predict "secondary islands," within the "primary islands" of figure 2.28. It must be stated, however, that this type of averaging-analysis cannot model the ergodic motion ("sea of stochasticity") observed in the numerical *Poincare'* plots. This is because the averaged equations will always be of hamiltonian form and, as such, will always possess a first integral of motion. Thus, irrespective of the order of approximation, all curves in the averaged phase planes correspond to a fixed value of the first integral and no chaotic motions are possible.

2.5. CONCLUDING REMARKS

The free oscillations of a class of strongly nonlinear, discrete, hamiltonian oscillators were examined. These oscillators have a potential function that is symmetric with respect to the origin of the configuration space, and they possess normal modes of free oscillation, analogous to the ones observed in linear systems. The nonlinear normal modes can be either similar or nonsimilar, depending on the linearity or not of their modal curves in the configuration space. Similar normal modes can be conveniently studied by means of linear and nonlinear "balancing diagrams" and their stability can be approximately determined by means of a linearized, Mathieu-type analysis. It was found that, when a single balancing diagram exists, the stability of the resulting similar normal modes is independent of the energy of oscillation. This, however, is not the case for systems that possess more than one balancing diagrams.

The "balancing equations" that determine the similar normal modes form an overdetermined set of algebraic equations; as a result, similar normal modes can only exist if the structural parameters of the system satisfy special conditions. In that sense, it can be stated that similar normal modes are not generic in strongly nonlinear oscillators. However, in cases of oscillators with internal resonances (i.e., with special symmetries), similar normal modes can exist and, in fact, in certain cases they represent the only possible form of free oscillations for the system.

Nonsimilar normal modes are described by sets of nonlinear functional equations that are singular at the maximum equipotential surface of the oscillator. These

functional equations are complemented by boundary conditions that assure that the modal lines intersect the maximum equipotential surface orthogonally. Asymptotic approximations to the nonsimilar normal modes can be computed (valid in open intervals of values of the displacements), provided that the nonsimilar modes in question "neighbor" similar ones. In that case a perturbation scheme is developed that leads to analytic, asymptotic expressions for the nonsimilar modes, valid for small values of the displacements.

Not all nonlinear normal modes are analytic continuations of linear ones, because bifurcations of normal modes are possible in nonlinear systems. As a result, the total number of nonlinear modes may exceed the degrees of freedom (DOF) of the oscillator (this is in direct contrast to what is observed in linear systems). As the degree of nonlinearity of the system increases, the bifurcations of normal modes become more complex and the number of additional normal modes increases. For systems with cubic nonlinearity and "1-1 resonance," the bifurcating modes appear in reciprocal pairs, and a hamiltonian pitchfork bifurcation of modes exists. When seventh order nonlinearity is considered, two saddle node and one pitchfork bifurcation can be detected. When the symmetry of the oscillator is perturbed, so is the bifurcation diagram of the normal modes. For oscillators with a single "balancing diagram," the nongeneric pitchfork bifurcations break into saddle-node ones and the normal modes of the system do not appear anymore in reciprocal pairs.

The global dynamics of strongly nonlinear oscillators can be effectively studied by means of *Poincare'* maps. This numerical technique was implemented to the study

of a strongly nonlinear oscillator with two-DOF. For low energies, the dynamics of the system appear to be smooth and totaly predictable. In fact, it was shown that a two-timing perturbation technique can analytically describe any possible low-energy motion. A basic feature of the low energy map is the existence of a homoclinic orbit. This trajectory occurs only after the bifurcation of normal modes has taken place and results from the identification of the stable and unstable manifolds of the unstable antisymmetric normal mode. It is the destruction of this orbit that generates some of the chaotic motions observed in high-energy *Poincare'* maps.

When the energy of oscillation is increased, a "sea of stochasticity" appears in the maps, indicating the existence of random-like, highly unpredictable, chaotic motions. These occur due to the nonintegrability of the hamiltonian system (i.e., the non-existence of a second analytic integral of motion, independent from the energy).

Large and small-scale chaotic motions are identified in the high-energy *Poincare'* maps. The large-scale chaotic motions are a direct result of the pitchfork bifurcation of normal modes: they appear after the bifurcation, when the antisymmetric mode is orbitally unstable, and they result from the transverse intersections of the stable and unstable manifolds of the antisymmetric mode (i.e., the destruction of the low-energy homoclinic orbit of the antisymmetric mode). Local, small-scale chaotic motions result from the breakdown of "rational invariant tori" of the system. They appear close to subharmonic orbits of the oscillator and are confined in specific regions of the map.

Note that a necessary condition for large-scale chaos is the orbital instability of the antisymmetric mode (since only then can large-scale transverse intersections of invariant manifolds occur). Thus, the bifurcations of normal modes appear to increase the complexity of the high-energy, free motions of the oscillator and in fact, one can state that the system after the bifurcation of the normal modes becomes "more chaotic."

The subharmonic orbits generated from the destruction of the "rational invariant tori" of the oscillation were analytically examined by constructing suitable subharmonic Melnikov functions. In principle, a similar Melnikov-type perturbation analysis could be used to analytically prove the existence of transverse intersections between the stable and unstable manifolds of the antisymmetric mode. However, the resulting homoclinic Melnikov function becomes exponentially small as the perturbation parameter tends to zero, and this causes a failure of the perturbation scheme.

As a final remark, it must be stated that although the specific numerical applications of this work involve only systems with two-DOF, the outlined methodologies are general, and therefore they can be applied to the study of the free oscillations of hamiltonian oscillators with arbitrary DOF. Of course, as the number of DOF and the degree of nonlinearity increase, the resulting algebraic expressions and numerical computations are expected to become more complicated.

3. EXACT STEADY STATE OSCILLATIONS

3.1. CONCEPTS - PREVIOUS WORK

In this section, the steady state motions of undamped, forced, discrete oscillators will be examined. To achieve this, the notion of "exact steady state" will be used. This concept was first introduced by Rosenberg, and was implemented in the study of strongly nonlinear, discrete oscillators.

To demonstrate the concept of nonlinear "exact steady state motion," consider first the forced oscillation of a single-degree-of-freedom (SDOF) system. A preliminary definition of a "cosine-like" function is appropriate at this point:

A function $s(t)$ is said to be "cosine-like", if:

- $s(t)$ is analytic in $-\infty < t < +\infty$

- $s(0) = 1,\ \dot{s}(0) = 0$

- $s(t)$ is a periodic function of t with least period T, and moreover $s(T/4) = 0$

- $s(t) = -s(T/2 - t)$ for every value of t, and $s(t+\epsilon) < s(t)$ for $0 < t < t + \epsilon \leq T/4$

The differential equation of motion of a SDOF oscillator excited by a "cosine-like" function $Pg(t)$, with $P > 0$ a constant, is given by:

$$\ddot{x} + f(x) = Pg(t) \tag{3.1}$$

The solution $x(t)$ of (3.1) corresponding to initial conditions $x(0) = X, \dot{x}(0) = 0$, is said to be an "exact steady state" (Rosenberg, 1966) if and only if the quantity

$x(t)/X$ is "cosine-like," of the same period as $g(t)$. Note that although both $x(t)$ and $g(t)$ are "cosine-like," in the general nonlinear case their ratio is not necessarily a constant (as in linear theory), but it typically depends on time. In (Rosenberg, 1966), it is proven that if $g(t)$ is "cosine-like," then necessary conditions for the existence of a steady state solution of (3.1) is that $f(x)$ is an analytic, odd function of x, that increases monotonically as x increases, and satisfies the inequality, $xf(x) > 0$.

The concept of "exact steady state" can be extended to multi-DOF oscillators by introducing the following general definition.

DEFINITION (Rosenberg, 1966)

Consider the forced, n-DOF, nonlinear oscillator:

$$\underline{\ddot{x}} = \underline{f}(\underline{x}) + \underline{g}(t) \tag{3.2}$$

where $\underline{x} \in R^n$ is the displacement vector, $\underline{f} \in R^n$ is the vector of (nonlinear) stiffness forces, $\underline{g}(t) \in R^n$ is a periodic forcing vector of least period T, and $\ddot{(\ )} \equiv d^2/dt^2$.

System (3.2) is said to be in an "exact steady state," if and only if, it "vibrates in unison" having as least period that of the forcing function.

Hence, at an "exact steady state" the system vibrates in a normal mode motion, and the forced problem is transformed to an equivalent free oscillation one. Thus, the analytic techniques developed in the previous section can be implemented to the study of forced nonlinear motions. An interesting question concerns the effect that

normal modes of free oscillations have on the exact steady motions. In classical linear theory, any forced response can be expressed as a superposition of modal responses. Moreover, linear steady state (resonant) motions always occur in the neighborhood of classical normal modes.

In the nonlinear case the principle of superposition generally fails. However, as shown by (Rosenberg, 1966), resonant motions in multi-DOF systems always occur in the neighborhood of normal modes. This is demonstrated in (Yang, 1968), where a complete forced steady state analysis is undertaken for a planar oscillator. In the same reference, the stability of the steady state oscillations is approximately studied by means of *Mathieu* equations. The general problem of the existence of exact steady state motions is addressed in (Kinney, 1965), where geometrical methods in the configuration space are used. Since exact steady states always occur in the neighborhood of modal lines, the question of existence of steady state forced oscillations hinges entirely on that of existence of modal lines. In (Kinney, 1965,1966), a multi-DOF system under periodic excitation is examined, and a geometrical method is used to find the exact steady states. In a specific application, a "homogeneous" two-DOF oscillator with $k-th$ order nonlinearity is considered. Assuming the forcing to be proportional to the $k-th$ power of a "*cam*-function," explicit analytical expressions for the steady state solutions are derived. For $k=3$ (i.e., for cubic nonlinearity), the "frequency response curves" (maximum response versus frequency of oscillation) of the system are given. It is shown that there exist values of frequencies for which as many as five steady states occur. However, an approximate stability

analysis indicates that only three of these are orbitally stable.

In (Hsu, 1960), the exact steady state of an undamped Duffing oscillator is computed by considering special elliptic function forcings. Hsu demonstrated that the known approximate harmonic solutions derived by iteration-perturbation techniques can be recovered from the exact steady state expressions if one expands the elliptic response in terms of the elliptic modulus and allows the nonlinearities and/or the displacements to become small. In (Harvey, 1958), "natural forcing functions" proportional to the nonlinear restoring forces are considered and applied to the forced Duffing problem.

It must be pointed out that a variety of perturbation techniques exist for analyzing steady state motions of resonant oscillators (for example see (Nayfeh, 1979),(Bogoliubov, 1961)). However, these techniques are only valid for cases of "weak nonlinearity," i.e., for systems that neighbor linear ones. Under these conditions, the nonlinear response can be expressed in a series, whose first term is the "unperturbed" linear oscillation. It is clear that these approximate solutions fail to describe the dynamic response when systems with strong nonlinearities are encountered since in such cases the linear solutions cannot be used as a basis for perturbation expansions.

An interesting approximate analysis of the forced motion of a two-DOF, weakly nonlinear system subject to harmonic excitation appears in (Szemplinska, 1980). It is shown that the resonant response is close to the normal mode oscillation (in agreement with Rosenberg's prediction), and that jumps between resonant states can occur. The approximate harmonic results were then verified by means of ana-

log computations. The stability of nonlinear systems under periodic excitation was approximately examined in (Hsu, 1964). The analysis is based upon a variational system of equations and it is shown how to obtain a single matrix whose eigenvalues determine the stability or instability of the steady motion. Finally, a variety of references address the problem of existence and stability of forced subharmonic and superharmonic motions in weakly nonlinear, single-DOF oscillators (Caughey, 1954), (Hsu, 1959), (Kronauer, 1966), (Levenson, 1967), (Musa, 1968).

In what follows, the steady state motions of a class of two-DOF oscillators with strong nonlinearity are examined. The analysis is general, since it can be applied to compute the forced response of systems with arbitrary DOF. However, this will not be attempted here, since the new analytical techniques introduced herein can be best demonstrated by examining relatively simple systems. In analogy to the free oscillations of these systems, it will be demonstrated that both "similar" and "nonsimilar exact steady states" can exist. Similar steady states can be realized only for special forms of the forcing functions, whereas nonsimilar steady state motions exist for an entire class of periodic forces. In the sequence, similar and nonsimilar steady states are examined separately.

3.2. SIMILAR STEADY STATE OSCILLATIONS

A "similar steady state motion" is a motion that corresponds to a straight line in the configuration space of the system. Hence, in a similar steady state, the oscillator vibrates as in a similar normal mode of free oscillation, and all coordinates oscillate "in-unison" (note that in linear theory, the only possible steady states are similar motions).

Consider a two-DOF oscillator of the general class defined in section 2. Suppose that the system is excited by a periodic (but not necessarily harmonic) force $p(t)$ and that the unforced system is in "1-1 resonance" (i.e., its linearized eigenvalues are equal). The differential equations describing the motion of the system are then given by:

$$\begin{aligned} \ddot{x}_1 + f_1(x_1) + f_2(x_1 - x_2) &= p(t) \\ \ddot{x}_2 + f_1(x_2) - f_2(x_1 - x_2) &= 0 \end{aligned} \tag{3.3}$$

where $f_i(\bullet)$, $i = 1, 2$ represent the (nonlinear) stiffnesses. Equation (3.3) is solved with the following set of initial conditions:

$$\begin{aligned} x_1(0) &= X_1 \qquad \dot{x}_1(0) = 0 \\ x_2(0) &= X_2 \qquad \dot{x}_2(0) = 0 \end{aligned} \tag{3.4}$$

The analytic expressions that will be derived in the sequence correspond to the specific set of initial conditions (3.4). For different initial conditions, the results should be modified accordingly.

According to Rosenberg's definition, the steady state motion of a multi-DOF system under periodic forcing is a motion in which all coordinates vibrate "in-unison," and

the period of the response is identical to that of the force. The basic question concerning the similar steady state problem is as follows:

Given a prescribed set of initial conditions (such as (3.4)), what is the form of the excitation $p(t)$ required for a similar steady motion?

A first step in answering this problem is to consider the linear case:

$$f_i(u) = k_i^2 u \quad , \qquad i = 1, 2 \tag{3.5}$$

Substituting (3.5) in the differential equations of motion, a classical, linear vibration analysis leads to the following harmonic steady state solution (corresponding to initial conditions (3.4)):

$$\begin{aligned} x_1(t) &= X_1 cos\omega t \\ x_2(t) &= c x_1(t) \\ p(t) &= \hat{p}(x_1(t)) = \frac{P}{X_1} = P cos\omega t \end{aligned} \tag{3.6}$$

and

$$\begin{aligned} \omega^2 &= k_1^2 - k_2^2(\frac{1-c}{c}) \\ \frac{P}{X_1} &= k_1^2 + k_2^2(1-c) - \omega^2 \\ X_2 &= c X_1 \end{aligned} \tag{3.7}$$

The steady state solution (3.6-3.7) is commonly studied by the frequency-response curves (or resonance plots), and because of linearity all solutions are orbitally stable. Note that at the steady state the forcing function is related to the displacement by a functional relation $\hat{p}(\bullet)$, which is linear in this case. Another feature of the solution is that at the steady state, the two differential equations of motion decouple (as in

case of a normal mode), and the two displacements x_1, x_2 are linearly related for all times (similar oscillation).

From the aforementioned, it is evident that nonlinear similar steady state motions exist only if the force $p(t)$ is related to the steady state displacements by a certain functional relation, and the coordinates are linearly related for all times:

$$p(t) = \hat{p}(x_1(t))$$
$$x_2(t) = cx_1(t) \tag{3.8}$$

The functional relation is generally nonlinear, and c is a scalar constant. Hence, the problem of finding similar steady states is transformed to the equivalent problem of finding a functional $\hat{p}(\bullet)$ and a modal constant c that uncouple the forced equations of motion. It will be shown that in order to achieve a similar steady state oscillation, special forms of the functionals $\hat{p}(\bullet)$ are required. On the contrary, nonsimilar steady states occur for a whole class of forcing functions. This is in direct analogy to what was observed with similar and nonsimilar normal modes of free oscillation: similar modes were computed by an overdetermined set of algebraic "balancing equations" and they occurred only for special values of the structural parameters of the oscillator. Nonsimilar normal modes, however, were described by sets of singular functional equations and they were typical for the class of nonlinear systems under consideration.

A two-DOF nonlinear system with "1-1 resonance" is examined in the sequence. As shown earlier, this system has always two similar modes of free oscillation (the symmetric and antisymmetric ones), and depending on the linear term of the coupling stiffness, additional (bifurcating) modes may occur. Thus, it is necessary to

distinguish between two cases: oscillators with bifurcating normal modes (for example, systems that possess a single "balancing diagram"), and systems where no bifurcation of modes can occur (i.e., cases where multiple balancing diagrams exist).

3.2.1. OSCILLATORS WITH BIFURCATING NORMAL MODES

3.2.1.1. ANALYSIS

Assuming that the coupling stiffness $f_2(\bullet)$ does not contain any linear term, and considering general, $k-th$ order nonlinearity (with k odd), the differential equations of motion take the form:

$$\begin{aligned} \ddot{x}_1 + f_{11}x_1 + f_{1k}x_1^k + f_{2k}(x_1 - x_2)^k &= p(t) \\ \ddot{x}_2 + f_{11}x_2 + f_{1k}x_2^k + f_{2k}(x_2 - x_1)^k &= 0 \end{aligned} \tag{3.9}$$

It will be assumed from hereon that the stiffness coefficients f_{ij} are nonnegative quantities (this is dictated from physical considerations). The same analysis, however, can be applied when this assumption does not hold. It was shown earlier that the linear terms of system (3.9) are always "balanced," and thus only one "balancing diagram" (that of nonlinear terms) exists. Also, depending on the value of the ratio $K_k = f_{2k}/f_{1k}$, a bifurcation of normal modes may exist, its precise form depending on the degree of nonlinearity k.

Assuming a functional relation between force and steady state displacement of the form,

$$p(t) = \hat{p}(x(t)) = \left(\frac{P}{X_1}\right)^k x_1^k(t) \tag{3.10a}$$

and considering the "similar" modal relation $x_2(t) = c\ x_1(t)$, the equations of motion at the steady state, become:

$$\begin{aligned} \ddot{x}_1 + f_{11}x_1 + [f_{1k} + f_{2k}(1-c)^k - (\frac{P}{X_1})^k]x_1^k = 0 \\ \ddot{x}_1 + f_{11}x_1 + [f_{1k}c^{k-1} - f_{2k}\frac{(1-c)^k}{c}]x_1^k = 0 \end{aligned} \qquad (3.10b)$$

Both equations have x_1 as dependent variable and must be solved with initial conditions given by (3.4), with $X_2 = cX_1$. Observe that the forced problem has been converted to a free oscillation one, and steady state motions can exist, provided that the coefficients of the respective powers of x_1 are equal. For this system, the linear terms are identical for all values of c (this is not the case in the following section, where the coupling stiffness contains a linear term), and therefore, one must balance the coefficients of the $k-th$ powers of the displacement:

$$f_{1k} + f_{2k}(1-c)^k - (\frac{P}{X_1})^k = f_{1k}c^{k-1} - f_{2k}\frac{(1-c)^k}{c} \equiv \mu_k \qquad (3.11)$$

For a given initial amplitude X_1 and force amplitude P, one can compute the modal constant c from equation (3.11), the displacement $x_1(t)$ by integrating by quadratures any one of equations (3.10b), and the quantity $x_2(t)$ from the modal relation $x_2 = c\ x_1$. General analytic integration formulas can be found in Appendix A.

The frequency of the steady state oscillation can be determined by considering the "complete" integrals of Appendix A, and for this particular application it is expressed as follows :

$$\omega = \omega(X_1, P) = \frac{\pi\Omega^{1/2}}{2\int_0^{\pi/2} [\ 1 + \frac{2\mu_k X_1^{k-1} v_k(\phi)}{(k+1)\Omega}\ ]^{-1/2} d\phi} \qquad (3.12)$$

where

$$v_k(\phi) = \frac{1 - cos^{k+1}(\phi)}{1 - cos^2(\phi)}$$
$$\Omega(X_1, P) = f_{11} + \frac{2\mu_k}{k+1} X_1^{k-1} \tag{3.13}$$

Equation (3.12) relates the amplitude X_1 to the frequency of oscillation ω, for a fixed value of the forcing P. Thus, it represents the frequency response curves of the oscillator, in analogy to the classical resonance curves of the linear theory.

Note that for $P = 0$ (no excitation), expression (3.12) gives the so-called "backbone curves" of free oscillation. These curves represent the dependence of the amplitude of free oscillation on the frequency of the motion, and they are as many as the number of normal modes of the system. The corresponding free oscillation values of c can be found from expression (3.11) by setting $P = 0$. This equation has always the solutions $c = \pm 1$ (corresponding to the symmetric and antisymmetric modes), and depending on the value of $K_k = f_{2k} / f_{1k}$, additional (bifurcating) modes are possible. The conclusion is that by varying the value of the structural parameter K_k, one can change the number of backbone curves (normal modes) of the system and thus invoke changes in the topological portrait of the response curves (3.12). This fact will be demonstrated in the next section.

The necessary forcing $p(t)$ for a steady state motion is given by expression (3.10b). Moreover, this is the *only* form of forcing that leads to a similar steady state for the system under investigation. This can be proved by considering alternative forms for the excitation $p(t)$: then one finds that there are no real values for c that uncouple the resulting steady state differential equations of motion.

In (Kinney, 1965), a geometrical method in the configuration space was used to study the steady state motion of a "homogeneous" system, i.e., a system with all stiffnesses proportional to the same power of the displacement. The system was excited by a *cam*-function (Rosenberg, 1963), and the response was expressed in terms of a generalized frequency λ. For a fixed value of the nonlinearity k, it can be shown that the results obtained in the present work are identical to that reported in (Kinney, 1965), provided that one relates the generalized frequency λ and the parameter μ_k (of equation (3.11)) by the relation:

$$\mu_k = c^{k-1}\lambda^2$$

However, the analysis presented in this work is slightly more general, in the sense that one does not require "homogenuity" in the stiffnesses (in this work, the linear parts of the stiffness $f_1(\bullet)$, is nonzero, $f_{11} \neq 0$).

3.2.1.2. FREQUENCY RESPONSE CURVES

As an application of the aforementioned theory, consider the case $k = 3$ (cubic nonlinearities). In this case, equation (3.11) becomes:

$$f_{13} + f_{23}(1-c)^3 - \left(\frac{P}{X_1}\right)^3 = f_{13}c^2 - f_{23}\frac{(1-c)^3}{c} \equiv \mu_3 \tag{3.14}$$

Equations (3.10b), combined with the set of initial conditions (3.4), lead to the following expression for the displacement $x_1(t)$ at the steady state:

$$\begin{aligned} x_1(t) &= X_1\ cn\ (\left[f_{11} + \mu_3 X_1^2\right]^{1/2} t\ ,\ k_1)\ ,\ \mu_3 > 0 \\ x_1(t) &= X_1\ sn\ (\left[f_{11} + \mu_3 X_1^2/2\right]^{1/2} t + K(k_2)\ ,\ k_2)\ ,\ 0 > \frac{\mu_3 X_1^2}{f_{11}} > -1 \end{aligned} \tag{3.15}$$

where $cn(\bullet,\bullet), sn(\bullet,\bullet)$ are elliptic functions (Byrd, 1956), $K(\bullet)$ is the complete elliptic integral of the first kind, and k_1, k_2 are elliptic moduli given by:

$$\begin{aligned} k_1^2 &= \frac{\mu_3 X_1^2}{2(f_{11} + \mu_3 X_1^2)} \\ k_2^2 &= \frac{-\mu_3 X_1^2}{2f_{11} + \mu_3 X_1^2} \end{aligned} \tag{3.16}$$

Note that in the above solutions, the possibility of unbounded motions (corresponding to values of μ_3 such that $\mu_3 X_1^2 \ / \ f_{11} \ < \ -1$) is excluded. This is because such motions cannot be realized for the oscillator under consideration (this statement will be mathematically proved later). The frequency-response curves at the steady state are computed by setting $k = 3$ in the general expressions (3.12-13):

$$\begin{aligned} \omega &= \frac{\pi(f_{11} + \mu_3 X_1^2)^{1/2}}{2K(k_1)} \quad , \quad \mu_3 > 0 \\ \omega &= \frac{\pi(f_{11} + \mu_3 X_1^2/2)^{1/2}}{2K(k_2)} \quad , \quad 0 > \frac{\mu_3 X_1^2}{f_{11}} > -1 \end{aligned} \tag{3.17}$$

where $K(\bullet)$ is the complete elliptic integral of the first kind, and the variable μ_3 is computed from equations (3.14).

In figure 3.1, the root c of equation (3.14) is schematically presented as a function of the structural parameter $K_3 \ = \ f_{23} \ / \ f_{13}$, for fixed values of P and X_1. These diagrams are the "forced balancing diagrams" of cubic terms and are analogous to the diagrams used for studying the normal modes of free oscillation. Note that since the coupling stiffness of the oscillator, $f_2(\bullet)$ (see equations (3.3) and (3.9)), does not contain any linear term, no linear diagram exists for the oscillator under consideration (this is because the linear terms in equations (3.10b) balance for every value of c).

Figure 3.1a, corresponds to zero forcing, and thus gives the modes of free oscillation of the system. Observe that at $K_3 = 1/4$, a pitchfork bifurcation occurs, and the antisymmetric mode exchanges stability becoming orbitally unstable. This means that depending on the ratio K_3 of the coefficients of the cubic terms of the stiffnesses, the system can have either two or four backbone curves (normal modes). In the latter case, one of the backbone curves represents orbitally unstable motions.

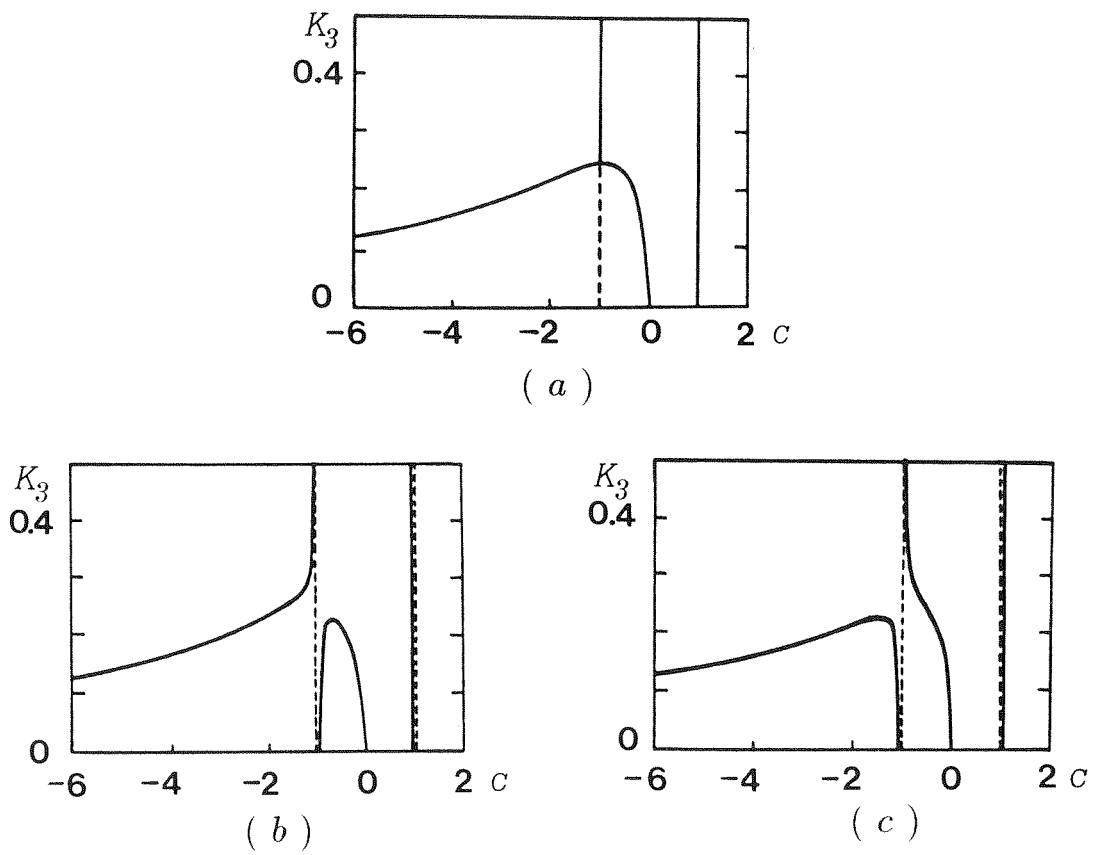

Figure 3.1. Forced balancing diagrams of the system with cubic nonlinearities : (a) $P = 0$ (b) $P/X > 0$ (c) $P/X < 0$.

When a forcing $P \neq 0$ is applied, figures 3.1b,c result, and it can be seen that the

pitchfork bifurcation is perturbed. In these diagrams, c denotes the value of the modal parameter for a steady state motion. For values of K_3 greater than $1/4$, one obtains at most two values for c, whereas for K_3 less than $1/4$, four such values exist. From these observations, one has a first indication that the topological portrait of the response curves changes quantitatively as K_3 is decreased below the bifurcation value $K_3 = 1/4$.

In figures 3.2 and 3.3, the frequency response curves (or resonance plots), are presented. Both diagrams correspond to the same value of the forcing amplitude $P = 0.5$, and the same values of the structural parameters $f_{11} = f_{13} = 1$. The response curves of figure 3.2 correspond to $K_3 = 0.4$ (where two normal modes exist), whereas those of figure 3.3 to $K_3 = 0.15$ (with four normal modes). To construct these curves, assign values to the initial condition X_1 and compute c and μ_3 from equations (3.14). Finally, evaluate the frequency of steady state motion from formulas (3.17).

Note the difference in the topology of the two sets of response curves. In the set of figure 3.2, there are two backbone curves (both orbitally stable), and at most five steady state solutions exist for a particular value of the frequency ω. In figure 3.3, however, a bifurcation of normal modes has occurred, giving rise to four backbone curves (of which one is orbitally unstable). Thus, the portrait of the response curves is much more complicated than in the previous case, and for a fixed value of the frequency, at most nine steady state solutions may occur. Therefore, it is concluded that the bifurcation of normal modes effects drastically the steady state

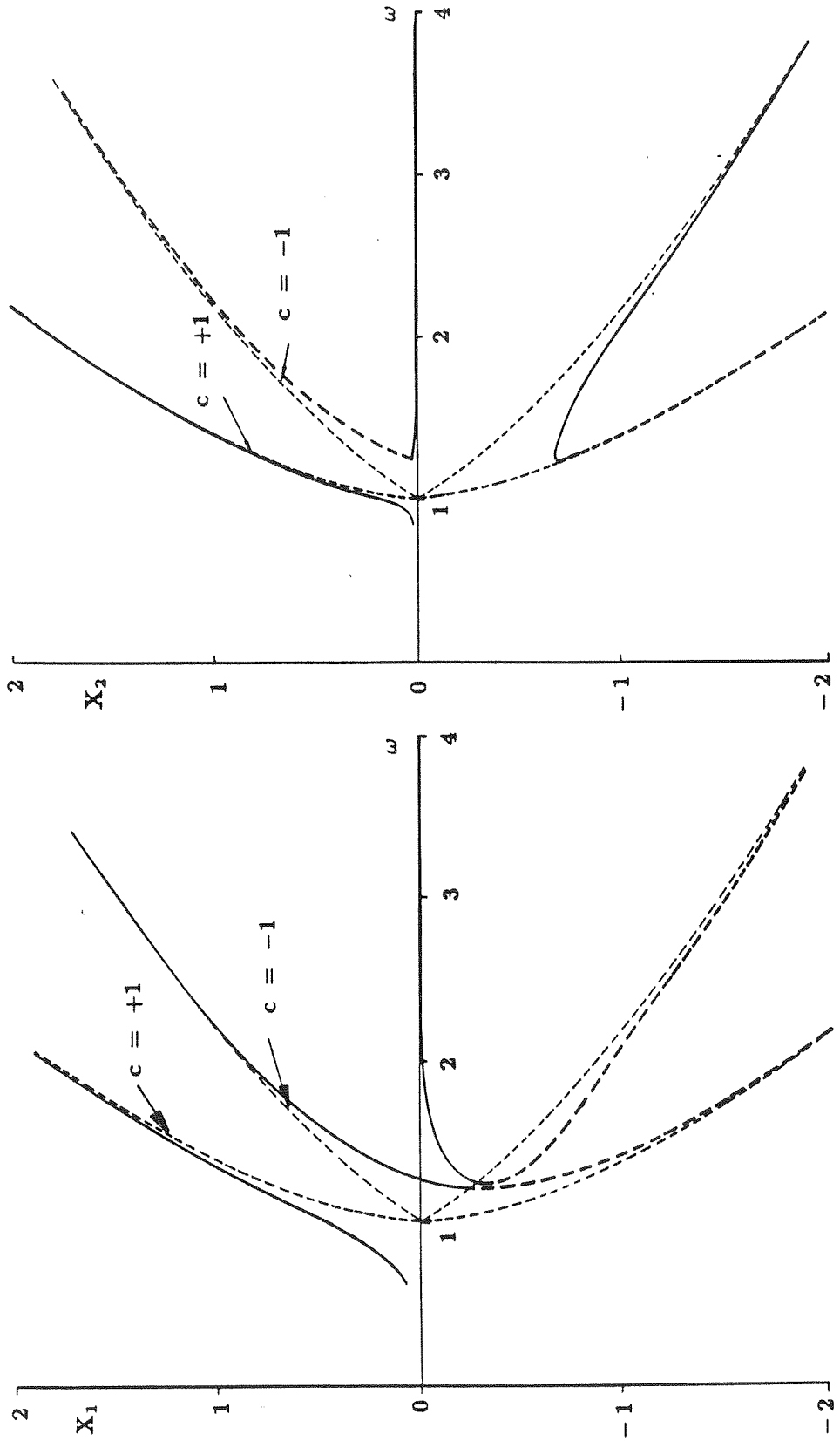

Figure 3.2. Frequency response curves corresponding to $K_3 = 0.40 > 1/4$.

Stable solutions ——— Unstable solutions - - - - - - - - - -

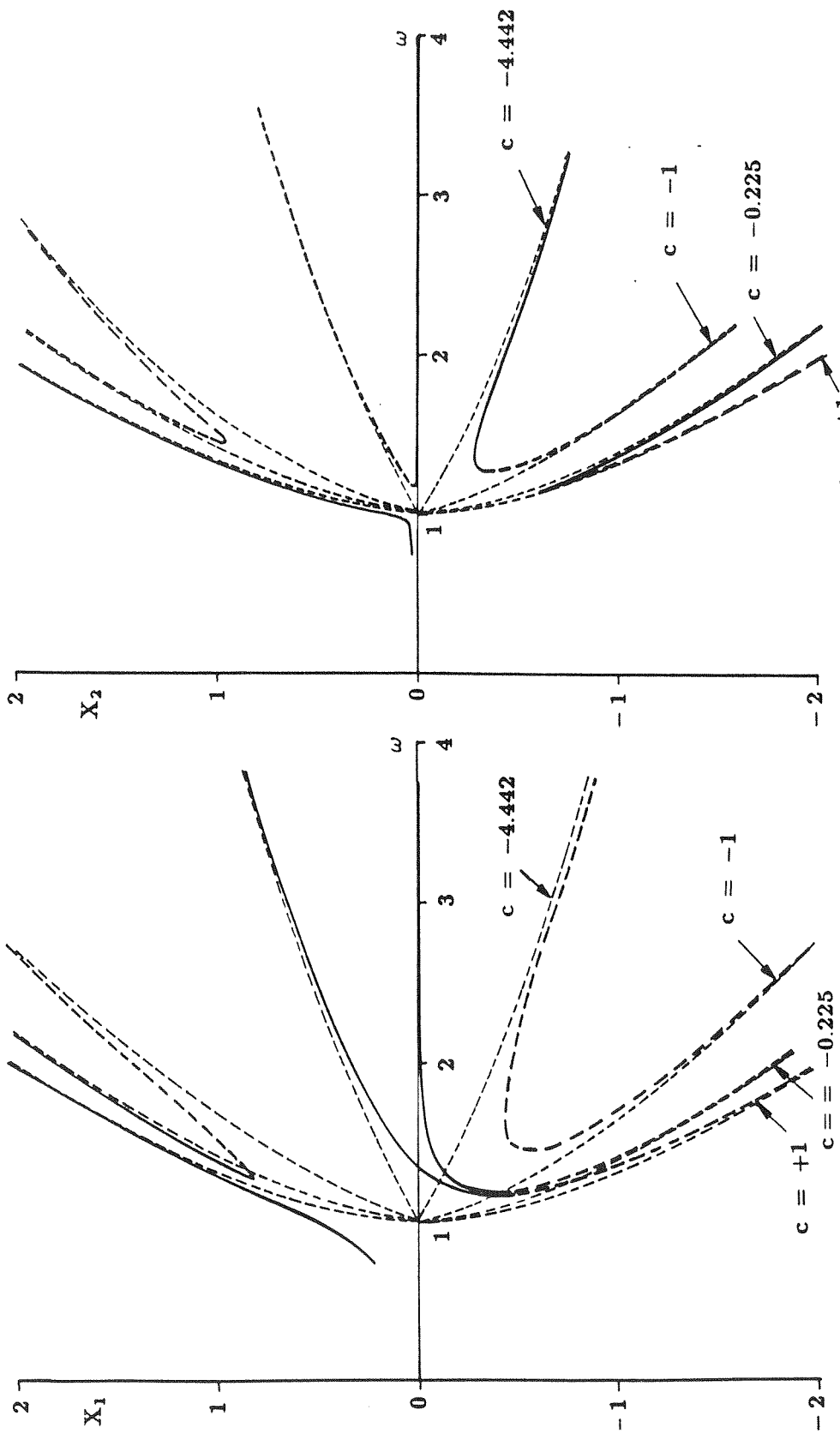

Figure 3.3. Frequency response curves corresponding to $K_3 = 0.15 < 1/4$.

Stable solutions ——— Unstable solutions - - - - - - - - - -

response of the oscillator. Note that since the oscillator under consideration is in "1-1 resonance," its dynamics are particularly "rich." For an oscillator which is "off-resonance" (i.e, with unequal linearized eigenvalues), one should expect less complicated steady-state response curves.

As far as the displacements of the system are concerned, one has to consider three distinct cases, depending on the value of the ratio of the frequency of oscillation ω over the square root of the linear term of spring $f_1(\bullet)$, $f_{11}^{1/2}$.

(a) Hardening Duffing response

If $\omega / f_{11}^{1/2} > 1$, then $\mu_3 > 0$, and the displacement $x_1(t)$ is obtained from the first of equations (3.15). The variable $x_2(t)$ is then computed from the modal relation $x_2 = c\, x_1$. The force necessary for the steady state is then :

$$p(t) = (\frac{P}{X_1})^3 x_1^3(t) \tag{3.18}$$

(b) Softening Duffing response

If $\omega / f_{11}^{1/2} > 1$, then $-f_{11} / X_1^2 < \mu_3 < 0$, and one has to use the second of equations (3.15) to compute $x_1(t)$. Note that

$$lim_{\mu_3 \to -f_{11}/X_1^2}\ k_2^2 = 1 \quad \Rightarrow \quad lim_{\mu_3 \to -f_{11}/X_1^2}\ K(k_2) = +\infty \tag{3.19}$$

Hence, it is concluded that

$$lim_{\omega \to 0}\ \mu_3 = -\frac{f_{11}}{X_1^2} \tag{3.20}$$

and as a result, no unbounded motions can be realized for the oscillator under

consideration (since this can only happen for $\mu_3 < -f_{11} / X_1^2$, which, in view of relation (3.19), implies that the frequency of oscillation ω is a negative quantity).

(c) *Harmonic response*

For the special case value of the frequency, $\omega = f_{11}^{1/2}$, one obtains $\mu_3 = 0$, and in that case the system responds harmonically:

$$x_1(t) = X_1 \, cos(f_{11}^{1/2} t) \; , \quad x_2(t) = c x_1(t) \tag{3.21}$$

$$c = \; [\; 1 + (f_{13}/f_{23}) \;]^{-1} \tag{3.22}$$

$$X_1 = P/(1+c) f_{13}^{1/3}$$

The necessary force for the harmonic steady state is then:

$$p(t) = P^3 cos^3(f_{11}^{1/2} t) \tag{3.23}$$

Note that these harmonic solutions are exact (since no approximation concerning the magnitude of the nonlinearity and the amplitude was made), but are only valid for a particular value of the frequency ω. Small perturbations of this value lead to softening- or hardening-type motions.

3.2.1.3. STABILITY ANALYSIS

The stability of the identified steady state periodic solutions is now examined, by introducing small perturbations in the exact steady state solutions (from this point, the steady state displacements for x_1, x_2, given by equations (3.15), will be denoted by $\hat{x}_1(t)$,and $\hat{x}_2(t)$ respectively):

$$\begin{aligned} x_1(t) &= \hat{x}_1(t) + \xi(t) \\ x_2(t) &= \hat{x}_2(t) + \eta(t) \end{aligned} \tag{3.24}$$

Substituting (3.24) into the forced equations of motion (3.9), and retaining only terms of first order in ξ and η, one obtains:

$$\begin{aligned} \ddot{\xi} + [f_{11} + 3f_{13}\hat{x}_1^2 + 3f_{23}(\hat{x}_1 - \hat{x}_2)^2]\xi - 3f_{23}(\hat{x}_1 - \hat{x}_2)^2\eta = 0 \\ \ddot{\eta} + [f_{11} + 3f_{13}\hat{x}_2^2 + 3f_{23}(\hat{x}_2 - \hat{x}_1)^2]\eta - 3f_{23}(\hat{x}_2 - \hat{x}_1)^2\xi = 0 \end{aligned} \tag{3.25}$$

Taking into account that at the exact steady state the relation $\hat{x}_2 = c\hat{x}_1$ holds, equations (3.25) are written as:

$$\begin{aligned} \ddot{\xi} + [f_{11} + 3f_{13}\hat{x}_1^2 + 3f_{23}(1-c)^2\hat{x}_1^2]\xi - 3f_{23}(1-c)^2\hat{x}_1^2\eta = 0 \\ \ddot{\eta} + [f_{11} + 3f_{13}c^2\hat{x}_1^2 + 3f_{23}(c-1)^2\hat{x}_1^2]\eta - 3f_{23}(c-1)^2\hat{x}_1^2\xi = 0 \end{aligned} \tag{3.26}$$

This is a set of coupled *Hill* equations that possess normal solutions (Kinney, 1965). Moreover, since the equations are linear, all their solutions can be expressed as linear combinations of the normal ones. Thus, the question of stability of $\xi(t)$ and $\eta(t)$ is reduced to the determination of the stability of the normal solutions of (3.26). These solutions are computed by requiring that (Kinney, 1965),

$$\eta(t) = K\xi(t) \tag{3.27}$$

and substituting this relation into (3.26), the following expressions result :

$$\begin{aligned} \ddot{\xi} + [f_{11} + 3f_{13}\hat{x}_1^2 + 3f_{23}(1-c)^2\hat{x}_1^2]\xi - 3f_{23}(1-c)^2\hat{x}_1^2 K\xi = 0 \\ \ddot{\xi} + [f_{11} + 3f_{13}c^2\hat{x}_1^2 + 3f_{23}(c-1)^2\hat{x}_1^2]\xi - \frac{3f_{23}(c-1)^2\hat{x}_1^2}{K}\xi = 0 \end{aligned} \tag{3.28}$$

These equations lead to identical solutions for $\xi(t)$, provided that the coefficients of $\xi(t)$ in both relations are equal. Imposing this condition, the following real values for K result:

$$K_{1,2} = \frac{f_{13}(1-c^2)}{2f_{23}(1-c)^2} \pm \left\{ 1 + \frac{f_{13}(1-c^2)}{2f_{23}(1-c)^2} \right\}^{1/2} \tag{3.29}$$

The normal solutions can then be computed from any one of equations (3.28), by setting $K = K_i,\ i = 1, 2$:

$$\ddot{\xi}_i + [\ f_{11} + (3f_{13} + 3f_{23}(1-c)^2 - 3f_{23}(1-c)^2 K_i)\hat{x}_1^2\ ]\xi_i = 0\ ,\ i = 1, 2 \qquad (3.30)$$

Finally, the solutions of the variational equations (3.26) are expressed as linear combinations of the normal solutions:

$$\begin{aligned} \xi(t) &= \xi_1(t) + \xi_2(t) \\ \eta(t) &= K_1\xi_1(t) + K_2\xi_2(t) \end{aligned} \qquad (3.31)$$

The stability of the variational equations (3.30) will be approximately examined by linearizing the response of the system. In order to achieve this, one expands the exact steady state solution $\hat{x}_1(t)$ in Fourier series and retains only the first harmonic terms to obtain the following approximate expression:

$$\hat{x}_1(t) = X_1 cos\omega t + \mathcal{O}(k^2) \qquad (3.32)$$

where k^2 is the square of the elliptic modulus, assumed to be of perturbation order. Substituting (3.32) into (3.30) and introducing the new time variable $\tau = \omega\, t$, one obtains the following approximate *Mathieu* equation:

$$\xi_i'' + (\delta_i + 2\zeta_i cos2\tau)\xi_i = 0\ \ ,\ \ i = 1, 2 \qquad (3.33)$$

where ξ is considered to be a function of τ and $(\bullet)'' \equiv d^2/d\tau^2$. The coefficients of the *Mathieu* equation are given by

$$\delta_i = \frac{f_{11}}{\omega^2} + \frac{\Lambda_i X_1^2}{2\omega^2}\ \ ,\ \ \zeta_i = \frac{\Lambda_i X_1^2}{4\omega^2}$$

$$\Lambda_i = 3f_{13} + 3f_{23}(1-c)^2 - 3f_{23}(1-c)^2 K_i$$

and the quantities K_i are computed from equation (3.29).

The stability analysis of equations (3.33) can be carried out by examining their stability characteristics in the *Stutt* diagram, in an exactly analogous way with that followed in section 2.2., where the linearized stability analysis of the normal modes of the same system was carried out.

The results of the stability analysis are presented at figures 3.2 and 3.3. From the diagrams of figure 3.2, observe that from a maximum of five steady state solutions, only three are orbitally stable. In figure 3.3, from a maximum of nine steady states, only four are orbitally stable. An interesting remark concerning the plots of figure 3.3 is that all steady state solutions neighboring the orbitally unstable backbone curve (of the antisymmetric mode) are also orbitally unstable. This leads to the conclusion that no stable steady motion can result in the vicinity of an orbitally unstable free oscillation. Finally, note that since no damping is present in the models, the phases of the steady states can only be 0 or 180 degrees.

Concluding the analysis of this section, it must be stated that response curves similar to those of figure 3.2 were reported elsewhere (Kinney, 1965) for "homogeneous" oscillators. However, in that reference, the stiffnesses did not contain any linear terms ($f_{11} = 0$) so that the backbone curves started from the origin of the frequency response diagrams. Thus, no softening-type or harmonic responses were possible, and the system had only hardening-type motions.

3.2.2. OSCILLATORS WITH NO BIFURCATING NORMAL MODES

3.2.2.1. COMPUTATION OF SIMILAR STEADY STATE SOLUTIONS

The examination of the similar steady motions of this class of systems has to be carried out on a case by case basis. To demonstrate the analysis, consider the "1-1 resonant" oscillator of the previous section, with differential equations of motion given by (3.3). In this case, however, it is assumed that the coupling stiffness $f_2(\bullet)$ contains a linear term:

$$\begin{aligned} f_1(u) &= f_{11}u + f_{13}u^3 \\ f_2(u) &= f_{21}u + f_{23}u^3 \end{aligned} \tag{3.34}$$

In section 2, it was shown that the presence of the linear term, $f_{21}\ u$, restricts the possible number of the normal modes of the system to two (the symmetric and antisymmetric ones). Therefore, in this case it is necessary to consider a forcing function $p(t)$ related to the steady state displacement by a functional relation of the form:

$$p(t) = \hat{p}(x_1(t)) = (\frac{P_1}{X_1})x_1(t) + (\frac{P_3}{X_1^3})x_1^3(t) \tag{3.35}$$

It will be shown that the functional relation (3.35) is the only one capable of producing a similar steady state oscillation. To prove this statement, the relation $x_2 = c\,x_1$ (that corresponds to a similar motion) is substituted into the equations of motion. Then, the following set of equations is obtained:

$$\begin{aligned} \ddot{x}_1 + x_1[f_{11} + f_{21}(1-c) - \frac{P_1}{X_1}] + x_1^3[f_{13} + f_{23}(1-c)^3 - \frac{P_3}{X_1^3}] = 0 \\ \ddot{x}_1 + x_1[-f_{21}(\frac{1-c}{c}) + f_{11}] + x_1^3[f_{13}c^2 - f_{23}\frac{(1-c)^3}{c}] = 0 \end{aligned} \tag{3.36}$$

where the usual set of initial conditions (3.4) is assumed, with $X_2 = cX_1$. To obtain a similar steady state oscillation, one requires that the coefficients in (3.36) of respective powers of x_1 be equal:

$$\begin{aligned} f_{11} + f_{21}(1-c) - \frac{P_1}{X_1} &= -f_{21}(\frac{1-c}{c}) + f_{11} = \lambda^2 \\ f_{13} + f_{23}(1-c)^3 - \frac{P_3}{X_1^3} &= f_{13}c^2 - f_{23}\frac{(1-c)^3}{c} = \mu^2 \end{aligned} \tag{3.37}$$

One imposes the additional restrictions that the above quantities be positive in order to investigate the "hardening-Duffing" response of the oscillator ($\mu^2 > 0$). However, a similar treatment can be followed for the examination of possible "softening-Duffing" responses (in that case one requires that the terms in the second of equations (3.37) be equal to $-\mu^2$).

In figures 3.4a and 3.4b, the roots c of equations (3.37) are presented as functions of the ratios $K_1 = f_{21}/f_{11}$ and $K_3 = f_{23}/f_{13}$, respectively. For fixed values of the forcings P_1, P_3, two such diagrams exist. The linear diagram represents solutions of the first equation of the set (3.37) (balancing the linear stiffness terms of the system), whereas the cubic diagram corresponds to the solutions of the second of equations (3.37) (balancing the cubic stiffness terms). For unforced motions ($P_1 = P_3 = 0$), the values of c satisfying both the linear and cubic diagrams are restricted to ± 1, corresponding to the symmetric and antisymmetric modes of free oscillation. When a forcing is applied, the balancing diagrams are perturbed, and it is necessary that the steady values of c satisfy both of them simultaneously.

Hence, in order for a steady state motion to exist, both balancing diagrams must be perturbed, and this is only achieved with a forcing of the form (3.35). This is

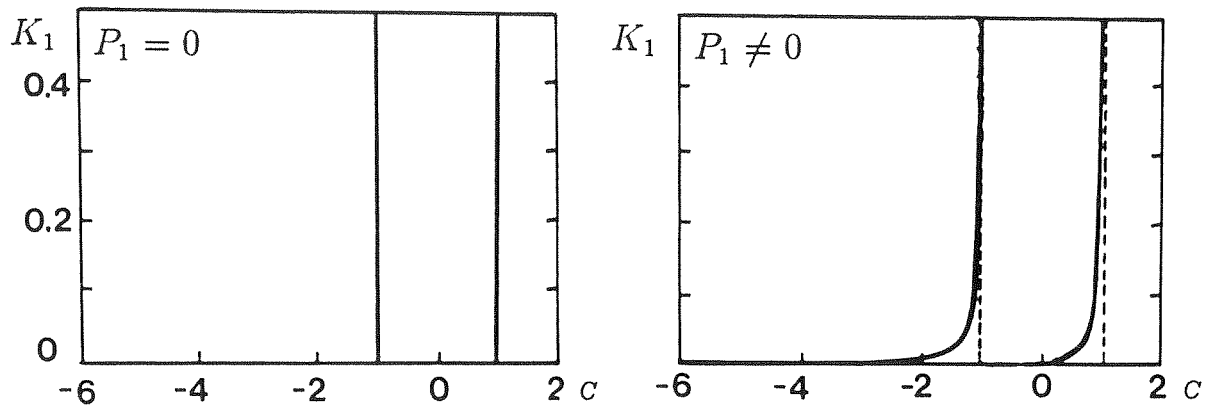

(a)

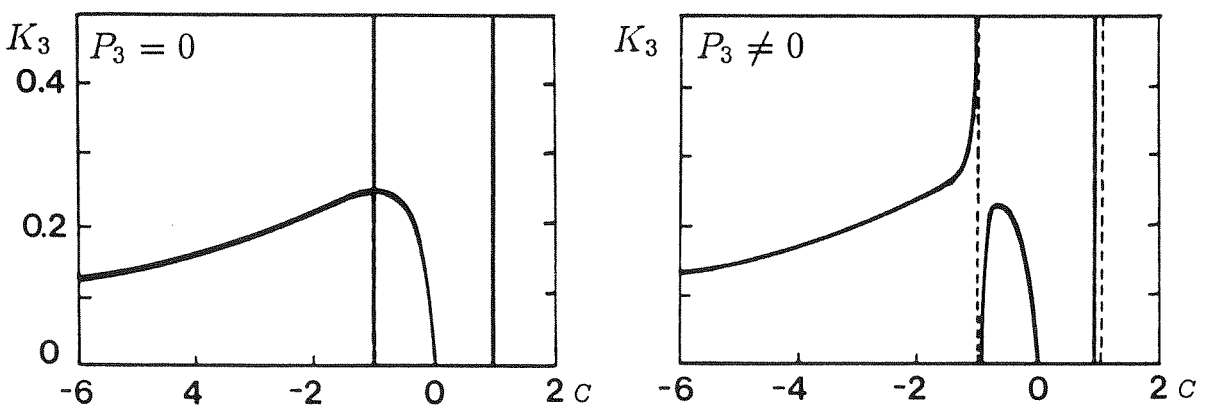

(b)

Figure 3.4. (a) Forced ($P_1 \neq 0$), and unforced ($P_1 = 0$) linear balancing diagrams.

(b) Forced ($P_3 \neq 0$), and unforced ($P_3 = 0$) cubic balancing diagrams.

because the force should contain a linear term (that distorts the linear diagram) as well as a cubic term in the displacement (that distorts the cubic diagram). It can be concluded, therefore, that when a system has more than one balancing diagram of free oscillation, the steady state excitation should be such as to perturb all these diagrams simultaneously. Thus, the necessary force for an exact steady state should be expressed in a series form, the number of terms depending in the number of the balancing diagrams. Moreover, each term of the series should be proportional to a power of the displacement that is equal to the nonlinearity of the balancing diagram that it perturbs.

Taking into account expressions (3.37), the steady state response of the oscillator is computed as follows:

$$x_1(t) = X_1 cn(qt, k) \quad , \qquad x_2(t) = c x_1(t) \tag{3.38}$$

where

$$q^2 = \lambda^2 + \mu^2 X_1^2 \quad , \quad k^2 = \mu^2 X_1^2 / 2q^2 \tag{3.39}$$

and

$$\begin{aligned} c &= f_{21}/(f_{11} + f_{21} - \lambda^2) \\ P_1/X_1 &= (f_{11} - \lambda^2)(f_{11} + 2f_{21} - \lambda^2)/(f_{11} + f_{21} - \lambda^2) \\ \mu^2 &= (f_{13} f_{21}^3 - f_{23}(f_{11} - \lambda^2)^3)/f_{21}(f_{11} + f_{21} - \lambda^2)^2 \\ P_3/X_1^3 &= f_{13} + f_{23}(1 - c)^3 - \mu^2 \end{aligned} \tag{3.40}$$

Note that all variables in relations (3.40) are expressed in terms of the quantity λ^2, and this is related to the frequency of steady state oscillation, ω, by:

$$\omega = \frac{\pi q}{2K(k(\lambda))} = \frac{\pi[\lambda^2 + \mu(\lambda)^2 X_1^2]^{1/2}}{2K(k(\lambda))} \tag{3.41}$$

where the usual notation for the complete elliptic integral of the first kind and the elliptic modulus have been used. Expression (3.41) relates the amplitude of the steady state oscillation, X_1, to the frequency ω ; therefore, it represents the steady state frequency response curves of the system. The force is computed by combining equations (3.35) and (3.38):

$$p(t) = P_1 cn(qt, k) + P_3 cn^3(qt, k) \tag{3.42}$$

When no force is applied, i.e., when $P_1 = P_3 = 0$, equations (3.38-41) lead to the free oscillation solution. As mentioned earlier, two such motions exist for the oscillator under consideration:

$$\begin{aligned} &c = +1,\ \lambda^2 = f_{11},\ \mu^2 = f_{13}\ \ (Symmetric\ mode) \\ &c = -1,\ \lambda^2 = f_{11} + 2f_{21},\ \mu^2 = f_{13} + 8f_{23}\ \ (Antisymmetric\ mode) \end{aligned} \tag{3.43}$$

Using these expressions for λ^2 and μ^2, one can compute the "backbone" response curves from equation (3.41). As long as the linear coefficient of the stiffness $f_2(\bullet)$, is nonzero, one obtains only two such curves, one corresponding to $c = +1$, and the other to $c = -1$. Therefore, in contrast to what was found in the previous section, the topological portrait of the frequency response curves *does not change* when a structural parameter of the oscillator changes. This is a direct result of the fact that no bifurcation of modes is possible for the system under consideration, and thus, no additional "backbone" curves can exist.

Consider now the case where $P_1,\ P_3 \neq 0$. Relations (3.40) indicate that if either one of P_1 or P_3 is taken as a constant, the other must be made dependent on the frequency of oscillation, ω. This leads to difficulties of interpretation of the similar steady state solution, since one has to define an acceptable constant "forcing

amplitude" for the excitation. To resolve this issue, one can use the perturbation methodology of (Hsu, 1960) who studied the exact steady state of a single-degree-of-freedom (SDOF) oscillator (this perturbation analysis is performed in the next section). Note that although solution (3.38-41) is difficult to interpret physically, nevertheless it is an exact similar steady state solution for the (strongly) nonlinear problem. Moreover, it will be proved that, as the nonlinearities of the system become small, the derived solution degenerates to the well known approximate harmonic oscillation of the weakly nonlinear oscillator that are obtained by standard, approximate techniques.

As a last remark, note that the forcing form (3.42) is the only one leading to a similar steady state motion. If the excitation is taken to be merely proportional to the steady displacement, and the similar condition is imposed, one finds a "pseudo-steady state" oscillation, namely a periodic motion valid only for a particular value of the frequency ω (Vakakis, 1988). However, there exists an infinite set of periodic excitations that lead to nonsimilar steady motions.

3.2.2.2. PERTURBATION ANALYSIS

The analysis of this section is similar to that carried in (Hsu, 1960), where the forced motion of a strongly nonlinear SDOF oscillator is examined. In order to justify the perturbation method, it is necessary that the nonlinearities and/or the displacements of the system be small, so that the quantities $f_{i3}\ X_1^2,\ i = 1, 2$, be of

perturbation order:

$$0 < f_{i3} X_1^2 \ll 1 \quad , i = 1,2 \tag{3.44}$$

Since the coefficients of the linear terms of the stiffnesses are finite quantities (i.e., $f_{i1} = \mathcal{O}(1)$, $i = 1,2$), assumptions (3.44) indicate that the elliptic modulus squared, k^2, is also of perturbation order (see expressions (3.39)). Thus, one can consider a perturbation expansion of the elliptic functions with respect to their modulus, and retain only terms of order up to k^2. This is done in Appendix C; substituting the associated Fourier expressions in equation (3.42), one obtains:

$$p(t) = P_1(a_1 cos\omega t + a_3 cos3\omega t) + P_3(b_1 cos\omega t + b_3 cos3\omega t) + \mathcal{O}(k^4) \tag{3.45}$$

where the coefficients of the Fourier series, a_i and b_i, can also be expanded in powers of k^2, as follows :

$$\begin{aligned} a_1 &= 1 - \frac{k^2}{16} + ... \\ a_3 &= \frac{k^2}{16} + ... \\ b_1 &= \frac{3}{4} - \frac{35k^2}{64} + ... \\ b_3 &= \frac{1}{4} + \frac{6k^2}{128} + ... \end{aligned} \tag{3.46}$$

Eliminating the quantity λ^2 from the expressions of P_1 and P_3 (equations (3.40)), and rearranging terms, one obtains the following formulas for the forces:

$$\begin{aligned} \frac{P_3}{X_1^3} &= f_{13} + f_{23}(1-c)^3 - (\frac{2k^2q^2}{X_1^2}) \\ \frac{P_1}{X_1} &= (2k^2 - 1)q^2 + f_{11} + f_{21}(1-c) \end{aligned} \tag{3.47}$$

Substituting for P_1 and P_3 in equations (3.45), one gets an expression for the force acting to the system, correct to $\mathcal{O}(k^2)$:

$$p(t) = \{\mathcal{A}_1 X_1 + \mathcal{A}_3 X_1^3\} cos\omega t + \{\mathcal{B}_1 X_1 + \mathcal{B}_3 X_1^3\} cos3\omega t + \mathcal{O}(k^4) \tag{3.48}$$

where

$$\mathcal{A}_1 = [(2k^2 - 1)q^2 + f_{11} + f_{21}(1-c)]a_1$$

$$\mathcal{A}_3 = [f_{13} + f_{23}(1-c)^3 - \frac{2k^2q^2}{X_1^2}]b_1$$

$$\mathcal{B}_1 = [(2k^2 - 1)q^2 + f_{11} + f_{21}(1-c)]a_3$$

$$\mathcal{B}_3 = [f_{13} + f_{23}(1-c)^3 - \frac{2k^2q^2}{X_1^2}]b_3$$

A similar expansion in terms of k^2 can be carried out for the response of the system $x_1(t)$ (equation (3.38)):

$$x_1(t) = a_1 X_1 cos\omega t + a_3 X_1 cos3\omega t + ... = X_1 cos\omega t + \mathcal{O}(k^2) \tag{3.49}$$

From expression (3.49), it can be concluded that for k^2 sufficiently small, the system response contains a dominant harmonic term of frequency ω, and small additional higher harmonic terms. Moreover, if one requires that

$$\begin{aligned}
&[(2k^2 - 1)q^2 + f_{11} + f_{21}(1-c)]X_1 a_1 + [f_{13} + f_{23}(1-c)^3 - \frac{2k^2q^2}{X_1^2}]X_1^3 b_1 = P_0 \\
&[(2k^2 - 1)q^2 + f_{11} + f_{21}(1-c)]X_1 a_3 + [f_{13} + f_{23}(1-c)^3 - \frac{2k^2q^2}{X_1^2}]X_1^3 b_3 = 0
\end{aligned} \tag{3.50}$$

then, correct to $\mathcal{O}(k^2)$, the oscillator is excited with a harmonic force $p(t) = P_0\ cos\omega t$, and responds harmonically with a frequency equal to that of the excitation. In the aforementioned equations, P_0 is the constant magnitude of the harmonic excitation. Thus, for weak nonlinearities and/or displacements, the similar steady state solution (3.38-41) degenerates to an approximate harmonic one. To investigate this approximate harmonic motion, it is necessary to eliminate the variables q and c from expressions (3.50). This is achieved as follows.

First, consider expression (3.41), and expand the complete elliptic integral $K(k)$ in terms of its modulus:

$$\omega^2 = \frac{q^2}{(1+k^2/2)} + \mathcal{O}(k^4) \tag{3.51}$$

Then, use the first of equations (3.40) to express λ^2 as a function of c:

$$\lambda^2 = -f_{21}(\frac{1-c}{c}) + f_{11} \tag{3.52}$$

Substituting (3.52) and the third of equations (3.40) into (3.39), obtain the following alternative expression for q^2:

$$q^2 = -f_{21}(\frac{1-c}{c}) + f_{11} + [f_{31}c^2 - f_{32}\frac{(1-c)^3}{c}]X_1^2 \tag{3.53}$$

An elimination of the variable q^2 is now possible, by a combination of (3.51) and (3.53):

$$(1+\frac{k^2}{2})\omega^2 = -f_{21}(\frac{1-c}{c}) + f_{11} + [f_{31}c^2 - f_{32}\frac{(1-c)^3}{c}]X_1^2 \tag{3.54}$$

Equations (3.50) and (3.54) can now be regarded as a set of three equations with three unknowns, namely, X_1, c and k^2. Trivial but lengthy algebraic manipulations lead to a set of equations that describe the approximate harmonic steady state solution of the "weakly nonlinear" system, correct to $\mathcal{O}(k^2)$:

$$f_{11} + f_{21}(1-c) - \omega^2 - \frac{P_0}{X_1} + [f_{13} + f_{23}(1-c)^3]X_1^2\{\frac{7\omega^2 - f_{11} - f_{21}(1-c)}{9\omega^2 - f_{11} - f_{21}(1-c)}\} = 0$$

$$c = f_{21}/(f_{11} + f_{21} - \omega^2)$$

$$k^2 = \frac{4[f_{13} + f_{23}(1-c)^3]X_1^2}{9\omega^2 - [f_{11} + f_{21}(1-c)]} \tag{3.55}$$

For a fixed value of the forcing amplitude P_0, one can eliminate c from the first two equations (3.55) and obtain the frequency response curves of the steady state

oscillation. Note that the approximate steady state solution (3.55) is valid for all frequencies, except those in the neighborhood of $\omega = (f_{11} + f_{21}(1-c))/9$. Close to that frequency, the denominator of the last of equations (3.55) becomes a small quantity, leading to large values for the elliptic modulus k^2. Thus, the assumptions of the perturbation analysis are violated, since k^2 is not any more of perturbation order. Also note that from the first of equations (3.55) one requires that (the quantity c is of $\mathcal{O}(1)$):

$$f_{11} + f_{21}(1-c) - \omega^2 - \frac{P_0}{X_1} = \mathcal{O}(k^2) \tag{3.56}$$

The above equation represents the linear steady state solution. Therefore, it is concluded that the approximate harmonic steady solution must be in the neighborhood of the linear one.

In figure 3.5, the frequency response curves of the approximate steady state solutions corresponding to $f_{11} = 1, f_{21} = 4, f_{13} = 0.07, f_{23} = 0.1$ and $P_0 = 0.05$ are presented. The stability question of this type of approximate steady state motions is addressed elsewhere (Kinney, 1966), (Hsu, 1964), and it can be shown that two branches of solutions are orbitally unstable.

Summarizing, it was demonstrated that the exact similar steady state solution (3.38-41) (that is valid for strongly nonlinear systems), is a generalization of the approximate harmonic steady state solution, since it degenerates to this later motion when the nonlinearities and/or the displacements become small. As pointed by (Hsu, 1960), however, the exact steady state solution can also give rise to an approximate subharmonic oscillation. To study this type of motion, one has to

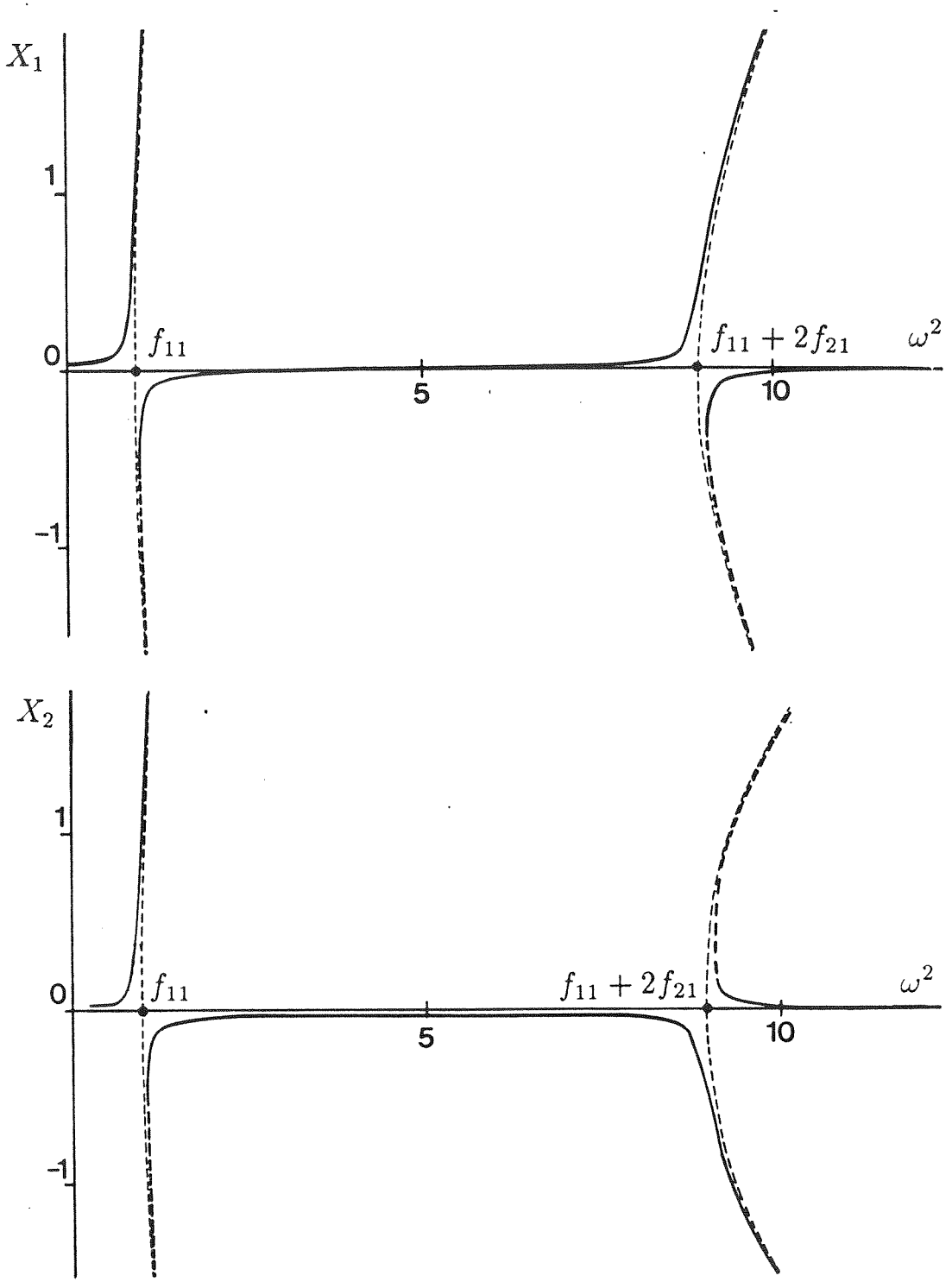

Figure 3.5. Approximate harmonic steady state responses.

Stable ———— Unstable - - - - - - -

impose the following conditions, similar to (3.50):

$$[(2k^2-1)q^2+f_{11}+f_{21}(1-c)]X_1a_1+[f_{13}+f_{23}(1-c)^3-\frac{2k^2q^2}{X_1^2}]X_1^3b_1=0$$
$$[(2k^2-1)q^2+f_{11}+f_{21}(1-c)]X_1a_3+[f_{13}+f_{23}(1-c)^3-\frac{2k^2q^2}{X_1^2}]X_1^3b_3=P_0 \tag{3.57}$$

Under these restrictions, the weakly nonlinear system is excited by a harmonic force and responds harmonically with a frequency equal to one third of that of the excitation:

$$p(t)=P_0cos3\omega t+\mathcal{O}(k^4)$$
$$x_1(t)=X_1cos\omega t+\mathcal{O}(k^2) \tag{3.58}$$

Clearly, this is the well known subharmonic phenomenon.

3.2.3. DISCUSSION

In section 3.2 the similar steady state motions of a class of "1-1 resonant" oscillators were examined. Although only systems of two-DOF were investigated, the presented methodology can be extended to systems of arbitrary DOF by considering each time suitable forcing functions and introducing linear relations between the coordinates of the system. One can then uncouple the equations of motions of the oscillator by defining "forced balancing diagrams," in a way similar to that presented in this work. Since no assumptions concerning the amount of the nonlinearity were made, the analytic expressions are valid for strongly nonlinear systems in contrast to results of conventional, approximate methods that only hold for oscillators with "weak nonlinearities."

It was shown that the selection of the functional equation that relates the force with

the displacement, is of paramount importance when the similar steady state motions of strongly nonlinear discrete systems are studied. In this work this problem was solved by choosing the excitation in such a way as to transform the forced motion to an equivalent free oscillation. This was achieved by using a matching procedure to uncouple the steady state equations of motion of the system. The resulting "forced balancing diagrams" can then be used to find the appropriate values of the modal constants c; the steady state oscillation can then be analytically expressed by an integration by quadratures.

Two categories of strongly nonlinear oscillators were examined. The first category consists of systems that possess additional modes of free oscillation. The force is taken proportional to the displacement raised to a power equal to that of the nonlinearity. It was shown that for this type of oscillators, the topological portrait of the frequency response curves may change, if a certain structural parameter changes. This is a direct consequence of the bifurcation of normal modes of the free oscillation of the system: the variation of a certain structural parameter may introduce additional (bifurcated) "backbone" curves, and these increase the complexity of the steady state response diagrams.

The second category consists of systems that possess only two modes of free oscillation. In this case, the functional equation relating the force and the displacement contains linear and nonlinear terms. Since no bifurcation of normal modes is possible, the topology of the response curves remains unaltered for changes of the structural parameters of the oscillator.

Specific numerical applications of the theory were given for systems with cubic nonlinearities. For a system with a linear term in its coupling stiffness, $f_2(\bullet)$, a difficulty of interpretation of a constant "forcing amplitude," was encountered. However, perturbation analysis indicates that the exact steady state is a generalization of the well-known approximate harmonic steady response of the corresponding weakly nonlinear system excited by a harmonic force.

Finally, it must be stated that although only "1-1 resonant" systems were examined, the same analysis can be applied to systems that are "off-resonance." Since these systems also possess normal modes (see section 2), their steady state motions can be regarded as perturbations of their free oscillations. Accordingly, exact analytic expressions can be obtained by imposing the conditions for similar motion and by constructing "forced balancing diagrams."

3.3. NONSIMILAR STEADY STATE OSCILLATIONS

In the previous sections the similar steady state motions of strongly nonlinear forced oscillators were examined by considering special periodic forcing functions, i.e., forces that were related by certain functional relations to the steady state displacements. It was concluded that similar forced motions could only be realized for a very restricted set of forces, and in that sense they resembled the similar normal modes of free oscillation (since they too existed only for systems with special symmetries).

However, in nonlinear systems, nonsimilar steady state motions may exist. In a nonsimilar steady motion, the system oscillates as in a nonsimilar normal mode, where the functional relations between the coordinates are generally nonlinear. In what follows, it will be shown that these nonsimilar forced motions exist for a whole class of periodic excitations; in that sense, nonsimilar steady states are generic for the oscillators under investigation, in contrast to the similar steady states that require special forcing conditions (this is in analogy to the nonsimilar normal modes that were shown to be generic for the class of nonlinear systems under consideration).

Two types of nonsimilar steady state motions are analyzed. In the first case, the nonsimilar steady motion is caused by a force proportional to the steady state displacement. Since the resulting forced oscillator cannot oscillate in a similar motion, nonsimilar steady state oscillations are considered. In the second case, a general periodic excitation is applied to the system, and a theorem on the necessary and sufficient conditions that this force must satisfy in order to lead to a nonsimilar

steady state motion is given. In both cases, an asymptotic methodology similar to that applied for the problem of the nonsimilar modes is followed.

3.3.1. SPECIAL FORCING FUNCTIONS

3.3.1.1. ASYMPTOTIC ANALYSIS

Consider the two-DOF system of the previous section with equations of motion given by relations (3.3):

$$\begin{aligned} \ddot{x}_1 + f_1(x_1) + f_2(x_1 - x_2) &= p(t) \\ \ddot{x}_2 + f_1(x_2) - f_2(x_1 - x_2) &= 0 \end{aligned} \tag{3.3}$$

where the stiffnesses $f_i(\bullet)$ are given by:

$$\begin{aligned} f_1(u) &= u + u^3 \\ f_2(u) &= K_1 u + K_3 u^3 \end{aligned} \tag{3.59}$$

As usual, the usual set of initial conditions, is assumed :

$$\begin{aligned} x_1(0) = X_1 \quad \dot{x}_1(0) = 0 \\ x_2(0) = X_2 \quad \dot{x}_2(0) = 0 \end{aligned} \tag{3.60}$$

In section 3.2.2 it was shown that the unforced system possesses only two normal modes of free oscillation, and that *similar* steady state motions exist if and only if the forcing function $p(t)$ is selected according to the functional relation (3.35). Thus, it is of interest to investigate the possibility of existence of any additional nonsimilar steady state motions when the applied force is general and does not necessarily satisfy relation (3.35).

To this end, consider a linear functional relation between the force and the steady state displacement of the form:

$$p(t) = (\frac{P}{X_1})x_1(t) \tag{3.61}$$

In writing (3.61), it was assumed that a steady state oscillation occurs where the coordinate $x_1(t)$ oscillates with a maximum amplitude X_1. Taking into account the expressions for the stiffnesses and the force, the differential equations of motion become:

$$\begin{aligned} \ddot{x}_1 + x_1(1+\epsilon) + x_1^3 + K_1(x_1 - x_2) + K_3(x_1 - x_2)^3 = 0 \\ \ddot{x}_2 + x_2 + x_2^3 + K_1(x_2 - x_1) + K_3(x_2 - x_1)^3 = 0 \end{aligned} \tag{3.62}$$

where $\epsilon = -P/X_1$. Regarding for the moment ϵ as a fixed, structural parameter, the steady state problem is converted to an equivalent free oscillation one. *Note, however, that this equivalence only holds at the steady state.* For $\epsilon = 0$ (unforced motion), two similar normal modes exist, corresponding to $c = \pm 1$. For $\epsilon \neq 0$, it can be easily shown that the equivalent problem cannot possess similar normal modes (since there do not exist any real values for the modal constant c, that match simultaneously the linear and cubic terms of equations (3.62)). Thus, no similar steady state solutions exist for the forced problem, and it is necessary to search for nonsimilar steady state motions.

The *nonsimilar* normal modes of the equivalent problem (3.62), are computed by imposing a functional relation between the coordinates of the form:

$$x_2 = \hat{x}_2(x_1) \tag{3.63}$$

Using the methodology of section 2.3 (where nonsimilar normal modes were analyzed), it can be shown that the function $\hat{x}_2(\bullet)$ must satisfy the following functional

equation:

$$-2\hat{x}_2''\{\frac{x_1^2-X_1^2}{2}(1+\epsilon+K_1)+\frac{x_1^4-X_1^4}{4}+\int_{X_1}^{x_1}[K_3(\xi-\hat{x}_2(\xi))^3-K_1\hat{x}_2(\xi)]d\xi\}-$$

$$-\hat{x}_2'\{x_1(1+\epsilon)+x_1^3+K_1x_1-K_1\hat{x}_2+K_3(x_1-\hat{x}_2)^3\}+$$

$$+\hat{x}_2+\hat{x}_2^3+K_1\hat{x}_2-K_1x_1+K_3(\hat{x}_2-x_1)^3=0 \qquad (3.64)$$

where $(\bullet)' \equiv \frac{d(\bullet)}{dx_1}$. This functional equation is singular at $x_1 = X_1$ (i.e., at the maximum equipotential surface of the equivalent free system), but, as shown earlier, the solution can be successfully approximated by an asymptotic series. There is a "boundary condition" for the functional equation (3.64), resulting from the requirement that the modal line of the nonsimilar normal mode of the equivalent problem intersects orthogonally the maximum equipotential surface:

$$-\hat{x}_2(X_1)'\{X_1(1+\epsilon)+X_1^3+K_1X_1-K_1\hat{x}_2(X_1)+K_3(X_1-\hat{x}_2(X_1))^3\}+$$

$$+\hat{x}_2(X_1)+\hat{x}_2^3(X_1)+K_1\hat{x}_2(X_1)-K_1X_1+K_3(\hat{x}_2(X_1)-X_1)^3=0 \qquad (3.65)$$

Assuming that the quantity ϵ is small (i.e., that the excitation is weak), one can find an asymptotic approximation for the nonsimilar normal mode of the equivalent free problem (3.64-65), using the perturbation technique outlined in section 2.3. Since ϵ depends on the applied forcing magnitude, the resulting nonsimilar mode corresponds to a nonsimilar steady state oscillation. Summarizing, the nonsimilar steady motion can be asymptotically approximated by transforming the forced problem (at the steady state) to an equivalent free oscillation one that can be approximately solved by applying the asymptotic methods outlined in previous sections.

In what follows, the asymptotic solution for the nonsimilar steady state motion is outlined. Details of the perturbation analysis have been omitted since it is analogous to the one performed in section 2.3. The nonlinear modal line of the steady state is expressed as follows:

$$\hat{x}_2(x_1) = \hat{x}_2^{(0)}(x_1) + \hat{x}_2^{(1)}(x_1) + ... \tag{3.66}$$

where the zero-th order approximation, $\hat{x}_2^{(0)}(\bullet)$, is computed by considering the balance of the $\mathcal{O}(1)$ terms in (3.64-65):

$$\hat{x}_2^{(0)}(x_1) = c\, x_1 \quad , \quad c = c_{(\pm)} = \frac{\epsilon}{2K_1} \pm \{1 + (\frac{\epsilon}{2K_1})^2\}^{1/2} \tag{3.67}$$

where $\epsilon = -P/X_1$. The first order approximation $\hat{x}_2^{(1)}(\bullet)$ is then expressed in the form:

$$\hat{x}_2^{(1)} = a_{21}^{(1)} x_1 + a_{23}^{(1)} x_1^3 + a_{25}^{(1)} x_1^5 + ... \tag{3.68}$$

The coefficients $a_{2j}^{(1)}$ are computed by considering $\mathcal{O}(\epsilon)$ terms. Their analytic expressions are identical with formulas (2.63), obtained for the free oscillation problem of section 2.3.3:

$$a_{21}^{(1)} =$$

$$\frac{-T_5^{(1)}X_1^2 - L_2^{(1)}X_1^4(T_3^{(1)} + T_4^{(1)}X_1^4) + 5L_2^{(1)}X_1^4(T_1^{(1)} + T_2^{(1)}X_1^2)}{-(1 + 3L_1^{(1)}X_1^2 + 5L_3^{(1)}X_1^4)(T_1^{(1)} + T_2^{(1)}X_1^2) + (1 + L_1^{(1)}X_1^2 + L_3^{(1)}X_1^4)(T_3^{(1)} + T_4^{(1)}X_1^2)}$$

$$a_{23}^{(1)} = \frac{(T_1^{(1)} - T_3^{(1)})a_{21}^{(1)}}{6T_1^{(1)}X_1^2 + 3T_2^{(1)}X_1^4} \equiv L_1^{(1)}a_{21}^{(1)}$$

$$a_{25}^{(1)} = \frac{-T_5^{(1)}}{20T_1^{(1)}X_1^2 + 10T_2^{(1)}X_1^4} + \frac{[L_1^{(1)}(-T_3^{(1)} + 9T_1^{(1)}) + T_2^{(1)} - T_4^{(1)}]a_{21}^{(1)}}{20T_1^{(1)}X_1^2 + 10T_2^{(1)}X_1^4} \equiv$$

$$\equiv L_2^{(1)} + L_3^{(1)}a_{21}^{(1)} \tag{3.69}$$

where, in this case,

$$
\begin{aligned}
T_1^{(1)} &= 1 - \frac{P}{X_1} + K_1(1-c) \\
T_2^{(1)} &= 1 + K_3(1-c)^3 \\
T_3^{(1)} &= 1 + K_1(1+c) \\
T_4^{(1)} &= 3K_3(1-c)^2 c + 3c^2 + 3K_3(1-c)^2 \\
T_5^{(1)} &= -c - cK_3(1-c)^3 + c^3 + K_3(c-1)^3
\end{aligned}
\tag{3.70}
$$

Summarizing, in the nonsimilar steady state the system oscillates as in a nonsimilar normal mode; the motion in the configuration plane is a curved modal line given by:

$$
\hat{x}_2(x_1) = (c + a_{21}^{(1)})x_1 + a_{23}^{(1)} x_1^3 + + a_{25}^{(1)} x_1^5 + \mathcal{O}(\ \epsilon x_1^7,\ \epsilon^2) \tag{3.71}
$$

Depending on the value of c, two modal lines exist, the one corresponding to forced steady motions occurring in the neighborhood of the symmetric ($c = +1$) mode, and the other corresponding to forced oscillations in the vicinity of the antisymmetric ($c = -1$) one. The time response, $x_1 = x_1(t)$, can be found by an integration by quadratures of the first of equations (3.62), with x_2 given by relation (3.71):

$$
\begin{aligned}
t = t(x_1) = \\
= \pm \int_{X_1}^{x_1} \frac{d\xi}{\{\ I_1^{(1)}(X_1^2 - \xi^2) + \frac{I_3^{(1)}}{2}(X_1^4 - \xi^4) + \frac{I_5^{(1)}}{3}(X_1^6 - \xi^6) + \mathcal{O}(\epsilon x_1^7, \epsilon^2)\ \}^{1/2}} \equiv \\
\equiv \pm \int_{X_1}^{x_1} G(X_1, \xi) d\xi
\end{aligned}
\tag{3.72}
$$

where

$$
\begin{aligned}
I_1^{(1)} &= 1 - \frac{P}{X_1} - a_{21}^{(1)} + K_1(1-c) \\
I_3^{(1)} &= 1 - K_1 a_{23}^{(1)} + K_3(1 - c - a_{21}^{(1)})^3 \\
I_5^{(1)} &= -K_1 a_{51}^{(1)} - 3K_3(1 - c - a_{21}^{(1)})^2 a_{23}^{(1)}
\end{aligned}
\tag{3.73}
$$

and

$$G(X_1,P,\xi)\equiv\frac{1}{\{\ I_1^{(1)}(X_1^2-\xi^2)+\frac{I_3^{(1)}}{2}(X_1^4-\xi^4)+\frac{I_5^{(1)}}{3}(X_1^6-\xi^6)+\mathcal{O}(\epsilon x_1^7,\epsilon^2)\ \}^{1/2}} \tag{3.74}$$

The frequency response curves corresponding to the nonsimilar steady state motion are computed by expressing the frequency of the steady oscillation as a function of the displacement amplitudes X_1 and X_2. The details can be found in section 2.3.3, and the derived analytical expression for the frequency is as follows:

$$\omega=\omega(X_1,P)=\frac{\pi}{-\int_{X_1}^{0}G(X_1,P,\xi)d\xi} \tag{3.75}$$

The frequency response curves corresponding to the nonsimilar steady state motion were computed using the asymptotic solution (3.75). The results appear in figure 3.6, for $P=0.1, K_1=1.3$ and $K_3=0.6$. To check the accuracy of the series solution, the equations of motion were numerically integrated with a fourth order Runge-Kutta algorithm, and the exact initial conditions for the nonsimilar steady states found. This was achieved by fixing each time the amplitude X_2 to its theoretical, asymptotic value, and subsequently "tuning" the amplitude X_1 until a modal line appeared in the configuration plane. In figure 3.6, the exact solutions are superimposed to the asymptotic ones, and clearly, the agreement is satisfactory for low values of the displacements.

Some of the steady state solution branches will be shown to be orbitally unstable. However, since the steady state problem is converted to an equivalent free one, it is possible to find numerically even the unstable steady states by computing

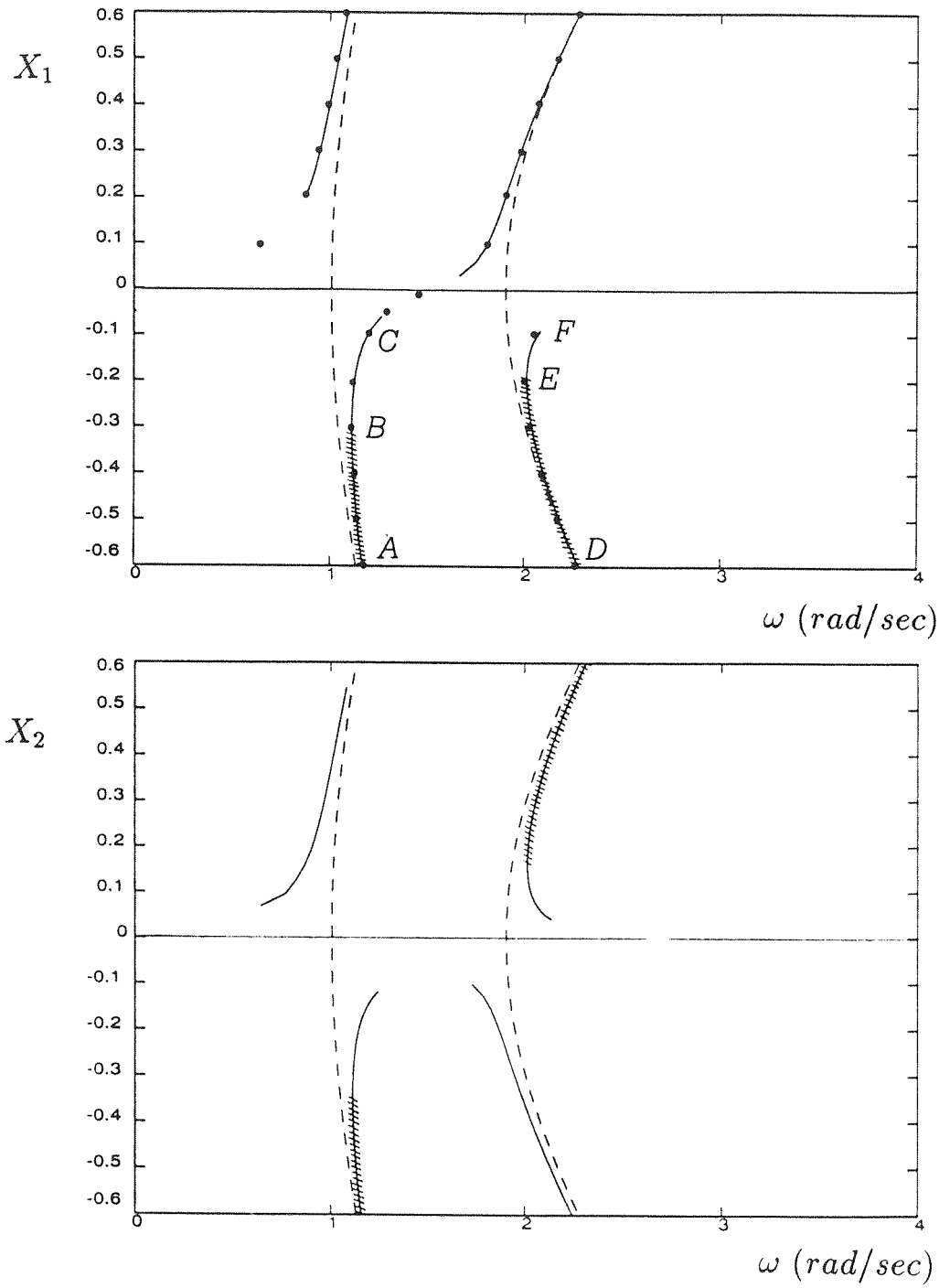

Figure 3.6. Frequency Response curves for the nonsimilar steady state oscillations.

Asymptotic solutions ———, Numerical (exact) solutions ●

Unstable motions ##########

the nonsimilar mode of the equivalent free problem. Since the equivalent problem has two nonsimilar normal modes that result as perturbations of orbitally stable similar ones, the "equivalent" nonsimilar modes are expected to be orbitally stable and as such can be numerically detected. However, this does not imply that the forced problem has only stable steady solutions, since its equivalence with the free problem holds *only* at the steady state. To investigate the stability of the steady state motion, one has to examine the effects that small perturbations have on the forced response.

3.3.1.2. STABILITY CONSIDERATIONS

To examine the stability of the nonsimilar steady state solution (3.71-75), one introduces small perturbations $\xi(t)$ and $\eta(t)$ to the forced response, as follows:

$$\begin{aligned} x_1(t) &= \hat{x}_1(t) + \xi(t) \\ x_2(t) &= \hat{x}_2(t) + \eta(t) \end{aligned} \tag{3.76}$$

In the above equations, $\hat{x}_1(t)$ and $\hat{x}_2(t)$ denote the exact nonsimilar steady state motions. Substituting (3.76) into the equations of motion (3.3), taking into account the chosen functional relation for the force (3.61), and noting that $\hat{x}_1(t)$ and $\hat{x}_2(t)$ satisfy the steady state relations (3.62), one obtains the following set of variational equations:

$$\begin{aligned} \ddot{\xi} + \xi + 3\hat{x}_1^2\xi + K_1(\xi - \eta) + 3K_3(\hat{x}_1 - \hat{x}_2)^2(\xi - \eta) = 0 \\ \ddot{\eta} + \eta + 3\hat{x}_2^2\eta + K_1(\eta - \xi) + 3K_3(\hat{x}_2 - \hat{x}_1)^2(\eta - \xi) = 0 \end{aligned} \tag{3.77}$$

where terms of order higher than ξ or η were discarded. Equations (3.77) form a set of coupled *Hill*-equations. Since the steady motion is nonsimilar, one cannot apply

the approximate stability analysis that was used in section 3.2.1.3 for the similar steady state motions. Hence, it is necessary to apply *Floquet* theory in order to determine the stability of the variational equations. Details of the theory can be found in standard books of differential equations (for example (Arnold, 1982)). In this work only an outline will be presented.

The technique applies to linear vector fields of the form,

$$\dot{\underline{x}} = \underline{A(t)}\,\underline{x} \tag{3.78}$$

where $\underline{x}$ is an n-vector and $\underline{A(t)}$ is a time-dependent, periodic system matrix, of minimum period T. It is numerical in essence, since it relies on the computation of a certain "fundamental solution matrix" of the system. The components of this matrix are the solutions of (3.78) corresponding to the following two separate sets of initial conditions:

$$x_k = \delta_{kj} \quad , \quad k = 1, ..., N \quad , j = 1, ..., N$$

$$\dot{x}_k = 0$$

and

$$\dot{x}_k = \delta_{kj} \quad , \quad k = 1, ..., N \quad , j = 1, ..., N$$

$$x_k = 0$$

where the quantity δ_{ij} is *Kronecker's*-delta function. Evaluation of the "fundamental solution matrix" at $t = T$ (the period of the time-varying system matrix $A(t)$), leads to the "*Floquet* matrix" of the system. A basic theorem of *Floquet* theory states that, if all the eigenvalues of the "*Floquet* matrix" lie inside the unit circle, then all the solutions of the vector field (3.78) are stable.

The variational equations (3.77) can be put in the form (3.78), by introducing new variables $u = \dot{\xi}$ and $v = \dot{\eta}$, and transforming the two second order differential equations into a set of four, first order ones. Then *Floquet* theory can be applied to the new set of equations. The steady state responses $\hat{x}_1(t)$ and $\hat{x}_2(t)$ were numerically evaluated by integrating equation (3.72) and by taking into account the expression for the modal line (3.71). The "*Floquet* matrix" of equations (3.77) was then computed and its eigenvalues found by a numerical technique. The results appear in figure 3.7, were the eigenvalues of the "*Floquet* matrix" corresponding to the nonsimilar steady state solutions of figure 3.6, are presented. At figure 3.7a, the eigenvalues associated with a branch of steady solutions "neighboring" the symmetric mode, are shown (points A, B and C correspond to respective points in the frequency response plots of figure 3.6). Note that at point B, one of the eigenvalues leaves the unit circle, indicating orbital instability of the respective branch of solutions.

Observe, however, that the remaining steady state solutions correspond to eigenvalues of unit modulus (since they lie *on* and not *inside* the unit circle). Hence, the diagram of figure 3.7a cannot prove orbital stability for these branches and a direct integration of the equations of motion is needed to determine their stability. To explain this, recall that at the nonsimilar steady state, the forced motion is equivalent to a free oscillation, and as a result, at the steady motion the oscillator is virtually hamiltonian. Thus, the corresponding eigenvalues of the "*Floquet* matrix" at the steady state must occur in reciprocal pairs, and moreover, the product of their

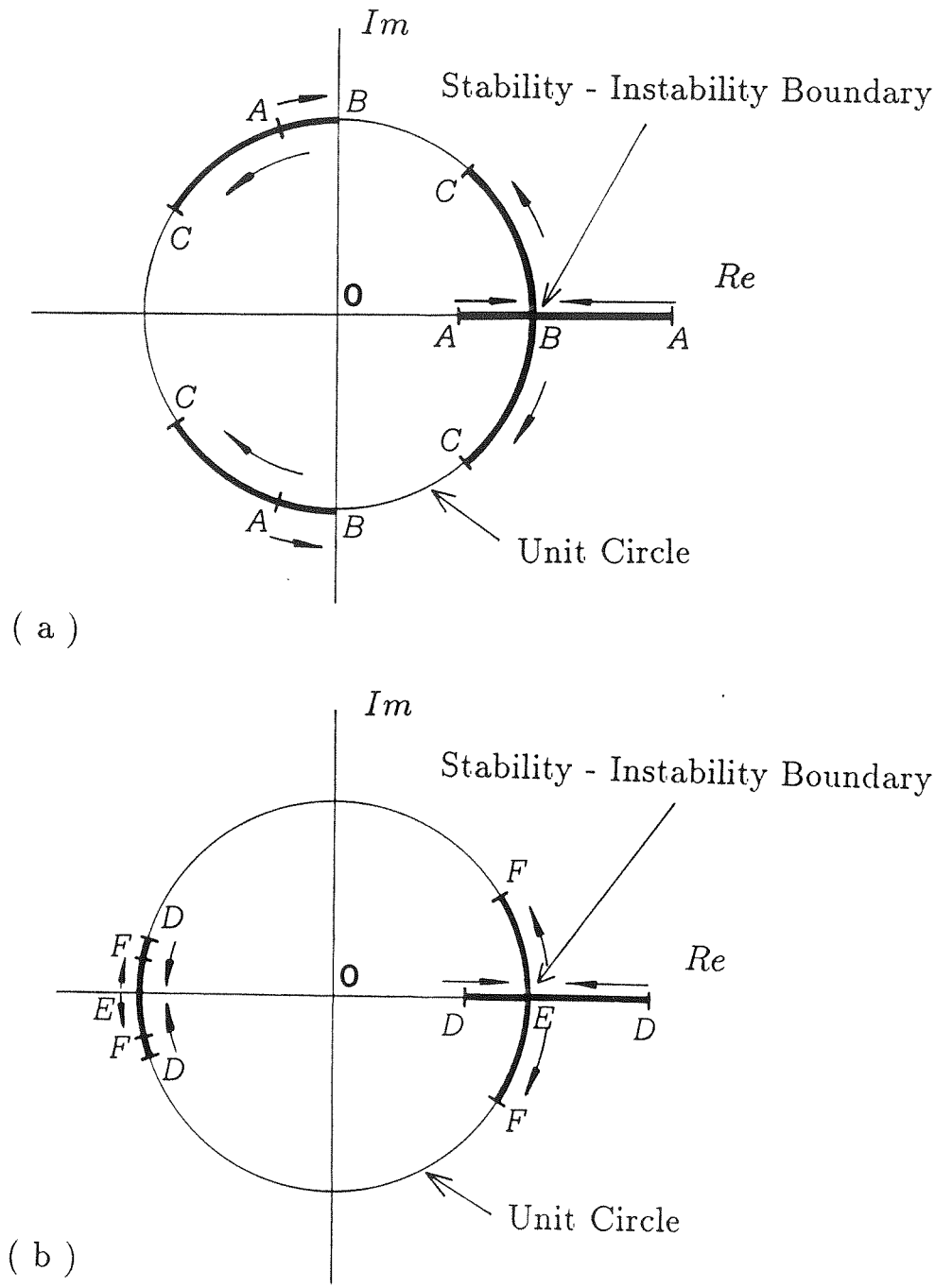

Figure 3.7. Eigenvalues of the *Floquet* matrix of the variational equations: non-similar steady state solutions in the vicinity of (a) the symmetric mode, (b) the antisymmetric mode.

moduli must be equal to unity (Arnold, 1982). Clearly, this requirement eliminates the possibility of a pair of eigenvalues lying inside the unit circle; thus, one cannot prove orbital stability for the remaining branches of solutions. A direct numerical integration of the equations of motion indicates that the solution branches in question correspond to orbitally stable nonsimilar steady state motions.

In figure 3.7b, the eigenvalues corresponding to a branch of steady states occurring in the vicinity of the antisymmetric mode are shown. Again, some of the solutions are proven to be orbitally unstable. Moreover, it can be shown that all the other steady motions presented in figure 3.6 are orbitally stable.

To check the aforementioned stability results, a direct numerical integration of the equations of motion using a fourth order Runge-Kutta algorithm was carried out. The stability of a particular steady state motion was evaluated by introducing perturbations in the exact values of the initial conditions (necessary for the steady state oscillations). At figure 3.8a, the effect of perturbing the exact initial conditions of an orbitally stable mode are shown. The exact initial conditions for the steady state motion are

$$(\; x_1(0), \dot{x}_1(0), x_2(0), \dot{x}_2(0) \;) = (\; 0.3, 0, -0.338052, 0 \;)$$

and the stability is examined by introducing a 5.3% perturbation in the initial condition for $x_2(0)$. It can be seen that this only results in a slight amplitude modulation of the response, whereas, overall, the waveform remains essentially unaffected. This cannot be stated, however, for the perturbed response of figure 3.8b. This motion corresponds to a 1.7% perturbation in $x_2(0)$ of an orbitally unstable steady state

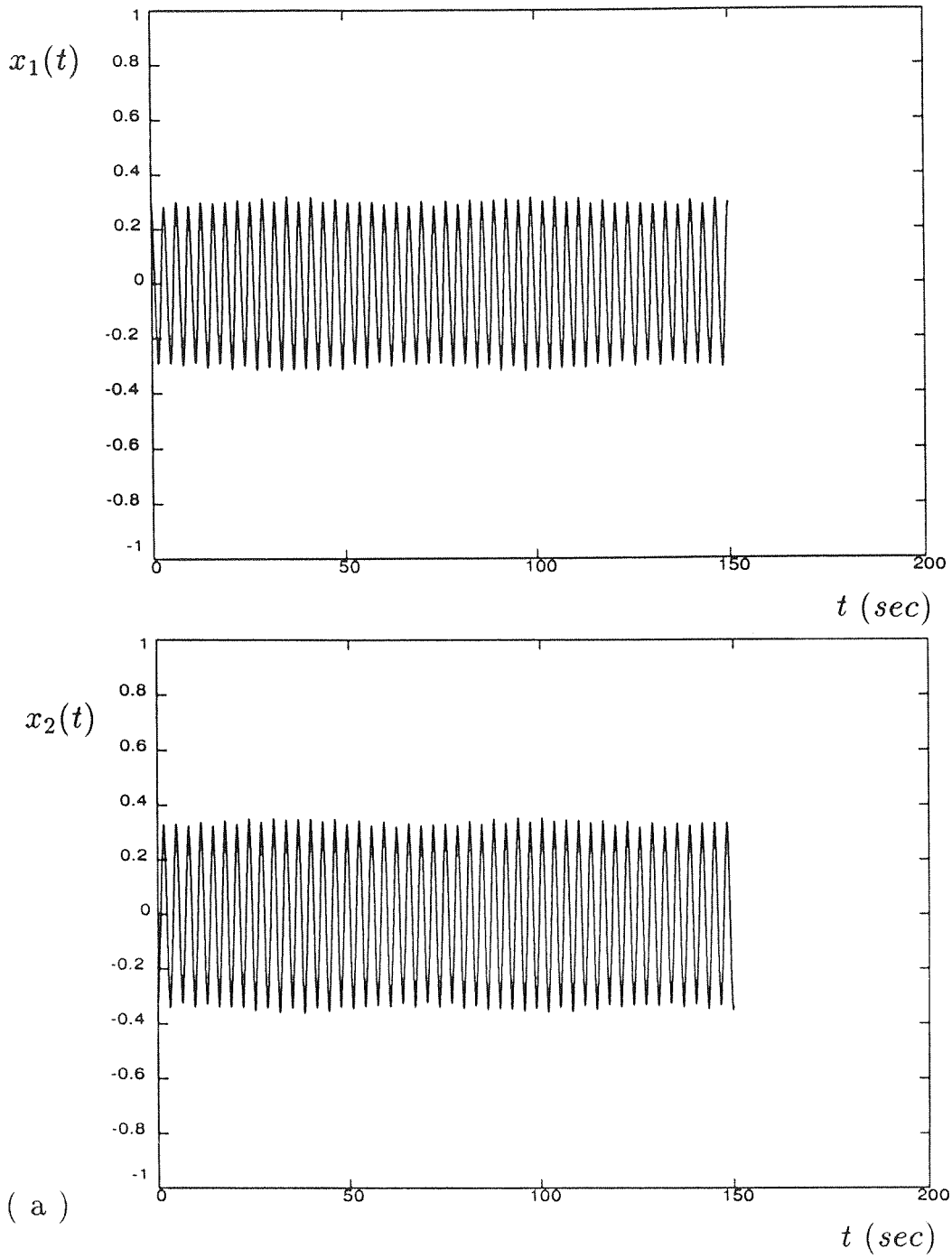

Figure 3.8. Effects of perturbations in the initial conditions of the steady state solutions:

(a) Orbitaly stable motion, perturbation 5.3% in the initial condition $x_2(0)$.

(b) Orbitaly unstable motion, perturbation 1.7% in the initial condition $x_2(0)$.

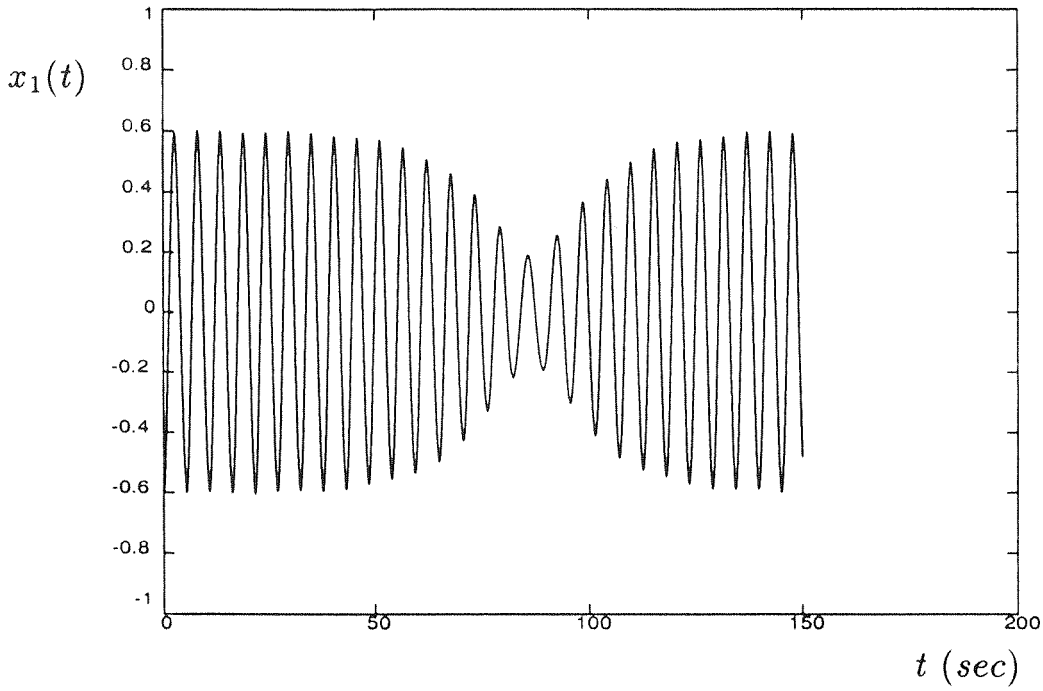
$x_1(t)$
1
0.8
0.6
0.4
0.2
0
-0.2
-0.4
-0.6
-0.8
-1
0
50
100
150
200
t (sec)

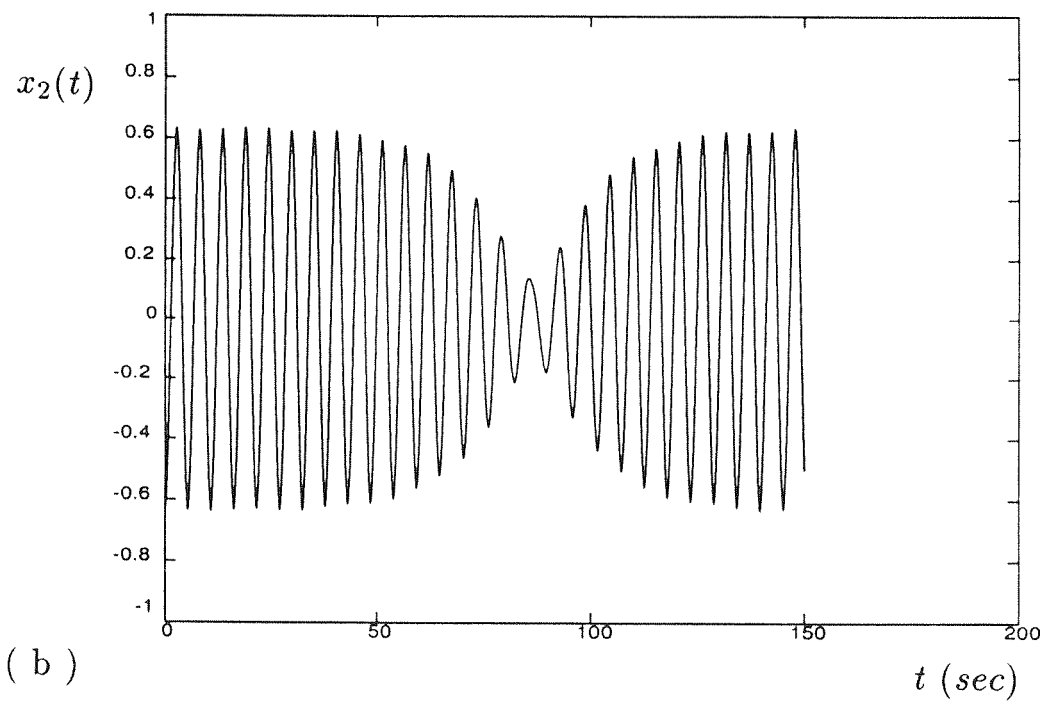
$x_2(t)$
1
0.8
0.6
0.4
0.2
0
-0.2
-0.4
-0.6
-0.8
-1
0
50
100
150
200
t (sec)

(b)

motion, with exact initial conditions:

$$(x_1(0), \dot{x}_1(0), x_2(0), \dot{x}_2(0)) = (-0.6, 0, -0.636263, 0)$$

Observe that, although the perturbation is small (it is almost five times lower than that of the first case), it has drastic effects on the waveform of the response. A large amplitude modulation results, and the waveform of the perturbed motion is nowhere near that of the original steady state.

3.3.2. GENERAL PERIODIC FORCING FUNCTIONS

Until now, the similar and nonsimilar steady motions of the class of nonlinear systems under investigation were examined by considering special forcing functions. A basic feature, however, of nonlinear discrete systems is that, depending on the form of the excitation, they may possess multiple steady state solutions (in contrast to the linear case, where only steady harmonic oscillations can be realized). A basic question therefore arises:

Suppose that a nonlinear oscillator of the general class of systems under investigation is acted upon by a periodic excitation. Under what conditions will this force produce an exact steady state motion?

Two remarks are appropriate at this point. First, the required conditions must depend on the degree of nonlinearity of the system, as well as on its structural parameters. Second, a steady state motion for the class of undamped oscillators under investigation can be materialized only for a specific set of initial conditions.

This is because in undamped systems, initial transients do not decay with time (as in systems with damping). As a result, one has to initiate the motion with specific initial conditions in order to obtain a periodic, steady state response. Thus, there exist two sub-problems resulting from the aforementioned general question:

- The first problem concerns the derivation of the necessary and sufficient conditions that a periodic force must satisfy in order to lead to an exact steady state.

- Then, given such a periodic excitation, one has to compute the specific set of initial conditions of the oscillator that lead to an elimination of the initial transients of the response and give rise to a periodic steady state motion.

In the following sections a general methodology for addressing the above problems is outlined. Then, an application of the theory is given for a two-DOF oscillator with cubic nonlinearity.

3.3.2.1. ASYMPTOTIC ANALYSIS

Consider the general n-DOF nonlinear, undamped system, excited by n forces $p_i(t)$:

$$\ddot{x}_i = f_i(x_1, ..., x_n) + \epsilon p_i(t) \ , \quad i = 1, ..., n \tag{3.79}$$

subject to the set of initial conditions ,

$$x_i(0) = X_i \ , \quad \dot{x}_i(0) = 0 \ , \quad i = 1, 2, ..., n \tag{3.80}$$

The forces $p_i(t)$ are assumed to be "weak" (since their amplitudes are proportional to the small parameter ϵ) and periodic with least common period T. The methodology that will be followed is similar to the asymptotic technique presented in section

2.3.3, where the problem of nonsimilar normal modes was addressed. Its basic features can be found in (Mikhlin, 1974), but certain aspects of the analysis presented in this work are completely new.

The nonconservative system (3.79) can be viewed as a perturbation of a conservative one, corresponding to $\epsilon = 0$. In what follows, it is assumed that the unperturbed system possesses normal modes of free oscillation, and that the steady state motions of the perturbed system result as perturbations of the normal modes of the free oscillator. Hence, one can develop an asymptotic approximation to the steady state oscillation, where the leading term is the unperturbed normal mode motion. The details of this approximate solution are outlined below.

Suppose that the system (3.79) oscillates in a steady state motion. Then, the response $x_1 = x_1(t)$ is periodic with minimum period T (equal to that of the excitation); therefore, at the steady state, one can express the time variable t as a single-valued function of x_1, for t in the interval $[0, T/2)$. Symbolically one can write:

$$t = t(x_1) \quad , \quad t \in [\, 0, T/2 \,) \tag{3.81}$$

Using (3.81), one can eliminate the variable t from expression (3.79), and obtain the following equivalent autonomous system:

$$\ddot{x}_i = f_i(x_1, \ldots, x_n) + \epsilon p_i(t(x_1)) = f_i(x_1, \ldots, x_n) + \epsilon \hat{p}_i(x_1) \ , \quad i = 1, \ldots, n \tag{3.82}$$

where $\hat{p}_i(x_1) \equiv p_i(t(x_1))$. *Note that the equivalence between systems (3.79) and (3.82) holds only at the steady state.* The system (3.82) is autonomous and has

a form similar to that of the systems examined in section 2.3.2. Thus, the forced problem is converted to an equivalent free oscillation and the steady state motion of the original system corresponds to a normal mode of the equivalent free system. Thus, an asymptotic analysis similar to that of section 2.3.2 can be followed, with only minor modifications.

The nonsimilar normal modes of the equivalent problem (3.82) are expressed in the form:

$$x_i = \hat{x}_i(x_r) \quad , \quad i = 1, ..., n, \quad i \neq r \tag{3.83}$$

In analogy to equation (2.40) of section 2.3.2, the nonlinear functions $\hat{x}_i(\bullet)$ satisfy $(n-1)$ functional equations of the form:

$$2\Big[h - V(\hat{x}_1(x_r), ..., \hat{x}_n(x_r))\Big] \Big[1 + \sum_{k=1, k\neq r}^{n} (\frac{d\hat{x}_k}{dx_r})^2\Big]^{-1} \frac{d^2\hat{x}_i}{dx_r^2} +$$

$$+ [f_r(\hat{x}_1(x_r), ..., \hat{x}_n(x_r)) + \epsilon\hat{p}_r(\hat{x}_1(x_r))]\frac{d\hat{x}_i}{dx_r} = f_i(\hat{x}_1(x_r), ..., \hat{x}_n(x_r)) + \epsilon\hat{p}_i(\hat{x}_1(x_r)) \tag{3.84}$$

where, $i = 1, 2, ..., n \quad , i \neq r$, h is the total (fixed) energy, and V is the potential energy of the equivalent conservative system (3.82).

Complementing the aforementioned functional equations, there exist $(n-1)$ boundary orthogonality conditions that guarantee that the modal lines intersect orthogonally the maximum equipotential surface of the equivalent system:

$$[f_r(\hat{x}_1(X_r), ..., \hat{x}_n(X_r)) + \epsilon\hat{p}_r(\hat{x}_1(X_r))]\Big\{\frac{d\hat{x}_i}{dx_r}\Big\}_{x_r = X_r} =$$

$$= f_i\,(\hat{x}_1(X_r), ..., \hat{x}_n(X_r)) + \epsilon\hat{p}_r(\hat{x}_1(X_r)) \tag{3.85}$$

A detailed asymptotic analysis will be carried out in the next section, where a forced two-DOF oscillator with cubic nonlinearity is examined. The general steps of the asymptotic solution are as follows.

First, one introduces the following series expressions for the functions $\hat{x}_i(\bullet)$ and $t(\bullet)$:

$$\begin{aligned} \hat{x}_i(x_r) &= \sum_{k=0}^{\infty} \epsilon^k \hat{x}_i^{(k)}(x_r) \ , \quad i = 1, ..., n \ , i \neq r \\ t(x_1) &= \sum_{k=0}^{\infty} \epsilon^k t^{(k)}(x_1) \end{aligned} \tag{3.86}$$

The functions $\hat{x}_i^{(k)}(\bullet)$ and $t^{(k)}(\bullet)$ represent successive approximations to the steady state motion, and the zero-th order terms ($k = 0$) correspond to the normal modes of the unperturbed system (with $\epsilon = 0$). If the approximations of order $0, ..., (k-1)$ are known, the $k-th$ order approximations are found by substituting equations (3.86) into the functional equations (3.84) and the boundary conditions (3.85), and disregarding higher order approximations (of order $k+1$,...). Then "$k-th$ order functional equations" and "$k-th$ order boundary conditions" result.

The $k-th$ order approximation $\hat{x}_i^{(k)}$ is itself expressed in a series representation:

$$\hat{x}_i^{(k)}(x_r) = \sum_{j=1,3,5,...}^{\infty} a_{ij}^{(k)} x_r^j \tag{3.87}$$

$i = 1, 2, ..., n \ , \quad i \neq r$. Note that only even terms are included in the series because of the symmetries of the modal line in the configuration space. The real scalars $a_{ij}^{(k)}$ are determined by substituting the series (3.87) in the "$k-th$ order functional relations" and the "$k-th$ order boundary conditions," and matching coefficients of respective powers of x_r.

Moreover, successive approximations for the amplitude X_r are obtained by requiring that at each level of approximation the period of the steady state motion be equal to T. The asymptotic solution converges in any open sub-interval of $[-X_r, X_r]$, but not at the limiting values $x_r = \pm X_r$. A rigorous mathematical proof regarding the convergence of the above asymptotic scheme can be found in (Manevich, 1972).

Summarizing, at each level of approximation the forced system is reduced to an equivalent autonomous one and the steady state motion to an equivalent nonsimilar normal mode. The equivalent normal mode can then be conveniently studied using the asymptotic technique of section 2.3.2. Thus, one proves that to each normal mode of the unperturbed system (resulting for $\epsilon = 0$) corresponds a steady state motion and that the trajectory of the forced steady motion in the configuration space is similar to that of a normal mode of an equivalent conservative system (Mikhlin, 1974).

To demonstrate the outlined asymptotic analysis, a specific application is given.

3.3.2.2. SYSTEM WITH CUBIC NONLINEARITY: BASIC THEOREM

Consider the oscillator with cubic nonlinearity of section 3.3.1, acted by a weak periodic excitation $\epsilon p(t)$ ($|\epsilon| \ll 1$), of period T:

$$\begin{aligned} \ddot{x}_1 + x_1 + x_1^3 + K_1(x_1 - x_2) + K_3(x_1 - x_2)^3 &= \epsilon p(t) \\ \ddot{x}_2 + x_2 + x_2^3 + K_1(x_2 - x_1) + K_3(x_2 - x_1)^3 &= 0 \end{aligned} \tag{3.88}$$

As usual, the set of initial conditions (3.60) is assumed. If no excitation exists

($\epsilon = 0$), the system has two similar normal modes, corresponding to modal constants $c = \pm 1$. When $\epsilon \neq 0$, the normal modes are perturbed, and the conditions on the forcing function for an exact steady state motion should be found.

If such a steady oscillation occurs, the responses of the system are periodic, (of period T); then, one can express the time variable t as a function of the displacement x_1, i.e., $t = t(x_1)$, where t is restricted in the range $t \in [0, T/2)$. Thus, in principle one can eliminate the time dependence in the expression of the forcing function, and symbolically write $\hat{p}(x_1) \equiv p(t(x_1)),\ t \in [0, T/2)$. As a result, at the steady state, the forced problem (3.88) is equivalent to an autonomous one, described by the following set of equations:

$$\begin{aligned} \ddot{x}_1 + x_1 + x_1^3 + K_1(x_1 - x_2) + K_3(x_1 - x_2)^3 &= \epsilon \hat{p}(x_1) \\ \ddot{x}_2 + x_2 + x_2^3 + K_1(x_2 - x_1) + K_3(x_2 - x_1)^3 &= 0 \end{aligned} \tag{3.89}$$

for $t \in [\,0, T/2\,)$. As mentioned earlier, a nonsimilar normal mode of the equivalent system (3.89), corresponds to a nonsimilar steady state motion for the original forced problem (3.88). Consider now such a motion, with a modal line in the configuration space given by $x_2 = \hat{x}_2(x_1)$. The function $\hat{x}_2(\bullet)$ must then satisfy the functional relation:

$$\begin{aligned} &-2\hat{x}_2'' \frac{(x_1^2 - X_1^2)}{2}(1 + K_1) + \frac{(x_1^4 - X_1^4)}{4} - \\ &-2\hat{x}_2'' \int_{X_1}^{x_1} [K_3(\xi - \hat{x}_2(\xi))^3 - K_1 \hat{x}_2(\xi) - \epsilon \hat{p}(\xi)] d\xi - \\ &-\hat{x}_2' \{\, x_1 + x_1^3 + K_1 x_1 - \hat{x}_2 K_1 + K_3(x_1 - \hat{x}_2)^3 - \epsilon \hat{p}(x_1)\} + \\ &+\hat{x}_2 + \hat{x}_2^3 + K_1 \hat{x}_2 - K_1 x_1 + K_3(\hat{x}_2 - x_1)^3 = 0 \end{aligned} \tag{3.90}$$

and the orthogonality boundary condition:

$$-\hat{x}_2'(X_1)\{\ X_1 + X_1^3 + K_1 X_1 - \hat{x}_2(X_1)K_1 + K_3(X_1 - \hat{x}_2(X_1))^3 - \epsilon\hat{p}(X_1)\}+$$

$$+\hat{x}_2(X_1) + \hat{x}_2(X_1)^3 + K_1\hat{x}_2(X_1) - K_1 X_1 + K_3(\hat{x}_2(X_1) - X_1)^3 = 0 \qquad (3.91)$$

where primes denote differentiation with respect to x_1. Note that, in contrast to the case of free oscillation, the amplitude of the response X_1 is an unknown quantity and has to be evaluated by the asymptotic technique.

The modal line of the equivalent autonomous system is asymptotically approximated by

$$\hat{x}_2(x_1) = \hat{x}_2^{(0)}(x_1) + \epsilon\hat{x}_2^{(1)}(x_1) + \mathcal{O}(\epsilon^2) \qquad (3.92)$$

and the various orders of approximation are evaluated separately.

ZERO – TH ORDER APPROXIMATION

The zero-th approximation $\hat{x}_2^{(0)}(\bullet)$ is found by substituting (3.92) into the functional equations (3.90-91) and considering only terms of $\mathcal{O}(1)$. The resulting responses correspond to the similar normal modes of the "unperturbed" system (with $\epsilon = 0$):

$$\hat{x}_2^{(0)}(x_1) \ = \ c\, x_1 \quad , \quad c \ = \ \pm 1 \qquad (3.93)$$

Moreover, the time response $x_1 = x_1(t)$ is given in terms of an elliptic function:

$$x_1(t) = X_{10}\ cn(qt, k) \qquad (3.94)$$

where

$$q^2 = \lambda^2 + \mu^2 X_{10}^2\ , \quad k^2 = \mu^2 X_{10}^2/2q^2$$

and

$$\lambda^2 = 1 + K_1(1-c) \quad , \quad \mu^2 = 1 + K_3(1-c)^3$$

The quantity X_{10} denotes the first order approximation to the amplitude of oscillation X_1, and is a yet unknown quantity. To compute X_{10}, one has to impose an additional condition, namely, that the oscillation (3.94) is of period T. This is because, at the steady state, the forced oscillation is of the same period with that of the excitation. Thus, one requires that:

$$\omega = \frac{\pi q}{2K(k)} = \frac{2\pi}{T} \tag{3.95}$$

The only unknown parameter in (3.95) is X_{10}, and this quantity is easily evaluated by a numerical root-finding technique (in this work, the method of bisection was used).

The relations (3.93-95) give the zero-th order approximation to the steady state oscillation that, as mentioned previously, coincides with the free motion of the oscillator.

FIRST ORDER APPROXIMATION

A higher order approximation to the steady state motion can be obtained, if one substitutes the asymptotic approximation (3.92) into the functional relations (3.90-91), and considers only $\mathcal{O}(\epsilon)$ terms. Then, the following two functional equations for $\hat{x}_2^{(1)}(\bullet)$, result:

$$-2\hat{x}_2^{(1)\prime\prime}\{\ [1 + K_1(1-c)]\frac{(x_1^2 - X_{10}^2)}{2} + [1 + K_3(1-c)^3]\frac{(x_1^4 - X_{10}^4)}{4}\ \}-$$

$$-\hat{x}_2^{(1)\prime}\{\ [1+K_1(1-c)]x_1+[1+K_3(1-c)^3]x_1^3\ \}+$$

$$+\hat{x}_2^{(1)}\{\ [1+K_1(1+c)]+3c^2x_1^2\ \}+\hat{p}_0(x_1)\ =0 \tag{3.96}$$

and

$$-\hat{x}_2^{(1)\prime}(X_{10})\{\ [1+K_1(1-c)]X_{10}+[1+K_3(1-c)^3]X_{10}^3\ \}+$$

$$+\hat{x}_2^{(1)}(X_{10})\{\ [1+K_1(1+c)]+3c^2X_{10}^2\ \}+\hat{p}_0(X_{10})\ =0 \tag{3.97}$$

The term $\hat{p}_0(\bullet)$ that appears in the above equations represents the first order approximation to the function $\hat{p}(\bullet)$ that results when the time t is expressed as a function of x_1. Hence, to compute $\hat{p}_0(\bullet)$, one has to "invert" the functional relation (3.94) and solve for t as a function of x_1. This "inversion" is carried out as follows (Byrd, 1954):

$$\frac{x_1}{X_{10}}=cn(qt,k)\ \Rightarrow\ t=t(x_1)=\frac{1}{q}F(\ sin^{-1}\ [1-(x_1/X_{10})^2]^{1/2}\ ,\ k\ ) \tag{3.98}$$

where $F(\bullet,\bullet)$ is the complete elliptic integral of the first kind. Note that the above relation only holds for $t\ \in\ [0,T/2)$ (or equivalently for x_1 monotonically decreasing in $[\ X_{10},-X_{10}\ ))$, since only then there exists a single-valued representation $t=t(x_1)$. Taking into account (3.98), the function $\hat{p}_0(x_1)$ is found by eliminating the time variable t from the expression of the force $p=p(t)$:

$$\hat{p}_0(x_1)\equiv p\ (\ \frac{1}{q}F(\ sin^{-1}\ [1-(x_1/X_{10})^2]^{1/2}\ ,\ k\ )\ ) \tag{3.99}$$

Thus, an explicit, analytic expression is obtained for the function $\hat{p}_0(x_1)$, which in turn can be substituted into the functional equations (3.96-97)) to obtain the first order approximation $\hat{x}_2^{(1)}(x_1)$. Note, however, that the above expression is very

complicated and, thus, of no practical help for the analysis. In order to obtain a more useful expression for $\hat{p}_0(x_1)$, one has to introduce a change of variables.

The "amplitude function," $am(\bullet,\bullet)$, is introduced at this point, defined as (Byrd, 1954):

$$cn(u,k) = cos\phi \quad \Rightarrow \quad \phi = am(u,k) \tag{3.100}$$

Then, from equation (3.98), one can write:

$$cn(qt,k) = cos\phi \quad \Rightarrow \quad \phi = am(qt,k) \tag{3.101}$$

or, solving for the variable t:

$$t = \frac{1}{q} am^{-1}(\phi,k) \quad \Rightarrow t = \frac{1}{q}\ F(\phi,k) \tag{3.102}$$

where the relation $am^{-1}(\bullet,\bullet) = F(\bullet,\bullet)$ was used (Byrd, 1956), and $F(\bullet,\bullet)$ is the complete elliptic integral of the first kind. Thus, instead of expressing t as a function of x_1 (equation (3.98)), one can write it as a function of the newly introduced variable ϕ. Then, eliminating the time dependence from the forcing function $p = p(t)$, one obtains:

$$\hat{p}_0(x_1) \equiv \tilde{p}_0(\phi) \equiv p(\ \frac{1}{q}\ F(\phi,k)\ ) \tag{3.103}$$

The quantity $\tilde{p}_0(\phi)$ represents the first order approximation to the forcing function, when the time variable t is evaluated according to the zero-th order solution. In that sense, it is exactly analogous to expression (3.99), where the displacement x_1 is used as the independent variable.

Note at this point that the displacement x_1 can be also expressed in terms of the new variable ϕ, as:

$$x_1 = \tilde{x}_1(\phi) = X_{10} cos\phi \tag{3.104}$$

Equations (3.103-104) provide a means for computing an alternative, simplified expression for the required function $\hat{p}_0(x_1)$. To achieve this, one has to expand the expression (3.103) of $\tilde{p}_0(\phi)$ in a "generalized Fourier series" with respect to the variable ϕ (Bejarano, 1988,1989), (Margallo, 1988).

Referring to equation (3.102) and taking into account certain properties of the complete elliptic integral of the second kind, it can be shown that:

$$t \in [\, 0,\ +T/2\,) \iff \phi \in [\, 0,\ +\pi\,)$$

$$t \in [\, -T/2,\ 0\,) \iff \phi \in [\, -\pi,\ 0\,)$$

Clearly, in each of the above time intervals, the representation $t = t(x_1)$ has meaning (i.e., is a single-valued function). Moreover, the above relations, coupled with the assumption that the forcing function $p(t)$ is periodic with period T, lead to the conclusion that the function $\tilde{p}_0(\phi)$ is periodic in ϕ, with a period equal to 2π. It can be, therefore, expanded in "generalized Fourier series" as follows:

$$\tilde{p}_0(\phi) = \sum_{n=0}^{\infty} A_n cosn\phi + \sum_{m=1}^{\infty} B_m sinm\phi \tag{3.105}$$

where the coefficients A_n and B_m are computed by the well-known Fourier series formulas:

$$\begin{aligned} A_0 &= \frac{1}{2\pi} \int_{-\pi}^{\pi} \tilde{p}_0(\phi)\ d\phi \\ A_n &= \frac{1}{\pi} \int_{-\pi}^{\pi} \tilde{p}_0(\phi) cosn\phi\ d\phi \\ B_m &= \frac{1}{\pi} \int_{-\pi}^{\pi} \tilde{p}_0(\phi) sinm\phi\ d\phi \end{aligned} \tag{3.106}$$

Consider now the first approximation for the displacement, $\hat{x}_2^{(1)}(x_1)$, and express it in the following series form:

$$\hat{x}_2^{(1)}(x_1) = a_{21}^{(1)} x_1 + a_{23}^{(1)} x_1^3 + a_{25}^{(1)} x_1^5 + ... \tag{3.107}$$

or transforming into the new variable ϕ :

$$\hat{x}_2^{(1)}(x_1) \equiv \tilde{x}_2^{(1)}(\phi) = a_{21}^{(1)} X_{10} cos\phi + a_{23}^{(1)} X_{10}^3 cos^3\phi + a_{25}^{(1)} X_{10}^5 cos^5\phi + ... \tag{3.108}$$

Substituting now for $x_1 = \tilde{x}_1(\phi), \hat{p}_0(x_1) = \tilde{p}_0(\phi)$ and $\hat{x}_2^{(1)}(x_1) = \tilde{x}_2^{(1)}(\phi)$ into the functional equations of the first approximation (3.96-97), one obtains the following set of equations containing only trigonometric terms of the variable ϕ:

$$\begin{aligned}
&(-6a_{23}^{(1)} X_{10} cos\phi - 20 a_{25}^{(1)} X_{10}^3 cos^3\phi)\ \{\ T_1^{(1)} X_{10}^2 (cos^2\phi - 1) + T_2^{(1)} \frac{X_{10}^4}{2} (cos^4\phi - 1)\ \} + \\
&+(-a_{21}^{(1)} - 3a_{23}^{(1)} X_{10}^2 cos^2\phi - 5a_{25}^{(1)} X_{10}^4 cos^4\phi)\{\ T_1^{(1)} X_{10} cos\phi + T_2^{(1)} X_{10}^3 cos^3\phi\ \} + \\
&+(a_{21}^{(1)} X_{10} cos\phi + a_{23}^{(1)} X_{10}^3 cos^3\phi + a_{25}^{(1)} X_{10}^5 cos^5\phi)\{\ T_3^{(1)} + T_4^{(1)} X_{10}^2 cos^2\phi\ \} + \\
&+c\ \{\ \sum_{n=0}^{\infty} A_n cosn\phi + \sum_{m=1}^{\infty} B_m sinm\phi\ \}\ =\ 0
\end{aligned} \tag{3.109}$$

and

$$\begin{aligned}
&+(-a_{21}^{(1)} - 3a_{23}^{(1)} X_{10}^2 - 5a_{25}^{(1)} X_{10}^4)\{\ T_1^{(1)} X_{10} + T_2^{(1)} X_{10}^3\ \} + \\
&+(a_{21}^{(1)} X_{10} + a_{23}^{(1)} X_{10}^3 + a_{25}^{(1)} X_{10}^5)\{\ T_3^{(1)} + T_4^{(1)} X_{10}^2\ \} + c \sum_{n=0}^{\infty} A_n\ =\ 0
\end{aligned} \tag{3.110}$$

where terms of order $\mathcal{O}(x_1^7) = \mathcal{O}(cos^7\phi)$, or higher, were omitted, and

$$\begin{aligned}
T_1^{(1)} &= 1 + K_1(1 - c) \\
T_2^{(1)} &= 1 + K_3(1 - c)^3 \\
T_3^{(1)} &= 1 + K_1(1 + c) \\
T_4^{(1)} &= 3c^2
\end{aligned} \tag{3.111}$$

An exact steady state motion can only occur, provided that one is able to evaluate the coefficients $a_{2j}^{(1)}$ in the above expressions, by suitably matching coefficients of respective powers of $cos\phi$ and $sin\phi$. To do this, it is needed that the terms $cos\ n\ \phi$ and $sin\ n\ \phi$ be expanded in terms of powers of $cos\phi$ and $sin\phi$.

Considering the functional equations (3.109-110), the following general remarks can be made as far as the generalized series of the forcing function is concerned:

1) For a steady state motion to occur, it is necessary that the coefficients of the sine-terms of the generalized series of the force, be zero :

$$B_m \ = \ 0 \ , \quad m = 1, 2, 3, ... \qquad (3.112a)$$

This is because, in the functional equation (3.109), terms containing powers of $sin\phi$ cannot be balanced for any values of the coefficients $a_{2j}^{(1)}$. In fact, condition (3.112a) can be shown to be equivalent to the statement that the steady state response of the undamped oscillator is either in-phase or out-of-phase with the excitation.

In order to prove this, note that a basic assumption of the outlined steady state analysis is that the initial conditions of the system are given by equations (3.60), i.e., that they correspond to zero initial velocities for the coordinates x_1 and x_2. Hence, the steady state oscillation of the system is expected to be an even function of t, and since the system is undamped, the periodic excitation must be either in-phase or out-of-phase, with the displacements. Thus, it is necessary that the forcing function be an even function of t in the interval of oscillation $t \ \in \ [-T/2, \ T/2)$, or equivalently, that $\tilde{p}_0(\phi)$ be an even function of ϕ in the interval $\phi \ \in \ [-\pi, \ \pi)$.

This requirement, however, is equivalent to the statement that the Fourier series of $\tilde{p}_0(\phi)$ do not contain any sine-components.

Thus, in order to obtain an exact steady state oscillation, one must impose a first major restriction on the class of periodic excitations, namely, that their generalized Fourier series do not contain any sine-components.

2) A second restriction on the coefficients of the Fourier series (3.105) results from the fact that there exist only odd powers of $cos\phi$ in the functional equations (3.109-110). Hence, in order to be able to balance the various terms of these equations, it is necessary that the Fourier series of $\tilde{p}_0(\phi)$ do not contain any even cosine-terms:

$$A_{2j} \;=\; 0 \quad , \quad j = 0, 1, 2, ... \qquad (3.112b)$$

This condition is an immediate result of the fact that the nonlinearities of the oscillator under consideration are of odd degrees, and thus, there exist no even powers of $cos\phi$ to balance the odd cosine-terms of the generalized Fourier series of the excitation.

3) In particular, for $j = 0$, equation (3.112b) states that the generalized Fourier series of the excitation $p(t)$ must not contain any constant term:

$$\int_{-\pi}^{\pi} \tilde{p}_0(\phi) d\phi = \int_{-\pi}^{\pi} p(\frac{1}{q} F(\phi, k))\; d\phi = 0 \qquad (3.112c)$$

Equation (3.112c) is the equivalent for the system with cubic nonlinearity, of the analogous (trivial) condition satisfied by harmonic forces in linear steady state motions, namely that:

$$\int_{-T/2}^{T/2} p(t) dt = 0 \quad (\; \textit{Linear theory} \;) \qquad (3.113)$$

In fact, one can easily show that when the coefficients of the nonlinear terms in the equations of motion vanish, equation (3.112c) degenerates to the expression (3.113). Note, however, that condition (3.113) *does not* imply (3.112c).

Summarizing, it was found that in order for a steady state to exist (or equivalently, in order for the functional equations to have solutions for the coefficients $a_{2j}^{(1)}$), certain restrictions concerning the class of admissible periodic excitations must be posed. These are *necessary conditions* for a steady state motion and are given by equations (3.112a,b). In the sequence it will be shown that if these conditions are met, one can always compute numerical values for the coefficients $a_{2j}^{(1)}$, or equivalently one can always obtain an exact nonsimilar steady state oscillation. Thus the aforementioned conditions will also be proven to be *sufficient.*

Assume at this point that conditions (3.112a,b,c) are satisfied. Then, a balancing of respective powers of $cos\phi = x_1/X_{10}$ in equation (3.109), leads to the following values for the coefficients $a_{2j}^{(1)}$, $j = 3, 5, ...$:

$$a_{23}^{(1)} = \frac{(T_1^{(1)} - T_3^{(1)})a_{21}^{(1)}}{6T_1^{(1)}X_{10}^2 + 3T_2^{(1)}X_{10}^4} - \frac{cS_1^{(1)}/X_{10}}{6T_1^{(1)}X_{10}^2 + 3T_2^{(1)}X_{10}^4} \equiv$$

$$\equiv L_1^{(1)}a_{21}^{(1)} + L_2^{(1)}$$

$$a_{25}^{(1)} =$$

$$= \frac{(L_1^{(1)}(9T_1^{(1)} - T_3^{(1)}) + T_2^{(1)} - T_4^{(1)})a_{21}^{(1)}}{20T_1^{(1)}X_{10}^2 + 10T_2^{(1)}X_{10}^4} + \frac{-(cS_3^{(1)}/X_{10}^3) + L_2^{(1)}(9T_1^{(1)} - T_3^{(1)})}{20T_1^{(1)}X_{10}^2 + 10T_2^{(1)}X_{10}^4} \equiv$$

$$\equiv L_3^{(1)}a_{21}^{(1)} + L_4^{(1)} \qquad (3.114)$$

where $T_j^{(1)}$, $j = 1, 2, 3, 4$ are given by expressions (3.111) and,

$$\begin{aligned} S_1^{(1)} &= A_1 - 3A_3 + 5A_5 + ... \\ S_3^{(1)} &= 4A_3 - 20A_5 + ... \\ S_5^{(1)} &= 16A_5 + ... \end{aligned} \tag{3.115}$$

The terms A_j appearing in the above sums are the coefficients of the cosine "generalized Fourier series" (equations (3.105-106)).

The coefficient $a_{21}^{(1)}$ is computed by substituting expressions (3.114) into the "boundary orthogonality condition"(3.110):

$$a_{21}^{(1)} = L_5^{(1)} \ / \ L_6^{(1)} \tag{3.116}$$

where

$$L_5^{(1)} = (3L_2^{(1)}X_{10}^2 + 5L_4^{(1)}X_{10}^4)(T_1^{(1)}X_{10} + T_2^{(1)}X_{10}^3) -$$

$$-(L_2^{(1)}X_{10}^3 + L_4^{(1)}X_{10}^5)(T_3^{(1)} + T_4^{(1)}X_{10}^2) - c(S_1^{(1)} + S_3^{(1)} + S_5^{(1)})$$

and

$$L_6^{(1)} = X_{10}(1 + L_1^{(1)}X_{10}^2 + L_3^{(1)}X_{10}^4)(T_3^{(1)} + T_4^{(1)}X_{10}^2) -$$

$$-X_{10}(1 + 3L_1^{(1)}X_{10}^2 + 5L_3^{(1)}X_{10}^4)(T_1^{(1)} + T_2^{(1)}X_{10}^2)$$

Equations (3.114-116) provide asymptotic approximations for the coefficients of the terms of the modal curve corresponding to the nonsimilar steady state motion. Note, however, that the outlined asymptotic solution is only valid for sufficiently small values of ϵ (i.e., for weak periodic excitations) and for a sufficiently small neighborhood of the origin of the configuration plane (since terms of $\mathcal{O}(x_1^7)$ or higher

were omitted). One can improve the validity of the solution for large amplitudes by computing higher order coefficients $a_{2j}^{(1)}$, $j = 7, 9, ...$ At the steady state, the system oscillates in a nonsimilar motion, described by a modal curve of the form:

$$\hat{x}_2(x_1) = (c + \epsilon a_{21}^{(1)})x_1 + \epsilon a_{23}^{(1)} x_1^3 + \epsilon a_{25}^{(1)} x_1^5 + \mathcal{O}(\ \epsilon x_1^7,\ \epsilon^2) \tag{3.117}$$

Since c can take either the value $+1$, or -1, the system has two possible nonsimilar steady state motions, each one occurring in the neighborhood of a similar normal mode of the unforced (unperturbed) system. Moreover, the time responses of the system can be evaluated by substituting the modal relation (3.117) into the first of the equations of motion (3.89), and integrating by quadratures. Note, however, that in order to do this, one must also substitute an appropriate expression for the force $\hat{p}(x_1)$. This is achieved, by considering the generalized Fourier series (3.105), expanding the trigonometric terms $cos\ n\ \phi$ in powers of $cos\phi$, and eliminating the resulting trigonometric terms by use of formula (3.104). Then the following asymptotic approximation for the force results:

$$\epsilon\hat{p}(x_1) = \epsilon S_1^{(1)} \frac{x_1}{X_{10}} + \epsilon S_3^{(1)} \frac{x_1^3}{X_{10}^3} + \epsilon S_5^{(1)} \frac{x_1^5}{X_{10}^5} + \mathcal{O}(\epsilon x_1^7, \epsilon^2) \tag{3.118}$$

and the quantities $S_j^{(1)}$ are given in terms of the coefficients of the generalized Fourier series, A_n, by expressions (3.115).

The final expression for the time response of the coordinate x_1, is given by:

$$t = t(x_1) =$$

$$= \pm \int_{X_{10}}^{x_1} \frac{d\xi}{\{\ I_1^{(1)}(X_{10}^2 - \xi^2) + \frac{I_3^{(1)}}{2}(X_{10}^4 - \xi^4) + \frac{I_5^{(1)}}{3}(X_{10}^6 - \xi^6) + \mathcal{O}(\epsilon x_1^7, \epsilon^2)\ \}^{1/2}} \tag{3.119}$$

where

$$I_1^{(1)} = 1 - \epsilon a_{21}^{(1)} + K_1(1-c)$$

$$I_3^{(1)} = 1 - \epsilon K_1 a_{23}^{(1)} + K_3(1 - c - \epsilon a_{21}^{(1)})^3 \qquad (3.120)$$

$$I_5^{(1)} = -\epsilon K_1 a_{51}^{(1)} - 3K_3(1 - c - \epsilon a_{21}^{(1)})^2 \epsilon a_{23}^{(1)}$$

The $(+)$ or $(-)$ signs are used alternatively so that a monotone increase of the time variable results. Note that, in writing expressions (2.69), it was assumed that the initial conditions of the system were $x_1\ (0) = X_{10}, \dot{x}_1(0) = 0, x_2(0) = X_{20}, \dot{x}_2(0) = 0$. For a different set of initial conditions, the limits of integration should be modified accordingly. Once the relation $x_1 = x_1(t)$ has been determined, the time response of the coordinate x_2 can be easily computed by means of the (nonlinear) modal relation (3.117).

An improved approximation for the amplitude of steady state oscillation, X_1, can be derived by imposing the additional requirement that the period of the steady motion is equal to T (i.e., equal to the period of the excitation):

$$-\int_{X_1}^{0} \frac{d\xi}{\{\ I_1^{(1)}(X_1^2 - \xi^2) + \frac{I_3^{(1)}}{2}(X_1^4 - \xi^4) + \frac{I_5^{(1)}}{3}(X_1^6 - \xi^6)\}^{1/2}} = T/4 \qquad (3.121)$$

The root of the above equation, $X_1 = X_{11}$, represents an improved approximation to the amplitude of oscillation that replaces the zero-th order approximation X_{10}.

From the outlined analysis, it can be concluded that if conditions (3.112a,b) are met, then a nonsimilar steady state oscillation results. Therefore, these conditions are not only necessary, but also sufficient for a steady state motion. The stability of the resulting nonsimilar steady oscillation can be examined by the *Floquet* methodology outlined in previous sections.

The results of this section can be summarized in the form of a theorem, as follows.

THEOREM

Consider a two-DOF oscillator with cubic nonlinearity, excited by a periodic excitation $p(t)$, and equations of motion given by (3.88). Provided that the excitation is sufficiently small, and that the initial conditions are given by equations (3.60), a necessary and sufficient condition for an exact steady state motion is that the "generalized Fourier series" of the excitation is of the form:

$$\tilde{p}_0(\phi) = \sum_{j=0}^{\infty} A_{2j+1} \; cos(2j+1)\phi$$

where

$$A_{2j+1} = \frac{1}{\pi} \int_{-\pi}^{\pi} \tilde{p}_0(\phi) cos(2j+1)\phi \; d\phi$$

and the function $\tilde{p}_0(\bullet)$ is evaluated by the expression:

$$\tilde{p}_0(\phi) = p(\frac{1}{q} F(\phi, k))$$

In the above equations, $F(\bullet, \bullet)$ is the incomplete elliptic integral of the first kind, and the quantities q and k depend on the structural parameters of the oscillator and the period of the external force.

Moreover, at the steady state the system generally oscillates as in a nonsimilar normal mode.

What the above theorem states is that there exists a whole class of periodic functions for the oscillator under consideration that lead to an exact steady state motion. In

the next section some of these functions will be examined. Note that the theorem can be easily extended to the case of n-DOF, undamped oscillators with cubic nonlinearity. In that case, one has to consider n functional equations and n boundary orthogonality conditions in order to compute the modal line in the configuration space; however, the analysis for the steady state motion is carried out in exactly the same way with that followed in this section.

If the nonlinearity of the system is not cubic, but of a general even power, the expression defining the quantity $\tilde{p}_0(\phi)$ should be modified accordingly. However, the argument of the function in the right-hand side of the equation defining $\tilde{p}_0(\phi)$ will generally be a complicated expression, and it might not even be possible to be expressed in terms of tabulated functions.

Finally, a remark must be made as far as the unperturbed system, corresponding to $\epsilon = 0$, is concerned. In this section it was assumed that the free system contained two similar normal modes of free oscillation. The same methodology, however, can be applied for oscillators that have nonsimilar normal modes. In such cases, one finds asymptotic approximations for the nonsimilar normal modes, and subsequently computes the nonsimilar steady state oscillations that result when these modes are perturbed by weak periodic forcing functions. Then one can prove that in the vicinity of each nonsimilar free motion, there exists an exact nonsimilar steady state.

3.3.2.3. NUMERICAL APPLICATIONS

In this section specific periodic forcing functions will be considered, and numerical evaluations of some exact, nonsimilar steady state motions will be carried out. As mentioned previously, a whole class of periodic forcing functions exist that produce exact steady states of the oscillator with cubic nonlinearities described by equations (3.88). These forces must satisfy the conditions of the theorem of the previous section.

The first type of force to be considered is the harmonic cosine forcing function:

$$\epsilon p_1(t) \;=\; \epsilon P_1 \; cos\omega t \tag{3.122}$$

In the sequence it is shown that this type of force satisfies the requirements of the theorem of the previous section, and thus, may lead to exact, nonsimilar steady state motions. The zero-th order approximation for the amplitude X_1 is evaluated by numerically solving equation (3.95). Substituting the expressions for q and k, this equation takes the form:

$$\omega \;=\; \frac{\pi\{\,[1+K_1(1-c)]+[1+K_3(1-c)^3]X_{10}^2\,\}^{1/2}}{2K\,(\,\frac{[1+K_3(1-c)^3]X_{10}^2/2}{[1+K_1(1-c)]+[1+K_3(1-c)^3]X_{10}^2}\,)} \tag{3.123}$$

In the above expression, $K(\bullet)$ is the complete elliptic integral of the first kind. Setting $K_1 = 1.3$, $K_3 = 0.7$ and $c = \pm 1$, one can compute the amplitude X_{10}, as a function of the frequency of the external force, ω. The solutions of equation (3.123) are presented in graphical form at figure 3.9. The presented curves correspond

to free oscillations in either the similar ($c = +1$) or the nonsimilar normal mode ($c = -1$), and therefore they are the "backbone curves" of the unperturbed, free system.

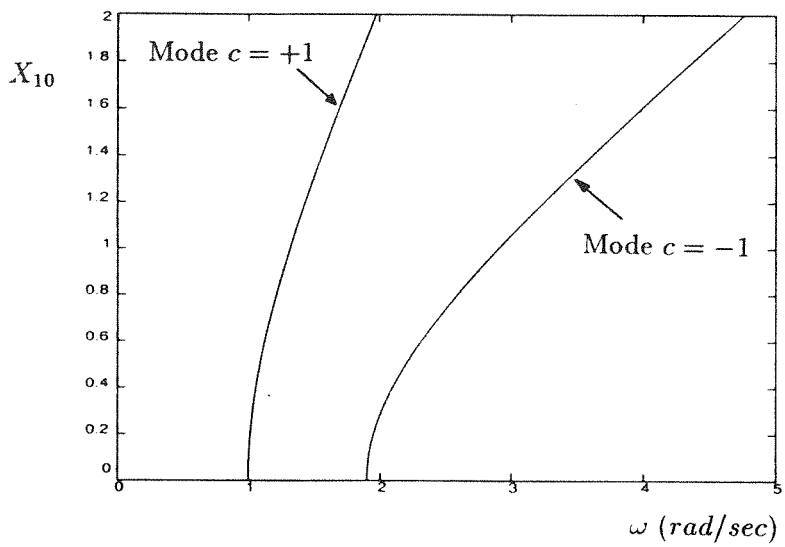

Figure 3.9. "Backbone curves" of the unperturbed oscillator ($\epsilon = 0$).

The free response of the oscillator is then given by:

$$x_1(t) = X_{10} cn(qt, k) \ , \quad x_2(t) \ = \ \pm \ x_1(t) \tag{3.124}$$

To compute the asymptotic approximation of the steady state, one has to evaluate the "generalized Fourier coefficients" of the forcing function. The first order representation of the forcing function, $\tilde{p}_0(\phi)$, is given in this case by:

$$\tilde{p}_0(\phi) = P_1 \ cos \ (\ \frac{\omega F(\phi, k)}{\{[1 + K_1(1-c)] + [1 + K_3(1-c)^3] X_{10}^2\}^{1/2}} \ ) \tag{3.125}$$

Using this representation, the "generalized Fourier coefficients" of the excitation are computed by numerically integrating expressions (3.106). A typical set of Fourier

coefficients is presented below. These values correspond to $\epsilon P_1 = 0.1$, and two different values for the parameters ω and c.

Set 1 : $c = +1,\ \omega = 1.25$

$$A_1 = +0.101498,\ A_3 = -0.001543,\ A_5 = +0.000046,\ ...$$

Set 2 : $c = -1,\ \omega = 2.15$

$$A_1 = +0.100921,\ A_3 = -0.000938,\ A_5 = +0.000017,\ ...$$

Moreover, numerical integration shows that all even cosine-, and all sine-Fourier coefficients are zero. Thus, by the theorem of the previous section, the cosine forcing function can lead to an exact steady state motion. An asymptotic approximation to this motion can be subsequently computed by means of the analytical formulas (3.114-116) derived in the previous section.

The exact steady state motions corresponding to the aforementioned sets of Fourier coefficients were computed. The first set corresponds to $\omega = 1.25$ and $c = +1$. From the plot of figure 3.9, the corresponding value of X_{10} was found to be $X_{10} = 0.8726866$. This value corresponds to a free oscillation of the unforced oscillator in the $c = +1$ similar normal mode. Thus, the zero-th order approximation for the amplitude X_2 is $X_2 = X_{20} = 0.8726866$ (i.e., identical to the amplitude of x_1). After evaluating the coefficients of the modal line, $a_{21}^{(1)}$, $a_{23}^{(1)}$ and $a_{25}^{(1)}$, an improved estimate for the amplitude of oscillation X_1 was obtained by means of equation (3.121). The improved estimate was computed as $X_1 = X_{11} = 0.9300499$. The amplitude of

oscillation of coordinate x_2 was then evaluated by means of the nonlinear modal relation (3.117), with $x_1 = X_{11}$. The resulting improved estimate for the amplitude X_2 was found to be $X_2 = X_{21} = 0.9012262$. Summarizing, the first order asymptotic analysis leads to improved estimates for the amplitudes of oscillation X_1 and X_2. This is schematically presented in the following notation, where the subscripts $(j0)$ and $(j1)$, $j = 1, 2$ refer to initial and improved estimates, respectively:

$$(X_{10}, X_{20}) = (0.872686, 0.872686) \longrightarrow (X_{11}, X_{21}) = (0.930049, 0.901222) \tag{3.126}$$

The second set of Fourier coefficients corresponds to $\omega = 2.15$ and $c = -1$. A similar asymptotic analysis was carried out, and the improved results are presented below.

$$(X_{10}, X_{20}) = (0.456623, -0.456623) \longrightarrow (X_{11}, X_{21}) = (0.464247, -0.496311) \tag{3.127}$$

To check the validity of the analytic results, a direct numerical integration of the forced equations of motion was carried out, with initial conditions $x_1(0) = X_{11}, \dot{x}_1(0) = 0, x_2(0) = X_{21}, \dot{x}_2(0) = 0$. The results are presented in figures 3.10 and 3.11. In these graphs, the representation of the forced motion in the configuration plane, as well as the time signals of the response x_1 and the excitation, are shown. Note that these numerical solutions confirm the existence of exact steady

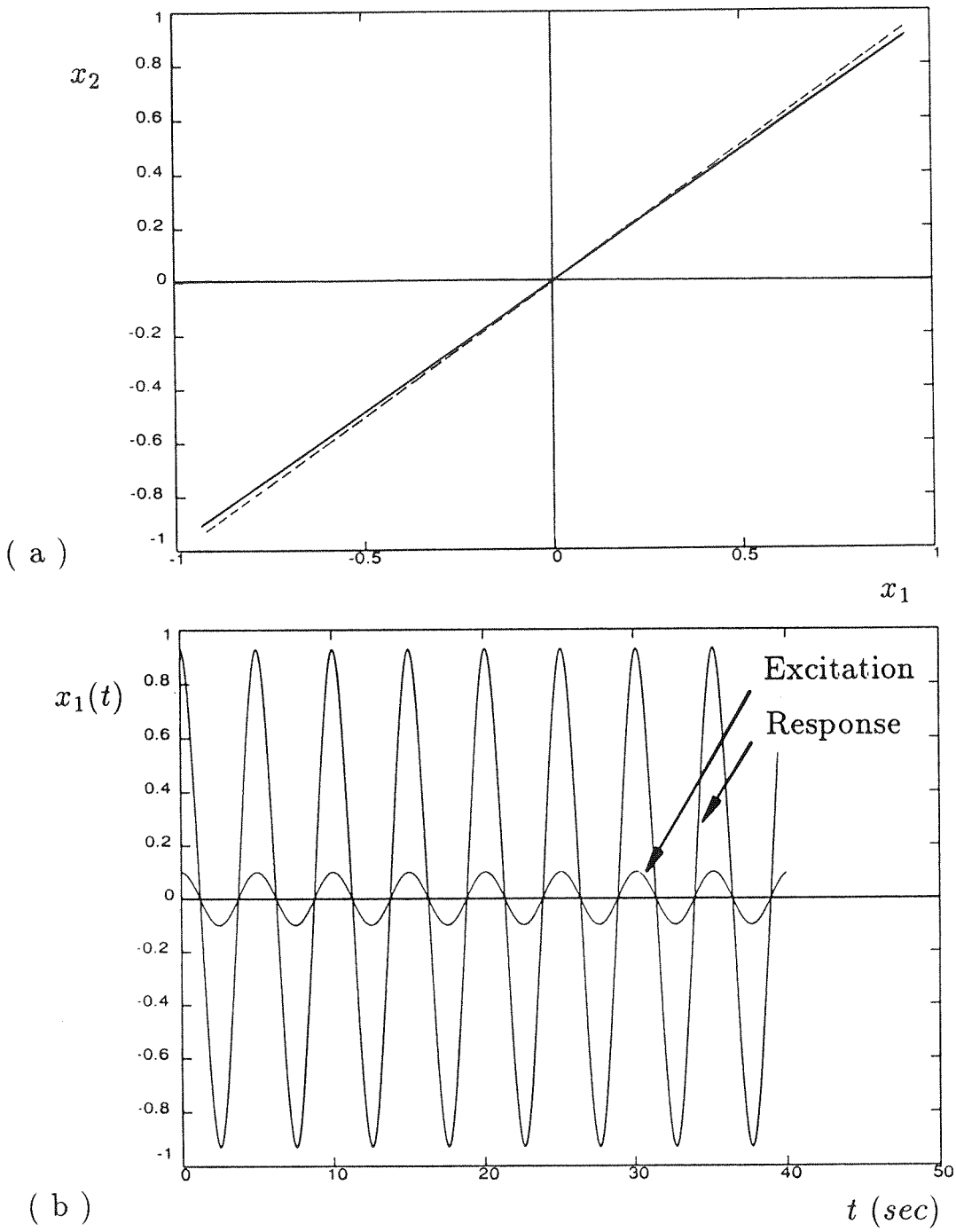

Figure 3.10. Nonsimilar steady state oscillation in the neighborhood of the similar normal mode $c = +1$, corresponding to $K_1 = 1.3$, $K_3 = 0.7$, and $\omega = 1.25$. Forcing function given by (3.122): (a) Modal curve (b) Time signals.

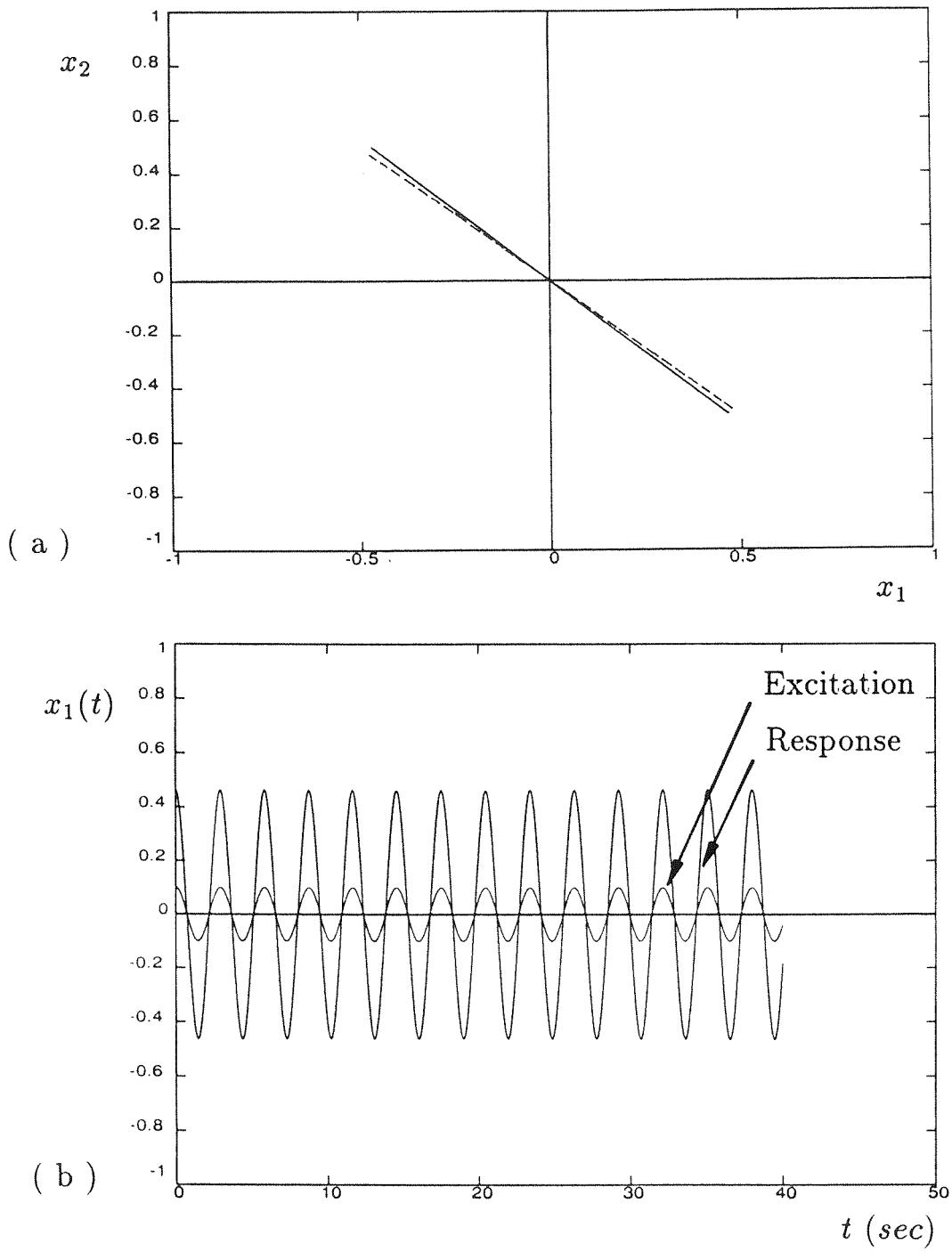

Figure 3.11. Nonsimilar steady state oscillation in the neighborhood of the similar normal mode $c = -1$, corresponding to $K_1 = 1.3$, $K_3 = 0.7$, and $\omega = 2.15$. Forcing function given by (3.122): (a) Modal curve (b) Time signals.

state motions corresponding to the analytically predicted initial conditions. Moreover, these motions can be theoretically and numerically proven to be orbitally stable.

A variety of nonsimilar steady state solutions was analytically computed and numerically verified. In general, the asymptotic approximations were found to be satisfactory as long as they remained in the neighborhood of the normal modes of the unperturbed system. The majority of these steady states were found to be orbitally stable, but two branches of orbitally unstable solutions were also identified.

The second periodic forcing function considered is given by:

$$p_2(t) = \frac{P_2}{2}\ tan^{-1}\ \{\frac{2\alpha cos\omega t}{1-\alpha^2}\} \tag{3.128}$$

This complicated periodic function can be shown to satisfy the requirements of the theorem of the previous section, and it can therefore produce exact steady state motions. The structural parameters of the oscillator were $K_1 = 1.3$ and $K_3 = 0.7$, the forcing amplitude was chosen to be $\epsilon P_2 = 0.15$, and the parameter α appearing in (3.128) was given the value $\alpha = 0.5$. The results of the asymptotic analysis for two selected values of ω are presented below, and the numerical integrations of the forced equations of motion (based on the analytically derived estimates for the initial conditions), are shown in figures 3.12 and 3.13.

Set 1 : $\omega = 1.25,\ c = +1$

$$(X_{10}, X_{20}) = (0.872686, 0.872686) \longrightarrow (X_{11}, X_{21}) = (0.915668, 0.894198) \tag{3.129}$$

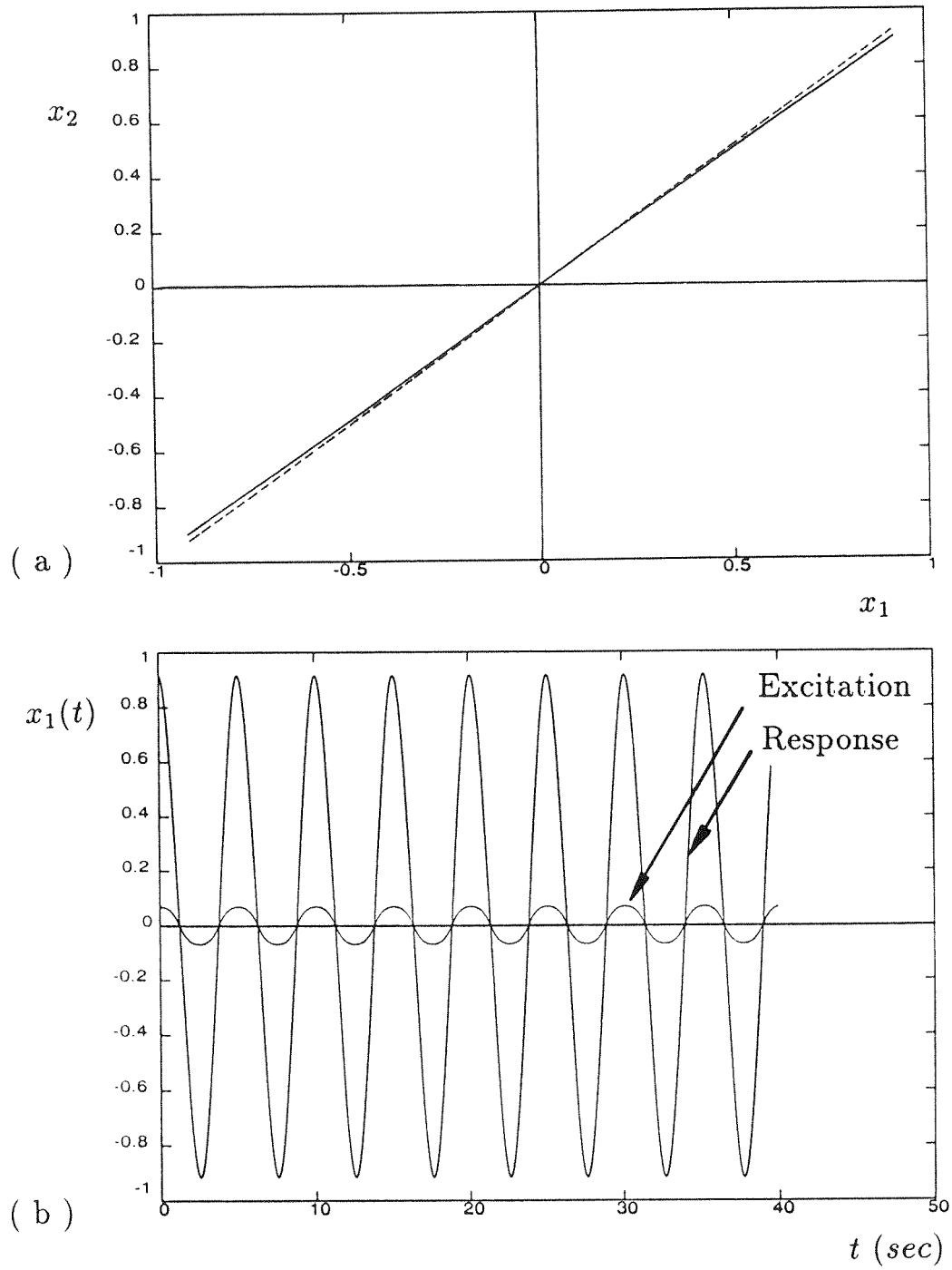

Figure 3.12. Nonsimilar steady state oscillation in the neighborhood of the similar normal mode $c = +1$, corresponding to $K_1 = 1.3$, $K_3 = 0.7$, and $\omega = 1.25$. Forcing function given by (3.128): (a) Modal curve (b) Time signals.

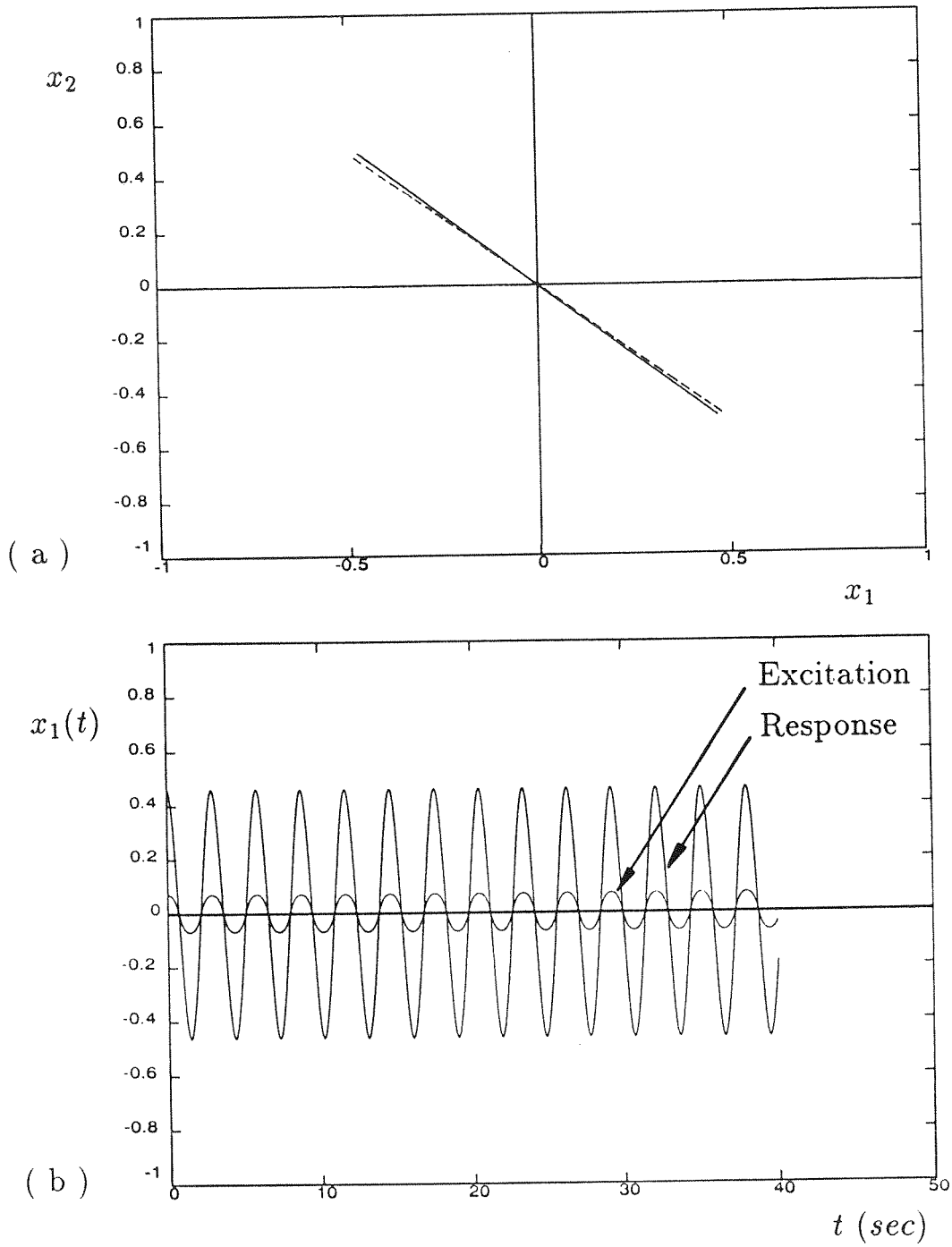

Figure 3.13. Nonsimilar steady state oscillation in the neighborhood of the similar normal mode $c = -1$, corresponding to $K_1 = 1.3$, $K_3 = 0.7$, and $\omega = 2.15$. Forcing function given by (3.128) : (a) Modal curve (b) Time signals.

Set 2 : $\omega = 2.15,\ c = -1$

$$(X_{10}, X_{20}) = (0.456623, -0.456623) \longrightarrow (X_{11}, X_{21}) = (0.462823, -0.486446) \tag{3.130}$$

Both of the resulting steady state motions are orbitally stable. Again, the numerical integrations confirm the existence of exact steady state motions corresponding to the theoretically predicted values of initial conditions.

Although only two forms of periodic excitations were considered in this section, it is evident that one can find an infinity of such forcing functions satisfying the conditions of the basic theorem of the previous section, and thus producing exact steady state motions of the oscillator under consideration. In fact, one can construct such functions by requiring that their "generalized Fourier series" contain only even cosine-terms. Then, one could use the asymptotic methodology presented in the previous section to compute the resulting steady state oscillation.

3.3.3. DISCUSSION

In the previous section, exact, nonsimilar, steady state oscillations were examined. It was shown that during these motions, the system oscillates as in a nonsimilar normal mode of free oscillation; as a result, it was established that the forced oscillator at the steady state is equivalent to an unforced free system, whose parameters, however, are modified according to the specific form of the forcing function.

Initially, the forcing function was taken to be proportional to the steady state displacement. Then, the nonsimilar normal modes of the resulting equivalent free

oscillator were analyzed by the asymptotic technique of section 2.3. These normal modes were then shown to correspond to nonsimilar steady state motions of the forced system. The stability of the steady oscillations was examined by *Floquet* theory, i.e., by numerically integrating the equations of motion and computing the eigenvalues of the corresponding "*Floquet* matrix."

The validity of the asymptotic analytical solutions was found to be limited to the neighborhoods of the normal modes of the unforced oscillator. This is because the modal curves representing the exact steady state in the configuration plane were expressed in a series whose dominant terms corresponded to the free oscillations of the unforced systems. Moreover, the asymptotic analysis was carried out only up to the first order of approximation; therefore, it was only justified when the steady state solution is at "distance ϵ" from the unperturbed response (the normal modes). Also, the outlined analytical expressions were valid for small amplitudes, since terms of order x_1^7, or higher, were omitted. However, one could extend the validity of the approximate solutions, even to large amplitudes, by computing additional coefficients of the asymptotic series.

For systems with cubic nonlinearities and general periodic excitations, i.e., not given as functions of the steady state amplitudes, one has to introduce expansions of the forcing functions in "generalized Fourier series" with respect to a parameter ϕ. This parameter is related to the solution of the zero-th approximation, i.e., the free oscillation of the system and, in fact, is an elliptic "amplitude" function. It was shown that in doing so, one obtains convenient representations for the forces that

can be subsequently used in corresponding functional equations for computing the nonsimilar steady state motions. Using this methodology, a general theorem was stated on the necessary and sufficient conditions that a periodic force must satisfy in order to produce a steady state motion of the oscillator with cubic nonlinearity. As a result of this theorem, the general class of periodic functions that can produce steady state motions in systems with cubic nonlinearity was identified. Moreover, the theorem can be extended to systems with arbitrary degrees of nonlinearity, and with many DOF.

The theorem is valid only for weak excitations and assumes that the unforced (unperturbed) system has nonlinear normal modes. This is because for large forcing amplitudes, one has to take into account higher order terms that were omitted in the presented analysis. Again, the resulting asymptotic expressions are valid only in the neighborhoods of the unperturbed normal modes since the steady state solutions are assumed to result as perturbations of the free oscillations of the unforced system.

The accuracy of the theoretical results was tested by numerically integrating the equations of motion of the system. The asymptotically computed sets of initial conditions were used for the numerical integrations, and the existence of the theoretically predicted steady motions was verified: corresponding to each prescribed set of initial conditions, a modal curve in the configuration plane existed, indicating the presence of an exact steady state oscillation.

3.4. CONCLUDING REMARKS

The exact steady state motions of the class of strongly nonlinear, discrete, undamped oscillators under investigation were examined. During these motions the systems oscillate as in a nonlinear normal mode, and the coordinates are linearly or nonlinearly related for all times. It was shown that exact steady state oscillations always occur in the neighborhoods of the normal modes of the unforced systems. Thus, although the principle of linear superposition does not hold for this class of nonlinear oscillators, the existence and the number of normal modes greatly influences the forced responses.

Similar steady state oscillations can only be achieved for special periodic excitations that can be expressed as functions of the steady state displacements. Since no damping exists, during such motions, the responses are either in phase or out of phase with the excitation, and in addition, they are linearly related for all times. It was shown that explicit analytic expressions describing the steady state motion can be derived. Moreover, these analytical formulas are valid for strong nonlinearities and/or large amplitudes of oscillation. The stability of the responses was approximately studied by a linearized technique.

It was found that for a system in "1-1 resonance," with cubic nonlinearities and bifurcating normal modes of free oscillation, the topology of the steady state frequency response curves changes when a bifurcation of normal modes of the unforced system takes place. At most eight steady states were identified for a given value of the frequency of excitation. Of this total number, only five where found to be

orbitaly stable, and which one was ultimately realized depended on the selection of initial conditions. Note that if a small amount of damping is added to the system, then one should expect certain "jump-phenomena" between the various steady state motions. Also of interest would be to investigate in that case the domain of attraction of each one of the stable steady oscillations. This can be certainly achieved for low energies of motion, but when the amplitude is increased one expects to find chaotic motions and possibly fractal boundaries between the domains of attraction.

For systems in "1-1 resonance" and no additional modes of free oscillation, at most three steady state motions could be realized for any fixed value of the frequency of external excitation. Exact solutions for the frequency response curves were derived, but a difficulty of interpretation of the results was encountered since it was not possible to directly define a convenient amplitude for the exciting force. However, a perturbation analysis indicates that the exact steady state motions of these systems degenerate to well known approximate harmonic steady states found by standard techniques for weakly nonlinear systems.

Although the analytical expressions for the similar steady states hold for strongly nonlinear systems and large amplitudes of oscillation, their validity is restricted from the fact that they can only be realized for special forms of the excitation. To overcome this limitation, nonsimilar steady state motions were considered, i.e., oscillations represented in the configuration space of the system by curves (and not necessarely straight lines). It was shown that there exists a general class of periodic excitations that can produce such exact nonsimilar motions. This class consists

of forcing functions with "generalized Fourier series" that contain only even cosine terms. Moreover, the way in which these "generalized series" are defined depends on the degree of nonlinearity of the system.

In this work, a detailed analysis of a two-DOF system with cubic nonlinearity was carried out, and it was shown that close to each of the normal modes of the unforced oscillator, a pair of exact nonsimilar steady state responses exists. To prove this, the forced problem was transformed to an equivalent unforced one; in the sequence, the asymptotic analysis of section 2.3.3 was implemented to find the nonsimilar normal modes of the transformed system. These oscillations were then shown to correspond to nonsimilar steady states of the original forced problem. In general, it can be stated that nonsimilar steady state oscillations are generic for the class of oscillators under investigation, in the sense that they can be realized for a general class of periodic excitations, and not just for special forms of the forcing functions.

Finally, a general conclusion from this work is that the concept of "nonlinear normal mode" can be successfully used for studying the forced response of nonlinear discrete oscillators. This surprising result comes from the fact that steady state motions result as perturbations of normal modes, *provided that the system is excited by a suitable "admissible" periodic forcing function.* Although harmonic functions may be included in the general class of admissible excitations, it is evident that there is a need to consider alternative forms of forces when the forced behavior of strongly nonlinear oscillators is examined. This conclusion outlines a limitation of conventional methods, since they consider only harmonic excitations and assume

only predominantly harmonic responses. In this work no such assumptions were made, since the general nonsimilar steady state responses were expressed in asymptotic series whose dominant terms consisted of normal mode motions. Hence, for weak excitations, and close to the corresponding normal modes, the steady solutions derived in this section are expected to be more accurate than those obtained by conventional methodologies.

PART II: MODAL IDENTIFICATION: ANALYSIS OF INTERFERING MODES AND EXAMINATION OF THE EFFECTS OF WEAK NONLINEARITIES

4. INTRODUCTION

4.1. OVERVIEW

In Part I of this work, the finite amplitude oscillations of a class of strongly nonlinear, undamped, discrete systems, were examined. The effects of the nonlinearities in the dynamic behavior were investigated, and an insight into some of the complicated chaotic responses was gained. However, a majority of practical engineering structures is designed to operate in small amplitudes of motion. In such cases the nonlinear effects are small compared to the dominant linear terms and, consequently, the structural dynamic behavior may be considered as linear, or at most, as weakly nonlinear. A variety of approximate analytical techniques can then be applied to study the vibrational response.

A major concern regarding practical mechanical structures is to reliably identify their dynamic characteristics, i.e., their natural frequencies and modes of vibration. This is needed in order to control the vibrations of structural components; this is achieved by avoiding the excitation of the structural modes by external periodic forces that may lead to resonance phenomena and thus to possible mechanical failure. Such vibration studies are incorporated in the design of mechanical components, and involve both numerical and experimental procedures.

In the numerical part of the analysis, the structure is usually modelled by a finite-element, or a finite difference model, and its dynamic properties are extracted by extensive computer simulations. The analytical models involve a certain amount

of approximations and simplifications (as all models of real structures do!); hence, the numerical analysis needs to be verified by some experimental procedure. This is performed by means of experimental modal testing, i.e., a test were a structure is excited by a controlled excitation, with simultaneous data acquisition. Extraction of the structural modal parameters is then carried out by performing a modal analysis of the measured response.

Thus, modal analysis, or modal identification, is a collection of techniques for determining the modal properties of practical structures based on the assumption that the dynamic structural response can be expressed as a linear superposition of the responses of individual modes. Hence, an essential assumption of modal analysis concerns the linearity of the structure, since only then the principle of modal superposition can be applied. The basic objectives of modal analysis can be outlined as follows:

- Validation and refinement of Finite-element structural models, and/or performance of correlation studies between numerical and experimental data in order to identify possible causes of disrepancies between predicted and measured data sets.

- Construction of mathematical models of the structure for subsequent use in Substructure synthesis analyses, or in analytical studies of the effects of possible structural modifications (design optimization of the structure).

- Construction of modal models of the structure in certain frequency ranges in order to develop robust structural control algorithms for vibration of shock isolation.

A wide range of modal analysis methods can be found in the literature: methods in the frequency or in the time domain, deterministic or stochastic, with single or multiple inputs and outputs, etc. A basic problem (and limitation) inherent in the majority of modal analysis techniques,is their inaccurate performance when structures with interfering (or closely spaced) modes, or systems with certain amounts of stiffness or damping nonlinearities, are encountered.

Conventional identification techniques are highly effective on systems whose modes are well spaced. There are, however, limitations on the applicability of these methods to systems with interfering modes, i.e., modes with very closely spaced natural frequencies and large differences in their dampings and participation factors (modal constants). In these cases, the results of modal analysis using conventional methods are generally inaccurate. More importantly, when heavy mode interference occurs, the number of "peaks" observed in the measured Frequency Response Functions (FRF), may not necessarily correspond to the actual number of modes in the examined frequency range. Hence, certain modes of the structure might be overlooked by a conventional modal analysis routine. This results in incomplete characterization of the dynamic performance of the structure, and subsequently, in serious mismatches between the theoretical predictions of the eigenproperties of the structure (derived for example by a finite element program) and the experimentally extracted ones.

Problems with interfering modes arise often in engineering practice. This is observed in systems with symmetries in their spatial distribution or in repetitive structures with light damping. As mentioned in (Pappa, 1990), finite element simulations of a

large space structure, such as the Space Station "Freedom," indicate large "clusters" of closely spaced modes (namely 366 modes under 1 Hz and 3000-4000 modes below 20 Hz). As pointed out in the same reference, if the identification results are to be used for creating reliable models of such structures, they must describe accurately the experimental dynamic response: if the extracted modal parameters are in error, or if the number of identified modes is much smaller than the actual number of modes in the frequency range of interest, an incomplete description of the dynamics result. Thus, there is a need for developing techniques that can reliably analyze interfering modes, i.e., modes whose FRF is distorted by the presence of nearby modes.

An additional problem encountered in practical engineering structures is that of the presence of nonlinearities. These can be material (stiffnesses or damping) nonlinearities, or they can result from the geometry of the structural components. An additional cause for nonlinear behavior can be the presence of friction between two contacting mechanical components, the occurence of impacts between several structural members during operation, or the attachments (boundary conditions) of the structure with the ground or with some other structure.

For example, in cases where dry friction occurs, or clearances exist between certain structural components, the structural response is a nonlinear function of the excitation. Then, the basic assumption of linearity is violated, nonlinear distortions exist in the measured FRF and conventional modal identification algorithms fail to accurately predict the modal parameters of the system. Therefore, an addi-

tional challenge in modal analysis is to analyze the distortions in the FRF caused by nonlinear effects, to detect the type of nonlinearities present in the system and to possibly quantify (measure) their amount. This would enable the analyst not only to identify the linear modal properties with improved accuracy, but also to find the possible sources of the nonlinearities. This in turn could lead to possible design modifications of the structure, with subsequent elimination of the nonlinear distortions.

4.2. OBJECTIVES - OUTLINE OF WORK

The general aim of this part of the work is to develop refined algorithms for identifying closely spaced (interfering) modes, and to analytically study the distortions in the frequency response plots caused by stiffness or damping structural nonlinearities. The modal analysis will be performed in the frequency domain, assuming that the structure is excited by a single harmonic force.

Initially, the Nyquist plot of a system with two closely spaced modes, will be considered. Restricting the frequency close to the natural frequency of one of the modes (the "perturbed mode"), the interaction of the "perturbing mode" will be approximated by expanding its FRF in a Taylor series with respect to the frequency variable, and retaining only the first two terms. Geometrical arguments will then be used to construct an identification algorithm that takes into account distortions in the Nyquist plot due to mode interference.

In the sequence, vibrating modes with weak nonlinearities will be considered. The

first order effects of the nonlinearities on the steady state response will be computed, by means of an "equivalent linearization" technique, and the resulting nonlinear distortions in the FRF will be detected and quantified. The general objective will be to construct an approximate algorithm that leads to accurate estimates for the modal parameters and the perturbing weak nonlinear effects.

The applicability of the outlined techniques will be tested with theoretically generated and experimental data, and the limitations of the proposed methodologies will be discussed.

5. MODAL ANALYSIS OF INTERFERING MODES

5.1. PREVIOUS WORK

A comprehensive presentation of some of the existing algorithms for modal identification can be found in (Ewins, 1984) and in the general review article by (Rades, 1985). Also, a very interesting and detailed discussion about some of the most popular modal analysis methods is given in the thesis by N.Maia (Maia, 1988). Generally, modal analysis algorithms can be classified in certain major categories.

Depending on the domain where the identification is carried out, modal analysis techniques can be characterised as *time-domain*, or as *frequency-domain* methods. As pointed out in (Maia, 1988), generally, time-domain algorithms tend to provide best results when a large frequency range or a large number of modes exist in the data, whereas frequency-domain methods give best results for restricted frequency ranges and limited number of modes. Depending on the number of modes that a modal analysis algorithm can analyze, there is an additional classification between *single - degree - of - freedom (SDOF)* and *multi - degree - of - freedom (MDOF)* methods. Note, however, that this classification holds for frequency-domain methods only, since all time-domain methods are MDOF ones.

Furthermore, modal analysis algorithms that can be applied to only one frequency response function (FRF) at a time are characterised as *single - input - single - output (SISO)* methods, whereas those that can simultaneously analyze many FRF are classified as *multiple - input - multiple - output (MIMO)* methods. Other meth-

ods assume a single excitation of the structure, but analyze measurements from different points. These are referred to as *single - input - multiple - output (SIMO)* methods. Considering the type of model that a modal analysis algorithm assumes for the structure, one can further distinguish between *indirect* and *direct* methods. If the structure is simulated by a modal model, i.e., if the unknowns are the modal parameters of the system, the algorithm is characterised as *indirect.* Otherwise, if a spatial model is assumed, i.e., if one seeks to directly determine the system matrices, the modal analysis is *direct* (Maia, 1988). A last classification has to do with the deterministic or stochastic nature of the model that the algorithm uses to simulate a practical system. Hence, modal analysis methods can be categorized as *deterministic* or *stochastic.* The advantage of the stochastic methods is that they can effectively take into account the "pollution" of the measured experimental data by noise, whereas in the deterministic methods this is difficult to achieve. However, a disadvantage of the stochastic methods is that they are generally more computationally involved and, furthermore, their algorithms are generally more difficult to physically interpret.

Examples of indirect, time-domain methods are the "Complex Exponential Method" (Brown, 1979), (Spitznogle, 1970), where the impulse response functions obtained from inverse Fourier transforms of the FRF are analyzed; and the "Ibrahim Time Domain Method" (Ibrahim, 1973, 1976), (Pappa, 1981), where the free decay time responses of the system are curve fitted, and a "Double Least Squares procedure" is used to obtain estimates for the modal parameters. A representative of time

domain, direct methods is the "Autoregressive Moving Average Method (ARMA)" (Gersch, 1979, 1982), where the system to be identified is modelled by a linear ordinary differential equation, which in turn is discretized to a difference equation by sampling the time response in equal time intervals. The difference equation is then fitted to the measured data by numerically minimizing a suitably defined error function.

There exists a variety of indirect, SDOF, frequency domain methods. In the "Peak Amplitude Method" (Pendered, 1963), the natural frequencies of the system are identified as the frequencies corresponding to the "peaks" of the FRF. The remaining modal parameters are then found by considering the slopes of the "peaks" and their relative magnitudes. In (Pendered, 1965), the natural frequencies are identified as corresponding to the points where the real part of the FRF vanishes. In the now classical paper of Kennendy and Pancu (Kennendy, 1947), it is shown that close to the natural frequencies, the Nyquist plots of systems with hysteretic damping are almost circular. Thus, circles can be fitted to the resonance regions of the measured FRF. The natural frequencies are then identified as the points of maximum frequency separation of the Nyquist points, whereas the modal dampings and modal constants are computed by considering the "half power points" and the diameters of the circle fits. Extensions of this method for systems with viscous damping can be found in (Klosterman, 1971). In (Marples, 1973), an analytic formula for calculating the hysteretic modal damping is given. In (Vakakis, 1985) and (Ewins, 1989), the result of Marples is extended, and analytical expressions for deriving not only the

modal damping, but also the natural frequency from the circle fit, are presented. In (Dobson, 1987), complex modes are considered and the dynamic stiffness FRF (inverse of the receptance) is analyzed by a refinement process that minimizes errors due to unaccounted, out-of-range modes.

A list and a discussion of various indirect, MDOF methods can be found in (Ewins, 1984) and (Maia, 1988). Some typical references of this class of methods are (Gaukroger, 1973) where a simultaneous least-squares fit of the Nyquist plot of several modes is attempted, and (Ewins, 1982), (Maia, 1989), where lightly damped structures are considered, and mathematical models with real modes are fitted to the measured FRF.

A restriction concerning the majority of the aforementioned modal analysis methods is their inaccurate performance when "interfering" modes are analyzed, i.e., modes whose measured FRF is perturbed by the presence of near-by modes. This is the case when closely spaced modes in the frequency domain (i.e., whith natural frequencies very close to each other) are considered. Also, modal interference can result between moderately spaced modes that have, however, large differences in the values of their modal dampings and/or modal constants. A discussion about indicators and criteria for modal interference in the FRF, can be found in (Marples, 1973), (Vakakis, 1985), (Traill-Nash, 1967). Unfortunately, not much work has been done regarding the problem of modal interference, and thus, only a few modal analysis techniques exist dealing with systems containing closely spaced modes.

In (Montalvao e Silva, 1986), regions of the Nyquist plots of interfering modes where

the SDOF identification algorithms yield relatively accurate results are defined. A "mode interference criterion" is then introduced and applied iteratively to correct the initial poor estimates of the modal parameters. The main feature of the methodology is that it can lead to estimations of the "rigid body rotations" of the modal circles caused by modal interaction and, hence, to better estimates for the phases of the modes. However, the technique requires interaction from the part of analyst and its success essentially depends on his/her experience, since there are certain constants that are assigned empirical numerical values. In (Maia, 1988), the real and imaginary parts of the inverse of the receptance FRF are examined. It is shown that complex modes that are practically indistinguishable in the Nyquist plots can be reliably recognized when their inverse receptance plots are considered. Therefore, it is concluded, that an accurate indicator for detecting closely spaced modes is the examination of alternative representations of the measured data, other than the classical Nyquist plots.

An interesting iterative algorithm using a circle-fit SDOF method is outlined in (Robb, 1988), where the FRF of closely spaced motions is considered. After identifying the first of the two modes, the (generally inaccurate) modal estimates are used to regenerate a SDOF frequency response, which in turn is subtracted from the (total) measured FRF. Then, the second mode is expected to dominate the remaining FRF, and it can be identified with improved accuracy by means of a SDOF modal analysis technique. The iterations can be continued by subtracting each time the identified mode and modal analyzing the remaining response. A criterion to stop

the iterative procedure was that the difference of two consecutive iterations be less than a prescribed small amount. A more detailed presentation of this algorithm will be given later, since it will be used in association with some refined, proposed modal analysis methods.

In (Dobson, 1987), the theoretical FRF of two closely spaced modes is analyzed by a different iterative technique. No "circle-fitting" is involved, since the technique is based upon difference equations. The dynamic stiffness FRF (inverse of receptance) is analyzed by a repetitive, refinement process that minimizes errors due to unaccounted out-of-range modes and noise. This is achieved by modifying the SDOF expressions of the receptance by adding certain residual effects representing out-of-range modes. A different approach is used in (Dossing, 1986), where a deconvolution of the measured FRF is used, leading to a "mode spectrum" where each line represents a damped natural frequency of the structure. Application of this method shows that it can lead to separation of closely spaced modes, especially when the interference is caused by differences in the modal constants (participation factors). Finally, in (Lee, 1990), a time-domain method based on a "suboptimum maximum likelihood" discrete estimation scheme is applied to the problem of closely spaced modes. This "stochastic" methodology is computationally involved, takes into account noise in the measured data, and utilizes special forms of Autoregressive Moving-Average with exogeneous inputs (ARMAX) models. Theoretical, heavily interfering modes were analyzed and as shown, the method leads to very accurate modal estimates even for noisy data.

In what follows, the Nyquist plot of a system with two closely spaced modes, is considered. Restricting the frequency close to the natural frequency of one of the modes (the "perturbed mode"), the interaction of the "perturbing mode" is approximated by expanding its FRF in a Taylor series with respect to the frequency variable, and retaining only the first two terms. Geometrical arguments are then used that lead to an identification algorithm that takes into account distortions in the Nyquist plot due to mode interference. According to the aforementioned classification of modal analysis methods, this algorithm is in the frequency-domain, indirect, SISO, and deterministic. Moreover, it can be considered as an extension for the case of closely spaced modes of the conventional SDOF technique described in (Ewins, 1989). Hence, a synopsis of this SDOF method is appropriate at this point in order to demonstrate its poor performance when interfering modes are considered.

5.2. LIMITATIONS OF A CONVENTIONAL SDOF METHOD

In this section, a brief presentation of a conventional SDOF modal analysis method will be given. Although the method gives accurate modal estimates when well separated modes are considered, its performance is inaccurate when interfering modes are encountered. This limitation is inherent to the general class of conventional algorithms, and this stresses the importance of developing refined modal analysis methods that take into account modal interference. The SDOF methodology presented in this section will be implemented later in the applications section, in

association with a refined, new identification algorithm.

Consider an N-mode system with light hysteretic damping. One does not lose in generality by this assumption, since it can be shown that for low values of damping the hysteretic and viscous models give almost identical performances. The FRF of the system can then be expressed as follows:

$$a_{jk}(\omega) = \sum_{s=1}^{N} \frac{{}_sA_{jk}}{\omega_s^2 - \omega^2 + i\eta_s\omega_s^2} \cong \frac{{}_rA_{jk}}{\omega_r^2 - \omega^2 + i\eta_r\omega_r^2} + {}_rB_{jk} \qquad (\omega^2 \quad close \ to \ \omega_r^2) \tag{5.1}$$

where $a_{jk}(\omega)$ is the receptance FRF, defined as the ratio of the steady state displacement at coordinate j divided by a harmonic force acting at coordinate k. The quantity ω is the frequency of steady state vibration in (rad/sec); ω_s is the s-th natural frequency; η_s is the loss factor of the s-th mode; ${}_sA_{jk}$ is the complex modal constant of the s-th mode; and $i = \sqrt{-1}$. The effect of the (N-1) remaining modes on mode r is denoted by the term ${}_rB_{jk}$. For well separated modes, it can be assumed that this is a constant complex quantity (Ewins, 1984).

The plot of equation (5.1) in the complex plane with ω as the varying parameter is shown in figure 5.1a. It can be seen that in the region where $\omega \simeq \omega_r$, the receptance plot is a circle displaced from the origin by the complex constant ${}_rB_{jk}$ (Ewins, 1984). Considering three points A, B and C corresponding to frequencies squared $\omega_A^2, \omega_A^2 - d\omega^2$, and $\omega_A^2 + d\omega^2$ respectively, one defines the quantity Δ as follows (see figure 5.1a for a definition of the angles):

$$\Delta \equiv \frac{1}{tan(\frac{\Delta\theta}{2})} - \frac{1}{tan(\frac{\Delta\phi}{2})} \tag{5.2}$$

As shown in (Ewins, 1989), the value of Δ does not depend on the frequency increment $d\omega^2$, but only on the frequency ω_A of the center point A:

$$\Delta = \frac{2}{\eta_r}(1 - \frac{\omega_A^2}{\omega_r^2}) \tag{5.3}$$

Thus, for each triad of points, the quantity Δ can be regarded as a function of the frequency of the center point, and it can be plotted in a diagram versus frequency (figure 5.1b, "Δ - plot"). This plot is a straight line passing through zero at the natural frequency of the system, with a slope equal to $tan\mu = 2/\eta_r\omega_r^2$.

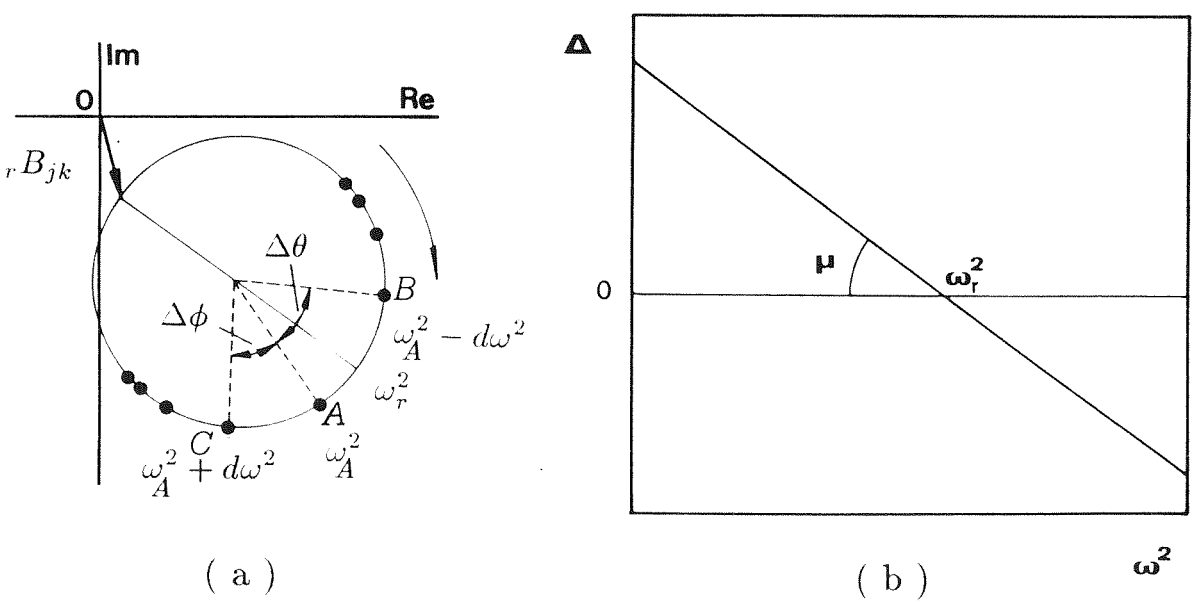

Figure 5.1. Δ-Plot method for modal analysis: (a) Nyquist plot of the FRF of an isolated mode.(b) Δ-Plot of a theoretically generated mode.

The Δ - plot is constructed by circle-fitting FRF points in the resonance region of a mode and by measuring the angles formed by lines connecting points on the modal circle. The modal parameters can then be conveniently estimated by considering the zero-crossing of the graph and its slope. Note that circle fitting is not a simple process (Brandon, 1983), and careful consideration should be given to it since it affects essentially the success of modal analysis. In this work, the circle-fitting algorithm outlined in (Moltalvao e Silva, 1988) was used, and the optimum circle fit was obtained by minimizing a certain scalar error by means of a least-squares procedure (this error is denoted by e_2 in that reference). In figure 5.2, the Δ-plot constructed from experimentally measured data from the blade of a turbine engine is presented. The predicted linear pattern can be clearly detected, and the modal parameters can be accurately extracted by a least squares straight line fit.

Both theoretical and experimental data were analyzed by this method in (Ewins, 1989). In the same reference, a discussion of the advantages and limitations of the methodology is carried out, and its performance is compared with that of other circle-fitting interpolation algorithms. The method is found to work accurately for well-spaced FRF points in the Nyquist plot, but it is affected by noise when the central angles between subsequent points are small (as in cases of heavily damped modes). In such cases, the quantity Δ results by differencing large quantities and is sensitive to experimental errors. In addition, when closely spaced modes are considered relation (5.1) does not apply since mode interference cannot be accurately approximated by a single complex constant ${}_rB_{jk}$, and the modal estimates derived

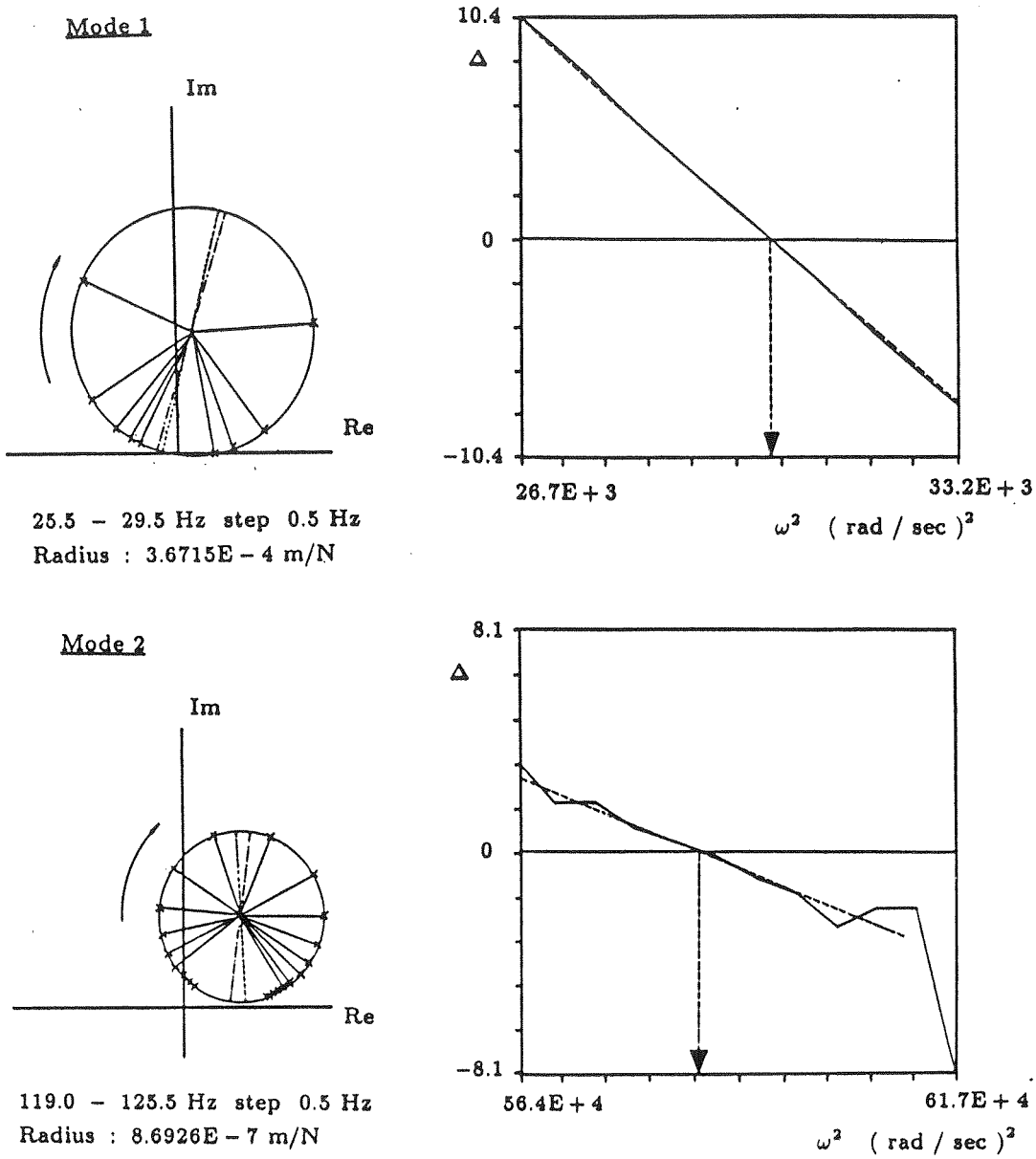

Figure 5.2. Modal analysis of an experimental FRF : (a) Circle fit in the resonance region.(b) Δ-Plot.

by the Δ - plot method are not satisfactory any more.

This is clearly shown in figure 5.3, where the Δ - plots of two theoretically-generated, interfering modes are displayed. For comparison, the straight lines corresponding to the isolated modes are also shown. Note that the modal interference distorts the theoretically predicted straight lines by displacing and curving them. The estimates for the natural frequency and the modal damping are, therefore, inaccurate and modal analysis based on this methodology is no longer satisfactory.

From the aforementioned discussion, it is clear that a refined algorithm should be developed for investigating closely spaced modes; one that takes into account distortions of the Δ - plots such as those observed in figure 5.3.

5.3. ANALYSIS OF MODAL INTERFERENCE

Consider again the N-DOF system with hysteretic damping, and assume that there exists a pair of closely spaced modes r and m. Close to the natural frequency of one of these modes, mode r say, the receptance takes the form

$$a_{jk}(\omega) = \sum_{s=1}^{N} \frac{{}_{s}A_{jk}}{\omega_s^2 - \omega^2 + i\eta_s\omega_s^2} \cong$$

$$\cong \frac{{}_{r}A_{jk}}{\omega_r^2 - \omega^2 + i\omega_r^2\eta_r} + \frac{{}_{m}A_{jk}}{\omega_m^2 - \omega^2 + i\omega_m^2\eta_m} + {}_{rm}B_{jk}$$

$$(\omega \simeq \omega_r) \qquad (5.4)$$

where ${}_{rm}B_{jk}$ is the effect that the $(N-2)$ remaining modes have on the resonance region of the r^{th} mode (constant complex). Since the frequency ω is restricted in

the neighborhood of the r^{th} natural frequency ω_r, it can be stated that

$$1 - \frac{\omega^2}{\omega_r^2} = \mathcal{O}(\epsilon) \tag{5.5}$$

where $|\epsilon| \ll 1$ is a small quantity and as before, $\mathcal{O}(\bullet)$ denotes order of magnitude.

A measure of the difference between the natural frequencies of the interfering modes is given by the quantity D, defined as

$$D \equiv \frac{\omega_m^2 - \omega_r^2}{\omega_r^2} \tag{5.6}$$

Although D is a small quantity (since the modes are closely spaced), it will be assumed that the frequency ω is chosen close enough to ω_r, so that D has a much greater magnitude than ϵ. Thus, if the modes are very closely spaced, one should restrict the range of the frequency to a very small neighborhood of the r^{th} natural frequency.

The FRF of the "perturbed" mode will be now approximated by the first two terms of its Taylor expansion with respect to the frequency. This will lead to a simplified model of mode interference which will be used subsequently for the construction of a modal analysis algorithm. To this end, expand the FRF of the m^{th} mode in a Taylor series about zero with respect to the frequency variable $(1 - \frac{\omega^2}{\omega_r^2})$, and retain only the first two terms:

$$\frac{{}_mA_{jk}}{\omega_m^2 - \omega^2 + i\omega_m^2\eta_m} =$$

$$= \frac{{}_mA_{jk}/\omega_r^2}{i\eta_m + D(1 + i\eta_m)} - \frac{(1 - \frac{\omega^2}{\omega_r^2}){}_mA_{jk}/\omega_r^2}{[\, i\eta_m + D(1 + i\eta_m)\,]^2} + \mathcal{O}[(1 - \frac{\omega^2}{\omega_r^2})^{\,2}\,]$$

$$(\ \omega^2 \simeq \omega_r^2\ ) \tag{5.7}$$

Substitute now equation (5.7) into (5.4), to obtain the following approximate expression for the receptance of the system in the neighborhood of the r^{th} natural frequency:

$$a_{jk} \cong \frac{{}_rA_{jk}}{\omega_r^2 - \omega^2 + i\omega_r^2\eta_r} + {}_{rm}C_{jk}(1 - \frac{\omega^2}{\omega_r^2}) + {}_{rm}\tilde{B}_{jk} + \mathcal{O}[\,(1 - \frac{\omega^2}{\omega_r^2})^{\,2}\,]$$

$$(\ \omega^2 \simeq \omega_r^2\ ) \qquad (5.8)$$

where ${}_{rm}C_{jk}$ and ${}_{rm}\tilde{B}_{jk}$ are complex constants (i.e. they do not depend on the frequency) given by

$${}_{rm}C_{jk} = \frac{{}_mA_{jk}/\omega_r^2}{[\ i\eta_m + D(1 + i\eta_m)\ ]^2}\ , \quad {}_{rm}\tilde{B}_{jk} = {}_{rm}B_{jk} + \frac{{}_mA_{jk}/\omega_r^2}{i\eta_m + D(1 + i\eta_m)} \qquad (5.9)$$

Note from the above expression that there exists an $\mathcal{O}(\epsilon)$ frequency-dependent correction given by the second term of equation (5.8) ; this causes the distortion of the relative spacing of the FRF points in the Nyquist plot. Note that when modes m and r are well separated, the quantity D is large. In that case, the frequency-dependent term becomes negligible (since it contains D squared in the denominator) and equation (5.8) reduces to the form (5.1), that is the case of an isolated mode.

A geometrical interpretation of the derived analytical results will now be given (this formulation will be used in later sections). In figure 5.4a, the two modal circles corresponding to the two interfering modes are drawn. It was assumed that $\omega_r^2 < \omega_m^2$ (this does not restrict, however, the generality of the analysis). Mode r will be denoted as the "perturbed" mode while mode m will be the "perturbing" one. Referring to figure 5.4a, it is clear that the receptance FRF of the system can

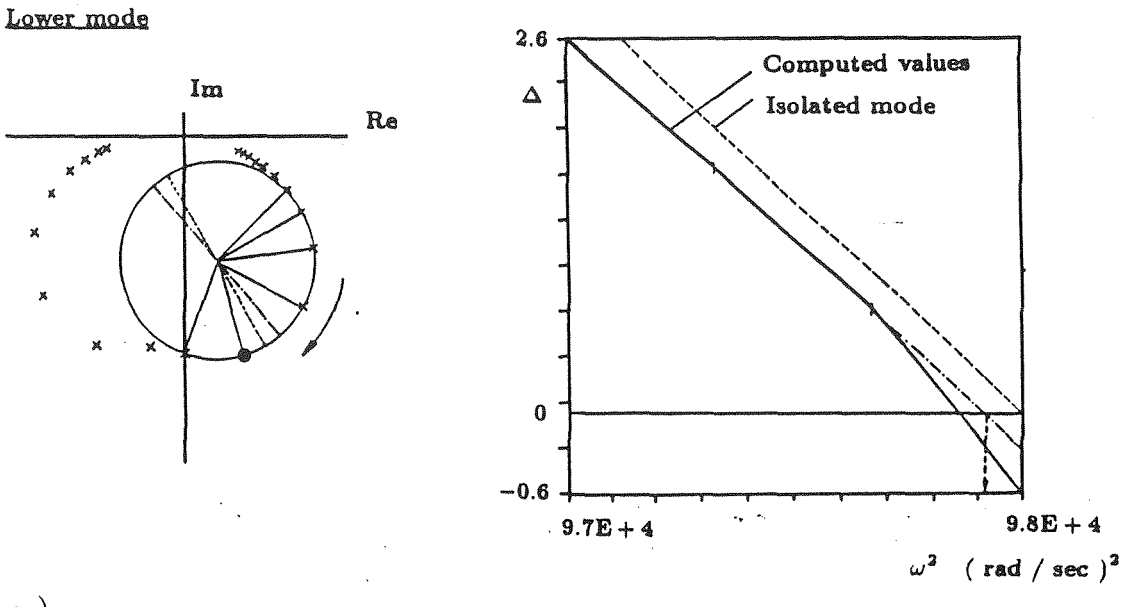

(a)

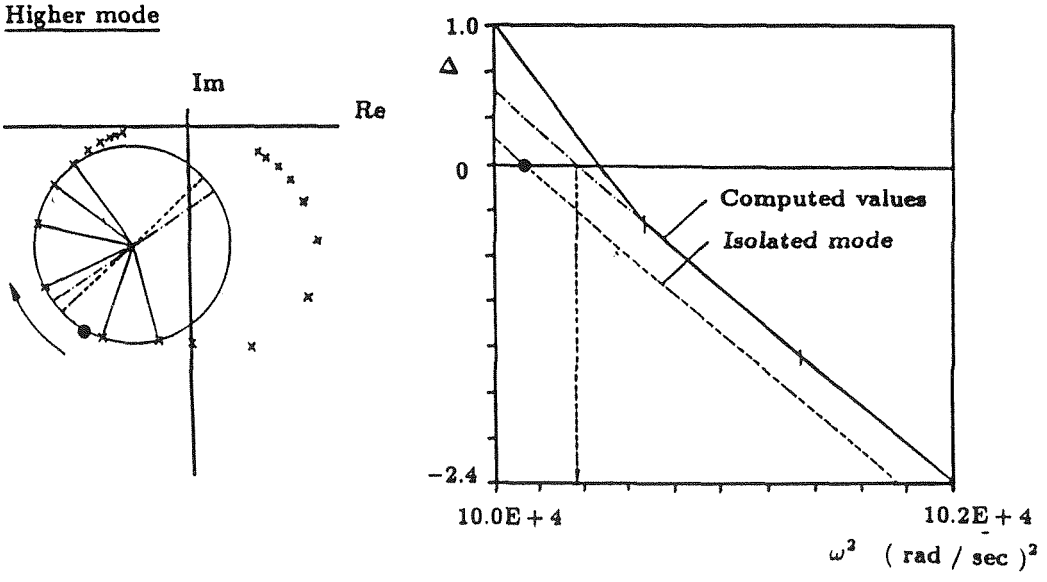

(b)

Figure 5.3. Distorted Δ-Plots of two interfering modes: (a) Lower mode (b) Higher mode

be represented by the vectorial summation

$$a_{jk} \cong \overline{OK_1} + \overline{OK_2} + \overline{OK_3} \quad (\omega^2 \simeq \omega_r^2) \tag{5.10}$$

where $\overline{OK_3}$ is a frequency-independent vector representing the interference of the remaining $(N-2)$ modes (in equation (5.4) this quantity is represented by the complex constant ${}_{rm}B_{jk}$). Since the frequency is restricted to be close to the resonance of the r^{th} mode, large variations in the amplitude and phase are anticipated for the vector $\overline{OK_1}$, in contrast to vector $\overline{OK_2}$ that has a relatively small variation. Thus, to the first order of accuracy, for $\omega^2 \simeq \omega_r^2$, the vector $\overline{OK_2}$ can be assumed to vary along the tangent of the m^{th}-modal circle at $\omega^2 = \omega_r^2$ (figure 5.4b). This, however, is equivalent with taking the Taylor expansion of the FRF of the m-mode about $\omega^2 = \omega_r^2$ and retaining only the two first terms (equation (5.7)). The approximate combined response of the system (valid in the resonance region of the r-th mode), can then be expressed as follows:

$$a_{jk} \cong \overline{OK_1} + \overline{OK_{2r}} + \overline{\Delta OK_{2r}} + \overline{OK_3} + \mathcal{O}(\epsilon^2) \quad (\omega^2 \simeq \omega_r^2) \tag{5.11}$$

where $\overline{OK_{2r}}$ is the response of mode m at $\omega^2 = \omega_r^2$ (a frequency-independent quantity) and $\overline{\Delta OK_{2r}}$ is a frequency-dependent vector with a constant direction (fixed by the phase of the complex quantity ${}_{rm}C_{jk}$, eq.(5.9)). This is the direction of the tangent on mode m, at frequency ω_r^2. Note that equation (5.11) is equivalent to the analytical formula (5.8) and, in fact, it is the geometrical representation of that expression.

Referring now to figure 5.5, consider three points A, B, and C on the r^{th} modal circle, corresponding to frequencies squared $\omega^2, \omega^2 - d\omega^2$, and $\omega^2 + d\omega^2$ respectively.

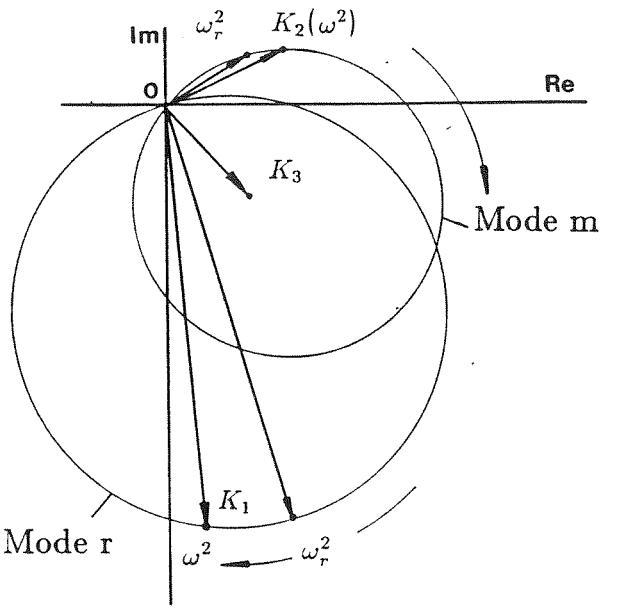

(a)

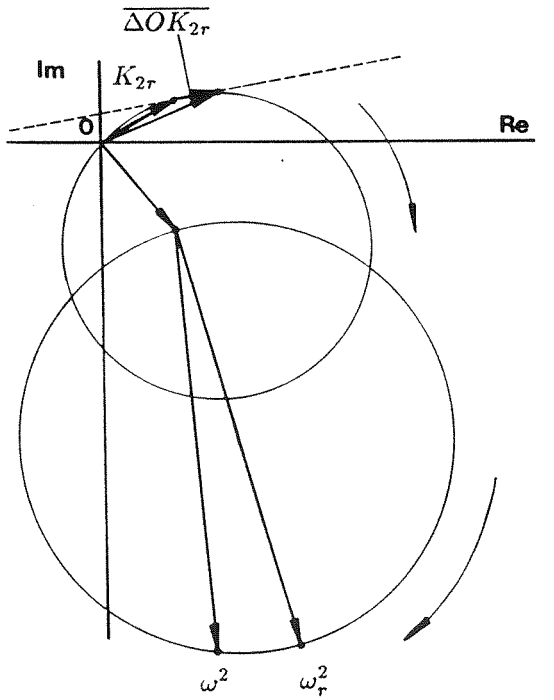

(b)

Figure 5.4. Geometry of modal interference : (a) Exact representation (b) First order approximation (equation 5.8).

This triad of points is distorted due to the interfering effects of the remaining (N-1) modes, as follows.

• First, the triad is distorted to the position $A_1B_1C_1$. This distortion results from the rigid translation of the modal circle by the vector $\overline{OK_{2r}}+\overline{OK_3}$. This interference does not affect the *relative* spacing of the points in the triad, and so the ideal SDOF distribution of points on the r-th modal circle is preserved.

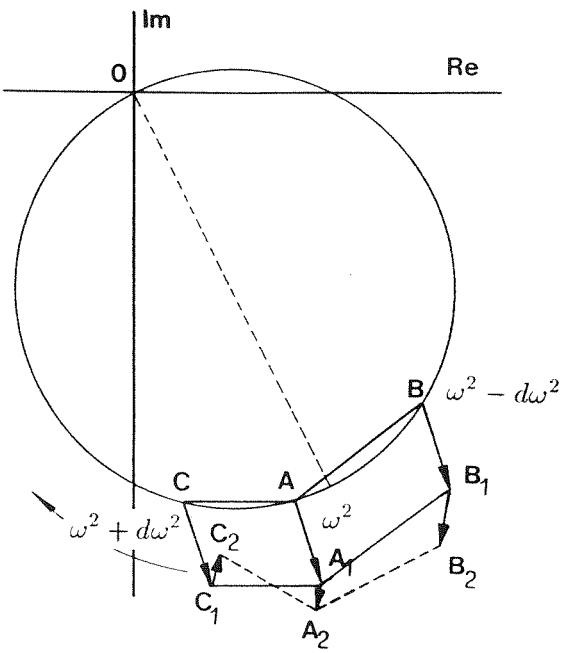

Figure 5.5. Distortion of a triad of points (B C A) caused by interference from a closely spaced mode (first order of approximation, equation (5.8)).

• A secondary distortion is caused by the distorting effects of mode m. This is a frequency-dependent interference, and is represented by the vectors $\overline{\Delta OK_{2r}}$ of figure 5.4b. Since these vectors have a constant direction, it can be stated that, correct to $O(\epsilon)$, points A_1, B_1 and C_1 are distorted in the same direction by vectors

(see figure 5.5):

$$A_1A_2 =_{rm} C_{jk}(1 - \frac{\omega^2}{\omega_r^2})$$
$$B_1B_2 = A_1A_2 +_{rm} C_{jk}\frac{d\omega^2}{\omega_r^2}, \qquad C_1C_2 = A_1A_2 -_{rm} C_{jk}\frac{d\omega^2}{\omega_r^2} \tag{5.12}$$

Clearly, this secondary frequency-dependent interference modifies the ideal SDOF frequency distribution of the modal circle since the relative position of the points in the triad is altered.

From the aforementioned discussion, it is evident that a closely spaced "polluting" mode introduces alterations in the relative spacing of points in the Nyquist plot of the perturbed mode. In what follows, the geometric arguments in the complex plane will be used to develop a refined identification algorithm that takes into account frequency - dependent distortions due to modal interference.

5.4. IDENTIFICATION ALGORITHM FOR INTERFERING MODES

Consider again the distorted Nyquist plot of the "polluted" mode (figure 5.6). The distorted FRF points are denoted by double-primes in what follows, and it is exactly these points that are measured during a modal analysis experiment. Referring to the triad of points $B''A''C''$ on the "perturbed" r^{th} modal circle, the relation between the lengths $A''B''$ and $A''C''$ of the distorted plot and the corresponding "unperturbed" ones AB and AC, will now be examined. Since one is only interested in the *relative* displacements of points B'' and C'' with respect to the center point of the triad A'', one translates the triad (BAC) by the constant vector AA'' so that point A coincides with point A'' of the distorted plot. By using simple geometrical

relations, it can be stated that (see figure 5.6 for a definition of the various segments and angles):

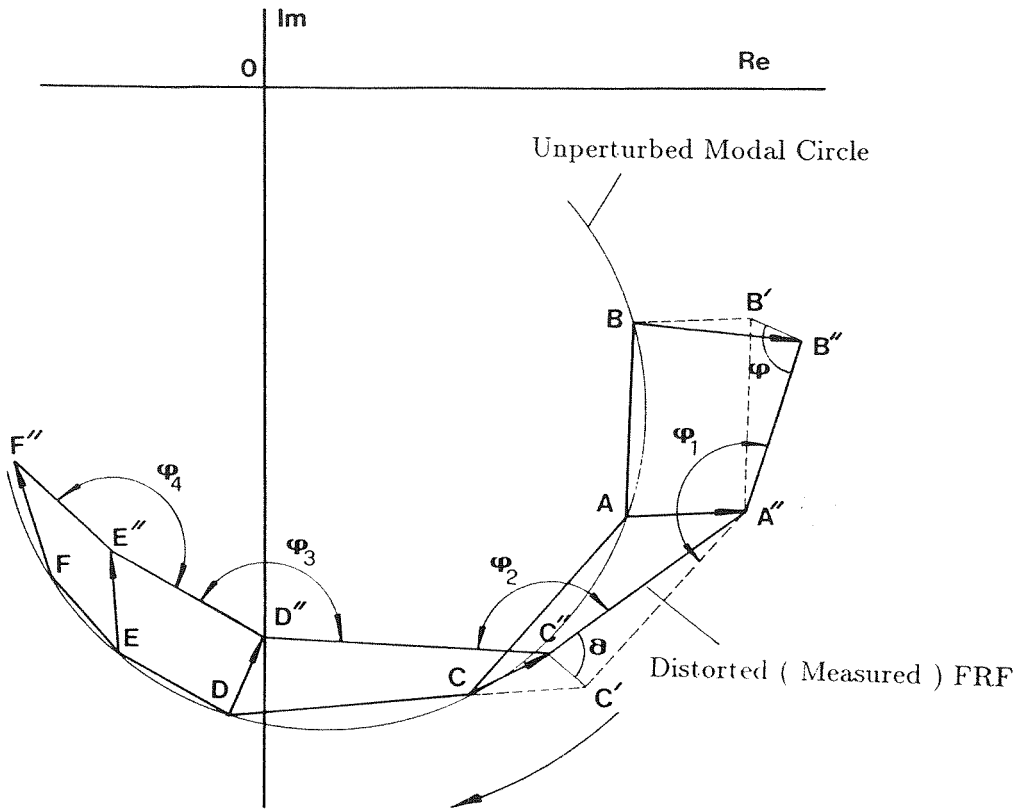

Figure 5.6. Distorted Nyquist plot. Frequencies of points: $B, B'' \rightarrow \omega^2 - d\omega^2$, $A, A'' \rightarrow \omega^2$, $C, C'' \rightarrow \omega^2 + d\omega^2$, $D, D'' \rightarrow \omega^2 + 2d\omega^2$, $E, E'' \rightarrow \omega^2 + 3d\omega^2$, $F, F'' \rightarrow \omega^2 + 4d\omega^2$.

$$\begin{aligned} (AB)^2 = (A''B')^2 &= (A''B'')^2 + x^2 - 2(A''B'')x\cos\phi \\ (AC)^2 = (A''C')^2 &= (A''C'')^2 + x^2 - 2(A''C'')x\cos\theta \end{aligned} \tag{5.13}$$

where $x = |B'B''| = |C'C''| = |_{rm}C_{jk}|d\omega^2/\omega_r^2$, and $\theta = \phi_1 + \phi - 180°$. The quantities $(A''B''), (A''C'')$ and ϕ_1 are directly measurable from the Nyquist plot of the FRF, and the lengths $(AB), (AC)$ can be expressed as functions of the modal

parameters of the r^{th} mode since A, B, C belong to the "unperturbed" r^{th} modal circle (see Appendix D for the actual expressions).

Dividing the first of equations (5.13) by the second and using the equations derived in the Appendix D for lengths (AB) and (AC), one obtains the following relation for the distorted triad $(B''A''C'')$:

$$\frac{1+(y+\frac{z(z-1)}{y})^2}{1+(y+\frac{z(z+1)}{y})^2} = \frac{(\frac{A''B''}{A''C''})^2 + w^2 - 2(\frac{A''B''}{A''C''})wcos\phi}{1+w^2+2wcos(\phi+\phi_1)} \qquad (5.14a)$$

where

$$y = \eta_r\omega_r^2/d\omega^2, \qquad z = (\omega_r^2-\omega^2)/d\omega^2, \qquad w = x/(A''C'')$$

The following remarks can be made, as far as relation (5.14a) is concerned. First, this expression characterizes the frequency distribution of a single triad of points corresponding to frequencies squared $\omega^2 - d\omega^2, \omega^2, \omega^2 + d\omega^2$. There are four unknown variables in this equation, namely z, related to the natural frequency ω_r^2; y , related to the modal damping η_r; and w and ϕ, related to the frequency-depended interference of the perturbing mode. All the other variables can either be measured directly from the Nyquist plot (lengths $(A''B'')$ and $(A''C'')$), or are fixed by the frequencies of the points of the particular triad (quantities $\omega^2, d\omega^2$). Note that the variables appearing in equation (5.14a) are all normalized, so that their values are of comparable orders of magnitude (this is important for the numerical evaluation of the unknowns).

Considering subsequent triads $(A''C''D''), (C''D''E'')$ and $(D''E''F'')$ (see figure

5.6), one obtains three additional equations :

$$\frac{1+\left(y+\frac{(z-1)(z-2)}{y}\right)^2}{1+\left(y+\frac{(z-1)z}{y}\right)^2}=\frac{1+w^2+2w\cos(\phi+\phi_1)}{\left(\frac{C''D''}{A''C''}\right)^2+w^2-2\left(\frac{C''D''}{A''C''}\right)w\cos(\phi+\phi_1+\phi_2)} \tag{5.14b}$$

$$\frac{1+\left(y+\frac{(z-2)(z-3)}{y}\right)^2}{1+\left(y+\frac{(z-2)(z-1)}{y}\right)^2}=\frac{\left(\frac{C''D''}{A''C''}\right)^2+w^2-2\left(\frac{C''D''}{A''C''}\right)w\cos(\phi+\phi_1+\phi_2)}{\left(\frac{D''E''}{A''C''}\right)^2+w^2+2\left(\frac{D''E''}{A''C''}\right)w\cos(\phi+\phi_1+\phi_2+\phi_3)} \tag{5.14c}$$

$$\frac{1+\left(y+\frac{(z-3)(z-4)}{y}\right)^2}{1+\left(y+\frac{(z-3)(z-2)}{y}\right)^2}=\frac{\left(\frac{D''E''}{A''C''}\right)^2+w^2+2\left(\frac{D''E''}{A''C''}\right)w\cos(\phi+\phi_1+\phi_2+\phi_3)}{\left(\frac{E''F''}{A''C''}\right)^2+w^2-2\left(\frac{E''F''}{A''C''}\right)w\cos(\phi+\phi_1+\phi_2+\phi_3+\phi_4)} \tag{5.14d}$$

Thus, a set of four nonlinear equations with four unknowns is obtained. The four variables can be found by numerically solving these equations. Unfortunately, there is not a single numerical methodology that solves unconditionally simultaneous nonlinear equations (Press, 1988): the convergence of existing methodologies depends on the complexity of the problem under investigation and on the choice of initial estimates for the unknowns. In this work, the steepest-descent minimization algorithm was used for finding the solutions (software package *EUREKA*). Its convergence proved to be very good for modes with moderate interference, particularly when good initial estimates for the modal parameters were provided (the final errors of the minimization scheme was of the order of 10^{-8}). From the authors's experience, good initial estimates for solving this set of equations are

$$w_0=0, \quad \varphi_0=0, \quad y_0=\tilde{\omega}_r^2\tilde{\eta}_r/d\omega^2, \quad z_0=(\tilde{\omega}_r^2-\omega^2)/d\omega^2 \tag{5.15}$$

where $\tilde{\omega}_r$ and $\tilde{\eta}_r$ are estimates of the natural frequency and the modal damping derived by implementing an approximate SDOF Identification algorithm. It must be pointed out, however, that when heavy mode interference is present, the convergence of the numerical solution is poor. This had to be expected, since as discussed earlier, the proposed identification algorithm does not accurately model the distortions of the Nyquist plots in such cases. An additional note of caution must be made with regard to the choice of initial estimates. If these values are not selected appropriately (i.e., if they are far from the exact solutions), the numerical algorithm does not converge. This is a general feature of numerical minimization techniques and, in fact, inadequate initialization is one of the main problems of this class of methodologies (Press, 1988).

Summarizing, the outlined method examines the frequency spacing of six points in the resonance region of a coupled mode and leads to a single estimate for the natural frequency, the modal damping, and the modal interference. The method takes into account $O(\epsilon)$ frequency-dependent distortions caused by a nearby mode, where ϵ is a measure the size of the neighborhood around the natural frequency of the mode in which the analyzed FRF points lie. Thus, application of this methodology is limited to the neighborhood of the natural frequency of the examined mode.

A basic assumption of the method is that the receptance can be represented by the approximate formula (5.8), and that terms of order ϵ^2 or higher are negligible. Although this assumption holds for cases of modes with comparable dampings and modal constants, it is violated when heavy interference exists –for example when the

frequency response of an overdamped mode is much smaller than that of a closely spaced, lightly damped one (such a case is examined in the Applications part of this work). For such cases, the resonance response of the overdamped mode does not dominate over the interfering effects of the perturbing mode and there is a need to take into account higher order terms in expansion (5.7). A more complicated expression replaces equation (5.8), and the geometrical picture of modal interference is altered. In cases of heavy interference, the proposed algorithm does not lead to accurate results; but, as shown in the next section, it can be used to obtain good initial estimates for initializing a convergent iteration scheme.

Ending this section, the basic steps of the proposed identification algorithm are outlined.

1) Consider six points in the resonance region corresponding to frequencies squared $\omega_i^2 = \omega^2 + (i-1)d\omega^2, i = 0, ..., 5$ (note that ω^2 is the frequency of the *second* point).

2) Compute the lengths of the segments connecting the points and the angles that are being formed by these segments (angles ϕ_1, ϕ_2, ϕ_3 and ϕ_4 of figure 5.6).

3) Solve the set of nonlinear algebraic equations (5.14) for y, z, w, and ϕ. To this end the "steepest-descent" optimization algorithm can be used. Good initial guesses for the unknowns are given by relations (5.15). The modal parameters of the mode are then given by:

$$\omega_r^2 = zd\omega^2 + \omega^2, \quad \eta_r = yd\omega^2/(zd\omega^2 + \omega^2) \tag{5.16}$$

4) Circle-fit the triad of points containing the natural frequency estimate and compute

the modulus of modal constant of the mode as

$$|_rA_{jk}| =_r D_{jk}\omega_r^2\eta_r \tag{5.17}$$

where $_rD_{jk}$ is the diameter of the circle-fit. A note of caution is appropriate at this point. When "heavy interference" exists, the modal circle will be significantly distorted, so that the measured estimate of the modal diameter from the circle-fit will be erroneous. Thus, the computed value for the modal constant is accurate only in cases where moderate interference occurs. This conclusion is in accordance with the remarks made earlier, concerning the limitations of the proposed methodology with regard to modes with heavy interference.

5) Compute the phase of the mode directly from the circle-fit, given by the angle between the diameter passing through the natural frequency estimate and the real axis.

5.5. APPLICATIONS OF THE PROPOSED METHOD

The validity of the proposed technique was tested by analyzing both theoretically generated and experimental data. Generally, it was found that, provided that the assumptions of the theory are met, the method works satisfactorily and leads to modal estimates of improved accuracy. However, when "heavy" modal interference occurs, the proposed method gives inaccurate estimates and there is a need to use it iteratively in order to obtain the correct values for the modal parameters.

5.5.1. MODAL ANALYSIS OF THEORETICALLY GENERATED FRF

A variety of theoretically generated data of closely spaced modes were analyzed by the proposed algorithm. It was found that in general, the extracted modal estimates were of improved accuracy compared with those derived by standard SDOF circle-fitting routines.

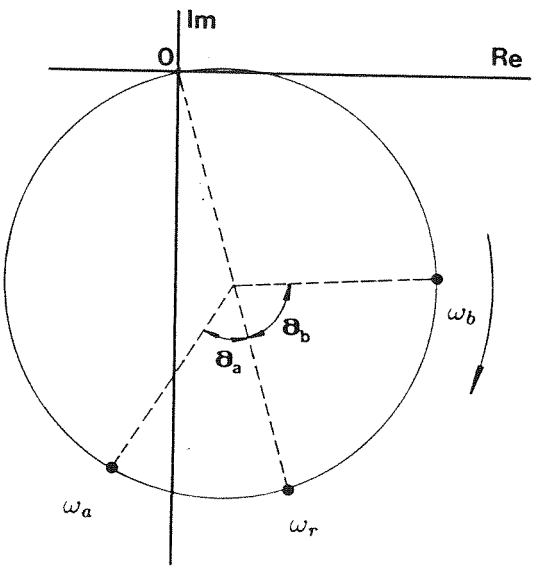

Figure 5.7. Central angles for determining the estimate for the modal damping.

For comparison purposes, modal estimates derived by means of two conventional SDOF algorithms will also be computed. The first is the Δ-plot method outlined in section 5.2 and the second is an algorithm based on an interpolation technique. Details for this interpolation methodology can be found in (Ewins, 1984, 1989) and its main features are now presented. After circle-fitting the FRF Nyquist plot, the natural frequency estimate is computed by finding the point of the modal circle

where the FRF points are most widely spaced. Mathematically, this is equivalent to solving the following equation:

$$\frac{d}{d\omega}\left(\frac{d\omega^2}{d\theta}\right)_{\omega=\omega_r} = 0 \tag{5.18}$$

where ω_r is the natural frequency, and θ represents a central angle on the modal circle. Equation (5.18) is solved by an interpolation algorithm, and once the natural frequency estimate has been obtained, the modal damping is computed by the following formula:

$$\eta_r = \frac{(\omega_a^2 - \omega_b^2)}{\omega_r^2[tan(\theta_a/2) + tan(\theta_b/2)]} \tag{5.19}$$

The angles θ_a and θ_b correspond to two (arbitrary) FRF points on the modal circle, each on a different side of the point corresponding to ω_r (see figure 5.7).

DATA SET 1

The theoretical modal parameters for the first set of interfering modes can be found in table 5.1 (this is the set of closely spaced modes whose Δ-Plots are shown at section 5.2). The two modes have the same amount of damping and identical magnitudes of modal constants; modal interference is caused by the close spacing of their natural frequencies. The frequency ranges analyzed are 49.8 - 50.2 Hz for the lower mode (8 data points) and 50.2 - 50.6 Hz for the higher one (8 data points). The extracted modal parameter values are listed in table 5.1.

A general conclusion is that a single application of the proposed algorithm improves the accuracy of the extracted modal parameters, especially those of the natural frequencies and the modal constants. The differences observed between the extracted

Table 5.1. Results of Modal Analysis of Data Set 1.

Mode	Modal Parameter	Nominal Values	Interpolation Meth.	Δ-Plot Meth.	Proposed Meth.
1	Nat.Frequency (Hz)	50.00	49.944	49.957	50.012
	Modal Damping	0.010	0.0138	0.0073	0.0086
	Magn.Modal Const.	1.000	1.6866	0.8096	0.9593
	Phase (deg)	0°	+39.41°	+34.53°	+13.59°
2	Nat.Frequency (Hz)	50.40	50.456	50.441	50.388
	Modal Damping	0.010	0.0137	0.0071	0.00853
	Magn.Modal Const.	1.000	1.6851	0.8273	0.9661
	Phase (deg)	-10°	-56.32°	-49.58°	-25.13°

phases and their theoretical values are not caused by an inaccuracy of the method, but rather by a rigid body rotation of the closely spaced mode as a whole, caused by the presence of the nearby mode (see (Marples, 1973) and (Montalvao e Silva, 1986) for a discussion of this phenomenon). This can be seen in figure 5.8, where the theoretical and the predicted positions of the natural frequencies for both modes are shown. It is clear that the phase angles corresponding to the theoretical positions of the natural frequencies are shifted with respect to their nominal values (found in table 5.1). In the next application it will be shown that by using an iterative procedure one can improve the estimates for the phase angles.

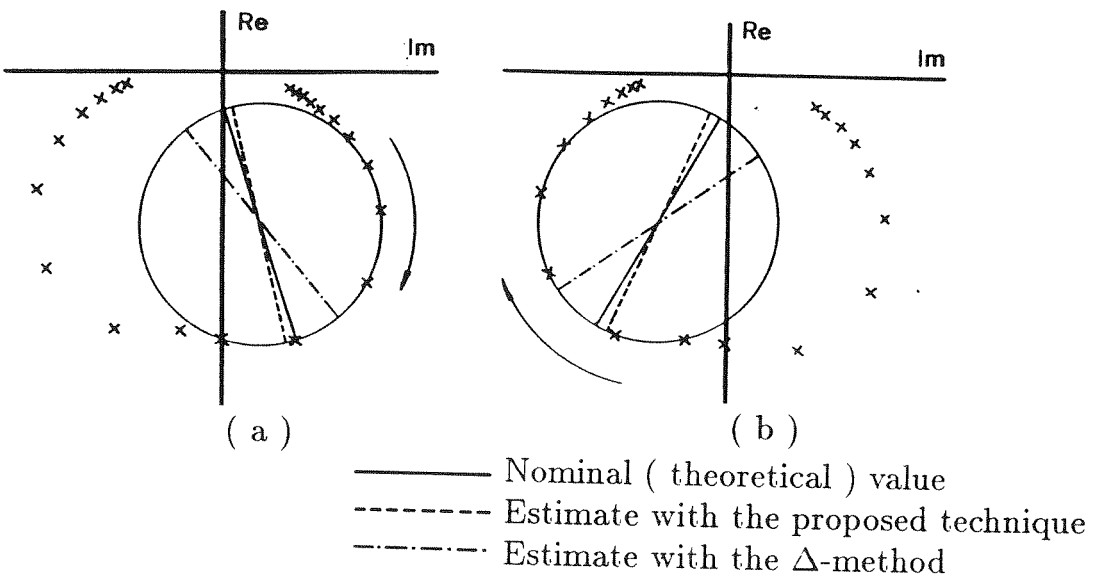

Figure 5.8. Natural frequency estimates for the modes of Data Set 1.

To test the robustness of the method, the theoretically generated data was "polluted" with random "noise" with a maximum peak of 10% of the nominal values, applied uniformly on the frequency range of interest. It was found that the method

still can be applied, although with a reduced accuracy on the modal estimates (5 – 10%).

DATA SET 2

The second set of theoretical data consists of a pair of "heavily" interfering modes. The theoretical values of the modal parameters are as follows:

Mode 1	*Mode 2*
Nat. freq.: 87.0 Hz	Nat. freq.: 87.5 Hz
Modal damp.: 0.05	Modal damp.: 0.01
Modulus Mod. Const.: 1.0	Modulus Mod. Const.: 1.0
Phase: 45 deg	Phase: -70 deg

The relative frequency separation in this data set is of the order of 0.6%, i.e., smaller than that of the previous data set (where the frequency separation was of the order 0.8%). Moreover, in this case there is a considerable difference in the two modal dampings, so that the lightly damped mode completely dominates the FRF.

This can be seen in the combined frequency response of figure 5.9a, where there appears to be only one "peak." Careful examination of the Δ - plot of the FRF (figure 5.9b) over the same frequency range indicates the presence of a lower over-damped mode since the Δ - plot is found to be curved at lower frequencies (ideally it should be a straight line).

Although the algorithm can be successfully applied for finding the modal parameters of the (lightly damped) higher mode, it cannot be implemented in the analysis of the (overdamped) lower one, since its resonance response is much smaller in magnitude

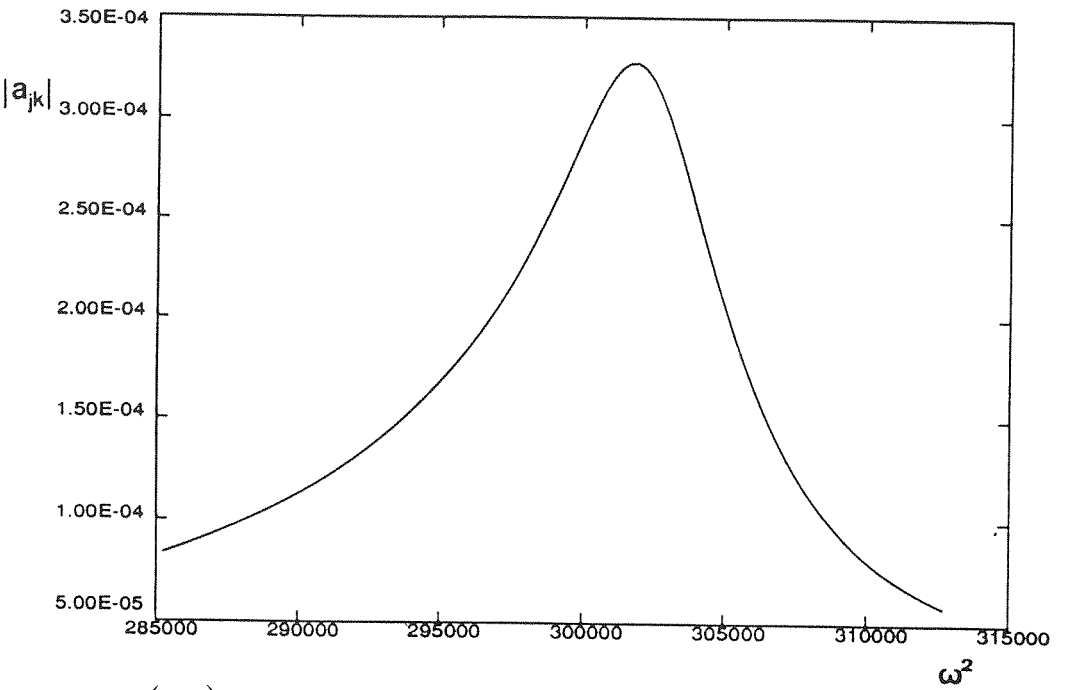

(a)

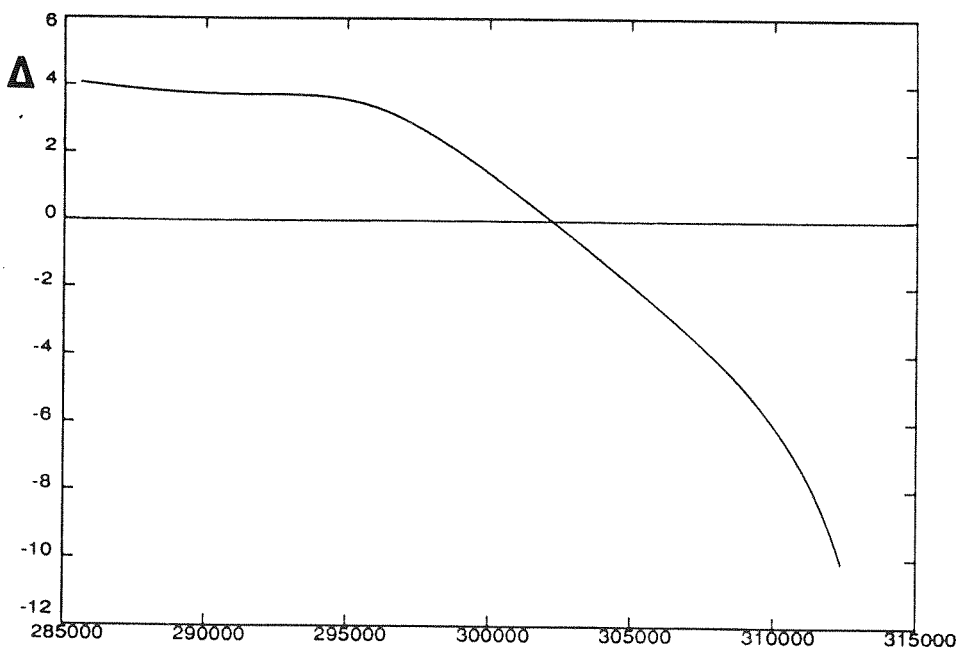

(b)

Figure 5.9. Heavy modal interference, Data Set 2 : (a) Combined FRF (b) Δ-plot of the response.

than the residual effects of the higher mode in the same frequency range. Thus, the approximate expression (5.8) cannot accurately approximate the FRF in the resonant region of the lower mode, and higher order terms must be taken into account. An iterative method will thus be implemented. This is similar to that described in (Robb, 1988), with the essential difference, however, that in the present work the iterations are initalized by the proposed, refined technique. Thus, at step 1, the proposed algorithm is used to initialize the iterations and in subsequent steps, the SDOF Δ - plot method is applied to the analysis of the corresponding FRF.

Step 1. Estimates were computed for the modal parameters of the higher (dominant mode) by means of the algorithm outlined in the previous section. The results of the modal analysis are listed in the first line of table 5.2: they are very close to the nominal values of the mode.

Step 2. The identified mode was subtracted from the total response and the remaining FRF was analyzed by the Δ-plot methodology. The results are presented in figure 5.10a, were it is observed that the residual effects of the higher mode still dominate the FRF in higher frequencies (this can be concluded from the fact that the Δ - plot is not a straight line in this frequency range). However, in the lower frequencies a linear pattern can be identified which eventually disappears as the region dominated by the residual effects of the higher mode is approached. This curve can be straight-line fitted and extrapolated linearly to give estimates of the natural frequency and the modal damping (see Section 5.2). The estimates for the modal constant and the phase are derived by circle-fitting the FRF in the frequency

Table 5.2. Modal Analysis of Data Set 2 : Iteration steps.

Mode	Modal Parameter	Iteration Step				
		1	2	3	4	5
1	Nat.Freq. (Hz)		86.8717		87.0157	
	Modal Damping		0.05427		0.05179	
	Magn. Modal Const.		0.99538		1.01514	
	Phase (deg)		+34.92		+43.99	
2	Nat.Freq. (Hz)	87.5048		87.4970		87.4993
	Modal Damping	0.01048		0.01022		0.01009
	Magn. Modal Const.	1.05526		1.00774		1.00994
	Phase (deg)	-68.41		-69.04		-69.65

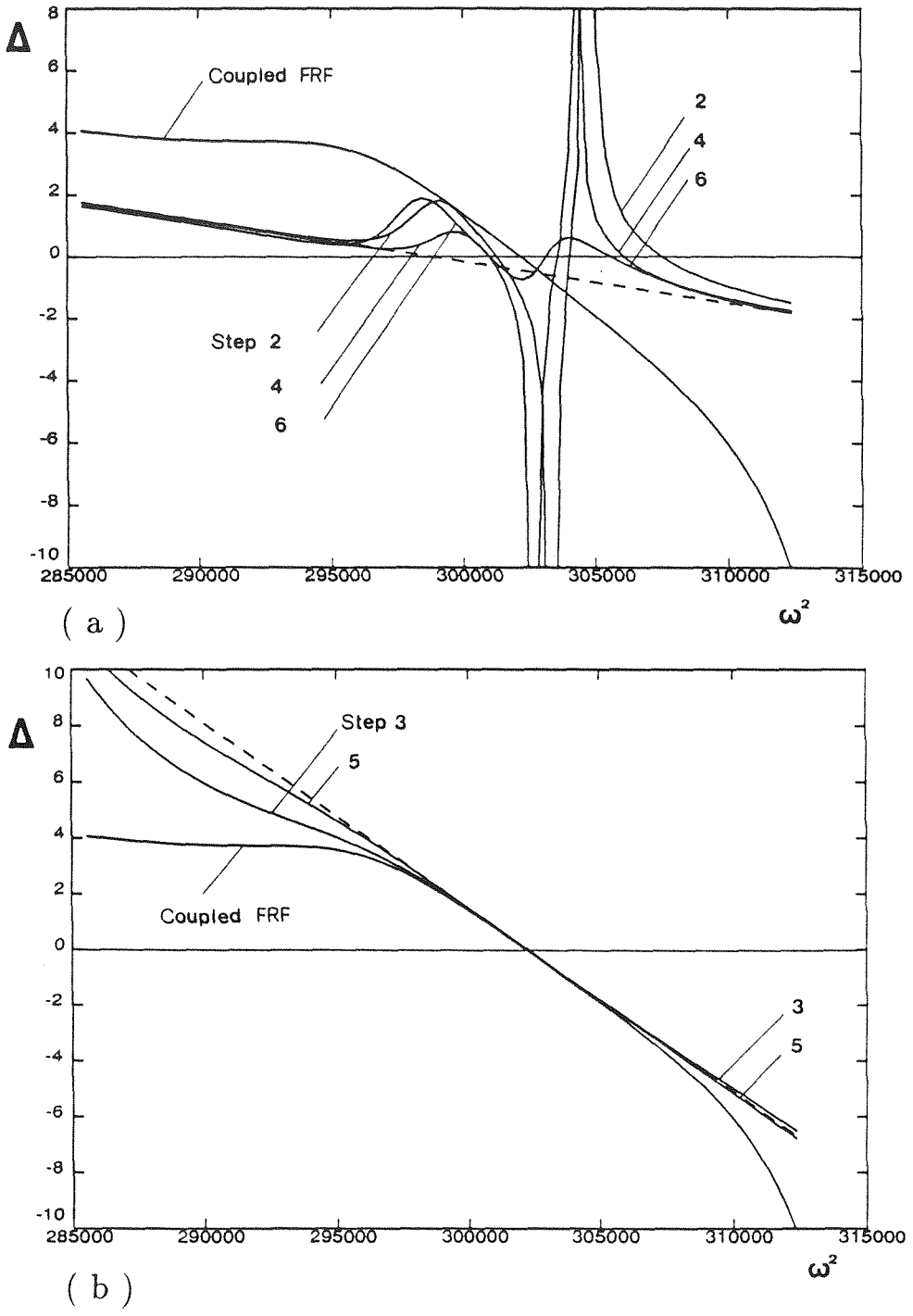

Figure 5.10. Modal analysis with the iterative technique, Data Set 2. Δ-plots (a) after subtracting the higher mode (b) after subtracting the lower mode.

----------Δ-plots of the isolated (unperturbed) modes.

range corresponding to the linear pattern of the Δ - plot (i.e., in this case, in the lower frequencies). The numerical estimates of the modal parameters are listed at table 5.2. Note that the extracted modal estimates are close to their nominal (theoretical) values.

Note that a zero-crossing of the Δ - plot can be detected in the higher frequencies of figure 5.10a. This should not be used for estimating the natural frequency since no clear linear pattern can be identified in that frequency range (circle-fitting the FRF in that frequency range leads to erroneous estimates for the modal parameters). In fact, the frequency corresponding to $\Delta = 0$ is where maximum spacing of frequency points in the Nyquist plot occurs. *Thus, the maximum frequency spacing criterion is not correct for detecting the natural frequency in this case*, and conventional SDOF methods utilizing this criterion for finding the natural frequency will lead to inaccurate results for the lower mode. In contrast, implementation of the Δ - plot formulation leads to the detection of the "optimum" frequency range for modal analysis, by identifying where linear patterns appear in the plot.

Step 3. The identified lower mode (from step 2) is subtracted from the total response and the remaining FRF is analyzed in a way similar to step 2. In figure 5.10b the Δ - plot of the remaining FRF is shown and it can be seen that it is closer to the ideal theoretical straight line than that of step 1.

The iteration scheme is continued by repeating the procedures outlined in steps 2 and 3. The results are presented in table 5.2, and the Δ-plots corresponding to the various iterations at figure 5.10. Alternatively, one could plot the Nyquist plots of

the receptances after the removal of the perturbing modes. However, the Δ-plots were preferred at this stage, in order to demonstrate that indeed linear patterns exist in such plots and also in order to identify the "optimum" regions of the FRF for circle-fitting. In figure 5.10a note that as the iterations proceed, the Δ - plots converge to the theoretical straight line of the higher mode. In figure 5.10b observe that the residual effects of the higher mode continue to distort the Δ - plots of the lower one; however, the linear patterns in lower frequencies become more and more apparent as the iteration steps increase.

DATA SET 3

The iterative method was applied to various examples of heavily interfering modes and the iterations were always found to converge to the nominal values of the modes. A case where the natural frequency separation of the modes is extremely small (less than 0.2 %), is now examined. The nominal values of the two closely spaced modes are as follows:

Mode 2	*Mode 1*
Nat. freq.: 55.0 Hz	Nat. freq.: 55.1 Hz
Modal damp.: 0.06	Modal damp.: 0.02
Modulus Mod. Const.: 0.8	Modulus Mod. Const.: 1.0
Phase: 60 deg	Phase: 40 deg

As many as 11 iterations were required for convergence. The combined FRF for this system is shown in figure 5.11, where there appears to be only one "peak." However, careful examination of the Δ-plot of the FRF over the frequency range indicates the

presence of a highly damped mode since the Δ-plot is found to be curved at lower frequencies. Although the Improved-SDOF algorithm can be successfully applied for finding the modal parameters of the more lightly damped mode, it cannot be used in the analysis of the highly damped one (its resonance response is much smaller in magnitude than the residual effects of the dominant mode in the same frequency range).

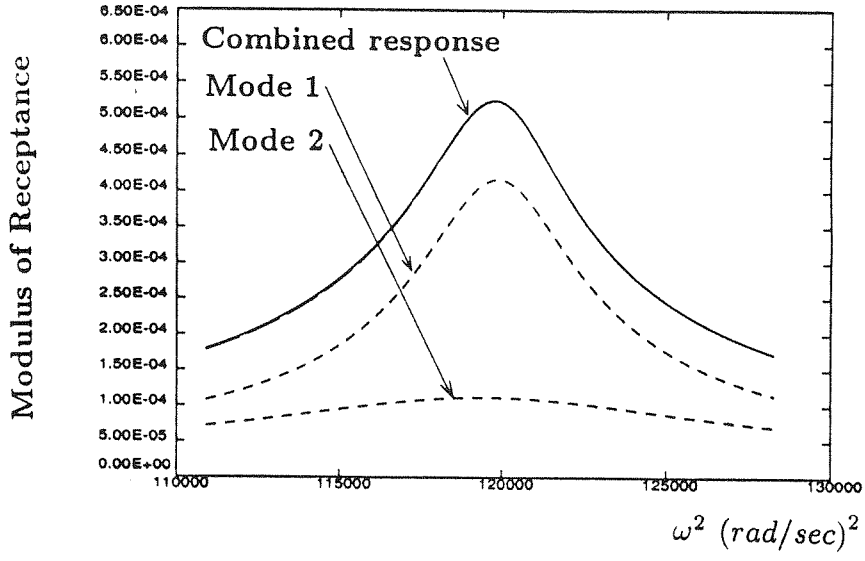

Figure 5.11. Theoretical FRF of Data Set 3.

The iterative algorithm is thus implemented. This proved to be a very challenging set of data. The iterations are given in table 5.3, and are graphically presented in figure 5.12.

Potential difficulties in the application of the iterative technique may arise in cases where the initial estimates for the modes are not very accurate (the convergence

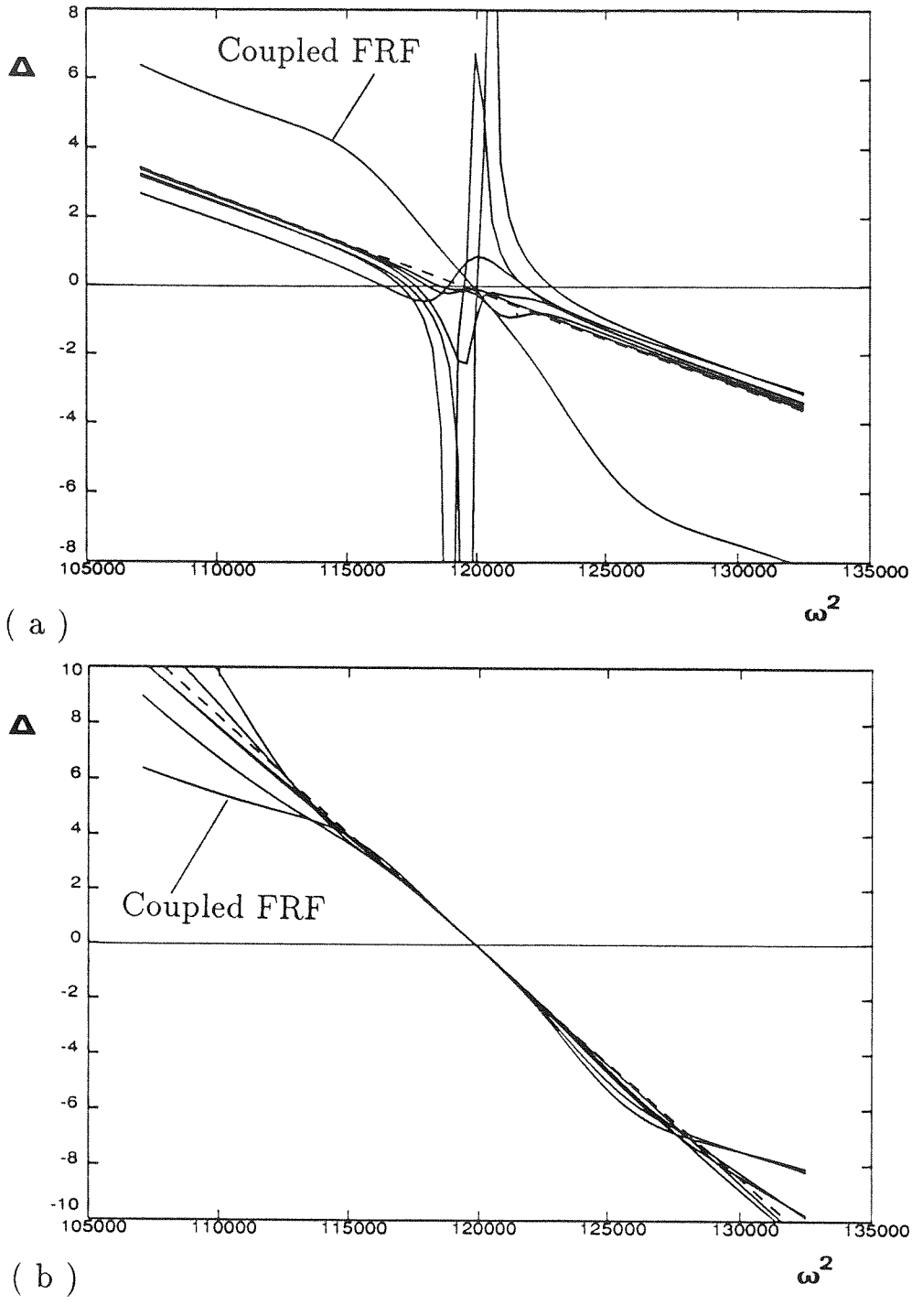

Figure 5.12. Modal analysis with the iterative technique, Data Set 3. Δ-plots (a) after subtracting the higher mode (b) after subtracting the lower mode.

– – – – – – – – Δ-plots of the isolated (unperturbed) modes.

Table 5.3.Modal Analysis of Data Set 3.

Step	Mode 2				Mode 1			
	Nat.Freq. (Hz)	Modal Damping	Magn.Modal Const.	Phase (deg)	Nat.Freq. (Hz)	Modal Damping	Magn.Modal Const.	Phase (deg)
1					55.1043	0.0204	1.1862	39.70
2	54.4314	0.0599	0.4201	68.44				
3					55.0910	0.0199	1.0784	43.39
4	54.8776	0.0621	0.6658	53.98				
5					55.0935	0.0200	1.0465	41.59
6	54.8250	0.0596	0.6872	59.20				
7					55.0941	0.0200	1.0244	42.42
8	54.9465	0.0602	0.7535	56.19				
9					55.0960	0.0200	1.0138	41.52
10	54.9958	0.0605	0.7824	58.06				
11					55.0987	0.0200	1.0054	40.46

Table 5.4. Results of Modal Analysis of the Experimental FRF.

Mode	Modal Parameter	Methodology		
		SDOF	Improved SDOF	MDOF
1	Nat.Freq. (Hz)	51.5039	51.5028	51.5017
	Modal Damping (10^{-4})	7.1909	6.5521	7.0001
	Magn. Modal Const.	0.1888	0.1720	0.1874
	Phase (deg)	+169.48	+174.69	+180.00
2	Nat.Freq. (Hz)	52.6833	52.6841	52.6825
	Modal Damping	7.6362	6.7556	7.5634
	Magn.Modal Const.	0.3110	0.2752	0.2982
	Phase (deg)	+177.97	+170.89	+180.00

of the steps may be considerably delayed). However, in such "demanding" cases, the linear patterns of the Δ-plots can help considerably the analyst in selecting "optimum" regions of the Nyquist plot for circle-fitting. This leads to an accelerated convergence of the iterations.

5.5.2. MODAL ANALYSIS OF AN EXPERIMENTAL FRF

The FRF of a practical structure is now analyzed in order to demonstrate the applicability of the proposed method with experimental data. The FRF consists of two interfering modes of a truss-structure with a frequency separation of the order of about 1.7% with respect to their natural frequencies. Although moderate levels of interaction are anticipated in this problem, it will be shown that the proposed technique leads to more accurate results than those obtained by means of the SDOF Δ-plot method. Thus, although the interfering effects between the two modes are not large, they will still be shown to affect the quality of the modal analysis.

For comparison purposes, the modal estimates resulting from the application of a MDOF identification technique will also be considered. This later methodology is parametric and minimizes the error between the curve-fit of a six-parameter theoretical model and the experimental data (the modes are assumed to be classically damped for simplicity). The minimization is carried out numerically and consists of a combination of the "pseudo-inverse" and the "steepest-descent" methodologies. More details about this algorithm can be found in (Caughey, 1990), and in (McVerry, 1979, 1983), where it was originally derived. For convenience, from now

on, the Δ-plot method will be referred as "SDOF," the proposed refined technique as "improved SDOF," and the numerical MDOF method as "MDOF."

The modal analysis results of the experimental FRF with the three aforementioned methods are shown in table 5.4. For this example, the numerical solution of equations (5.14) was achieved with an accuracy of 10^{-8}, and with no convergence complications.

In figure 5.13 the experimental and regenerated FRF plots are presented. From figure 5.13a it is seen that the regenerated curves based on the improved SDOF and the MDOF methods accurately describe the experimental response in the two resonance regions. In contrast, there exists a clear discrepancy between predicted and experimental points in the antiresonance region. This may be attributed to the fact that close to the antiresonance region, the magnitude of the FRF is very small. Thus, points in that region do not influence the modal analysis as much as FRF points with relatively large response, i.e., close to resonance. For the same reason, one expects the effects of external noise to be maximal in the antiresonance regions and minimal in the resonance ones. Another possible reason for the discrepancy in the antiresonance region may be residual effects of unaccounted higher modes, namely quasi-static responses of modes that lie outside the considered frequency range.

In the graphs of figure 5.13b, the Δ-plots are presented. An additional curve is plotted corresponding to SDOF modal analysis results. Note that the improved SDOF and the MDOF methods agree qualitatively and quantitatively quite well

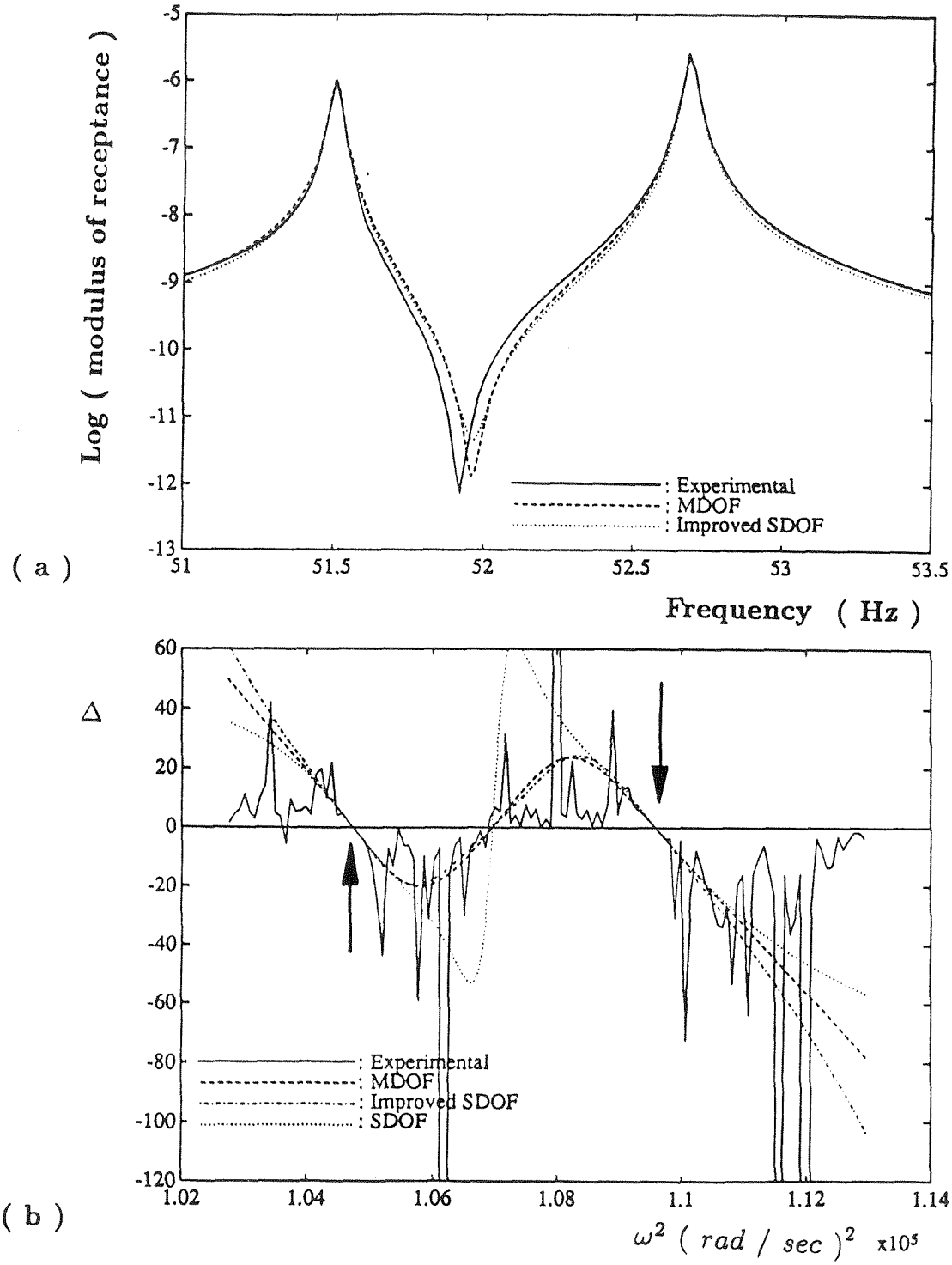

Figure 5.13. Modal analysis of the experimental FRF: (a) Measured and regenerated FRF (b) measured and regenerated Δ-plots.

with the experimental data over a wide frequency range. This cannot be stated for the SDOF method. Also observe that all regenerated curves approximate the experimental data very closely in the two resonance regions (denoted by arrows). Outside the resonance regions, the experimental data appear to be heavily polluted by noise, so agreement with the regenerated plots is nowhere nearly as good.

A general conclusion is that the SDOF methodology results in relatively inaccurate modal results in this example. Although the SDOF algorithm accurately curve-fits the resonance regions, its Δ-plot differs from those of other, more refined methodologies. This results from the fact that, in the SDOF method, modal interference (although small in this example) is not taken into account. A final note must be made concerning the agreement between the proposed method and the MDOF one. It seems that the approximate methodology outlined in this work captures the basic features of modal interference, since its results are in agreement with those obtained by the more exact MDOF technique. Moreover, the suggested method avoids the complicated numerical optimization schemes used in the MDOF approach.

5.6. DISCUSSION

Conventional SDOF modal analysis methods model the modal interference with a constant complex term that is added in the single mode FRF (eq. (5.1)). In this work this approximation is relaxed by Taylor expanding the FRF of the "perturbing" mode and retaining only the first two terms. The first term of the Taylor expansion is a complex constant which only causes rigid-body displacements of the

modal circle of the "perturbed" mode (SDOF approximation). The second term, however, is frequency dependent, thereby introducing distortions in the relative frequency spacing of points in the resonance region of the "perturbed" mode.

A geometrical representation of the distorted Nyquist plot was constructed, and based on this, an identification algorithm which takes into account first order frequency distortions caused by modal interference was developed. This algorithm is simple to apply, since it considers only angles and lengths measured directly from the experimental FRF plot. A possible complication may arise in the numerical solution of the set of algebraic equations (5.14), but as stated previously, good initial estimates for the unknown variables improve the convergence of the numerical solutions.

The proposed methodology can be applied in cases where the response of a mode in its resonant region is greater than the interfering terms of polluting closely spaced modes – wherever the approximate formula (5.8) holds. This is the case of closely spaced modes with comparable dampings and magnitudes of modal constants. In such cases, the proposed methodology is expected to give more accurate results compared to existing SDOF techniques, since it takes into account first order frequency-dependent distortions in the Nyquist plots (conventional SDOF do not consider such perturbations). An additional feature of the method is that it can approximately quantify the amounts of the frequency-dependent modal interference by computing the quantities w and ϕ in equations (5.14) (as previously explained, these variables represent the moduli and phases of the frequency-dependent interfering effects of

nearby modes). Thus, the analyst can determine the amount of interaction between two modes and test the validity of the SDOF assumption for approximating the FRF in the frequency range of interest.

The algorithm cannot be applied in cases of "heavy interference," i.e., closely spaced modes with large differentials in their modal dampings and modal constants. In such cases, the resonance modal response of the "perturbed" mode is orders of magnitude smaller than the distorting effects of nearby modes; thus, one needs to include higher order terms in eq. (5.8) in order to accurately model the modal interference. Even in such cases, however, the proposed algorithm can be used with the Δ - plot SDOF method in an iterative scheme which leads to very accurate estimates for the modal parameters. This iteration technique is not new (examples of its application with other modal analysis algorithms can be found in (Robb, 1988) for example). However, a new feature presented in this work is the potential of identifying "optimum" regions in the remaining FRF that are most effective for modal analysis. This can be achieved by detecting and line-fitting linear patterns in the Δ-plots of the remaining FRF.

A similar analysis with the one presented in this work can be performed when more than two closely spaced modes exist in the range of interest. Again, one of the modes can be designated as the "perturbed" one, whereas the remaining modes are "perturbing." The FRF of the perturbing modes can then be treated as in this work, leading to a more involved identification algorithm. When "heavy modal interference" occurs, then one could use the iteration scheme to separate

the individual modes. This can be achieved as in this work, with the additional complication, however, that more than two linear patterns in the Δ-plots should be considered.

The applicability of the method was tested with theoretical and experimental data. It was found that provided the theoretical assumptions are satisfied, the algorithm can lead to modal estimates of improved accuracy. The robustness of the analysis was tested by perturbing the theoretically generated data with random noise. Finally, a demonstration on the modal analysis of "heavily" interfering modes was given, where the proposed method was used in an iterative scheme with a SDOF algorithm.

6. EFFECTS OF WEAK NONLINEARITIES ON MODAL ANALYSIS

6.1. PREVIOUS WORK

A basic assumption of standard modal analysis techniques is that of linearity. Although the majority of engineering structures behaves almost linearly for low amplitudes of motion, there are cases where this does not hold. For example, in cases of nonlinear boundary conditions, of dry friction between sliding surfaces, of impacts, or of material nonlinearity, the nonlinear effects can be evident even for low energies of motion. In such cases, the frequency response functions (FRF) are distorted and modal analysis using conventional methods does not lead to accurate modal estimates.

The identification of nonlinear systems consists of various stages. Initially, one examines the FRF of the system in order to detect nonlinear distortions. Once the existence of nonlinear effects is established, one identifies the type and the spatial distribution of the nonlinearity, i.e., if it is of stiffness- or of damping-type, and if it is local or distributed in the system. The next step consists of the quantification of the nonlinearity. This stage is more demanding and includes many topics. The most basic problem is that of developing an accurate mathematical modelling of the nonlinear behavior. Note that the resulting model depends not only on the specific type of the excitation used for the modal test, but also on the frequency range of interest and on the amplitudes of the response. Having defined the range of validity

of the model, one has to compute its parameters by analyzing the experimental response. At a final step, the regenerated, theoretical FRF (based on the identified model) is compared with the measured response of the tested structure in order to determine the accuracy of the identification.

A general survey of existing nonlinear identification methods can be found in (Billings, 1980) and (Natke, 1982, 1987), where a brief synopsis of the various approaches is given. A detailed discussion about the existing excitation techniques for nonlinear identification is presented in (He, 1987). There are various types of external excitation for modal testing: harmonic, random, transient, periodic, etc. Depending on the specific aims of modal analysis, different forcing types should be implemented. Harmonic excitation is regarded as the best technique for identification of structural nonlinearities (He, 1987), (Natke, 1987). This is due to the fact that with harmonic excitation one can accurately control the level of the input force and can effectively investigate the nonlinear distortions of the FRF in the resonance regions for different levels of the response. Moreover, one can detect additional subharmonic or superharmonic responses that are a clear manifestation of nonlinear behavior. The limitation of harmonic excitation is that it is relatively slow compared with other excitation types. Random forcing is faster and results in the excitation of the structure with random levels of forces and phases at each frequency. However, the response at each frequency (obtained by a frequency analyzer), is the average of the responses due to all the random input forces. Thus, the resulting FRF does not contain any nonlinear distortions and resembles that of

a linear system. Therefore, random excitation is not suitable for identifying nonlinearities in structural components. However, it can be effectively used when one wants to find a linearized model that has similar vibrational characteristics with the actual structure over the frequency range of interest. Similar arguments can be made with regard to transient excitation. With transient testing, there are difficulties in controlling the forcing input at each frequency, as well as, the frequency range of the test. Thus, transient testing has basic limitations when applied for nonlinear identification. Also certain coherence problems may exist close to anti-resonances (He, 1987), (Cawley, 1986). In this work only harmonic excitations are considered since, as mentioned they are the most suitable forcing functions for exposing the nonlinear distortions of frequency response functions.

There exist various methods for analyzing and identifying the nonlinear FRF. As far as the computation of approximate nonlinear FRF is concerned, there exist the classical methods of "equivalent linearization" (Caughey, 1963), (Iwan, 1973), and "slowly varying parameters" (Nayfeh, 1979). The basic assumption of these methods is that the nonlinearities of the system are weak, so that under harmonic excitation, the nonlinear response is approximately harmonic. The FRF computed by these techniques contain nonlinear distortions, and the equivalent, linearized natural frequencies depend on the amplitude of the motion. A more detailed discussion of the "equivalent linearization" technique will be given in the next section.

A class of current nonlinear identification methods is based on the Hilbert transform (Simon, 1984), (Tomlinson, 1987). This transform is a means of computing

the imaginary part of a complex frequency response function from the real part (and vice versa), provided that the system under consideration is linear and causal. When nonlinear systems are considered, their impulse time responses are still causal, but their inverse Fourier transforms (used for computing the FRF) are not (Simon, 1984). Thus, the Hilbert transform of the real part of a nonlinear FRF is not identical to its imaginary part, and nonlinear distortions occur. This result can be used not only for detecting, but also for quantifying nonlinearities from the plots of the FRF.

An additional category of techniques is based on the work of Masri and Caughey (Masri, 1979, 1982a,b). These methods can be used for parametric or nonparametric modal analysis, and they are based on a model of a SDOF nonlinear oscillator with a general nonlinear restoring force. As a first step, the applied force and the resulting acceleration are measured at discrete time intervals. Based on these measurements, the (nonlinear) restoring force of the system is estimated at each time step directly from the equation of motion, and its (3-dimensional) plot versus amplitude and velocity constructed. The resulting 2-dimensional surface of the restoring force is interpolated into a grid and is subsequently curve-fitted by a set of Chebyshev polynomials. The result is an analytic representation of the restoring force as a function of the displacement and the velocity. An extension of this method can be found in (Worden, 1989), where it is shown that the method can also be used for detecting the spatial location of the nonlinearity in the structural model.

In (Rades, 1983), the nonlinear distortions of the Nyquist plots of FRF are studied

by means of equivalent linearization techniques. Both stiffness and damping nonlinearities are considered, and the modal parameters of the system are computed by considering two Nyquist plots corresponding to two different levels of external excitation and by measuring the frequencies of certain, suitably selected, Nyquist points. In (Haymon, 1978), the approximate "backbone curve" of the FRF is constructed, by measuring the "peak" amplitudes of the response for different levels of forcing. From that curve, the amount of stiffness nonlinearity can be estimated. An interesting method for detecting and measuring nonlinearities of SDOF systems, is presented in (Mertens, 1989). This method considers the plots of the inverse of the frequency response functions, and it studies the dependence of the equivalent stiffnesses and dampings of the system, on the displacements and velocities respectively. Hence, diagrams of equivalent stiffnesses and dampings versus displacements and velocities are constructed and subsequently used for the derivation of accurate estimates of the types and amounts of the nonlinearities present in the system. It must be pointed out, however, that the performance of this technique depends on the accuracy of the estimate of the mass of the SDOF model.

In (Tomlinson, 1979), a structure with a localized Coulomb (dry friction) damper, is considered. Instead of analyzing the (distorted) Nyquist plot of the FRF, the in-phase and quadrature components of the power dissipated during the steady state oscillation is examined. An identification technique is subsequently derived that leads not only to the quantification, but also to the detection of the location of the nonlinearity. The effects of single and multiple clearance-type nonlinearities on

the dynamic response are examined in (Tomlinson, 1984). Both symmetrical and asymmetrical clearance characteristics are considered, and their distorting effects on the corresponding FRF are studied both analytically (using equivalent linearization techniques), and numerically (with digital simulations). However, no identification algorithms are given, this being attributed to the complexity of the problem. A similar analysis was performed in (Comparin, 1989), where the method of harmonic balance was used to compute the primary resonance of an impact pair. A study of the topology of the FRF of this system is carried out and a comparison with the FRF of a system with clearance nonlinearities is made. (Natsiavas, 1990) examines "trilinear" oscillators (with motion limiting constraints), and provides some examples of Nyquist plots constructed from the computation of the exact steady state nonlinear response. Finally, a brief discussion on the application of ARMA models for analyzing nonlinear structures can be found in (Hunter, 1990).

Recently, multidimensional Fourier transforms of Volterra and Wiener kernels of nonlinear systems were applied to the problem of nonlinear system identification (Gifford, 1989a,b), (Frachenbourg, 1989). These represent higher order FRF for the nonlinear system and contain information about the nonlinear behavior that cannot be obtained by conventional (first order) FRF. In the aforementioned references, nonlinear multi-DOF parametric models were curve-fitted to measured Volterra kernel transforms, with encouraging results. This method appears to be the extension for the nonlinear case of the conventional curve-fitting procedure that is commonly applied to (first order) linear FRF. In addition, the calculation of higher order FRF

permits the mathematical modelling of the transfer of energy between various frequencies that takes place in systems with nonlinearities. A limitation of this method is that it cannot be applied to systems with discontinuous stiffnesses (such as clearances), and dampings (such as friction), since such systems do not have a Volterra series representation. An additional drawback is the computational effort required for computing high order kernels, and the requirements for large data memories, in order to store the computed results.

In this work, the method of equivalent linearization will be implemented to the study of the nonlinear distortions of the Nyquist plots of weakly nonlinear systems. In linear systems with hysteretic damping, it can be shown that the Nyquist plots in the resonance regions are almost circular, and moreover, that an estimate for the natural frequency can be obtained by computing the point of the Nyquist plot corresponding to maximum frequency separation. It will be shown that this method cannot always be applied when nonlinearity is present, since in that case, the Nyquist plots of the approximate harmonic FRF are distorted from the circular, theoretical form. Hence, a primary objective of this work is to analyze and quantify the distorted, weakly nonlinear Nyquist plots, and in the sequence, to derive methods for accurate identification of the nonlinearity, and the linear modal structural parameters.

There are only a few references in the literature that investigate the nonlinear distortions in the Nyquist plots. In (White, 1971), a system with cubic stiffness nonlinearity is considered, and it is found that the maximum frequency separation in the Nyquist plot does not occur at the linear natural frequency of the system.

In that paper, analytic expressions for the frequency corresponding to maximum frequency separation are derived and the response of a practical nonlinear structure is examined. In (Tomlinson, 1980), a similar analytical study is performed for a system with dry friction, and it is found that although this type of nonlinearity significantly distorts the Nyquist plot, the maximum frequency separation criterion is still valid for estimating the natural frequency. In what follows, a system with general stiffness and/or damping nonlinearity is examined, and analytical expressions for the frequency of maximum frequency separation of the distorted Nyquist plot are derived. These results are then compared with those of the two aforementioned references.

6.2. THE METHOD OF EQUIVALENT LINEARIZATION

Since the notions of "equivalent stiffness" and "equivalent damping" will be used in the following analysis, a brief discussion on the method of equivalent linearization will now be given. This is an approximate method for computing the main harmonic component of the steady state response of a weakly nonlinear system, excited by a harmonic excitation.

Consider a SDOF nonlinear system, with the following equation of motion:

$$\ddot{x} + b\dot{x} + \omega_r^2 x + \epsilon f(x, \dot{x}) = \epsilon P e^{i\omega t} \tag{6.1}$$

where b and ω_r are the linear viscous damping and natural frequency respectively, and $\epsilon f(x, \dot{x})$ represents the small nonlinear element of the restoring force. As usual, ϵ is a small parameter (of perturbation order), satisfying $|\epsilon| \ll 1$. Observe,

that in (6.1) both the applied force and the nonlinear component of the restoring force are considered to be of perturbation order.

Consider now the alternative system:

$$\ddot{x} + b\dot{x} + \omega_r^2 x + b_{eq}\dot{x} + \omega_{eq}^2 x + \mathcal{E}(x,\dot{x}) = \epsilon P e^{i\omega t} \tag{6.2}$$

This results from (6.1), by replacing the nonlinear component of the restoring force, by two linear terms in the displacement and the velocity, and an additional error term, given by the quantity $\mathcal{E}(x,\dot{x})$. The quantities ω_{eq}^2 and b_{eq} are termed the equivalent stiffness and damping respectively. The aim of the method of equivalent linearization is to compute these equivalent quantities in such a way, as to minimize (in a certain sense) the error $\mathcal{E}$. From (6.1-2), this error can be computed as :

$$\mathcal{E}(x,\dot{x}) = \epsilon f(x,\dot{x}) - \omega_{eq}^2 x - b_{eq}\dot{x} \tag{6.3}$$

Assume that the steady state motion of the oscillator is approximately harmonic (of the same period with that of the harmonic excitation),

$$x(t) = Xe^{i\omega t} = Ae^{i\phi}e^{i\omega t} \qquad (\ \textit{Steady state motion}\ ) \tag{6.4}$$

The quantity X is the complex amplitude of the steady state motion, A is its magnitude and ϕ its phase. The error $\mathcal{E}$ will be minimized in mean square, by considering the following quantity, defined at the steady state of the system:

$$< \mathcal{E}^2(x,\dot{x}) >_T \equiv \int_0^T \{\ f(x,\dot{x}) - \omega_{eq}^2 x - b_{eq}\dot{x}\ \}^2 dt \tag{6.5}$$

where $T = 2\pi/\omega$ is the period of the harmonic excitation (and of the approximate steady state response). The minimization of (6.5) is carried out with respect to the

two unknown quantities ω_{eq}^2 and b_{eq}, and provides a means for their determination:

$$\frac{\partial < \mathcal{E}^2(x,\dot{x}) >_T}{\partial \omega_{eq}^2} = 0 \Rightarrow \omega_{eq}^2 = \frac{\int_0^T x \epsilon f(x,\dot{x}) dt}{\int_0^T x^2 dt} \tag{6.6}$$

$$\frac{\partial < \mathcal{E}^2(x,\dot{x}) >_T}{\partial b_{eq}} = 0 \Rightarrow b_{eq} = \frac{\int_0^T \dot{x} \epsilon f(x,\dot{x}) dt}{\int_0^T \dot{x}^2 dt} \tag{6.7}$$

where in the above expressions x is evaluated at the steady state. Considering the real part of (6.4), one obtains $x = A\,cos\theta$, where $A = |X|$, and $\theta = \omega t + \phi$. Substituting for x in (6.6-7), and changing the variables of integration, one finds the following final expressions for the equivalent quantities:

$$\begin{aligned} \omega_{eq}^2 &= \frac{\epsilon \int_0^{2\pi} cos\theta \; f(\; Acos\theta, -\omega A sin\theta \;)\; d\theta}{\pi A} \\ b_{eq} &= \frac{\epsilon \int_0^{2\pi} -sin\theta \; f(\; Acos\theta, -\omega A sin\theta \;)\; d\theta}{\pi \omega A} \end{aligned} \tag{6.8}$$

Note that both equivalent quantities are of $\mathcal{O}(\epsilon)$, and that they depend on the amplitude of oscillation A and the frequency of the exciting force, ω. The amplitude of the approximate harmonic steady state motion, A, is determined by considering the linearized system that results when the (minimized) error $\mathcal{E}$ is omitted from equation (6.2):

$$\ddot{x} + b\dot{x} + \omega_r^2 x + b_{eq}\dot{x} + \omega_{eq}^2 x + = \epsilon P e^{i\omega t} \tag{6.9}$$

Fixing A and ω, the system (6.9) becomes linear, and the approximate steady state response can be evaluated by the following formula:

$$\frac{X}{\epsilon P} = \frac{A e^{i\phi}}{\epsilon P} = \{\; (\omega_r^2 + \omega_{eq}^2 - \omega^2) + i[\omega(b_{eq} + b)] \;\}^{-1} \tag{6.10}$$

From equation (6.10), the magnitude A and the phase ϕ of the response can be numerically evaluated. Moreover, assuming the level of the force to be constant, and

assigning different values to the frequency ω, the approximate FRF of the oscillator can be evaluated. Note that since the system is nonlinear, an examination of the stability of the approximate steady state is also needed. However, this problem can be solved by standard techniques (Nayfeh, 1979), and will not be considered here.

Assuming that the damping of the system is light (this holds in the majority of practical applications), one can replace the equivalent viscous damping b_{eq}, by an equivalent, hysteretic loss factor η_{eq}. It can be proven that no loss of generality results by doing so, since for light damping the differences between the viscous and hysteretic damping models are negligible. However, it must be pointed out that *the model of hysteretic damping is only valid at the steady state*, since the transient motion of a hysteretically damped system violates the assumption of causality (Crandall, 1970). The overall equivalent hysteretic loss factor of the system is defined by,

$$\eta_{eq} = \frac{\omega(b + b_{eq})}{(\omega_r^2 + \omega_{eq}^2)} \tag{6.11a}$$

and the approximate harmonic oscillation of the system is described by the following equation (correct to $\mathcal{O}(\epsilon)$):

$$\ddot{x} + (\omega_r^2 + \omega_{eq}^2)(1 + i\eta_{eq})x = \epsilon P e^{i\omega t} \tag{6.11b}$$

Summarizing, in the method of equivalent linearization, the weakly nonlinear system (6.1) is replaced by an equivalent linearized system (6.9). This is achieved by replacing the nonlinear component of the restoring force, by equivalent linearized stiffness and damping terms. These quantities are derived by minimizing a certain

error function, they only hold at the approximate steady state, and they depend on the amplitude of motion and the frequency of the external harmonic excitation.

6.3. SYSTEM WITH DAMPING NONLINEARITY

6.3.1. ANALYSIS

Consider a harmonically excited, N-DOF discrete oscillator with weakly nonlinear damping elements. The equations of motion are as follows:

$$\underline{M}\ \underline{\ddot{q}} + \underline{K}\ \underline{q} + \underline{F}(\underline{\dot{q}}) = \underline{Q}e^{i\omega t} \tag{6.12}$$

where $\underline{M}, \underline{K}$ are the constant mass and stiffness system matrices, and $\underline{F}$ is a matrix containing the linear and nonlinear damping elements. The vectors $\underline{q}$ and $\underline{Q}$ represent the coordinates of the system and the amplitudes of the exciting forces respectively. Transforming into the modal coordinates of the undamped, linear oscillator, one obtains:

$$\underline{m}\ \underline{\ddot{x}} + \underline{k}\ \underline{\dot{x}} + \underline{f}(\underline{\dot{x}}) = \underline{P}e^{i\omega t} \tag{6.13}$$

where,

$$\underline{q} = \underline{\Phi}\ \underline{x}$$

and $\underline{\Phi}$ is the matrix containing the linear eigenvectors of the undamped system. In the new coordinates, the matrices $\underline{m}$ and $\underline{k}$ are diagonal, but $\underline{f}$ need not be. However, assuming that the natural frequencies of the undamped system are well separated, that the linear damping matrix satisfies the conditions for classical normal modes (Caughey,1963), and that the nonlinear damping elements are of per-

turbation order, one can approximately neglect the off-diagonal terms of the matrix $\underline{f}$, and obtain N uncoupled equations of the form:

$$m_i\ddot{x}_i + k_i x_i + f_i(\dot{x}_i) = P_i e^{i\omega t} \qquad i = 1, ..., N \tag{6.14}$$

Note that in writing (6.14) it was assumed that the nonlinear function f_i depends only on the variable $\dot{x}_i$. The approximate equations (6.14) describe the motion of the system on a normal mode, and they are identical in form to (6.1) that describes the motion of a nonlinear SDOF oscillator. Assuming that the nonlinearities and the exciting forces are small, the method of equivalent linearization can be applied, and (6.14) is replaced by a linearized equation. It can be shown that in the absence of nonlinear stiffness elements, the equivalent stiffness of the system is zero:

$$\omega_{eq}^2 = 0 \tag{6.15}$$

Hence, the equivalent, linearized system of equation (6.14) takes the form:

$$\ddot{x}_i + \omega_{ir}^2(1 + i\eta_{ieq})x_i = \frac{P_i}{m_i} e^{i\omega t} \tag{6.16}$$

where,

$$\eta_{ieq} = \frac{\omega b_{ieq}}{\omega_{ir}^2} \tag{6.17}$$

and

$$b_{ieq} = \frac{\int_0^{2\pi} -sin\theta \; f_i(\; -\omega A_i sin\theta \;)\; d\theta}{m_i \pi \omega A_i} \tag{6.18}$$

In the above equations, $\omega_{ir}^2 = k_i/m_i$, and A_i is the amplitude of the approximate steady state, computed by (from now on, the subscript i is omitted):

$$\frac{P/m}{Ae^{i\phi}} = \omega_r^2 - \omega^2 + i\omega_r^2\eta_{eq} \tag{6.19}$$

The phase ϕ between the displacement and the force is computed by the relation:

$$tan\phi = -\frac{\omega_r^2 \eta_{eq}}{\omega_r^2 - \omega^2} \tag{6.20}$$

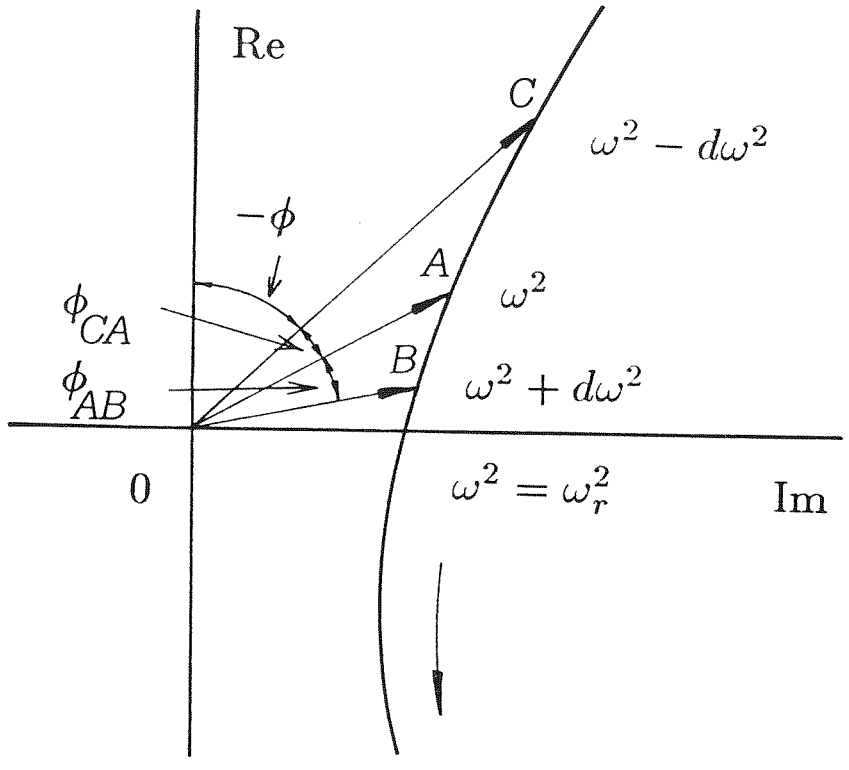

Figure 6.1. Inverse of the receptance of a system with nonlinear damping.

The complex quantity (6.19) has the form of the inverse of the receptance of a SDOF system, and its schematic plot for varying ω is presented in figure 6.1. When linear damping exists, the plot is a straight line that intersects orthogonally the imaginary axis, at $\omega^2 = \omega_r^2$. When the damping is nonlinear, the line is curved,

but it still intersects the imaginary axis at $\omega^2 = \omega_r^2$ (this is due to the fact that at this frequency the real part of (6.19) vanishes). Consider now three points C, A and B of the plot, corresponding to frequencies squared, $\omega^2 - d\omega^2, \omega^2$ and $\omega^2 + d\omega^2$ respectively. Referring to figure 6.1, the angles ϕ_{CA} and ϕ_{AB} connecting these points can be evaluated by the expressions:

$$\begin{aligned} \phi_{CA} &= tan^{-1}\left(\frac{\omega_r^2 \eta_{eq}(A(u),u)}{\omega_r^2 - u^2}\right)_{u^2=\omega^2-d\omega^2} - tan^{-1}\left(\frac{\omega_r^2 \eta_{eq}(A(u),u)}{\omega_r^2 - u^2}\right)_{u^2=\omega^2} \\ \phi_{AB} &= tan^{-1}\left(\frac{\omega_r^2 \eta_{eq}(A(u),u)}{\omega_r^2 - u^2}\right)_{u^2=\omega^2} - tan^{-1}\left(\frac{\omega_r^2 \eta_{eq}(A(u),u)}{\omega_r^2 - u^2}\right)_{u^2=\omega^2+d\omega^2} \end{aligned} \tag{6.21}$$

In equations (6.21), the explicit dependence of η_{eq} on the amplitude of motion, $A(\omega)$, and the frequency ω, are emphasized. Using some elementary algebraic and trigonometric formulas, the angles can be expressed as follows:

$$\begin{aligned} tan\phi_{CA} &= \frac{\omega_r^2(\omega_r^2 - \omega^2)\ \eta_{eq}^{(-)} - \omega_r^2(\omega_r^2 - \omega^2 + d\omega^2)\ \eta_{eq}^{(0)}}{(\omega_r^2 - \omega^2 + d\omega^2)(\omega_r^2 - \omega^2) + \omega_r^4\ \eta_{eq}^{(-)}\ \eta_{eq}^{(0)}} \\ tan\phi_{AB} &= \frac{\omega_r^2(\omega_r^2 - \omega^2 - d\omega^2)\ \eta_{eq}^{(0)} - \omega_r^2(\omega_r^2 - \omega^2)\ \eta_{eq}^{(+)}}{(\omega_r^2 - \omega^2 - d\omega^2)(\omega_r^2 - \omega^2) + \omega_r^4\ \eta_{eq}^{(0)}\ \eta_{eq}^{(+)}} \end{aligned} \tag{6.22}$$

where the following notation was adopted:

$$\begin{aligned} \eta_{eq}^{(-)} &= \{\eta_{eq}(A(u),u)\}_{u^2=\omega^2-d\omega^2} \\ \eta_{eq}^{(0)} &= \{\eta_{eq}(A(u),u)\}_{u^2=\omega^2} \\ \eta_{eq}^{(+)} &= \{\eta_{eq}(A(u),u)\}_{u^2=\omega^2+d\omega^2} \end{aligned} \tag{6.23}$$

The receptance of the modal response is found by inverting the quantity (6.19) in the complex plane, and its plot is shown in figure 6.2. A property of the complex inversion is that an angle formed by lines connecting the origin with two points in the original plane is preserved in the inverted plane. Thus, the points C', A' and B'

of the inverted (receptance) plot, corresponding to frequencies squared, $\omega^2 - d\omega^2, \omega^2$ and $\omega^2 + d\omega^2$, are connected by the same angles ϕ_{CA} and ϕ_{AB}, that connect the respective points C, A and B in the inverse receptance plot (figure 6.1).

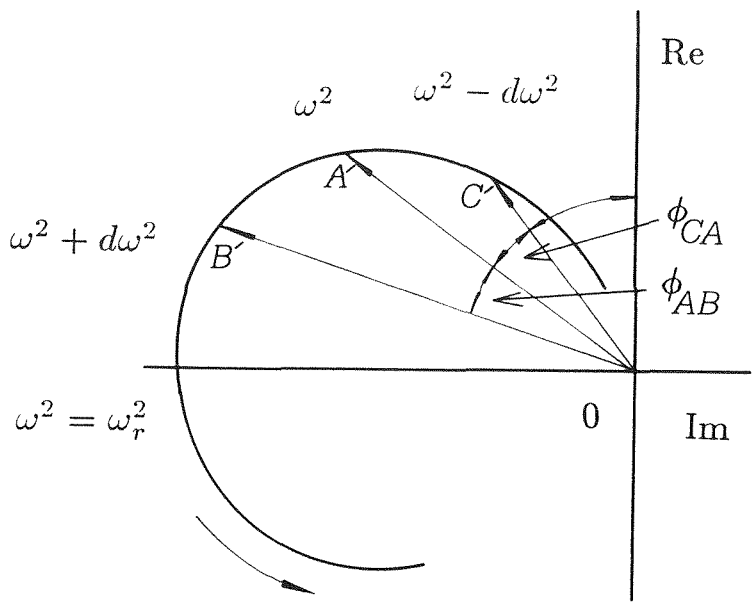

Figure 6.2. Receptance plot of a system with nonlinear damping.

Define at this point the quantity Δ, as follows:

$$\Delta = \frac{1}{tan\phi_{CA}} - \frac{1}{tan\phi_{AB}} \tag{6.24}$$

It will be shown that this quantity is the extension for the nonlinear case of the respective quantity defined for linear systems in section 5.2. To show this, consider the two circles passing through the origin of the complex plane and the points (B', A') and (A', C') respectively (figure 6.3). The central angles of the circles passing through these points are equal to one-half the angles ϕ_{AB} and ϕ_{CA} respectively. Thus, the quantity defined by (6.24) is analogous to the quantity Δ defined in sec-

tion 5.2 for linear systems (in that section, Δ was expressed in terms of the halves of the central angles connecting points of the circle fit of the measured data); hence, by using (6.24) one extends the Δ-Plot formulation developed for linear systems to the nonlinear case.

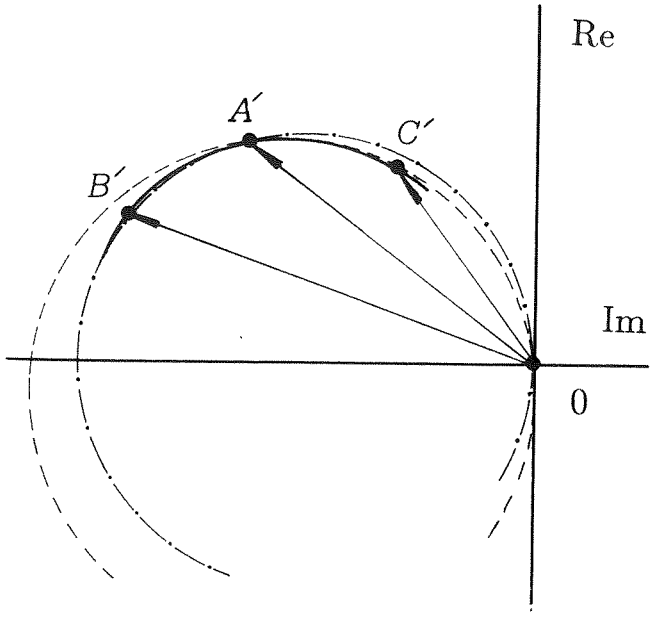

Figure 6.3. Circle-fitting for evaluation of the quantity Δ.

Note that in the linear case there exists a single circle passing through the origin and *all* the points of the Nyquist plot. In the nonlinear case, the Nyquist plot is distorted and no single circle-fit exists. Thus, in order to compute the nonlinear Δ-Plot, one must consider the circles passing through each couple of FRF points and the origin of the complex plane. However, for weak nonlinearities, the distortions of the Nyquist plots are small, and one can approximately circle-fit subsequent triads of frequency points; in doing so, one assumes that the two circles of figure 6.3 are nearly coincident, and that they can be approximately replaced by a circle passing

through the three FRF points. Then, the central angles of the approximate circle fit can be used for evaluating the Δ-quantity.

As a final comment regarding expression (6.24), note that the frequency where $\Delta = 0$, corresponds to the point of maximum frequency separation of the points of the Nyquist plot. This can be concluded from the fact that, at that frequency, the two central angles of the circle-fit become equal, and the derivative of the arc of the Nyquist plot with respect to the frequency is zero.

In section 5.2, it was shown that the linear Δ-quantity is a function only of the frequency of the center point of the triad (point A' in this case. However, when nonlinearity exists, this is not necessarely true. To find the expression for Δ one has to substitute in (6.24) the analytical expressions for the angles, given by relations (6.22). Since the resulting formulas become very complicated, a perturbation analysis will be applied at this point. Assuming that the increment of the frequency squared, $d\omega^2$, is small compared to the square of the linear natural frequency ω_r^2, one can expand the equivalent loss factor in Taylor series about a frequency ω_0, as follows:

$$\eta_{eq}(A(\omega_0^2 + d\omega^2), \omega_0^2 + d\omega^2) = \eta_{eq}(A(\omega_0^2), \omega_0^2) + \tilde{\eta}'(\omega_0^2)(\frac{d\omega^2}{\omega_r^2}) + \tilde{\eta}''(\omega_0^2)(\frac{d\omega^2}{\omega_r^2})^2 +$$

$$+ \mathcal{O}[\,(\frac{d\omega^2}{\omega_r^2})^3\,] \qquad (6.25)$$

The expansion coefficients appearing in (6.25) are computed as follows :

$$\tilde{\eta}'(\omega_0^2) \equiv \{\frac{\partial \eta_{eq}}{\partial(\omega^2/\omega_r^2)}\}_{\omega_0^2} + \{\frac{\partial \eta_{eq}}{\partial A}\}_{\omega_0^2}\{\frac{\partial A}{\partial(\omega^2/\omega_r^2)}\}_{\omega_0^2}$$

$$\tilde{\eta}''(\omega_0^2) \equiv \frac{1}{2}\{ \{\frac{\partial^2 \eta_{eq}}{\partial A^2}\}_{\omega_0^2} \{\frac{\partial A}{\partial(\omega^2/\omega_r^2)}\}^2_{\omega_0^2} + \{\frac{\partial \eta_{eq}}{\partial A}\}_{\omega_0^2} \{\frac{\partial^2 A}{\partial(\omega^2/\omega_r^2)^2}\}_{\omega_0^2} +$$

$$+\{\frac{\partial^2 \eta_{eq}}{\partial(\omega^2/\omega_r^2)^2}\}_{\omega_0^2} + \{2\frac{\partial^2 \eta_{eq}}{\partial A \partial(\omega^2/\omega_r^2)}\}_{\omega_0^2} \{\frac{\partial A}{\partial(\omega^2/\omega_r^2)}\}_{\omega_0^2} \} \qquad (6.26)$$

In deriving these expressions, it was assumed that η_{eq} depends explicitly on the amplitude A and the frequency ω, although there are cases where one of these variables is absent.

In addition, it is assumed that the frequency ω is very close to the linear natural frequency ω_r (this is the same with restricting the analysis to the resonance region of the mode), and that the equivalent loss factor η_{eq}, along with all of its partial derivatives, are small quantities. These requirements are summarized as follows:

$$\mathcal{O}(1 - \frac{\omega^2}{\omega_r^2}) = \mathcal{O}(\frac{d\omega^2}{\omega_r^2}) = \mathcal{O}(\eta_{eq}) = \mathcal{O}(\tilde{\eta}') = \mathcal{O}(\tilde{\eta}'') = \epsilon \qquad (6.27)$$

Moreover, the amplitude A and the ratio (ω^2/ω_r^2) are assumed to be of $\mathcal{O}(1)$.

Substituting now the expressions for the angles ϕ_{AB} and ϕ_{CA} in the expression for the Δ-quantity, equation (6.24), and taking into account the Taylor expansions (6.25), one obtains the following simplified expression for Δ :

$$\Delta = \frac{2}{\eta_{eq}^{(0)}}(1 - \frac{\omega^2}{\omega_r^2}) - 2\tilde{\eta}'(\omega^2) - \frac{2\tilde{\eta}'(\omega^2)}{\eta_{eq}^{(0)2}}(1 - \frac{\omega^2}{\omega_r^2})^2 + \mathcal{O}(\epsilon^2) \qquad (6.28)$$

where for a definition of $\eta_{eq}^{(0)}$, see equations (6.23). In deriving the above expression, terms of $\mathcal{O}(\epsilon^2)$, or higher, were omitted. The following remarks are made, as far as the analytic expression (6.28) is concerned.

• For damping nonlinearity, the quantity Δ depends explicitly on $d\omega^2$. The first term of the expression is of $\mathcal{O}(1)$, and corresponds to the unperturbed *linear* plot.

Indeed, this term is identical to expression (5.3) of section 5.2, where a system with linear hysteretic damping was examined. Hence, the damping nonlinearity introduces $\mathcal{O}(\epsilon)$ distortions in the Δ-plot (these are the second and third terms of equation (6.28)).

• Of interest is to compute the frequency ω_{ms} corresponding to $\Delta = 0$. By the construction of the Δ-quantity, ω_{ms} corresponds to the frequency of maximum frequency separation in the Nyquist plot. Setting the right-hand side of equation (6.28) equal to zero, one obtains the following analytic relation:

$$\frac{\omega_{ms}^2}{\omega_r^2} = 1 - \eta_{eq}(A(\omega_{ms}^2), \omega_{ms}^2)\ \tilde{\eta}'(\omega_{ms}^2) + \mathcal{O}(\epsilon^3) \tag{6.29}$$

This is a transcedental equation in ω_{ms}^2. However, by considering the orders of its terms, it can be concluded that $\omega_{ms} = \omega_r + \mathcal{O}(\epsilon^2)$. Hence, an interesting analytical result is that weak damping nonlinearity essentially leaves unaffected the point of maximum frequency separation in the Nyquist plot of the receptance. This confirms the result that Tomlinson derived for a SDOF with dry friction (Tomlinson, 1980). Although the Nyquist plot of the receptance is distorted, the frequency where maximum frequency separation occurs is essentially the same with that of the linear case.

• The slope of the Δ-plot at the point of maximum frequency separation is determined by differentiating (6.28) with respect to the frequency variable (ω^2/ω_r^2), and subsequently evaluating the resulting expression at $\omega = \omega_{ms} \simeq \omega_r$:

$$\left\{\frac{\partial \Delta}{\partial(\omega^2/\omega_r^2)}\right\}_{\omega_{ms}} = -\frac{2}{\eta_{eq}(A(\omega_r^2), \omega_r^2)} - 2\left\{\frac{\partial \tilde{\eta}'}{\partial(\omega^2/\omega_r^2)}\right\}_{\omega_r^2} + \mathcal{O}(\epsilon^2) \tag{6.30}$$

The first term is identical to the corresponding expression for a linear system (see section 5.2), whereas the additional term represents the perturbation due to the nonlinear damping.

The aforementioned results are derived by considering a single mode of the system (see figures 6.1 and 6.2). The obvious question is what happens when residual terms of nearby modes are also included. To answer this question, recall from section 5, that for well separated modes, and sufficiently close to the resonance region, the effects of out-of-range modes can be approximately modelled by a constant complex term that causes a rigid-body displacement of the resonance region. Therefore, for well separated modes, the *relative* spacing of the frequency points in the Nyquist plot remains unaffected. Since the Δ-quantity is evaluated by considering subsequent triads of Nyquist points, its value depends only on the relative spacing of the points in the resonance region and, therefore, is not affected by the residual effects of the out-of-range modes. However, when modes are closely spaced, the relative spacing of the Nyquist points is altered, and the aforementioned formulation cannot be applied.

6.3.2. NUMERICAL APPLICATION: DRY (COULOMB) FRICTION

As an application, a mode with weak dry friction was examined. The nonlinear restoring force is of the form,

$$f(\dot{x}) = F\ sgn(\dot{x}) \tag{6.31}$$

and the equation of motion is given by:

$$\ddot{x} + \omega_r^2 x + b\dot{x} + \frac{F}{m} sgn(\dot{x}) = \frac{P}{m} e^{i\omega t} \tag{6.32}$$

Note that in addition to dry friction, a linear viscous damping term is assumed. In the above equation, m represents the modal mass. The overall equivalent loss factor is computed from equations (6.8) and (6.11), as follows:

$$\eta_{eq} = \eta_{eq}(A, \omega) = \frac{2\omega\zeta_r}{\omega_r} + \frac{4R}{\pi A} \tag{6.33}$$

where A is the amplitude of the steady state motion, and $R = F/mP$, is the ratio of the friction force to the applied external excitation. In (6.33), the "critical viscous damping ratio," ζ_r, was used, related to b by the formula, $\zeta_r = b \;/\; 2\,\omega_r$. Note that the equivalent loss factor (6.33) has only meaning in the resonance region of the mode ($\omega \simeq \omega_r$), and only for small values of the friction force F.

The exact steady state solution of (6.32) was obtained in (Den Hartog, 1931) and (Yeh, 1966), and based on the results of these references, the Nyquist plots of the receptance were constructed for different values of the ratio R. The plots corresponding to $\omega_r = 2\pi$, and $\zeta_r = 0.008$ are presented in figure 6.4a. In deriving the receptances it was assumed that the steady states are continuous motions with no "stops" due to friction (for cases where this does not hold, see (Yeh, 1966)). In figure 6.4b, the associated Δ-Plots of the receptances are shown. These were constructed by circle-fitting subsequent triads of Nyquist points, and subsequently evaluating the corresponding central angles. Clearly, the theoretical prediction that the Δ-Plot vanishes at the linear natural frequency is verified. In fact, all the Δ-

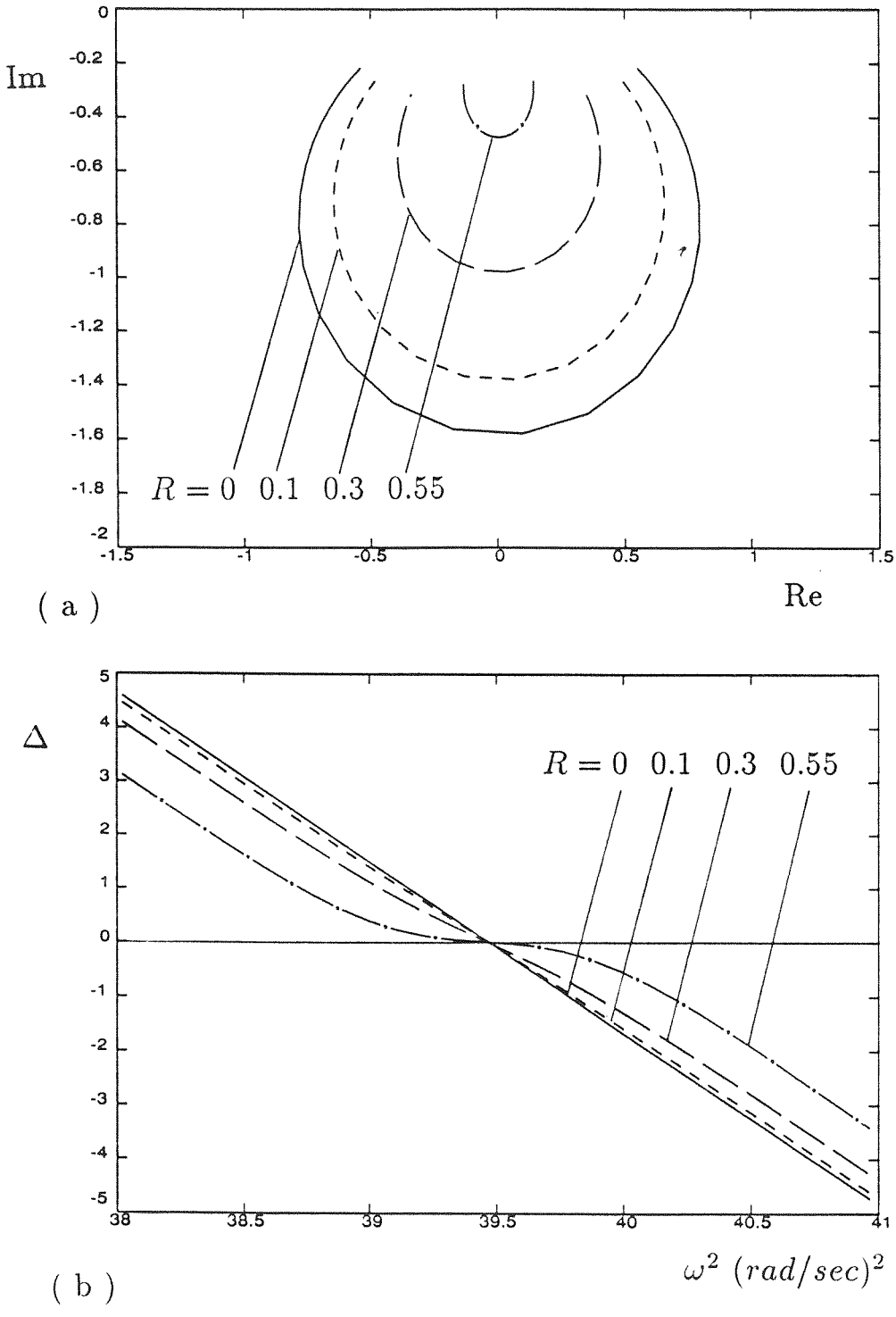

Figure 6.4. (a) Receptance plots for a system with dry friction, for different values of the parameter R (b) Resulting Δ-Plots.

plots vanish approximately at $\omega = \omega_r$ however, as the friction force is increased, the slopes of the Δ-Plots at the zero-crossing also decrease.

Of considerable interest is the "inverse" problem. Namely, regarding the Nyquist plots of figure 6.4a, as being measured from an experiment, to be able to identify the nonlinearity and the modal parameters by considering the Δ-Plots. To answer that problem, the following parametric technique for modal identification is proposed. In a later section a more general version of this technique will be presented.

The linear natural frequency is identified as the frequency where the plots become zero. The analytical approximation for the value of the slope of the Δ-Plot at the point of zero-crossing is given by equation (6.30). For dry friction this expression becomes:

$$\{\frac{\partial \Delta}{\partial(\omega^2/\omega_r^2)}\}_{\omega_{ms}} = -\{\ \zeta_r + \frac{2R}{\pi A(\omega_{ms})}\ \}^{-1} \tag{6.34}$$

where $\omega_{ms} \simeq \omega_r$. The slope is measured directly from the Δ-Plot, and the amplitude $A(\omega_{ms})$ of the motion is measured from a Bode plot of the receptance. Hence, by considering two Δ-Plots, corresponding to different values of the force amplitude, one can solve for the two unknown quantities R and ζ_r, and identify the friction force and the linear viscous damping ratio of the mode.

The results of the application of the aforementioned technique to a theoretically generated receptance with dry friction are summarized below.

Theoretical data	*Identified data*
Nat. freq.: 11.0000 Hz	Nat. freq.: 10.9909 Hz
Viscous ratio : 0.02500	Modal damp.: 0.02449
Friction force : 15.0000 Nt	Friction force : 13.5743 Nt

It can be seen that the identified parameters are close to their theoretical values. Based on these results, the regenerated receptance plots of figure 6.5 were constructed; for comparison purposes, the exact solutions are also shown.

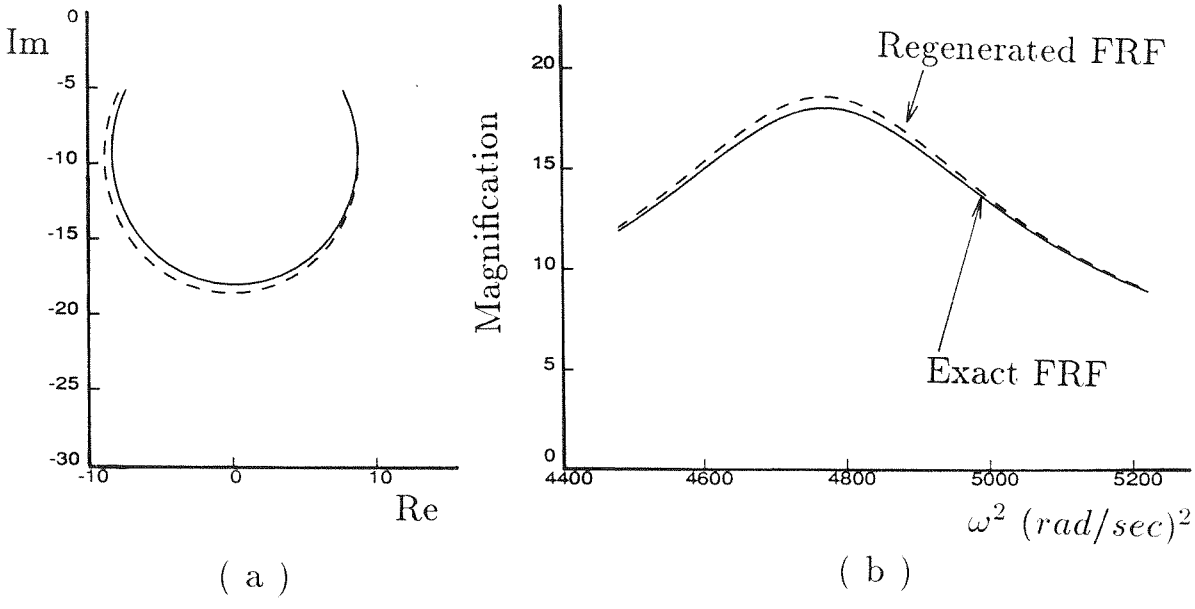

Figure 6.5. Theoretical and regenerated plots of the Magnification $(P/A\omega_r^2)$, for a mode with dry friction (a) Nyquist plot (b) Bode plot.

Summarizing, it was established that the numerical simulations confirm the analytical predictions. The Δ-Plots of systems with weak damping nonlinearities vanish at a frequency that is approximately equal to the linear natural frequency of the mode. The slopes of the Δ-Plots at the zero-crossings were analytically expressed

as functions of the modal parameters and the nonlinearity and were subsequently used for modal identification.

6.4. SYSTEM WITH STIFFNESS NONLINEARITY

6.4.1. ANALYSIS

When a mode contains stiffness nonlinearities, one can follow a similar methodology in order to study the nonlinear distortions of the receptance plots. Assuming that the steady state motion of the mode is described by a differential equation of the form,

$$m\ddot{x} + \omega_r^2(1 + i\eta)x + f(x) = Pe^{i\omega t}, \tag{6.35}$$

the inverse of the approximate receptance is given by:

$$\frac{P/m}{Ae^{i\phi}} = \omega_r^2 + \omega_{eq}^2 - \omega^2 + i\omega_r^2\eta \tag{6.36}$$

In the above equations, $f(x)$ is the nonlinear stiffness, η is the linear (constant) hysteretic loss factor and ω_{eq}^2 is the overall equivalent stiffness, given by:

$$\omega_{eq}^2 = \frac{\int_0^{2\pi} cos\theta \; f(\; Acos\theta \;)\; d\theta}{m\pi A} \tag{6.37}$$

Generally, the equivalent stiffness is a function of the amplitude of steady state oscillation, A.

As in section 6.3, one can construct the plot of the inverse of the receptance in the complex plane, using the frequency as the independent parameter. This plot is presented in figure 6.6, and is a straight line, intersecting orthogonally the imaginary

axis (compare this plot with that of figure 6.1, corresponding to nonlinear damping). The Nyquist plot of the receptance, resulting from the inversion of this line, is a circle. Thus, the linearized theory predicts a circular form for the receptance, i.e., identical in form with that of a linear mode with hysteretic damping. Again, three points corresponding to frequencies $\omega^2 \pm d\omega^2$ and ω^2 are considered, and the corresponding angles, ϕ_{CA} and ϕ_{AB}, are computed.

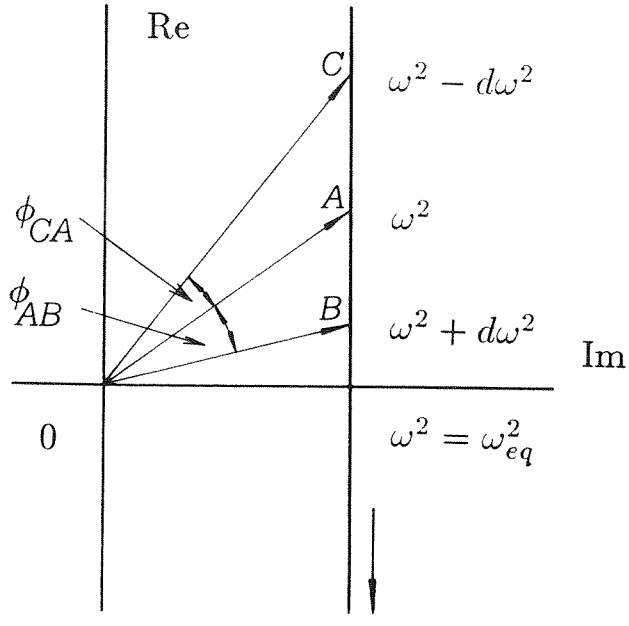

Figure 6.6. Inverse of the receptance of a system with nonlinear stiffness.

The quantity Δ is subsequently computed according to formula (6.24), and the result is simplified by use of perturbation analysis. In this case, it is assumed that the equivalent stiffness is of much smaller magnitude than that of the linear natural frequency:

$$\frac{\omega_{eq}^2}{\omega_r^2} = \mathcal{O}(\epsilon) \tag{6.38}$$

and additionally that:

$$\mathcal{O}(\eta) = \mathcal{O}(\frac{d\omega^2}{\omega_r^2}) = \mathcal{O}(\epsilon) \tag{6.39}$$

The corresponding expressions are too lengthy to be reproduced here, and only the main analytical results will be presented. It can be shown that the frequency of maximum frequency separation in the Nyquist plot (corresponding to the point where $\Delta = 0$), is given by the following analytical formula:

$$\frac{\omega_{ms}^2}{\omega_r^2} = 1 + \frac{\{\omega_{eq}^2\}_{\omega_{ms}}}{\omega_r^2} + \frac{2\{\omega_{eq}^2\}_{\omega_{ms}} - \{\omega_{eq}^2\}_{\omega_{ms}+d\omega^2} - \{\omega_{eq}^2\}_{\omega_{ms}-d\omega^2}}{2d\omega^2/\omega_r^2\eta^2} + \mathcal{O}(\epsilon^2) \tag{6.40}$$

In this expression, the increment of frequency squared, $d\omega^2$, can be assigned an arbitrary value, provided that the requirement (6.39) is satisfied.

So, in contrast to the case of damping nonlinearity, when nonlinear stiffness exists, the frequency of maximum frequency separation is shifted by $\mathcal{O}(\epsilon)$ terms. Note that the first two terms in the above expression give the approximate frequency of free oscillation of the nonlinear system (backbone curve). This is not, however, the frequency of maximum separation in the Nyquist plot, since there exists a third term (of comparable magnitude with the second) in equation (6.40). This term describes the unevenness of the distribution of ω_{eq} about the linear natural frequency ω_r, and as shown in the next section, it is also a measure of the asymmetry of the Bode plot of the receptance.

Equation (6.40) is the only analytical result of practical use. The expressions for the Δ-function and its slope at zero-crossing are lengthy and complicated, and cannot be easily implemented in modal identification procedures.

6.4.2. NUMERICAL APPLICATION: CUBIC STIFFNESS NONLINEARITY

To demonstrate the analysis, consider the case of cubic stiffness nonlinearity. The equation of motion (6.35) becomes:

$$m\ddot{x} + \omega_r^2 x + \alpha\omega_r^2 x^3 + 2\zeta_r\omega_r\dot{x} = Pe^{i\omega t} \tag{6.41}$$

where the parameter α is a measure of the nonlinearity and is assumed to be a small quantity. In this example, the damping is assumed to be viscous, but this does not complicate the analysis, since as mentioned earlier, for lightly damped systems, the viscous and hysteretic damping models are equivalent. The equivalent stiffness of the system is given by the well known formula,

$$\omega_{eq}^2(A) = \frac{3}{4}\alpha\omega_r^2 A^2, \tag{6.42}$$

and depends only on the amplitude of the steady motion. Accordingly, the linearized equivalent system becomes:

$$m\ddot{x} + (\omega_r^2 + \omega_{eq}^2)x + 2\zeta_r\omega_r\dot{x} = \frac{P}{m}e^{i\omega t} \tag{6.43}$$

The magnitudes of the approximate receptances are then computed by the following equation,

$$\frac{\omega_r^2 A}{P/m} = \{[\frac{\omega_{eq}^2}{\omega_r^2} - \frac{\omega^2}{\omega_r^2}]^2 + 4\zeta_r^2\frac{\omega^2}{\omega_r^2}\}^{-1/2}, \tag{6.44}$$

and their phases are given by:

$$tan\phi = \frac{2\zeta_r\omega/\omega_r}{(\omega_{eq}^2/\omega_r^2) - (\omega^2/\omega_r^2)} \tag{6.45}$$

The Bode plots of the receptances are presented in figure 6.7a, for different values of the forcing levels. These plots correspond to $\omega_r = 2\pi, \alpha = 0.025$ and $\zeta_r = 0.015$, and it can be seen that as the external forces increase, the asymmetries of the diagrams become more and more profound. Also shown in the same figure is the "backbone curve," corresponding to approximate, free oscillatory motions. It is assumed that the levels of excitation are small enough, so that there are no "jumps" in the receptance plots.

In figure 6.7b the Δ-Plots of the receptances are shown. Comparing these plots with those of figure 6.4b (corresponding to dry friction), it is concluded that the distortions in the receptances due to stiffness nonlinearities are fundamentally different than those resulting due to damping nonlinearities. In the present case, the frequency where the Δ-plot vanishes (and thus, the frequency of maximum frequency separation in the Nyquist plot) increases as the level of the excitation force increases. In fact, this is in agreement with the theoretical result (6.40) that predicts that, for modes with nonlinear stiffness, the frequency of zero-crossing is in $\mathcal{O}(\epsilon)$ distance from the linear natural frequency. Note that the frequencies corresponding to the backbone curve of the free system are not the frequencies where the Δ-Plot vanishes. This confirms the theoretical prediction that there exist distorting terms in the expression of ω_{ms} caused by the asymmetry of the Bode plot of the receptance.

In the sequence it will be shown how the analytic expression giving the frequency of maximum frequency separation (equation (6.40)) can be used for identifying the

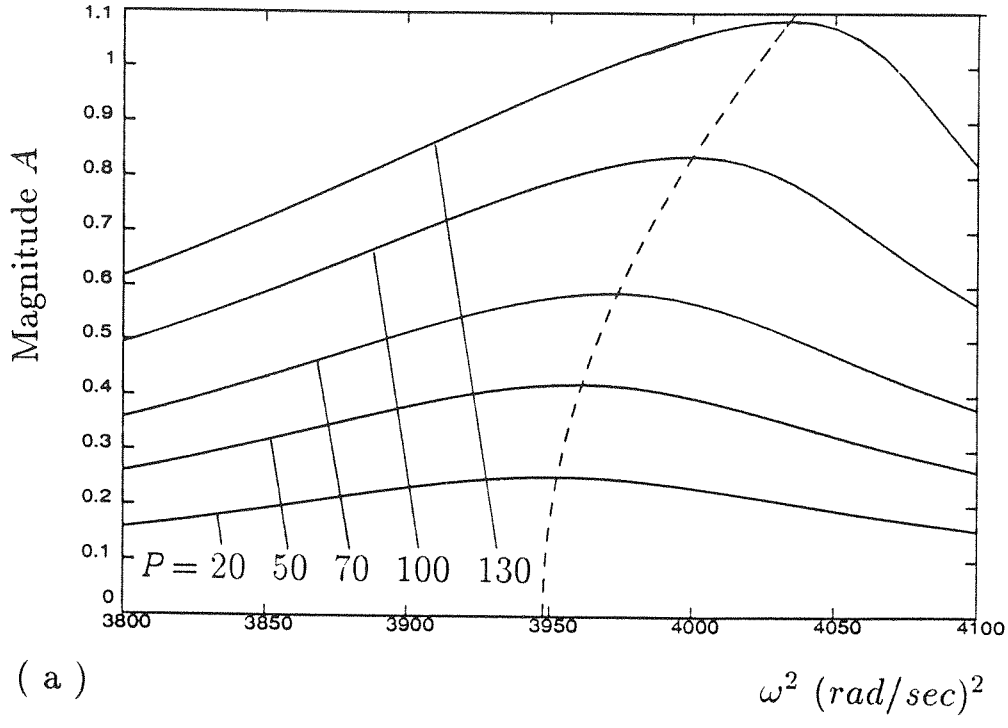

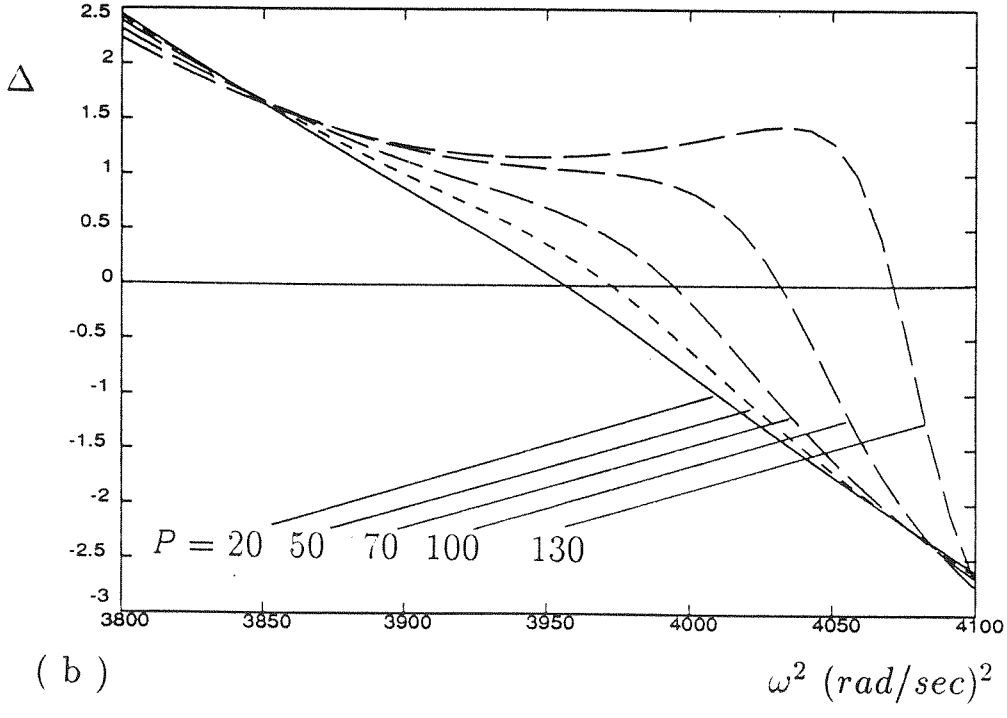

Figure 6.7. (a) Bode plots for a system with cubic stiffness nonlinearity, for different levels of external excitation (b) Resulting Δ-Plots.

stiffness nonlinearity. To achieve this, the nonlinearity will be assumed to be of the general form:

$$\frac{f(x)}{m} = \alpha\omega_r^2 x^n \tag{6.46}$$

where the unknown parameters α and n will be identified by analyzing the receptance plots. Assuming that n is a real exponent, the equivalent stiffness is computed from (6.37) as follows:

$$\omega_{eq}^2(A) = \frac{2\alpha\omega_r^2 A^{n-1}}{\pi^{1/2}} \frac{\Gamma((n+2)/2)}{\Gamma((n+3)/2)} \tag{6.47}$$

where $\Gamma(\bullet)$ is the Gamma function. Substituting this expression in (6.40), one obtains the following expression for the frequency of maximum frequency separation of the Nyquist plot of the receptance:

$$\omega_{ms}^2 - \omega_r^2 = \mathcal{T}(n) A^{n-1}(\omega_{ms}^2) + \frac{\mathcal{T}(n)}{(2d\omega^4/\omega_r^4(2\zeta_r)^2)} \{\, 2A^{n-1}(\omega_{ms}^2) - A^{n-1}(\omega_{ms}^2 + d\omega^2) -$$

$$- A^{n-1}(\omega_{ms}^2 + d\omega^2) \,\} \tag{6.48}$$

where $\mathcal{T}(n)$ depends only on the exponent of the nonlinearity and it is given by:

$$\mathcal{T}(n) = \frac{2\alpha\omega_r^2}{\pi^{1/2}} \frac{\Gamma((n+2)/2)}{\Gamma((n+3)/2)} \tag{6.49}$$

The identification procedure is as follows:

Step 1 : Identify the linear natural frequency and damping by considering the receptance plot corresponding to the lowest level of external excitation (see figure 6.7). Since the nonlinear stiffness is proportional to a power of the response, for low levels of excitation the nonlinear distortions are expected to be minimal. Hence,

the corresponding Δ-Plot is almost a straight line, and a SDOF identification can be approximately carried out.

Step 2: Consider in the sequence two additional receptance plots. In each case, identify the frequency ω_{ms} corresponding to the maximum frequency separation of the Nyquist plot (this can be achieved by identifying the frequency of zero-crossing of the corresponding Δ-Plot). Then, compute the amplitudes of steady state oscillations corresponding to frequencies squared, ω_{ms}^2 and $\omega_{ms}^2 \pm d\omega^2$. This can be carried out in the Bode plot of the receptance, by defining an arbitrary, but small, quantity $d\omega^2$. This calculation is graphically presented in figure 6.8.

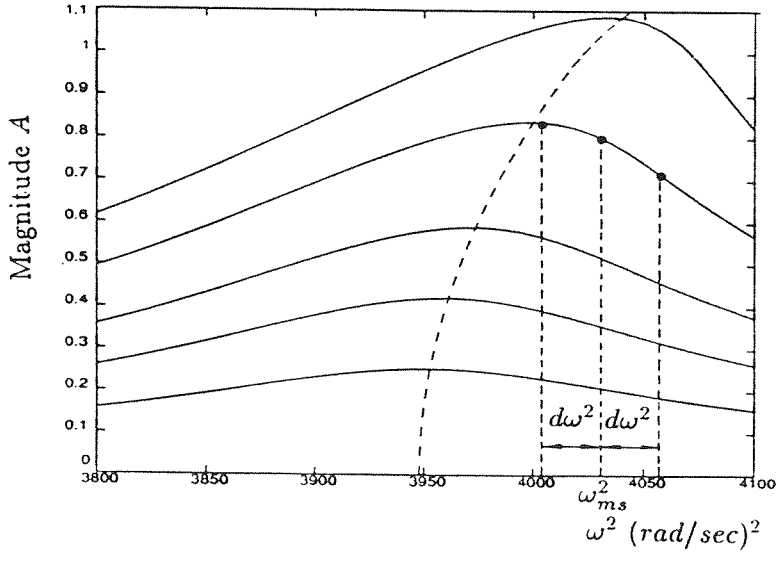

Figure 6.8. Calculation of the amplitudes of the receptance for modal identification.

Step 3: Use equation (6.48) and the computed quantities from the two receptance plots to construct a system of two nonlinear equations with two unknowns, namely, $\mathcal{T}(n)$, and n. Once these quantities are numerically determined, the amount of nonlinearity, α, is found by use of equation (6.49).

This technique was applied to the identification of the receptance plots of figure 6.7. Considering the receptance plot corresponding to the lowest excitation level (curve 1), the linear modal parameters were estimated (by making use of the linear SDOF methodology of section 5.2) as $\omega_r^2 = 3953.8\ (rad/sec)^2$ and $\zeta_r = 0.01545$. These estimates are very close to their theoretical values. Subsequently, curves 2 and 3 were used for estimating the order and the amount of the stiffness nonlinearity. The identified values are $n = 1.01841$ and $\alpha = 0.02337$. Thus, the method identified the nonlinearity as being almost cubic and of an amount that is very close to its nominal, theoretical value.

A series of additional computations was performed, considering each time a different set of receptance plots. The results were not as satisfactory as the ones obtained using curves 2 and 3. For example, using curves 2 and 4 one finds $n = 0.9228$, curves 2 and 5 give $n = 0.8636$, etc. This had to be expected, since as the level of excitation increases, the nonlinear effects become more apparent, and the approximate analysis based on the method of equivalent linearization loses accuracy. Hence, the outlined procedure should only be applied for low levels of excitation, where the nonlinearities are weak and the assumptions of the perturbation analysis are satisfied.

6.5. SYSTEM WITH COMBINED DAMPING AND STIFFNESS NONLINEARITIES: ANALYSIS OF EXPERIMENTAL DATA

In this final section, the general case of a mode with combined stiffness and damping nonlinearities will be examined. This situation is often encountered in engineering

practice, when more than one mechanism for nonlinearity exists in a practical structure.

Consider the steady state oscillation of a weakly nonlinear mode, with equivalent linearized stiffness $\omega_{eq}^2(A)$, and equivalent linearized loss factor $\eta_{eq}(A,\omega)$. These quantities approximate the actual stiffness and damping nonlinearities at the steady state. The inverse of the receptance can then be expressed as follows:

$$\frac{P}{X} = \omega_{eq}^2 - \omega^2 + i\omega_{eq}^2\eta_{eq} \tag{6.50}$$

where the notation of the previous two sections was used.

Working in a way similar to the previous two sections, and assuming that the nonlinear terms are small compared to the linear ones, it can be proven that the frequency, ω_{ms}, corresponding to the zero-crossing of the Δ-Plot (i.e., the frequency of maximum frequency separation in the receptance Nyquist plot) is given by the following analytical formula:

$$\frac{\omega_{ms}^2}{\omega_r^2} = 1 + \frac{\{\omega_{eq}^2\}_{\omega_{ms}}}{\omega_r^2} + \frac{2\{\omega_{eq}^2\}_{\omega_{ms}} - \{\omega_{eq}^2\}_{\omega_{ms}+d\omega^2} - \{\omega_{eq}^2\}_{\omega_{ms}-d\omega^2}}{2d\omega^2/\omega_r^2\{\eta_{eq}^2\}_{\omega_{ms}}} + \mathcal{O}(\epsilon^2) \tag{6.51}$$

This expression resembles the formula (6.40) that was derived for the case of nonlinear stiffness. Note, however, that in this case, the constant loss factor η in the denominator of (6.40) is replaced by the equivalent loss factor η_{eq}. From (6.51) it is concluded that ω_{ms}^2 differs from the square of the natural frequency, ω_r^2, by $\mathcal{O}(\epsilon)$ terms. When only nonlinear damping exists, the equivalent stiffness vanishes, and one finds that $\omega_{ms}^2 = \omega_r^2 + \mathcal{O}(\epsilon^2)$ (that is in full agreement with the results of section 6.3).

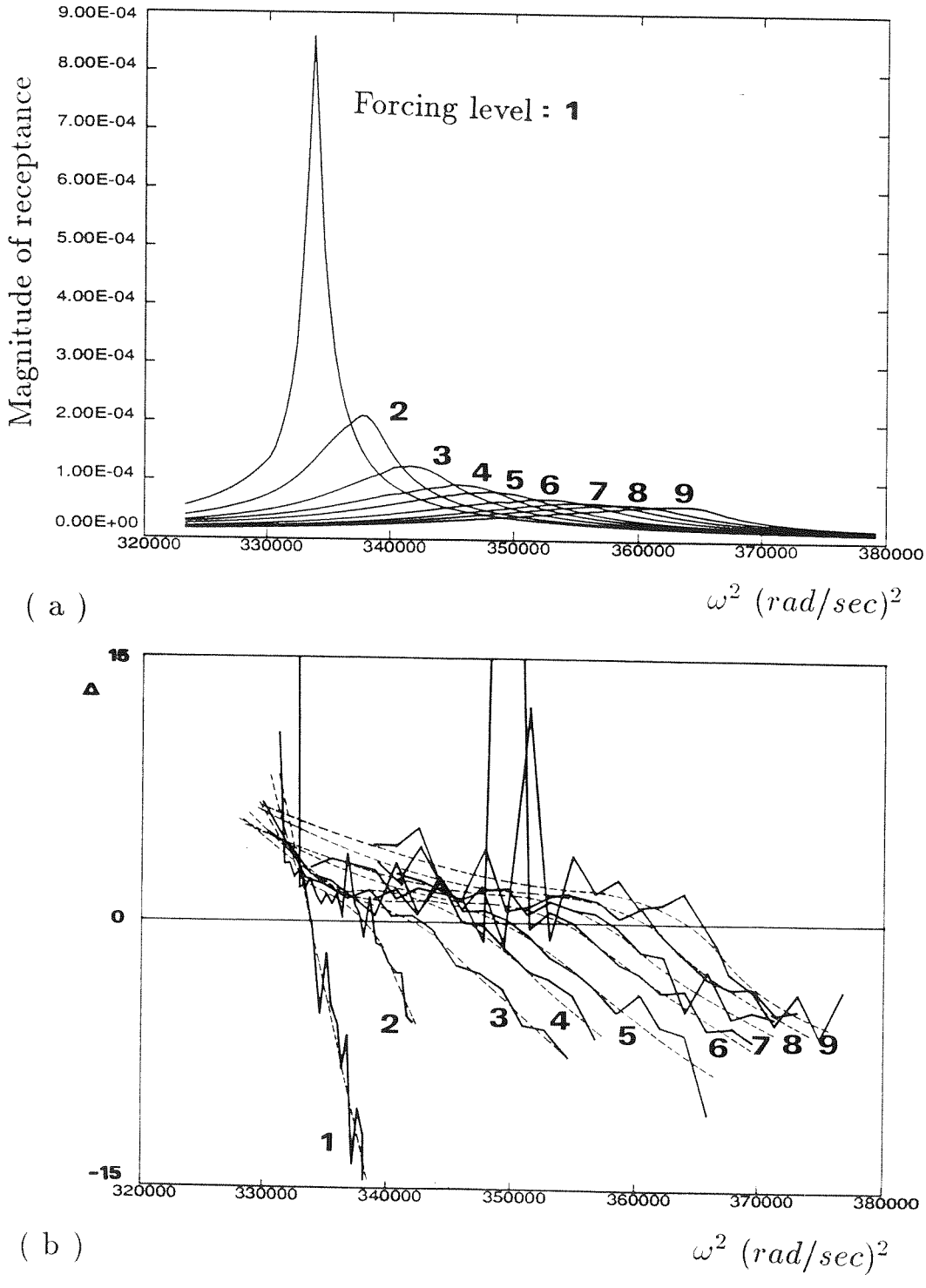

Figure 6.9. Experimental receptance plots (a) Bode diagrams (b) Δ-Plots.

As in section 6.4, the analytical result (6.51) can be used for modal identification of the nonlinearities and the modal parameters. The procedure of the previous section can be followed, i.e., one can initially identify the linear modal parameters from the plot corresponding to the lowest level of harmonic excitation, and subsequently use equation (6.51) and two additional receptance plots, to estimate the stiffness and damping nonlinearities.

This procedure was applied to the modal identification of an experimentally measured mode with combined damping and stiffness nonlinearities. The experimental data is taken from a high-frequency modal test of a truss structure, and the Bode plots of the receptance, corresponding to nine levels of external excitation, are presented at figure 6.9a. The j-th level, corresponds to a forcing magnitude that is j-times that of level 1. For low forcing (level 1), the response is almost linear and symmetric with respect to the frequency of maximum amplitude. The curves corresponding to levels 2 and 3 indicate a large increase in the modal damping and a low increase in the equivalent natural frequency. For higher level of forces, the modal damping appears to decrease, and the equivalent natural frequency, to slowly increase. Moreover, at high levels of force, asymmetries in the frequency responses (resulting from nonlinear distortions) are observed.

The Δ-plots of the receptances appear in figure 6.9b. Note that the plot corresponding to the first forcing is almost linear. As the level of excitation is increased, the Δ-Plots become curved and the frequency corresponding to the zero-crossing increases. Since the data are measured from an experiment, a certain amount of

measurement noise exists; however, the curves of the Δ-Plots are clearly detected, and they resemble the theoretical curves computed in the previous section.

The plots corresponding to forcing levels 1, 2, 3 and 4 will be examined in order to construct a model for the nonlinear force and to extract estimates for the linear modal parameters. The identification procedure will not be applied to receptances corresponding to higher forcing levels, since the obtained results will be inaccurate. This limitation of the method was demonstrated in the previous section with theoretical data, and is due to the fact that the analytical, perturbation results are not valid for high external forces. Hence, the approximate identification technique cannot be applied to strongly nonlinear FRF, and an alternative technique should be developed to study such cases.

The following general expression for the nonlinear force per unit modal mass will be considered. The first term of this formula models the nonlinear restoring force, whereas the second characterizes the nonlinear dissipation:

$$\frac{f(x,\dot{x})}{m} = kx^n + c|\dot{x}|^m \, sgn(\dot{x}) \tag{6.52}$$

Based on this model, the equivalent nonlinear quantities were computed as follows:

$$\begin{aligned} \omega_{eq}^2(A) &= \frac{2kA^{n-1}}{\pi^{1/2}} \frac{\Gamma((n+2)/2)}{\Gamma((n+3)/2)} \\ \eta_{eq}(A,\omega) &= \frac{2c\omega}{\pi^{1/2}} \frac{\Gamma((m+2)/2)}{\Gamma((m+3)/2)} \frac{(A\omega)^{m-1}}{\omega_r^2} \end{aligned} \tag{6.53}$$

where $\Gamma(\bullet)$ denotes the Gamma function.

From the receptance plot corresponding to forcing level 1, the loss factor of the mode is estimated as $\eta \simeq 2.009 \times 10^{-3}$, and the linear natural frequency as $\omega_r^2 \simeq 3.337 \times$

10^5 $(rad/sec)^2$. Moreover, the magnitude of the receptance corresponding to the natural frequency is found to be $A_1/P \simeq 8.594 \times 10^{-4}$. Substituting these estimates in the second of equations (6.53), one obtains the following alternative expression for the equivalent loss factor:

$$\eta_{eq}(A,\omega) \simeq 2.009 \times 10^{-3} \left(\frac{A}{8.594 \times 10^{-4}}\right)^{m-1} \left(\frac{\omega}{\omega_r}\right)^{m} \tag{6.54}$$

The expressions for ω_{eq} and η_{eq} are substituted in expression (6.51), and the receptance plots corresponding to forcing levels 2, 3 and 4 are examined. Evaluating the frequencies ω_{ms} directly from the experimentally measured Δ-Plots of figure 6.9b, and computing the corresponding magnitudes of the receptance from the Bode plots of figure 6.9a, an equation for ω_{ms} for each receptance plot is obtained. The resulting set of three equations with three unknowns, n, m and k, can be numerically solved, and the estimates for the exponents of the nonlinearities can be extracted. The exponent of the stiffness nonlinearity was computed as $n = 0.080753$, and that of the damping nonlinearity, as $m = -1.5168$. Hence, it is concluded that the restoring and dissipative components of the nonlinear force have the following approximate dependencies on the amplitude and the velocity respectively:

$$f_{restoring} \sim x^{0.080753}, \qquad f_{dissipative} \sim |\dot{x}|^{-1.5168}\, sgn(\dot{x}) \tag{6.55}$$

The mode has a weakly hardening stiffness behavior and a damping nonlinearity that is inversely proportional to a power of the velocity.

In figure 6.10, the equivalent loss factors at $\omega = \omega_{ms}$ are plotted for different forcing levels. Also shown in the same figure are the equivalent loss factors away from the

resonance region. These values were computed by considering the linear patterns of the experimental Δ-Plots for frequencies greater than ω_{ms}.

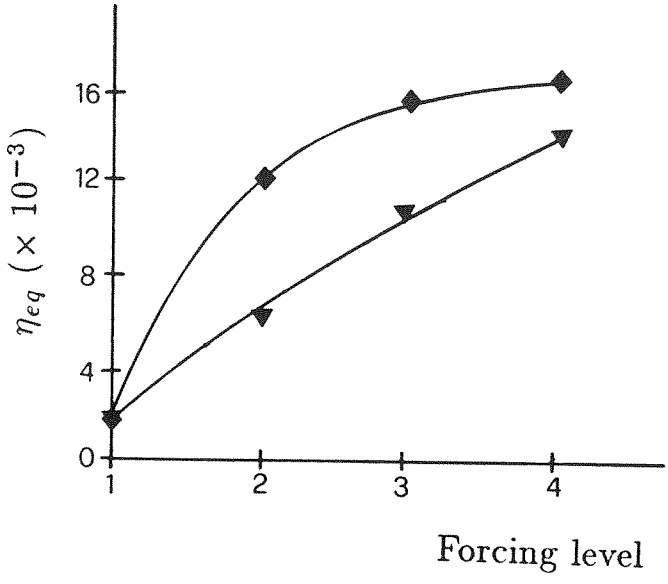

Figure 6.10. Equivalent loss factors : —▼— when $\omega = \omega_{ms}$, —◆— away from the resonance regions.

It must be pointed out that these results are based on the nonlinear mathematical model (6.52). Thus, if a different parametric model is used, the extracted nonlinear characteristics will differ. The outlined analysis provides only approximate estimates for the nonlinear behavior of the mode, and its results hold only for low levels of external excitations. A more complete nonlinear identification should also take into account information concerning the free oscillation of the structure (decay rates).

6.6. CONCLUDING REMARKS

The distortions in the receptance plots of weakly nonlinear modes were analyzed.

Analytical expressions for the frequencies of zero-crossings of the Δ-Plots were derived and subsequently used for identifying the weak nonlinearities. It was shown that when only nonlinear damping exists, the frequency of maximum frequency separation of the points in the receptance Nyquist plot is approximately equal to the linear natural frequency of the mode. However, when nonlinear stiffness nonlinearities exist, the frequency of maximum frequency separation shifts from the natural frequency, as the level of external excitation increases.

From the analytical results of this section, it can be concluded that the "maximum frequency separation criterion" (of linear modal identification techniques) cannot be used for extracting the natural frequency estimate from the Nyquist plot of the receptance. Instead, a technique that takes into account small nonlinear distortions is proposed. Since the method relies on perturbation analysis, it can only be applied to modes with weak nonlinearities, and for small levels of external excitation.

7. SUGGESTIONS FOR FURTHER WORK

The following research topics can be considered as extensions of this work:

- Use of Poincare maps to study the bifurcations of the similar modes of the system "off-resonance." In section 2.2.4. the linearized analysis indicated the existence of unstable regions in the balancing diagrams, corresponding to orbitally unstable similar modes. By investigating the global stability of the phase plane, the loss of stability of the similar modes could be analyzed; moreover, the existence of possible stable nonsimilar modes could be determined.

- Application of homoclinic Melnikov analysis for proving the existence of transverse homoclinic intersections for the two-DOF oscillator examined in section 2.4.3. This would rigorously prove the existence of an infinity of periodic orbits of the Poincare map and, thus, nonintegrability. In this work this was not possible since the homoclinic orbit appears in the slow-flow of the system (i.e., in the averaged equations), and the resulting Melnikov-functions are exponentially small. Hence, alternative forcing functions should be considered in order to introduce appropriate perturbations to the slow flow. Recent results by Holmes and Marsden, establishing upper and lower bounds for exponentially small Melnikov-functions, could be useful to this end.

- Examination of damped steady state motions. In this work only undamped motions were examined, and the displacements of the system were assumed to be functionally related at the steady state. When damping is introduced, the functional

steady state relations must also explicitly depend on the velocities. A theory analyzing the steady state motions of this class of oscillators has to be developed, and the general class of periodic excitations capable of producing steady state motions must be found.

- Application of the iterative algorithm for closely spaced modes, presented in section 5.5.1., to the modal analysis of experimental data containing nearly coincident modes. Investigation of the effects of measurement noise in the iterative procedure. Creation of refined multiple-input-multiple-output identification methods, suitable for structures with closely spaced modes. Comparison of the performance of the methods proposed in this work, with various existing SISO and MIMO identification algorithms.

- Study of alternative methods for quantifying structural nonlinearities. Development of techniques for detecting sources of nonlinearities in practical systems. Modelling and analysis of strongly nonlinear structures.

REFERENCES

PART I

Abramowitch M., Stegun I., 1965. Handbook of Mathematical Functions. Dover Publication, New York.

Anand G., 1972. Natural Modes of a Coupled Nonlinear System. Int.J.Nonlinear Mech. 7, pp. 81-91.

Arnold V., 1964. Instability of Dynamical Systems With Several Degrees of Freedom. Sov.Math.-Dokl. 5, pp. 581-585.

Arnold V., 1978a. Mathematical Methods of Classical Mechanics. Springer Verlag, New York.

Arnold V., 1978b. Geometrical Methods in the Theory of Ordinary Differential Equations. Springer Verlag, New York.

Arnold V., 1982. Ordinary Differential Equations. MIT Press, Cambridge, Massachusetts.

Atkinson C., 1961. On the Stability of the Linearly Related Modes of Certain Nonlinear two DOF Systems. J.Appl.Mech. 28, pp. 71-77.

Atkinson C., 1962. On a Superposition Method for Determining Frequencies of Nonlinear Systems. Proc. 4th U.S. Nat. Congress Appl. Mech., Berkeley, California.

Atkinson C., Bhatt S., Pacitti T., 1963. The Stability of the Normal Modes of Nonlinear Systems With Polynomial Restoring Forces of High Degree. J.Appl.Mech. 30, pp. 193-198.

Atkinson C., Taskett B., 1965. A Study of the Nonlinearly-Related Modal Solutions of Coupled Nonlinear Systems by Superposition Techniques. J.Appl.Mech. 32, pp. 359-364.

Auld B., 1961. On the Stability of the Linearly-Related Modes of Certain Nonlinear two DOF Systems. J.Appl.Mech. 30, pp. 635-636.

Bejarano D., Sanchez M., 1988. Generalized Exponential, Circular and Hyperbolic Functions for Nonlinear Wave Equations. J.Math.Phys. 29 (8), pp. 1847-1853.

Bejarano D., Sanchez M., 1989. Generalized Fourier Series for Nonlinear Systems. J.Sound Vib. 134 (2), pp. 333-341.

Bogoliubov N., Mitropolsky Y., 1961. Asymptotic Methods in the Theory of Nonlinear Oscillations. Gordon and Breach Science Publication, New York.

Byrd P., Friedman D., 1954. Handbook of Elliptic Integrals for Engineers and Physicists. Springer Verlag, New York.

Caughey T., 1954. The Existence and Stability of Ultraharmonics and Subharmonics in Forced Nonlinear Oscillators. J.Appl.Mech. 21 (1), pp. 327-335.

Cooke C., Struble R., 1966. On the Existence of Periodic Solutions and Normal Mode Vibrations of Nonlinear Systems. Quart.Appl.Math. 24 (3), pp. 177-193.

Erdelyi A., 1956. Asymptotic Expansions. Dover Publication, New York.

Greenberg H., Yang T.-L., 1971. Modal Subspaces and Normal Mode Vibrations. Int.J.Nonlinear Mech. 6, pp. 311-326.

Greenspan B., Holmes P., 1983. Homoclinic Orbits, Subharmonics and Global Bifurcations in Forced Oscillations. In "Nonlinear Dynamics and Turbulence," Pitman Advanced Publishing Program, New York.

Guckenheimer G., Holmes P., 1984. Nonlinear Oscillations, Dynamical systems and Bifurcations of Vector Fields. Springer Verlag, New York.

Harvey T., 1958. Natural Forcing Functions in Nonlinear Systems. J.Appl.Mech. 25, pp. 352-356.

Hayashi C., 1985. Nonlinear Oscillations in Physical Systems. Princeton Univ. Press, Princeton, New Jersey.

Holmes P., Marsden J., 1982a. Horseshoes in Perturbations of Hamiltonian Systems With two DOF. Comm.Math.Physics 82, pp. 523-544.

Holmes P., Marsden J., 1982b. Melnikov's Method and Arnold Diffusion for Perturbations of Integrable Hamiltonian Systems. J.Math.Physics 23, pp. 669-675.

Hsu C., 1959. On Simple Subharmonics. Quart.Appl.Math. 17 (1), pp. 102-105.

Hsu C., 1960. On the Application of Elliptic Functions in Nonlinear Forced Oscillations. Quart.Appl.Math. 17 (4), pp. 393-407.

Hsu C., 1964. On the Stability of Periodic Solutions of Nonlinear Dynamical Systems. In the Proc. CNRS "International Symposium on Forced Vibrations of Nonlinear Systems," 7-12 Sept., Marseille, France.

Hyams M., Month L., 1984. The Origin of Stability Indeterminacy in a Symmetric Hamiltonian. J.Appl.Mech. 51, pp. 399-405.

Johnson T., Rand R., 1979. On the Existence and Bifurcation of Minimal Normal Modes. Int.J.Nonlinear Mech. 14, pp. 1-12.

Kinney W., 1965. On the Geometrization of the Forced Oscillations of Nonlinear Systems Having Many DOF. Ph.D. Thesis, Univ. California, Berkeley.

Kinney W., Rosenberg R., 1966. On the Steady State Vibrations of Nonlinear Systems With Many DOF. J.Appl.Mech. 33 (2), pp. 406-412.

Kronauer R., Musa S., 1966. Necessary Conditions for Subharmonic and Superharmonic Synchronization in Weakly Nonlinear Systems. Quart.Appl.Math. 24 (2), pp. 153-160.

Levenson M., 1967. A Numerical Determination of Subharmonic Responses for the Duffing Equation: $\ddot{x} + \alpha x + \beta x^3 = F cos\omega t$ ($\alpha > 0$). Quart.Appl.Math. 25 (1), pp. 11-17.

Liapounov M., 1947. The General Problem of the Stability of Motion. Princeton Univ. Press, Princeton, New Jersey.

Lichtenberg A., Lieberman M., 1983. Regular and Stochastic Motions. Springer Verlag, New York.

Manevich L., Mikhlin I., 1972. On Periodic Solutions Close to Rectilinear Normal Vibration Modes. PMM 36 (6), pp. 1051-1058.

Margallo G., Bejarano D., Yuste B., 1988. Generalized Fourier Series for the Study of Limit Cycles. J.Sound Vib. 125 (1), pp. 13-21.

Mikhlin I., 1974. Resonance Modes of Near-Conservative Nonlinear Systems. PMM 38 (3), pp. 459-464.

Mishra A., Singh M., 1974. The Normal Modes of Nonlinear Symmetric Systems by Group Representation Theory. Int.J.Nonlinear Mech. 3, pp. 463-480.

Montaldi J., Roberts M., Stewart I., 1989. Existence of Nonlinear Normal Modes of Symmetric Hamiltonian Systems. Preprint, Mathematics Institute, Univ. of Warwick, Coventry, England.

Month L., Rand R., 1977. The Stability of Bifurcating Periodic Solutions in a two DOF Nonlinear System. J.Appl.Mech., pp. 782-783.

Month L., 1979. On Approximate First Integrals of Hamiltonian Systems With an Application to Nonlinear Normal Modes in a two DOF Nonlinear Oscillator. Ph.D. Thesis, Cornell Univ.

Month L., Rand R., 1980. An Application of the Poincare map to the Stability of Nonlinear Normal Modes. J.Appl.Mech. 47, pp. 645-651.

Musa S., Kronauer R., 1968. Sub- and Superharmonic Synchronization in Weakly Nonlinear Systems: Integral Constraints and Duality. Quart.Appl.Math. 25 (4), pp. 399-414.

Nayfeh A., Mook D., 1979. Nonlinear Oscillations. Wiley Interscience Publication, New York.

Pak C., Rosenberg R., 1968. On the Existence of Normal Mode Vibrations in Nonlinear Systems. Quart.Appl.Math. 26 (3), pp. 403-416.

Pak C., 1989. On the Stability Behavor of Bifurcated Normal Modes in Coupled Nonlinear Systems. J.Appl.Mech. 56, pp. 155-161.

Pecelli G., Thomas E., 1980. Stability of Modes for a Class of Nonlinear Planar Oscillators. Int.J.Nonlinear Mech. 15, pp. 57-70.

Persival I., Richards D., 1982. Introduction to Dynamics. Cambridge Univ. Press, Cambridge, England.

Porter J., Atkinson C., 1962. A Note on a new Stability Method for the Linear Modes of Nonlinear two DOF Systems. J.Appl.Mech. 30, pp. 258-262.

Rand R., 1971a. Nonlinear Normal Modes in two DOF Systems. J.Appl.Mech. 38, pp. 561.

Rand R., 1971b. A Higher Order Approximation for Nonlinear Normal Modes in two DOF Systems. Int.J.Nonlinear Mech. 6, pp. 545-547.

Rand R., 1973. The Geometrical Stability of Nonlinear Normal Modes in two DOF Systems. Int.J.Nonlinear Mech. 8, pp. 161-168.

Rand R., 1974. A Direct Method for Nonlinear Normal Modes. Int.J.Nonlinear Mech. 9, pp. 363-368.

Rand R., 1990. Personal Communication.

Rosenberg R., 1960. Normal Modes in Nonlinear Dual-Mode Systems. J. Appl. Mech. 27, pp. 263-268.

Rosenberg R., 1961. On Normal Vibrations of a General Class of Nonlinear Dual-Mode Systems. J.Appl.Mech. 28, pp. 275-283.

Rosenberg R., 1962. The Normal Modes of Nonlinear n-DOF Systems. J.Appl. Mech. 30, pp. 7-14.

Rosenberg R., 1963. The Ateb(h)-Functions and Their Properties. Quart. Appl. Math. 21 (1), pp. 37-47.

Rosenberg R., Kuo J., 1964. Nonsimilar Normal Mode Vibrations of Nonlinear Systems Having two-DOF. J.Appl.Mech. 31, pp. 283-290.

Rosenberg R., 1966. On Nonlinear Vibrations of Systems With Many DOF. Adv. Appl. Mech. 9, pp. 155-242.

Szemplinska - Stupnicka W., 1980. The Resonant Vibration of Homogeneous Nonlinear Systems. Int.J.Nonlinear Mech. 15, pp. 407-415.

Vakakis A., Caughey T., 1988. Free and Forced Vibration of Certain Strongly Nonlinear Systems. Dynamics Laboratory Report DYNL-88-1, Caltech, Pasadena, California.

Van der Pol B., Stutt M., 1928. On the Stability of the Solutions of Mathieu's Equations. Phil.Mag. 7-th series, 5, pp. 18.

Van Groesen E., 1983. On Normal Modes in Classical Hamiltonian Systems. Int. J. Nonlinear Mech. 18 (1), pp. 55-70.

Veerman P., Holmes P., 1985. The Existence of Arbitrarily Many Distinct Periodic Orbits in a two DOF Hamiltonian System. Physica 14D, pp. 177-192.

Veerman P., Holmes P., 1986. Resonance Bands in a two-DOF Hamiltonian System. Physica 20D, pp. 413-422.

Vito R., 1972a. Similar Normal Mode Vibrations in Certain Conservative Systems With two DOF. Int.J.Nonlinear Mech. 7, pp. 473-487.

Vito R., 1972b. An Approximate Method for Treating the Nonlinear Vibrations of Certain two DOF Systems. J.Appl.Mech. 39 (2), pp. 620-621.

Weinstein A., 1973. Normal Modes for Nonlinear Hamiltonian Systems. Inventiones Math. 20, pp. 47-57.

Wiggins S., 1989. Global Bifurcations and Chaos: Analytical Methods. Springer Verlag, New York.

Yang T.-L., 1968a. Symmetry Properties and Normal Mode Vibrations. Int. J. Nonlinear Mech. 3, pp. 367-381.

Yang T.-L., Rosenberg R., 1968. On Forced Vibrations of a Particle in the Plane. Int.J.Nonlinear Mech. 3, pp. 47-63.

Yen D., 1974. On the Normal Modes of Nonlinear Dual-Mass Systems. Int. J. Nonlinear Mech. 9, pp. 45-53.

PART II

Billings S., 1980. Identification of Nonlinear Systems: A Survey. IEE Proc. 127, Pt D, No 6, pp. 272-285.

Brandon J., Cowley A., 1983. A Weighted Least Squares Method for Circle-Fitting to Frequency Response Data. J.Sound Vib. 89, pp. 419-424.

Brown D., Allemang R., Zimmerman R., Mergeay M., 1979. Parameter Estimation Techniques for Modal Analysis. SAE Technical Paper, No 790221.

Caughey T., 1963. Equivalent Linearization Techniques. J. Acoust. Soc. Am. 35 (11), pp. 1706-1711.

Caughey T., Vakakis A., Moser A., 1990. Some Ideas on the Identification of Closely Spaced Modes. Presented in the 2end USAF/NASA Workshop on "System Identification and Health Monitoring of Precision Space Structures." March 27-29, Pasadena, California.

Cauley P., 1986. The Accuracy of Frequency Response Function Measurements Using FFT-based Analyzers With Transient Excitation. ASME J. Vibr., Acoust., Stress and Reliability in Design 108, pp. 45-49.

Comparin R., 1989. Nonlinear Frequency Response Characteristics of an Impact Pair. J. Sound Vib. 134 (2), pp. 259-290.

Crandall S., 1970. The Role of Damping in Vibration Theory. J. Sound Vib. 11 (1), pp. 3-18.

Den Hartog J., 1931. Forced Vibrations With Combined Coulomb and Viscous Friction. Trans. ASME, APM-53-9, pp. 107-115.

Dobson B., 1987. A Straight-Line Technique for Extracting Modal Properties From Frequency Response Data. Mech. Syst. Signal Proc. 1 (1), pp. 29-40.

Dossing O., 1986. A Method for Determining the Modal Frequencies of Structures With Coupled Modes. Proc. 4th Int. Modal Anal. Conf., Orlando, Florida.

Ewins D., Gleeson P., 1982. A Method for Modal Identification of Lightly Damped Structures. J. Sound Vib. 84, pp. 57-79.

Ewins D., 1984. Modal Testing: Theory and Practice. Research Studies Press, London, England.

Ewins D., Vakakis A., 1989. An Alternative Method for Modal Analysis. Int. J. Analyt. Exp. Modal Anal. 4 (4), pp. 144-149.

Frachebourg A., 1989. Using Volterra Models With Impact Excitation: A Simple Solution to Identify Nonlinearities. Proc. 7th Modal Anal. Conf., Las Vegas, Nevada.

Gaukroger D., Skingle C., Heron K., 1973. Numerical Analysis of Vector Response Loci. J. Sound Vib. 29 (3), pp. 341-353.

Gersch W., Martinelli F., 1979. Estimation of Structural System Parameters From Stationary and Non-Stationary Ambient Vibrations: An Exploratory Confirmatory Analysis. J.Sound Vib. 65 (3), pp. 303-318.

Gersch W., Brotherton T., 1982. Estimation of Stationary Structural System Parameters From Non-stationary Random Vibration Data: A Locally Stationary Model Method. J. Sound Vib. 81 (2), pp. 215-227.

Gifford S., Tomlinson G., 1989a. Recent Advances in the Application of Functional Series to Nonlinear Structures. J. Sound Vib. 135 (2), pp. 289-317.

Gifford S., Tomlinson G., 1989b. Understanding Multi-DOF Nonlinear Systems via Higher Order Frequency Response Functions. Proc. 7th Modal Anal. Conf., Las Vegas, Nevada.

Haymon G., 1978. Experimental Determination of Linear Damping Coefficients in Elastic Structures With Geometric Nonlinearity. Israel J. Tech. 16, pp. 64-69.

He J., 1987. Identification of Structural Dynamic Characteristics. Ph.D. Thesis, Imperial College, London.

Hunter N., 1990. Analysis of Nonlinear Systems Using ARMA Models. Proc. 8th Modal Anal. Conf., Orlando, Florida.

Ibrahim S., Mikulcik E., 1973. A Time-Domain Modal Vibration Test Technique. Shock Vib. Bull. 43 (4), pp. 21-37.

Ibrahim S., Mikulcik E., 1976. The Experimental Determination of Vibration Parameters From Time Responses. Shock Vib. Bull. 51 (3), pp. 43-72.

Iwan W., 1973. A Generalization of the Concept of Equivalent Linearization. Int. J. Nonlinear Mech. 8, pp. 279-287.

Kennendy C., Pancu C., 1947. Use of Vectors in Vibration Measurement and Analysis. J. Aero. Sc. 14 (11), pp. 603-625.

Klosterman A., 1971. On the Experimental Determination and use of Modal Representation of Dynamic Characteristics. Ph.D. Thesis, Univ. Cincinnati.

Lee J., Fassois S., 1990. A Stochastic Suboptimum Maximum Likelihood Approach to Structural Dynamics Identification. Proc. 8th Modal Anal. Conf., Orlando, Florida.

Maia N., 1988. Extraction of Valid Modal Properties From Measured Data in Structural Vibrations. Ph.D. Thesis, Imperial College, London.

Maia N., Ewins D., 1989. A new Approach for the Modal Identification of Lightly Damped Structures. Mech. Syst. Signal Proc. 3 (2), pp. 173-193.

Marples V., 1973. The Derivation of Modal Damping Ratios From Complex Plane Response Plots. J. Sound Vib. 124 (1), pp. 13-26.

Masri S., Caughey T., 1979. A Nonparametric Identification Technique for Nonlinear Dynamical Problems. J. Appl. Mech. 46, pp. 433-447.

Masri S., Sassi H., Caughey T., 1982a. Identification and Modeling of Nonlinear Systems. Nuclear Eng. and Design 72 (2), pp. 235-270.

Masri S., Bekey G., Sassi H., Caughey T., 1982b. Nonparametric Identification of a Class of Nonlinear Multi-DOF Dynamic Systems. J. Earthquake Eng. Str. Dynamics 10, pp. 1-30.

McVerry G., 1979. Frequency Domain Identification of Structural Models from Earthquake Records. Earthquake Engineering Research Report EERL 79-02. Dpt. of Civil Engineering, California Institute of Technology, Pasadena, California.

McVerry G., Beck J., 1983. Structural Identification of JPL Building 180 Using Optimally Synchronized Earthquake Records. Dpt. of Civil Engineering, Earthquake Engineering Research Report EERL 83-01. California Institute of Technology, Pasadena, California.

Mertens M., Van der Auweraer H., Vanherck P., Snoeys R., 1989. The Complex

Stiffness Method to Detect and Identify Nonlinear Dynamic Behavor of SDOF Systems. Mech. Syst. Signal Proc. 3 (1), pp. 37-54.

Montalvao e Silva J., Maia N., 1988. Single Mode Modal Identification Techniques for use With Small Microcomputers. J. Sound Vib. 124 (1), pp. 13-26.

Montalvao e Silva J., Maia N., 1989. Single Mode Modal Identification of Insufficiently Separated Modes. Proc. 4th Modal Anal. Conf., Los Angeles, California.

Natke H. (ed), 1982. Identification of Vibrating Structures. CISM Course and Lecture No 272, Springer Verlag, New York.

Natke H., 1987. Survey on the Identification of Mechanical Systems. Workshop on "Road Vehicle Systems and related Mathematics," June 20-25, Torino, Italy.

Natsiavas S., 1990. Steady State Vibration of Oscillators With Motion-Limiting Constraints. Proc. 8th Modal Anal. Conf., Orlando, Florida.

Nayfeh A., Mook D., 1979. Nonlinear Oscillations. Wiley Interscience Publication, New York.

Pappa R., Ibrahim S., 1981. A Parametric Study of the Ibrahim Time-Domain Identification Algorithm. Shock Vib. Bull. 51 (3), pp. 43-72.

Pappa R., 1990. Identification Challenges for Large Space Structures. Proc. 8th Modal Anal. Conf., Orlando, Florida.

Pendered J., Bishop R., 1963. A Critical Introduction to Some Industrial Resonance Testing Techniques. J. Mech. Eng. Science 5 (4), pp. 345-367.

Pendered J., 1965. Theoretical Investigation Into the Effects of Close Natural Frequencies in Resonance Testing. J. Mech. Eng. Science 7 (4), pp. 372-379.

Press W., Flannery B., Teukolsky S., Vetterling W., 1988. Numerical Recipes. Cambridge Univ. Press, Cambridge, England.

Rades M., 1983. On the Effects of Nonlinear Stiffness in Resonance Testing. Applied Mechanics, No 6, Academy of the Republic, Bucharest, Romania.

Rades M., 1985. Frequency-Domain Experimental Modal Analysis Techniques. Shock Vib. Digest 17 (6), pp. 3-15.

Robb D., 1988. User's Guide to Program MODENT. Dynamics Section, Dpt Mech. Eng., Imperial College, London.

Simon M., Tomlinson G., 1984. Use of the Hilbert Transform in Modal Analysis of Linear and Nonlinear Structures. J. Sound Vib. 96 (4), pp. 421-436.

Spitnogle F., Quazi A., 1970. Representation and Analysis of Time-Limited Signals Using a Complex Exponential Algorithm. J. Acoust. Soc. Am. 47 (5), pp. 1150-1155.

Tomlinson G., Hibbert J., 1979. Identification of the Dynamic Characteristics of a Structure With Coulomb Friction. J. Sound Vib. 64 (2), pp. 233-242.

Tomlinson G., 1980. An Analysis of the Distortion Effects of Coulomb Friction on the Vector Plots of Lightly Damped Systems. J. Sound Vib. 71 (3), pp. 443-451.

Tomlinson G., Lam J., 1984. Frequency Response Characteristics of Structures With Single and Multiple Clearance-Type Nonlinearity. J. Sound Vib. 96 (1), pp. 111-125.

Tomlinson G., 1987. Developments in the use of the Hilbert Transform for Detecting and Quantifying Nonlinearity Associated With Frequency Response Functions. J. Sound Vib. 1 (2), pp. 151-171.

Traill-Nash R., Long G., Bailey C., 1967. Experimental Determination of the Complete Dynamical Properties of a two-DOF Model Having Nearly Coincident Natural Frequencies. J. Mech. Eng. Science 9 (5), pp. 402-413.

Vakakis A., 1985. Complex Modes in Vibrating Systems. MSc Thesis, Imperial College, London.

White R., 1971. Effects of Nonlinearity due to Large Deflections in the Resonance Testing of Structures. J. Sound Vib. 16 (2), pp. 255-267.

Worden K., Tomlinson G., 1989. Application of the Restoring Force Surface Method to Nonlinear Elements. Proc. 7th Modal Anal. Conf., Las Vegas, Nevada.

Yeh G., 1966. Forced Vibrations of a two-DOF System With Combined Coulomb and Viscous Damping. J. Acoust. Soc. Am. 39, pp. 14-24.

APPENDICES

APPENDIX A: INTEGRATIONS OF SDOF UNDAMPED EQUATIONS OF MOTION

Consider the free oscillation of an undamped SDOF system with equation of motion:

$$\ddot{x} + f(x) = 0 \qquad (A-1)$$

and initial conditions, $x(0) = X, \dot{x}(0) = 0$. Assume that the system is "linearizable" about $x = 0$, i.e., that the restoring force can be expressed in the form:

$$f(x) = \sum_{i=1,3,5,\ldots} \frac{f^{(i)}(0)}{i!} x^i \qquad (A-2)$$

where $f^{(i)}(0)$ denotes the i-th derivative of f, evaluated at $x = 0$, and for simplicity is assumed to be a non-negative quantity.

Then, the free oscillation of the system can be obtained by quadratures, as:

$$t = t(x, X) = \frac{1}{\Omega(X)^{1/2}} \int_0^{cos^{-1}(x/X)} \{\, 1 + \sum_{i=3,5,\ldots} \frac{2f^{(i)}(0)X^{i-1}v_i(\phi)}{\Omega(X)(i+1)!} \,\}^{-1/2} d\phi \qquad (A-3)$$

where

$$v_i(\phi) = \frac{1 - cos^{i+1}\phi}{1 - cos^2\phi} - 1 \quad , \quad i = 3, 5, \ldots$$

$$\Omega(X) = \sum_{i=1,3,5,\ldots} \frac{2f^{(i)}(0)X^{i-1}}{(i+1)!}$$

Expression (A-3) can be regarded as an "incomplete" integral (in the same sense as the incomplete elliptic integrals and Beta functions, for example). The integrand is periodic with respect to the variable ϕ, and $t(x, X)$ is monotonic in the interval $0 < \phi < \pi/2$. Hence, the frequency of free oscillation of the motion (A-3) can be evaluated by considering the respective "complete" integral, i.e., by setting the upper limit of integration equal to $\pi/2$:

$$\omega = \omega(X) = \frac{\pi \Omega(X)^{1/2}}{2 \int_0^{\pi/2} \{ \, 1 + \sum_{i=3,5,\ldots} \frac{2 f^{(i)}(0) X^{i-1} v_i(\phi)}{\Omega(X)(i+1)!} \, \}^{-1/2} d\phi} \qquad (A-4)$$

If the function $f(x)$ is "non-linearizable" about $x = 0$, i.e., if:

$$f^{(j)}(0) = 0, \; j = 1, \ldots, p-2 \;\; , \;\; and \;\; f^{(p)}(0) \neq 0 \;\; , \;\; p = even$$

then the following relations replace equations (A-3,4):

$$t = t(x, X) =$$

$$= \frac{1}{\Theta(X)^{1/2}} \int_0^{cos^{-1}(x/X)} \{ \, [\frac{1 - cos^{p+1}\phi}{1 - cos^2\phi}][1 + \sum_{i=p+2,\ldots} \frac{2 f^{(i)}(0) X^{i-1} u_i(\phi)}{\Theta(X)(i+1)!}] \, \}^{-1/2} d\phi \qquad (A-5)$$

and

$$\omega = \omega(X) = \frac{\pi \Theta(X)^{1/2}}{2 \int_0^{\pi/2} \{ \, [\frac{1 - cos^{p+1}\phi}{1 - cos^2\phi}][1 + \sum_{i=p+2,\ldots} \frac{2 f^{(i)}(0) X^{i-1} u_i(\phi)}{\Theta(X)(i+1)!}] \, \}^{-1/2} d\phi} \qquad (A-6)$$

where

$$u_i(\phi) = \frac{1 - cos^{i+1}\phi}{1 - cos^{p+1}\phi} - 1 \;\; , \;\; i = p+2, \ldots$$

$$\Theta(X) = \sum_{i=p, p+2, \ldots} \frac{2 f^{(i)}(0) X^{i-1}}{(i+1)!}$$

APPENDIX B: COEFFICIENTS OF VARIATIONAL EQUATIONS (2.23)

The coefficients of the stability equations (2.23) of the system with combined cubic and quintic nonlinearities are computed as follows:

$$
\begin{aligned}
A_2 &= (1+c^2)^{-2}\{\ (c^2-1)c + K_3(1+c)^3(1-c)\ \} \\
A_3 &= 3(1+c^2)^{-2}\{\ (1-c^2)^2K_3 + 2c^2\ \} \\
A_4 &= (1+c^2)^{-2}\{\ (1-c)^4K_3 + 1 + c^4\ \} \\
A_5 &= (1+c^2)^{-3}\{\ (1-c)^6K_5 + 1 + c^6\ \} \\
A_6 &= 5(1+c^2)^{-3}\{\ (1+c^4)(1-c)^2K_5 + c^2(1+c^2)\ \} \\
A_7 &= 10(1+c^2)^{-3}\{\ (c^2-1)^3K_5\ \} \\
A_8 &= 10(1+c^2)^{-3}\{\ (1+c)^2(1-c)^4K_5 + c^2(1+c^2)\ \} \\
A_9 &= (1+c^2)^{-3}\{\ c(c^4-1) + (1+c)^5(1-c)K_5\ \} \\
A_{10} &= (1+c^2)^{-2}\{\ (1+c)^4K_3 + 1 + c^4\ \} \\
A_{11} &= (1+c^2)^{-3}\{\ (1+c)^6K_5 + 1 + c^6\ \}
\end{aligned}
\qquad (B-1)
$$

The quantities c, K_3, and K_5 are defined in section 2.2.3.

APPENDIX C: FOURIER EXPANSIONS OF ELLIPTIC FUNCTIONS

The Fourier expansions of the elliptic cosine and some of its powers are given by (Byrd, 1954):

$$
cn(qt,k) = \sum_{n=0}^{\infty} a_{2n+1} cos\frac{(2n+1)\pi qt}{2K(k)} \qquad (C-1)
$$

$$cn^2(qt,k) = 1 - \sum_{n=0}^{\infty} b_{2n+1} sin \frac{(2n+1)\pi qt}{2K(k)} \qquad (C-2)$$

$$cn^3(qt,k) = \sum_{n=0}^{\infty} d_{2n+1} cos \frac{(2n+1)\pi qt}{2K(k)} \qquad (C-3)$$

where

$$\begin{aligned} a_{2n+1} &= \frac{2\pi}{kK(k)} \frac{Q^{(2n+1)/2}}{1+Q^{2n+1}} \\ b_{2n+1} &= [\ \frac{1+k^2}{2k^3} - \frac{(2n+1)^2}{2k^3} \frac{\pi^2}{4K^2(k)}\ ] \frac{2\pi}{K(k)} \frac{Q^{(2n+1)/2}}{1-Q^{2n+1}} \\ d_{2n+1} &= \frac{1}{2k^2}[\ 2k^2 - 1 + (2n+1)^2 (\frac{\pi}{2K(k)})^2\ ] \frac{2\pi}{kK(k)} \frac{Q^{(2n+1)/2}}{1+Q^{2n+1}} \end{aligned} \qquad (C-4)$$

In the above expressions, $K(\bullet)$ is the complete elliptic integral of the first kind, k is the elliptic modulus, and Q is the elliptic nome, defined by:

$$Q = exp(-\pi K'(k)/K(k)) \quad , \quad K'(k) = K(1-k) \qquad (C-5)$$

The complete elliptic integral $K(k)$ can be expanded in terms of its modulus, as follows:

$$\frac{2K(k)}{\pi} = 1 + \frac{k^2}{2} + \mathcal{O}(k^4) \qquad (C-6)$$

Additional formulas regarding expansions of elliptic functions can be found in (Byrd, 1954).

APPENDIX D: ANALYTIC EXPRESSIONS FOR THE LINEAR SEGMENTS OF FIGURE 5.6

Consider the r^{th} term of the receptance series (corresponding to the r-th modal response):

$${}_r a_{jk}(\omega) = \frac{{}_r A_{jk}}{\omega_r^2 - \omega^2 + i\eta_r \omega_r^2} \qquad (D-1)$$

Three points A, B and C on the r^{th} Modal circle with frequencies squared $\omega^2, \omega^2 - d\omega^2, \omega^2 + d\omega^2$ respectively, are connected by linear segments of magnitude (see figure 5.6):

$$\begin{aligned}(AB)^2 &= \frac{|_rA_{jk}|^2}{\left(\omega_r^2\eta_r\right)^2} sin^2\left[tan^{-1}\frac{\left(\eta_r\omega_r^2\right)^{-1}d\omega^2}{1+\left(\eta_r\omega_r\right)^{-2}(\omega_r^2-\omega^2)(\omega_r^2-\omega^2+d\omega^2)}\right] \\ (AC)^2 &= \frac{|_rA_{jk}|^2}{\left(\omega_r^2\eta_r\right)^2} sin^2\left[tan^{-1}\frac{\left(\eta_r\omega_r^2\right)^{-1}d\omega^2}{1+\left(\eta_r\omega_r^2\right)^{-2}(\omega_r^2-\omega^2)(\omega_r^2-\omega^2-d\omega^2)}\right]\end{aligned} \qquad (D-2)$$

The above complicated expressions can be simplified by use of the trigonometric identity:

$$sin^2(tan^{-1}\psi) = \frac{\psi^2}{1+\psi^2}$$

Referring now to figure 5.6, the triad of points (BAC) is initially displaced to the new position

$$(BAC) \rightarrow (B'A''C')$$

where A'' is the point of the distorted Nyquist plot corresponding to frequency ω^2. The *relative* distortions of points B'' and C'' with respect to A'' can now be analytically computed. These distortions are represented by the segments $B'B''$ and $C'C''$ which are equal in magnitude and parallel, since the modal interference is approximated by first order terms, (equation (5.8)). From the geometrical construction it can be stated that:

$$(A''B')^2 = (AB)^2, \qquad (A''C')^2 = (AC)^2 \qquad (D-3)$$

The angles ϕ, θ and ϕ_1 (in degrees), are related by:

$$\phi_1 = 180 + \theta - \phi \Rightarrow \theta = \phi_1 + \phi - 180 \qquad (D-4)$$